Assembly pathway of the fungal COP9 signalosome

Dissertation

for the award of the degree

“Doctor rerum naturalium”

of the Georg-August Universität Göttingen

within the doctoral program “Microbiology and Biochemistry” of the

Georg-August University School of Science (GAUSS)

submitted by

Fruzsina Erzsébet Bakti

born in Nyíregyháza, Hungary

Göttingen, 2021

For my nephews and nieces

Az unokaöccseimnek és unokahugaimnak

Thesis Committee and members of the Examination Board:

Reviewer: **Prof. Dr. Gerhard Braus**
Department of Molecular Microbiology and Genetics,
Georg-August-Universität Göttingen

2nd Reviewer: **Prof. Dr. Kai Heimel**
Department of Microbial Cell Biology,
Georg-August-Universität Göttingen

3rd Reviewer: **Prof. Dr. Ralf Ficner**
Department for Molecular Structural Biology,
Georg-August-Universität Göttingen

Prof. Dr. Stefanie Pöggeler
Department of Genetics of Eukaryotic Microorganisms,
Georg-August Universität Göttingen

PD Dr. Michael Hoppert
Department of General Microbiology,
Georg-August-Universität Göttingen

PD Dr. Marcel Wiermer
Schwann-Schleiden Center,
Research Group Molecular Biology of Plant-Microbe Interactions,
Georg-August-Universität Göttingen

Date of the oral examination: 2022. February 28.

Declaration of independence

Herewith I declare that the dissertation entitled "**Assembly pathway of the fungal COP9 signalosome"** was written on my own and independently without any aids and sources other than indicated.

Fruzsina Erzsébet Bakti

Göttingen, 2021.12.16.

This work was conducted in the group of Prof. Dr. Gerhard H. Braus at the Department of Molecular Microbiology and Genetics, Institute of Microbiology and Genetics, Georg-August-Universität Göttingen.

Publications, which were published during the doctoral studies:

Fruzsina Bakti, Christoph Sasse, Thorsten Heinekamp, István Pócsi, Gerhard H. Braus (2018) Heavy metal-induced expression of PcaA provides cadmium tolerance to *Aspergillus fumigatus* and supports its virulence in the *Galleria mellonella* model. *Frontiers in Microbiology*. 9: 744.

Tri-Thuc Bui, Rebekka Harting, Susanna A. Braus-Stromeyer, Van-Tuan Tran, Miriam Leonard, Annalena Höfer, Anja Abelmann, **Fruzsina Bakti**, Oliver Valerius, Rabea Schlüter, Claire E. Stanley, Alinne Ambrósio, Gerhard H. Braus (2019) *Verticillium dahliae* transcription factors Som1 and Vta3 control microsclerotia formation and sequential steps of plant root penetration and colonization to induce disease. *New Phytologist*. 221: 2138–2159.

Part of this work will be published in:

Fruzsina Bakti, Helena Stupperich, Kerstin Schmitt, Oliver Valerius, Anna M. Köhler, Cindy Meister, Anja Strohdiek, Kai Heimel, Piotr Neumann, Ralf Ficner, Gerhard H. Braus (2022) Assembly of the native fungal COP9 signalosome. *In preparation*.

Table of contents

Summary

The conserved eight-subunit COP9 signalosome (CSN complex) controls the exchange of E3 ubiquitin cullin RING ligase receptors, and therefore the specificity of protein degradation in eukaryotic cells and it is required for multicellular development. The CSN complex of the filamentous fungus *Aspergillus nidulans* assembles through a seven-subunit pre-CSN complex, which is activated by the final integration of the catalytic CsnE deneddylase, thereby forming an eight-subunit CSN, as in humans. The goal of this work was to identify the assembly pathway of fungal pre-CSN complex *in vivo* by combined genetic and biochemical approaches. Loss of CsnE and the abolishment of the pre-CSN complex formation result in distinct fungal phenotypes. All fungal COP9 signalosome subunits are required for sexual development and secondary metabolism. Subunits of the pre-CSN complex additionally support wild type-like growth and asexual development. Functional GFP-CSN subunit fusions can complement the corresponding phenotypes. GFP-CSN subunit-based GFP-affinity enrichments combined with mass spectrometry allowed the identification of interacting CSN subcomplexes. The interactome analysis revealed, as one major result, that two distinct heterotrimeric CSN subcomplexes are intermediates of the assembly pathway. These heterotrimers, CsnA-CsnC-CsnH and CsnD-CsnF-CsnG, are formed independently of CsnB. CsnE cannot associate to either any of the heterotrimers or CSN subunits without CsnB, which supports that this subunit acts as link between the two trimeric subcomplexes. Subtle cellular feedback surveillance mechanisms control that equal CSN subunit amounts are available for CSN assembly. Accordingly, loss of *csn* subunit genes differentially changes protein levels of remaining CSN subunits. Subunits of both heterotrimeric subcomplexes are required to reach wild type-like CsnA protein amounts, which is part of the CsnA-CsnC-CsnH subcomplex. In contrast, relative protein levels of CsnD, which is part of the CsnD-CsnF-CsnG trimer, are increased, if the pre-CSN complex cannot be formed. CsnG is a prerequisite to connect subunits of the CsnD-CsnF-CsnG subcomplex and it is part of the surveillance for the cellular CsnD amounts. Furthermore, CsnA and, therefore the CsnA-CsnC-CsnH trimer, is required for appropriate CsnB amounts, because the inability to form CsnA-CsnC-CsnH reduces relative levels of the CsnB bridging protein. These results support a complex orchestration for providing sufficient levels of subunits for the correct CSN assembly pathway, which includes a mutual control of the formation of both trimers. In addition, the cellular abundance of the CsnE deneddylase and the CsnB linker are adjusted independently of each other. An additional level of control includes the cellular localization of CSN subunits. The stable octameric CSN complex is enriched in nuclei, whereas CSN subassemblies inhabit different cellular compartments. The CsnD-CsnF-CsnG trimer is predominantly nuclear localized, whereas CsnA-CsnC-CsnH is evenly distributed between nuclei and cytoplasm. Nuclear enrichment of the linker CsnB is independent of the deneddylase subunit, but depends on CsnA and, therefore, an intact CsnA-CsnC-CsnH trimer. This suggests that CsnB is transported into the nuclei together with CsnA. In summary, the fungal COP9 signalosome is assembled through two trimeric subcomplexes linked by CsnB, which enables final association with the CsnE deneddylase. Formation of the functional CSN complex requires a sophisticated interplay between mutual control of subunit protein levels, correct localization and sequential assembly.

Zusammenfassung

Das COP9 Signalosom (CSN Komplex) ist ein Proteinkomplex aus acht Untereinheiten, der in höheren Eukaryoten konserviert ist und für die multizelluläre Entwicklung benötigt wird. CSN kontrolliert den Austausch von Substrat-Rezeptoren von E3 Ubiquitin-Cullin-RING Ligasen und damit die Spezifität des Protein-Abbaus in eukaryotischen Zellen. Beim Aufbau des CSN Holokomplexes des filamentösen Pilzes *Aspergillus nidulans* wird im letzten Schritt die katalytische CsnE Deneddylase-Untereinheit in einen sieben-Untereinheiten Prä-CSN Komplex eingebaut. Hauptziel der Doktorarbeit war die *in vivo* Identifikation der zellulären Schritte, die für den Zusammenbau des Gesamtkomplexes aus den einzelnen CSN-Untereinheiten notwendig sind. Dafür wurden genetischen und biochemischen Methoden kombiniert. Alle CSN Untereinheiten werden für die sexuelle Entwicklung und den dazu gehörenden Sekundärmetabolismus benötigt. Daneben können einzelne Untereinheiten des Prä-CSN Komplexes das Wachstum der Kolonie und die asexuelle Entwicklung unterstützen. Entsprechende funktionelle GFP-CSN Fusionsproteine, die alle diese Phänotypen komplementieren können, wurden für GFP-Affinitätsanreicherungen und anschließende Massen-Spektrometrie in unterschiedlichen *csn*-Mutanten verwendet. Ein Hauptergebnis dieser Interaktom-Analyse war die Entdeckung von zwei heterotrimer Subkomplexen als Zwischenstufe für den Aufbau des CSN Komplexes. Diese beiden Trimere, CsnA-CsnC-CsnH und CsnD-CsnF-CsnG, werden unabhängig von CsnB gebildet. CsnE ist nicht in der Lage mit einem der beiden Trimere zu interagieren, wenn CsnB in der Zelle fehlt. CsnB ist daher notwendig, um die beiden Trimere zum Prä-CSN Komplex zu verbinden und damit die Inkorporation von CsnE als finalem Schritt der Komplexbildung zu ermöglichen. Die zellulären Proteinmengen für die einzelnen CSN Untereinheiten werden durch unterschiedliche Feedback-Mechanismen kontrolliert. Die Wild-Typ-Menge an CsnA Protein wird nur dann in der Zelle erreicht, wenn ausreichend Proteine für die anderen Untereinheiten der beiden Trimere vorhanden sind. CsnA wird andererseits benötigt, um ausreichende Mengen des Brücken-Proteins CsnB zu bekommen. Die Menge an CsnD, das ein Teil des CsnD-CsnF-CsnG Trimers darstellt, wird umgekehrt erhöht, wenn ausreichende Mengen anderer Untereinheiten des Prä-CSN Komplexes fehlen. Diese Ergebnisse weisen auf ein komplexes zelluläres Überwachungssystem, das die Proteinmengen für die beiden Trimere, für das Brückenprotein CsnB und die Deneddylase CsnE, und damit den akkuraten Aufbau des gesamten CSN Komplexes kontrolliert. Ein weiteres Kontrollsystem steuert die zelluläre Lokalisierung der CSN Untereinheiten. Der stabile acht-Untereinheiten CSN Holokomplex ist überwiegend im Zellkern lokalisiert. Der CsnD-CsnF-CsnG Subkomplex befindet sich auch vorwiegend im Nukleus, während das CsnA-CsnC-CsnH Trimer zwischen Zytoplasma und Zellkern verteilt ist. Die Anreicherung des Brückenproteins CsnB im Zellkern erfordert CsnA, aber nicht die CsnE Deneddylase. Vermutlich wird CsnB daher mit CsnA oder mit dem CsnA-CsnC-CsnH Trimer in den Kern transportiert. Insgesamt ergab die hier durchgeführte Analyse, dass der zelluläre Aufbau des COP9 Signalosoms bei *A. nidulans* über die Bildung zweier Trimere führt, die durch CsnB verknüpft werden. Dies ermöglicht dann die Inkorporation der CsnE Deneddylase als einziger Untereinheit des CSN Holokomplexes mit intrinsischer Enzymaktivität. Der Aufbauprozess erfordert ein vielfältiges Zusammenspiel zwischen wechselseitiger Kontrolle der Proteinmengen der Untereinheiten, deren korrekter zellulärer Lokalisierung und ihres sequentiellen Zusammenbaus.

1 Introduction

1.1 Cellular proteostasis

Proteins perform an enormous variety of biological functions. Proteostasis, the protein homeostasis in the cell, is a well-regulated interconnection between protein biosynthesis, regulation of protein activity as well as protein degradation in response to environmental and internal changes. Protein biosynthesis includes translation of corresponding mRNA, folding of the native protein, regulation of steady state amounts and assembly of protein complexes. Protein activity is controlled by various processes, as the attachment and removal of posttranslational protein modifications (PTMs). These can govern the subcellular localization as well as the stability of a protein. Protein degradation encompasses the break-down of proteins into amino acids, as building bricks for novel proteins, and also the disassembly protein complexes. Together, these elements of proteostasis control the fine-tuned regulation of protein amounts in the cell (Figure 1). Proteostasis involves the dynamic change of functional proteomes upon diverse intra- and extracellular signals as well as developmental programs and thus, it is essential for the cellular homeostasis (reviewed in Jayaraj *et al.*, 2020).

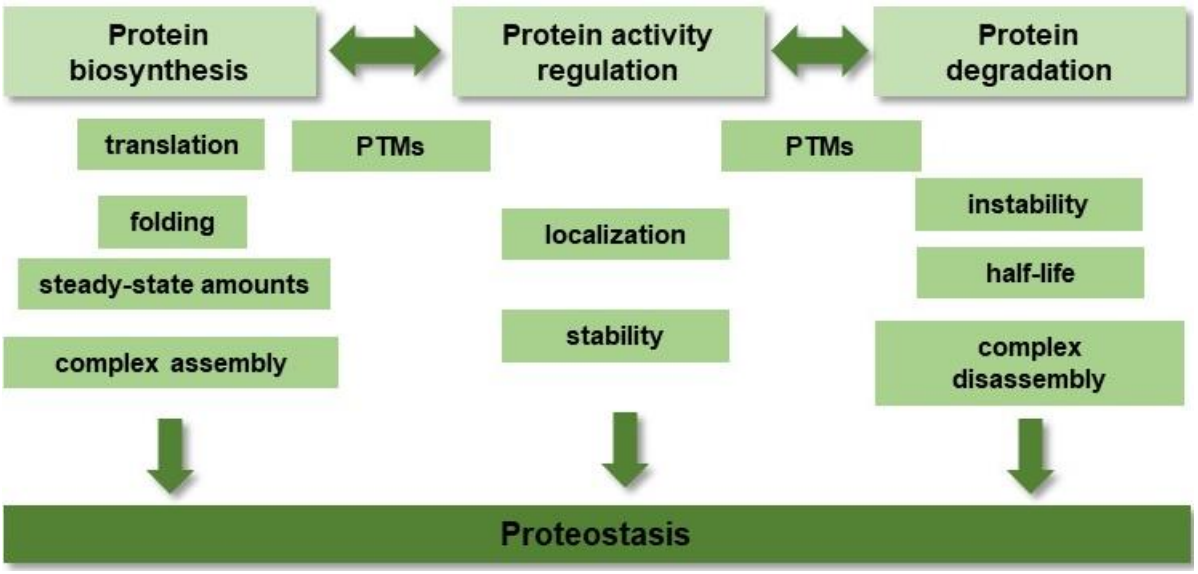

Figure 1. Elements of the proteostasis.
The protein homeostasis is a fine-tuned regulation and interconnection of protein biosynthesis, activity and degradation processes (reviewed in Jayaraj *et al.*, 2020).

1.2 Posttranslational protein modifications maintain the proteostasis

A dynamic and effective way to control activity, function, subcellular localization and life span of a protein is the attachment or detachment of posttranslational modifiers. PTMs take place during or after protein translation and can occur by addition of chemical groups or small proteins on specific amino acids of the protein. Dynamic PTMs include the reversible attachment of small protein modifiers, such as ubiquitin (Ub) and ubiquitin-like proteins (UBLs):

the neural precursor cell expressed developmentally down-regulated 8 (Nedd8), small ubiquitin-like modifier (SUMO) or autophagy-related 8 and 12 (Atg8 and Atg12).

UBL monomers and multi- and polymeric chains can be attached to the proteins, what confers various biological functions or fate to these acceptor protein substrates. For example, Ub monomers or multiple single Ub molecules can be attached on one or more acceptor sites of the substrate, resulting in mono- and multimonoubiquitination (reviewed in French *et al*., 2021). A Ub molecule has seven lysine residues (K6, K11, K27, K29, K33, K48, K63), which can bind another Ub molecule to build a polyubiquitin chain as result of repeated cycles of ubiquitin activating and conjugating (see in chapter 1.2.1). Ligation of a few to numerous Ub molecules results in multi- and polyubiquitination of the substrates. Various linear, unbranched polymeric Ub chains can be made, depending on whether the chain is formed by linkages between the same or different Ub residues, resulting in homotypic or mixed chains, respectively. There are branched Ub chains, where one Ub molecule forms two or more linkages with another. Ubiquitin can form mixed chains with other UBLs as well (reviewed in Cappadocia and Lima, 2018). These bear different biological purposes, similarly to different ubiquitin linkages (reviewed in Oh *et al.*, 2018 and in French *et al*., 2021). For example, monoubiquitination and K63 polyubiquitination of substrates can be a signal for the processes of endocytosis and transport as well as for DNA repair. K63 polyubiquitination can contribute to ribosome function and K48 and K11 polyubiquitin chains label protein substrates for destruction by the 26S proteasome in the ubiquitin-proteasome pathway (reviewed in Swatek and Komander, 2016). A well-regulated balance between polymeric and monomeric UBL modifications govern various cellular response mechanism (Bailly *et al.,* 2019; reviewed in Jackson and Durocher, 2013; and in Swatek and Komander, 2016). Thus, shortening of multi- or polymeric Ub chains, or detachment of these modifications from the substrates by deubiquitinating enzymes (DUBs) plays a key role in cellular homeostasis. Thereby, DUBs are also involved in the regulation of protein trafficking, DNA repair and oxidative stress (reviewed in Snyder and Silva, 2021).

1.2.1 Ubiquitin, Nedd8 and their activation, conjugation and ligation

Ubiquitin and Nedd8 are highly conserved in eukaryotes from fungi through plants to humans (Noventa-Jordão *et al*., 2000; von Zeska Kress *et al*., 2012; Sun *et al*., 1997; Rao-Naik *et al.*, 1998; Vijay-Kumar *et al.*, 1987; Whitby *et al.*, 1998). The Ub and Nedd8 amino acid sequences as well as their structures share great similarity. Both mature proteins consist of 76 amino acids with a C-terminal G75-G76 diglycine-motif and both have to be processed to expose these diglycine motifs prior to their attachment to a lysine residue of the substrate (reviewed in Neutzner and Neutzner, 2012; and in Enchev *et al.*, 2015) (Figure 2A and B). Ub is either translated together with a ribosomal protein or as a head-to-tail fusion of four Ub molecules and needs to be processed (monomerized) by DUBs. Nedd8 is translated as an 81 amino acid inactive precursor, which is processed to a 76 amino acid form by a ubiquitin C-terminal hydrolase (UCH) (Wada *et al.*, 1998). The subsequent activation, conjugation and ligation of the processed Ub and Nedd8 take place in analogous and conserved mechanisms by the interplay of specific E1, E2 and E3 enzymes (Figure 2C) (reviewed in Neutzner and Neutzner, 2012; in Mergner and Schwechheimer, 2014; in Cappadocia and Lima, 2018; Baek *et al.*, 2021). Ubiquitin or Nedd8 specific E1 enzymes activate Ub and Nedd8 in an energy-dependent reaction (Figure 2C).

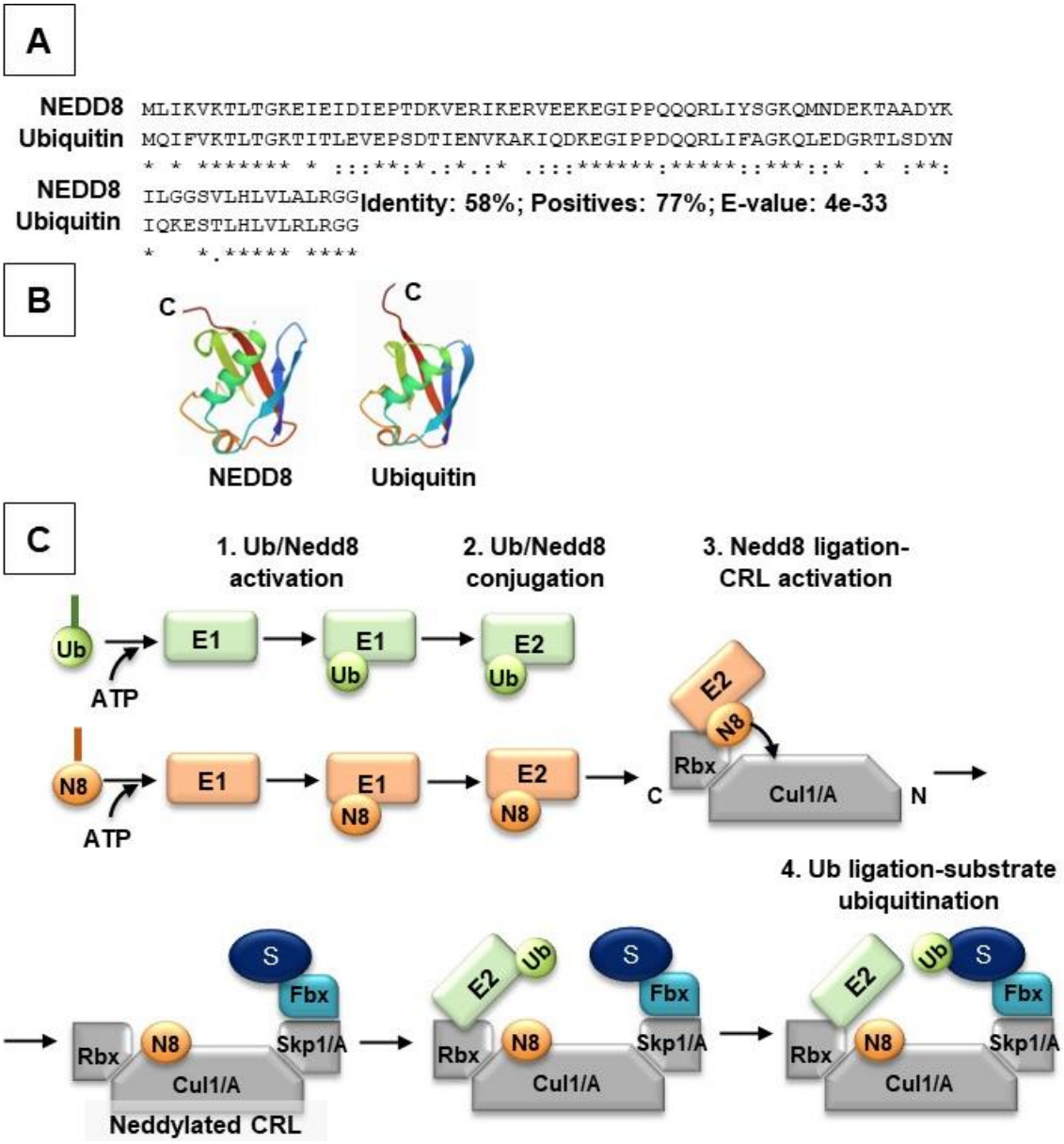

Figure 2. Ubiquitin and Nedd8 proteins and their substrate labeling cascades.
(**A**) Deduced amino acid sequence alignment of the human Ub and Nedd8 proteins reveals 58% identity and 77% similarity between the two sequences. `*´ conserved residues, `:´ strong similarity between the residues, `.´ weak similarity between the residues. (**B**) The structures of the activated human ubiquitin (PDB ID: 1UBQ and UniProt ID: P0CG48; Vijay-Kumar *et al*.,1987) and the activated human Nedd8 (PDB ID: 1NDD and UniProt ID: Q15843; Whitby *et al*., 1998) are shown, where C is the C-terminus. (**C**) Scheme of the E1-E2-E3 ubiquitin-like protein (UBL) Nedd8 (N8) and ubiquitin (Ub) activation-conjugation and substrate (S) labeling cascade. The SCF CRL complex is shown in C-terminal (C) to N-terminal (N) orientation.

The processed and activated ubiquitin and Nedd8 are transferred onto specific E2 UBL conjugating enzymes. Subsequently, the E2 enzymes are bound by E3 ligase complexes, which catalyze the ligation of UBLs to substrates. Such enzyme complexes are the HECT domain and the RING domain E3 ligases, which have distinct ubiquitinating mechanism (Metzger *et al.*, 2012). The largest group of RING-type E3 enzymes are the Skp1/A-Cul1/A-F-box cullin-RING E3 ligase (SCF CRL) complexes (reviewed in Deshaies and Joazeiro, 2009).

The SCF CRL complex carries a C-terminal Ub-loaded E2 enzyme through a RING-box (Rbx) protein and a protein substrate on the N-terminus (Figure 2C). Substrate receptors, like the F-box proteins, confer substrate binding and provide substrate specificity to the SCF complex. The F-box proteins are attached to the cullin1/A (Cul1/A) subunit of the CRL through an adaptor protein, such as Skp1/A (Zheng *et al.*, 2002). Substrate labeling by the SCF CRLs can only occur in an active state. The E2-bound CRL SCF activation requires neddylation of its Cul1 subunit. The cullin neddylation is the reversible attachment of a ubiquitin-like modifier Nedd8 on the Cul1 on the C-terminus by Nedd8-specific E2 enzymes, such as the Dcn1/A (Duda *et al.*, 2008; Kurz *et al*., 2005; von Zeska Kress *et al.*, 2012). Due to the CRL SCF neddylation, the conformation of the CRL SCF complex changes allowing the Ub-loaded E2 enzyme to stretch out to and ubiquitinate the substrate (Duda *et al.*, 2008).

1.2.2 Protein degradation by the ubiquitin-proteasome pathway contributes to maintenance of proteostasis

The destruction of no longer needed or dysfunctional proteins is a well-controlled process and it is essential for the maintenance of the proteostasis. Proteins can be degraded in the cytoplasm in protease-containing lysosomes or targeted by the 26S proteasome (reviewed in Ciechanover, 2005). Lysosomes are membrane-enclosed organelles containing proteolytic enzymes. Proteins are transported to the lysosomes in vesicles, which then fuse with the lysosome, where the break-down of proteins occurs. The ubiquitin-proteasome pathway (UPP) is a fine-tuned process. It involves an interplay of multi-subunit protein complexes for substrate recognition, labeling, recognition and degradation of labelled substrates (Figure 3) (reviewed in Ciechanover and Schwartz, 1998).

The UPP cycle starts with the E1-E2 ubiquitin activation-conjugation cascade followed by the substrate ubiquitination by an active, neddylated SCF CRL complex (Figure 2C and Figure 3, part 1). The ubiquitinated substrate is shuttled to the 26S proteasome by Ub-like domain containing proteins, such as the RAD23 (radiation sensitivity abnormal 23) (Figure 3, part 2) (Elsasser *et al.*, 2004). The 26S proteasome comprises of a 19S regulatory and a 20S core particle, where the regulatory particle is divided to two further clusters (more details in chapter 1.3.2 and Figure 6). The ubiquitinated substrate is recognized by the lid of the regulatory particle and the polyubiquitin chain is cleaved from the substrate by the proteasomal DUB enzyme Rpn11 and recycled for the cellular Ub pool. The substrate is passed through the base of the regulatory particle, where it is unfolded at cost of ATP and subsequently degraded within the 20S core particle (Figure 3, part 3). DUBs are proteases with a specificity for ubiquitin, ubiquitin chains and conjugates. They catalyze the cleavage or trimming of polyubiquitin chains (reviewed in Snyder and Silva, 2021). There are proteasome-specific DUBs, such as UCH37 and Usp14, which shorten polyubiquitin chains at the proteasome (reviewed in Lee *et al.*, 2011) and also other, not proteasome-specific DUBs, like the ubiquitin specific protease 15/A (Usp15/A) (Meister *et al.*, 2019).

The deactivation of the SFC CRL complex occurs by the deconjugation of Nedd8 from the Cul1 subunit in its substrate-free state (Mosadeghi *et al*, 2016). The COP9 signalosome (CSN complex) recognizes and binds the substrate-free SCF CRL complex. Csn5/E, the intrinsic Nedd8-specific isopeptidase of the CSN complex catalyzes the cleavage of Nedd8 from the Cul1, thereby inactivates the SCF CRL complex (Lingaraju *et al*, 2014) (Figure 3, part 4). Another deneddylase is the Deneddylase 1/A (Den1/A) protein, which has distinct protein

substrates (Coleman *et al*., 2017; Christmann *et al*., 2013; Schinke *et al.*, 2016). Interactions between the CSN complex and the second cellular deneddylase DenA (human DEN1 ortholog) were shown in *A. nidulans* (Christmann *et al*., 2013), where CSN subunits regulate the Den1/A stability during asexual differentiation of the fungus (Schinke *et al*., 2016).

The deneddylated SCF CRL complex is recognized by the substrate receptor-adaptor exchange factor, the Cand1/A complex (Pierce *et al.*, 2013; Köhler *et al.*, 2019). The Cand1/A complex binds to the deneddylated SCF CRL complex and through this, the substrate adaptor Skp1/A and the substrate receptor F-box protein dissociate from the SCF CRL (Figure 3, part 5). With the dissociation of the substrate adaptor and receptor, a new substrate labeling cycle can start. Cycles of SCF CRL neddylation-deneddylation result in its assembly-disassembly and thus, its activation and deactivation. This provides the dynamic exchange of protein substrates and thereby contributes to multicellular development and maintenance of the proteostasis.

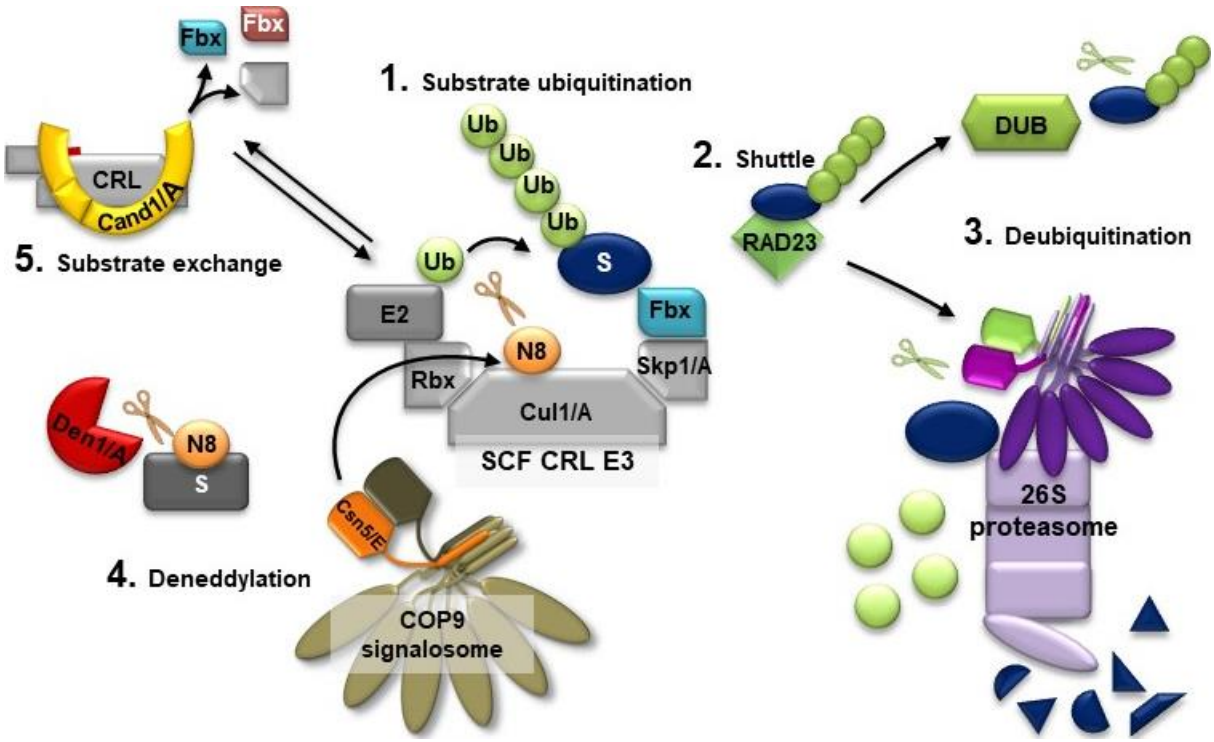

Figure 3. The substrate labeling and degradation machinery of the ubiquitin-proteasome pathway.
1. The cullin subunit of the E3 cullin ring ligase (CRL) is modified by Nedd8 (N8) on the C-terminus (C). This allows a conformational change, thus the E2-carrying ubiquitin reaches the substrate (S) bound on an F-box substrate receptor on the N-terminal end (N) of the cullin. **2.** The ubiquitinated substrate is shuttled to the 26S proteasome, for example by Ub-like domain protein RAD23. **3.** The ubiquitinated substrate is recognized, bound, unfolded by the lid particle of the 26S proteasome and the ubiquitin chain is removed from the substrate, allowing the recycling of both. Other deubiquitinating enzymes (DUBs) are able to trim the polyubiquitin chain. **4.** The COP9 signalosome recognizes the substrate-unbound and yet neddylated CRL and removes the Nedd8 modification. The Deneddylase 1/A (Den1/A) protein is able to cleave Nedd8 from various substrates. **5.** After the cullin deneddylation and dissociation of the substrate, a receptor-adaptor exchange factor, the Cand1/A complex binds to the cullin. Cand1/A binding allows the exchange of the substrate receptors, and thus, a new substrate can be attached and the cycle starts new.

1.3 ZOMES are regulators of protein synthesis and turnover

The `ZOMES´ appellation refers to three evolutionary conserved orthologous complexes: the eukaryotic translational elongation initiation factor 3 (eIF3), the COP9 signalosome and the 26S proteasomal lid, which contribute to the maintenance of the cellular proteostasis. The ZOMES share similar architecture (Figure 4), suggesting that they derive from the same ancestor, albeit, they are involved in distinct cellular functions (Lingaraju *et al.*, 2014; Lander *et al.*, 2012; Enchev *et al*., 2010; Scheel and Hofmann, 2005).

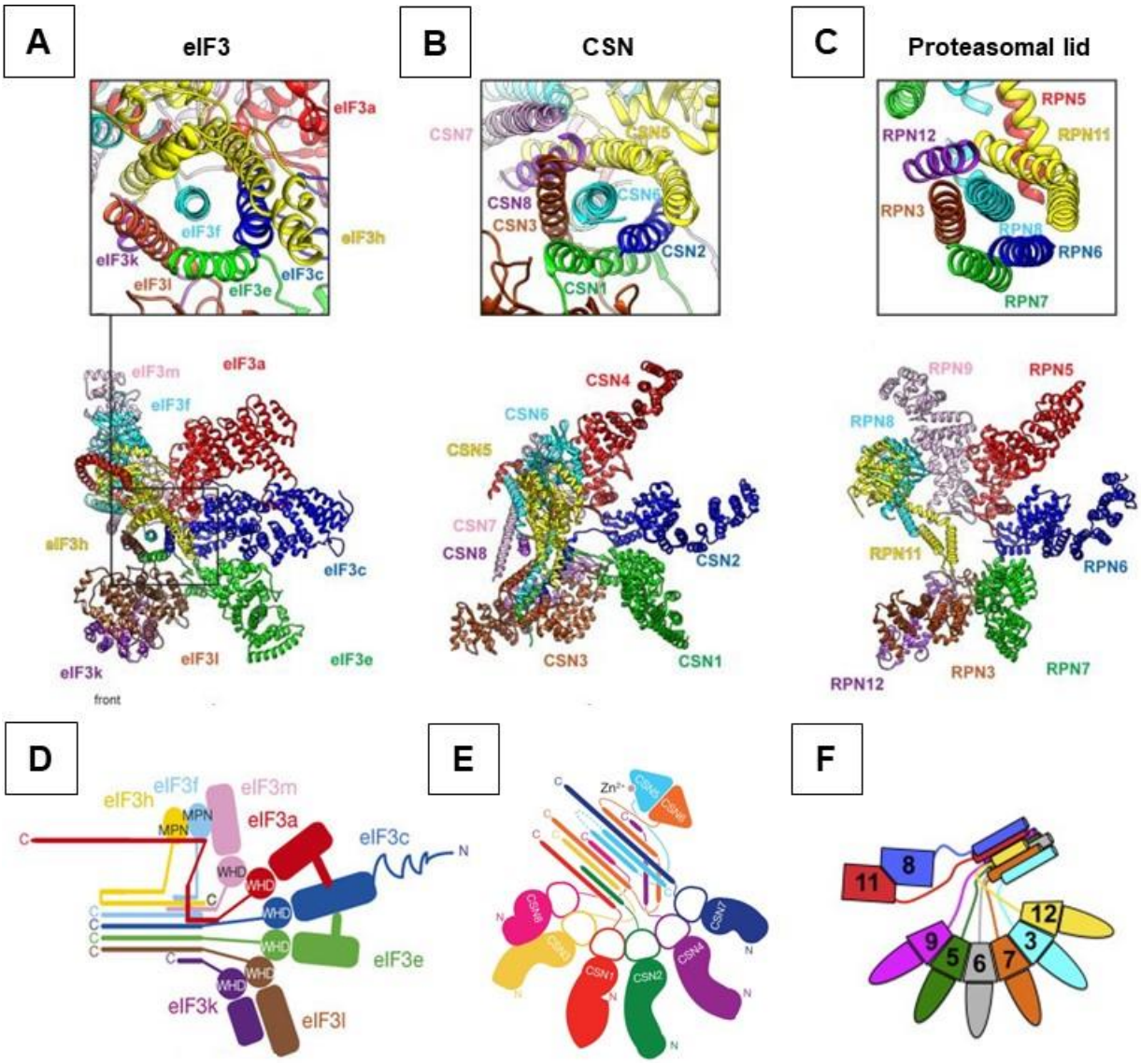

Figure 4. Topological similarities between the ZOMES complexes.
Architecture of the (**A**) mammalian eIF3 octameric core, (**B**) human COP9 signalosome and (**C**) the yeast 26S proteasomal lid particle. The close-ups above the complexes show the helical bundles of the eIF3, CSN and the proteasomal lid, respectively. The parts (**A**)-(**C**) are adapted from des Georges *et al.*, 2015. (**D**) Organization of the octameric core of the mammalian eIF3 (des Georges *et al.*, 2015). (**E**) Organization of the human COP9 signalosome subunits (Lingaraju *et al*, 2014). (**F**) Organization of the yeast proteasomal lid (Estrin *et al.*, 2013).

The eIF3 is a regulator of translation of proteins, whereas the CSN complex and the proteasomal lid are involved in protein catabolic processes. Their accurate function and amount are essential for multicellular development. Misregulation of these complexes is described for human cancer types (reviewed in Silvera *et al*., 2010; Mani and Gelmann, 2005; Richardson and Zundel, 2005; Lee *et al.*, 2011). These relevant complexes compose of eight canonical subunits and each have their equivalent representative in the two corresponding complexes (Table 1).

Table 1. Composition and equivalent subunits of the ZOMES.
The COP9 signalosome subunits have equivalent 26S proteasomal lid particle and eIF3 complex subunits. Six PCI domain subunits and two MPN domain subunits form the ZOMES. The COP9 signalosome and the proteasomal lid bear Csn5/A and Rpn11 catalytic MPN+ domain containing subunits, whose equivalent is missing from the eIF3. The Csn5/A and Rpn11-like eIF3h bears an MPN domain without catalytic activity. Sem1 and CSNAP are proposed as the ninth subunits of the proteasomal lid and the COP9 signalosome, respectively (Kragelund *et al.*, 2016; Rozen *et al.*, 2015). A Sem1- or CSNAP-like protein was so far not identified for the eIF3 complex. The data is based on the work of Scheel and Hofmann, 2005 and the eIF3 subunits are collected from des Georges *et al.,* 2015 based on the homology in structural alignment of the octameric eIF3 core to the human CSN (Lingaraju *et al.*, 2014) and the yeast 26S proteasomal lid (Lander *et al.*, 2012). HsCSN: *Homo sapiens* COP9 signalosome, AnCSN: *Aspergillus nidulans* COP9 signalosome.

Domain	HsCSN /AnCSN	Proteasomal lid	eIF3
PCI	CSN1 /CsnA	Rpn7	eIF3e
PCI	CSN2 /CsnB	Rpn6	eIF3c
PCI	CSN3 /CsnC	Rpn3	eIF3l
PCI	CSN4 /CsnD	Rpn5	eIF3a
MPN+	CSN5 /CsnE	Rpn11	eIF3h (MPN)
MPN	CSN6 /CsnF	Rpn8	eIF3f
PCI	CSN7A,B /CsnG	Rpn9	eIF3m
PCI	CSN8 /CsnH	Rpn12	eIF3k
disordered protein	CSNAP	Rpn15/Sem1/Dss1	?

Six subunits contain a PCI domain, which stands for proteasome, COP9 signalosome and eukaryotic translational elongation initiation factor 3. The PCI domain is usually located on the C-terminus of the protein and comprises of two subdomains, a helical bundle/subdomain (HB/HD) closer to the N-terminus and a winged-helix (WH) subdomain closer to the C-terminus (Ellisdon and Stewart, 2012). Structural properties of the HB and WH subdomains provide the PCI domains with the ability to mediate and stabilize protein-protein interactions and thus, enable the assembly of multisubunit complexes (des Georges *et al*., 2015; Dambacher *et al.,* 2016; Lingaraju *et al*., 2014). The amino acid sequences of PCI domains do not suggest a catalytic activity, but other cellular functions are linked to this domain (Pick *et al*, 2009). For example, the PCI domain of the seventh COP9 signalosome subunit (Csn7) in *Drosophila melanogaster* binds to DNA directly and through this supposedly regulates the expression of specific genes with developmental relevance (Singer *et al.*, 2014). The ZOMES, in addition to the six PCI subunits, contain two subunits carrying a conserved

MPR1-PAD1 N-terminal (MPN) domain. The MPN domain superfamily has two main subclasses: the MPN and the MPN+ domain subclass (Maytal-Kivity *et al*, 2002). No catalytic activity is assigned to the MPN domain. On the contrary, the MPN+ domain possesses a Jab1/MPN/Mov34, short JAMM metalloenzyme motif, coordinating a Zn^{2+} ion (Ambroggio *et al.*, 2003) and thus, providing metalloprotease catalytic activity. JAMM motif containing MPN+ domain proteins, RPN11 and Csn5/E are found in both the 26S proteasomal lid and the CSN complex, respectively, whereas the eukaryotic translational elongation initiation factor 3 has two MPN subunits without catalytic activity (Table 1). Besides their catalytic activity, a role in CSN complex stabilizing was shown for the MPN domains of Csn5 and Csn6 in plants (Gusmaroli *et al*, 2007). The metalloprotease activity of the proteasomal lid and the CSN complex is conferred by a conserved glutamate and the downstream JAMM motif comprising of defined `H-x-H-x(7)-S-x(2)-D´ pattern, where `x´ are non-conserved residues (Maytal-Kivity *et al*., 2002; Wei and Deng, 2003). The mechanism of catalysis is very similar in both complexes and their JAMM motifs highly conserved, differing in only two amino acids (reviewed in Meister *et al.*, 2016). This difference shifts the specificity towards Nedd8 for the intrinsic deneddylase Csn5/E of the CSN complex and towards ubiquitin cleavage for the deubiquitinase Rpn11 of the lid. The ubiquitin and Nedd8-specific metalloprotease activities of the lid and the CSN complex are exerted exclusively by the eight-subunit holocomplexes (Yao and Cohen, 2002; Lingaraju *et al.*, 2014; Beckmann *et al.*, 2015). The catalytic center of Csn5/E and Rpn11 contain two insertion loops Ins-1 and Ins-2 (Echalier *et al.,* 2013; Worden *et al.*, 2014; Lingaraju *et al.*, 2014; Pathare *et al*., 2014). The Ins-1 is oriented towards the active site in Csn5 and in Rpn11, blocking the access to Nedd8 and Ub, respectively, thereby fulfilling an autoinhibitory function. Due to the autoinhibition, the complex-unbound freestanding Csn5/E and Rpn11 are unable to perform their isopeptidase activities, unless they are activated by conformational changes when integrated to the holocomplex (Lingaraju *et al.*, 2014; Beckmann *et al.*, 2015; Pathare *et al.*, 2014).

1.3.1 Structural organization and assembly of the eukaryotic translational elongation initiation factor 3

The eukaryotic translation initiation starts with the formation of the 43S preinitiation complex, which is the association to the ternary complex consisting of eIF3, eIF1, eIF1A to the 40S ribosomal subunit (reviewed in Jackson *et al.,* 2010). The 43S complex binds to the activated mRNA and scans it until the AUG start codon is reached. Then, the 48S initiation complex is formed. Finally, eIF5 and eIF5B promote joining of the 60S ribosomal subunit to the 48S initiation complex, and thereby an elongation-competent 80S ribosome is assembled (reviewed in Jackson *et al.,* 2010). The eukaryotic translational elongation initiation factor 3 is involved in the first steps of the eukaryotic translation as part of the initiation complex (reviewed in Hershey *et al.*, 2012; Hinnebusch, 2006), but the eIF3 complex might function independently of translation, because some eIF3 subunits interact also with the 26S proteasome (Sha *et al.*, 2010).

eIF3 is a ~800 kDa large complex comprising 13 subunits named eIF3a to eIF3m. The eIF3 consists of five peripheral subunits and a PCI/MPN octameric core, belonging to the ZOMES (Sun *et al.,* 2011; des Georges *et al*., 2015). The octameric core is formed of five PCI domain proteins (eIF3a, eIF3c, eIF3e, eIF3k, eIF3l) and two MPN domain proteins the eIF3f and eIF3h subunits (Table 1 and Figure 4). Homology search revealed that eIF3h is the

equivalent subunit of Csn5/E and Rpn11, although the MPN domain of eIF3h has no catalytic center (des Georges *et al*., 2015). The structural organization of the rabbit eIF3 complex reveals strong trimeric interactions between the eIF3e-eIF3l-eIF3k subunits and a quaternary interaction between the C-termini of the eIF3a-eIF3f-eIF3h-eIF3m subunits (Figure 5) (des Georges *et al.,* 2015). Binary interactions between the eIF3e-eIF3c and eIF3a-eIF3c subunits were found in mammalian systems (Sun *et al.*, 2011; des Georges *et al.,* 2015). The peripheral subunits are the eIF3b, eIF3i, eIF3g, eIF3d and eIF3j, where eIF3b-eIF3-g-eIF3i form a heterotrimer connected to the MPN/PCI core through eIF3a and is located at the mRNA entrance, whereas eIF3d is near to the mRNA exit. The eIF3b, eIF3i, eIF3g, eIF3d are stably linked to the octameric core module, whereas eIF3j is loosely attached to the complex (des Georges *et al.*, 2015).

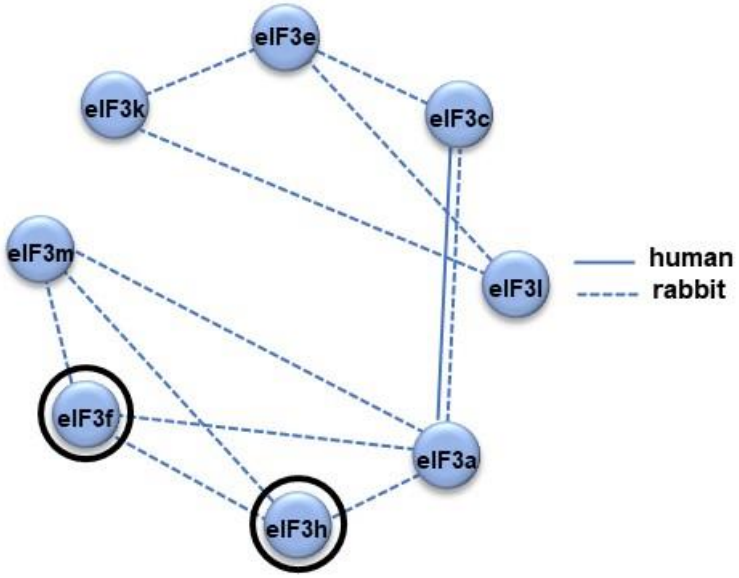

Figure 5. Interconnection of subunits of the eukaryotic translational elongation initiation factor 3.
The subunit cohesion within the eIF3 was determined *in vitro* with recombinantly expressed human eIF3 subunits and in reconstruction studies based on cryo-electron microscopy of the rabbit eIF3 (Sun *et al*., 2011; des Georges *et al.*, 2015). The rabbit eIF3 complex structure reveals strong trimeric interactions between the eIF3e-eIF3l-eIF3k and a quaternary interaction between the C-termini of the eIF3a-eIF3f-eIF3h-eIF3m subunits and the mammalian subassemblies include a strong dimeric interaction between eIF3c and eIF3a (Sun *et al*., 2011; des Georges *et al.*, 2015). The MPN domain-containing subunits are highlighted with black circles.

1.3.2 Structure, function and assembly of the 26S proteasome

Recent reviews summarize more than three decades of research on the 26S proteasomal structure and function (reviewed in Mao, 2021; and in Livneh *et al*., 2016). The proteasome is an approximately 2.5 MDa protein complex, which consists of a 20S core particle (CP) and a 19S regulatory particle (RP) (Figure 6). The 20S CP comprises four heptameric rings, two outer α- and two inner β-rings, forming a pore in which the protein substrate is destructed. Both rings build up from seven subunits, the α1 to α7 and β1 to β7, respectively. Among those, the β1, β2 and β5 subunits bare proteolytic properties. The 20S

CP is capped on either one or both ends by the 19S RP. The 19S acts in substrate recognition, binding, unfolding and shifting the substrate to the pore of the 20S core particle (Tomko *et al.*, 2010). The 19S cap can be further divided into the lid and the base particles. The base builds up from six AAA-type ATPases (Rpt1 to Rpt6) forming a ring and four regulatory particle non-ATPase subunits (Rpn1, Rpn2, Rpn10 and Rpn13).

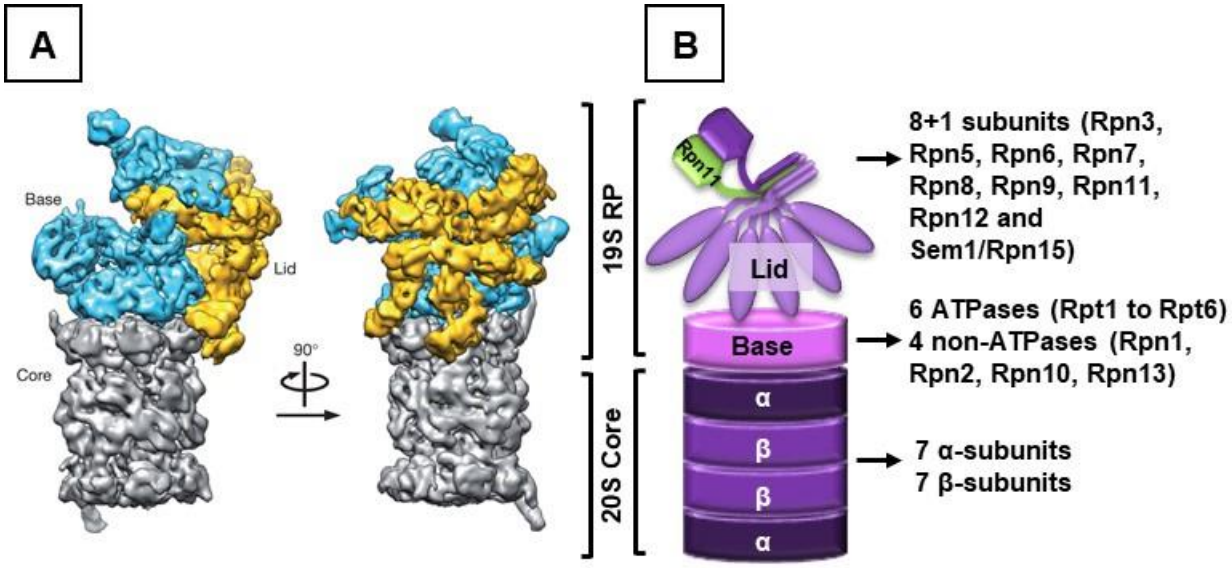

Figure 6. Negative-stain three-dimensional structure of the yeast 26S proteasome complex. (**A**) The structure is reconstructed after cryo-electron microscopy at approximately 15A° resolution (Lander *et al.*, 2012). The core particle is shown in grey, the base particle in cyan and the lid in gold. (**B**) Scheme shows the simplified topology of the 26S proteasome.

Rpn1, Rpn10 and Rpn13 function as ubiquitin receptors in substrate recognition. Rpn2 is a large scaffolding subunit, which binds Rpn13 and stretches towards Rpt1-Rpt2 and Rpt3-Rpt6. Nine subunits, the Rpn3, Rpn5-Rpn9, Rpn11, Rpn12 and Sem1 (alias Rpn15 or Dss1) form the lid particle (Table 1 and Figure 6). Six lid subunits contain a PCI domain and two subunits are MPN domains proteins. Sem1, the ninth subunit, is a disordered protein with connecting and stabilizing functions (reviewed in Kragelund *et al.*, 2016; Kolog Gulko *et al.*, 2018). The deubiquitination of the protein substrates occurs in the lid particle of the 19S RP by its intrinsic isopeptidase Rpn11. Lid-associated DUBs, like Usp14 and UCH37, also contribute to this process (reviewed in Lee *et al.*, 2011).

The 26S proteasome assembly follows a complex choreography with numerous steps, which involve self-assembly steps and partially rely on the assistance of various proteasome-specific chaperons, such as the assembly of the 20S core (Kunjappu and Hochstrasser, 2014). The formation of the 19S RP is not yet fully understood, but its two clusters, the base and the lid, are formed independently of each other. The assembly 19S RP base involves an Rpn2 and Rpn13 dimer, which is located in the close proximity of the Rpn11 isopeptidase subunit of the lid (Lander *et al.*, 2012). Although the assemblies of the base and the lid are independent processes, numerous inter-subcomplex linkages are described (Greene *et al.*, 2019; Glickman *et al.*, 1998), such as lid-base-core subunit interactions, which were identified using cross-linking methods in yeast (Lasker *et al.*, 2012). The assembly of the nine-subunit 19S lid in

yeast includes two main modules, the Rpn5-Rpn6-Rpn8-Rpn9 with Rpn8 in its center and an Rpn3-Rpn7-Sem1/Rpn15 module (Figure 7) (Sharon *et al.*, 2006).

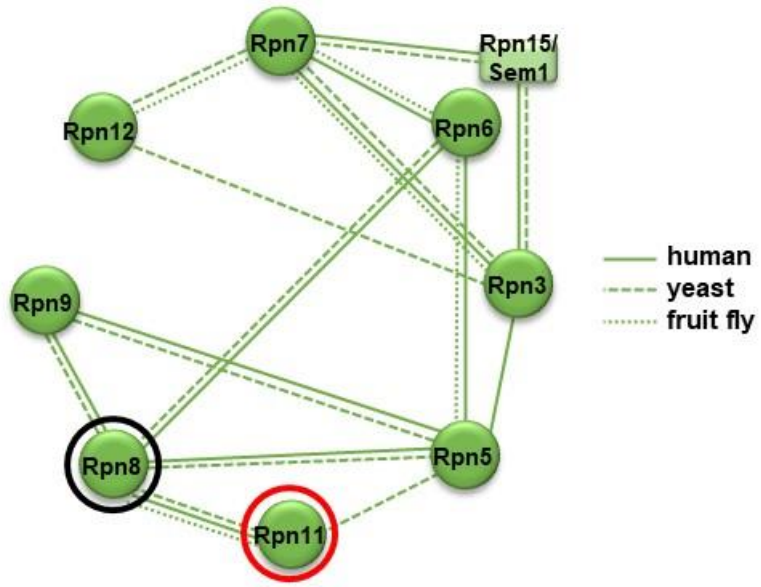

Figure 7. Interconnection of subunits of the 26S proteasomal lid.
Yeast-based reconstruction studies using deletion strains and biochemical methods revealed two main modules within the proteasomal lid (shown with dashed lines): interactions between Rpn5-Rpn6-Rpn8-Rpn9-Rpn11 and Rpn3-Rpn7-Sem1, where Rpn12 associates (Isono *et al.*, 2005; Sharon *et al.,* 2006; Fukunaga *et al*., 2010). Subunit cohesion within the proteasomal lid are indicated with continuos lines for human subunits (Bai *et al.*, 2019). The interactions within the lid are determined based on crystallography data of the fruit fly *Drosophila melanogaster* subunits and are indicated with dotted lines (Pathare *et al.*, 2012). The MPN domain-containing subunit is highlighted with a black circle and the MPN+ domain subunit is marked with a red circle.

It is suggested that the assembly of these modules is independent of Rpn11, though Rpn11 is required for the lid-base stabilization. Rpn11 joins the Rpn5-Rpn6-Rpn8-Rpn9 module, which is connected to the Rpn3-Rpn7-Sem1 module by Rpn6 through its interaction with Rpn7. Other yeast-based assembly assays with lid mutants also confirm an initiative core unit of Rpn5-Rpn6-Rpn8-Rpn9-Rpn11, which is attached to the Rpn3-Rpn7-Sem1 unit and completed by the incorporation of Rpn12 at last (Isono *et al.*, 2005; Fukunaga *et al*., 2010; Tomko and Hochstrasser, 2011). The lid modularity was further supported by data with the lid assembly in fruit flies and in humans (Pathare *et al.,* 2012; Bai *et al*., 2019). In *D. melanogaster*, the Rpn5-Rpn6-Rpn8-Rpn9-Rpn11 formation involved a Rpn5-Rpn6 and a Rpn8-Rpn11 interaction and the Rpn3-Rpn7 dimer, which provided surface for Rpn12 to bind and complete the assembly (Pathare *et al.,* 2012). In human cells the Rpn6 subunit conferred cohesion between the Rpn3-Rpn7-Sem1 and Rpn5-Rpn8-Rpn9-Rpn11 modules and is required for the stability of Rpn11 (Bai *et al.*, 2019).

1.3.3 The COP9 signalosome

The COP9 signalosome was discovered in plants as a regulator of light-sensing signaling, where *Arabidopsis thaliana* COP9 signalosome mutants showed constitutive

photomorphogenesis (COP) in the absence of light (Wei and Deng, 1992). Since then, three decades of research using diverse eukaryotic organisms, revealed information about the function, subcellular location, structure and interactome of the COP9 signalosome, but still numerous questions remain open.

1.3.3.1 Subunit organization within the CSN complex

The COP9 signalosome is an approximately 450 kDa holocomplex, consisting of eight conserved subunits (Table 2). The CSN subunits are named according to their descending molecular weight from Csn1/A to Csn8/H, where Csn1/A is the largest subunit (reviewed in Wei and Deng, 2003). The subunit composition of the CSN complex is conserved in eukaryotes from fungi through plants to humans (Table 2; Wei *et al*., 1998; Busch *et al*., 2007; Barth *et al*., 2016) whereby *Schizosaccharomyces pombe* and *Saccharomyces cerevisiae* have diverged CSN complexes (Harshuk-Shabso *et al.*, 2021; Mundt *et al*., 1999). Not only sequence and tertiary structure, but also the functional conservation of the CSN complex was demonstrated. The human Csn1, expressed in an *A. thaliana* Csn1 null mutant, can functionally incorporate into the plant CSN complex and fulfil its function (Kang *et al.*, 2000).

Table 2. The CSN subunits are highly conserved in eukaryotes.
The CSN subunits are highly conserved among eukaryotic reference organisms, where the second Csn2/CsnB and fifth, catalytic Csn5/CsnE subunits are the most conserved ones. *A. nidulans* CSN subunit amino acid (aa) sequences were used as query sequences (updated from Busch *et al.*, 2007). The domain positions are given for the *A. nidulans* CSN complex subunits, based on UniProt. Asterisks mark subunits with isoforms: hsCSN7B (27.8%), atCSN5B (53.2%), atCSN6B (31.1%). Glossary: *Aspergillus nidulans* (An), *Homo sapiens* (Hs), *Arabidopsis thaliana* (At), *Schizosaccharomyces pombe* (Sp) and *Saccharomyces cerevisiae* (Sc).

CSN subunit Hs/An	An UniProt ID	Length (aa)	Domain	Protein size (kDa)	aa identity (%) to			
					Hs	At	Sp	Sc
CSN1/CsnA	Q5BD89	498	PCI (249–430)	55.7	33.3	38.6	27.0	21.03
CSN2/CsnB	Q5B3U7	506	PCI (252–420)	58.1	51.1	48.1	46.1	23.58
CSN3/CsnC	Q5B0Y2	496	PCI (243–411)	55.2	26.0	23.4	20.1	-
CSN4/CsnD	Q9C467	408	PCI (194–374)	44.9	38.5	41.2	19.4	21.41
CSN5/CsnE	Q5BBF1	335	MPN+ (51–187) JAMM (134–147)	37.8	55.2	54.4*	38.8	30.0
CSN6/CsnF	Q5BB47	386	MPN (20–164)	42.1	31.1	29.9*	-	19.51
CSN7/CsnG	Q00648	327	PCI (4-165)	35.3	28.8*	29.5	27.0	26.88
CSN8/CsnH	P0C624	212	PCI (26-193)	23.9	22.4	18.9	-	-

Apart from the eight subunit COP9 signalosome holocomplex, **CSN subassemblies or CSN mini complexes** were reported in *in vitro* studies (Kotiguda *et al.*, 2012; reviewed in Dubiel *et al*., 2015). Reconstruction analyses of recombinantly expressed human CSN subunits coupled with LC-MS/MS measurements revealed modules within the complex *in vitro* (Sharon *et al.*, 2009). Such modules are the Csn4-Csn5-Csn6-Csn7 and the Csn1-Csn3-Csn8-Csn2 module (Figure 8) (Sharon *et al.*, 2009), which could also be partially verified in plants (Kotiguda *et al.*, 2012).

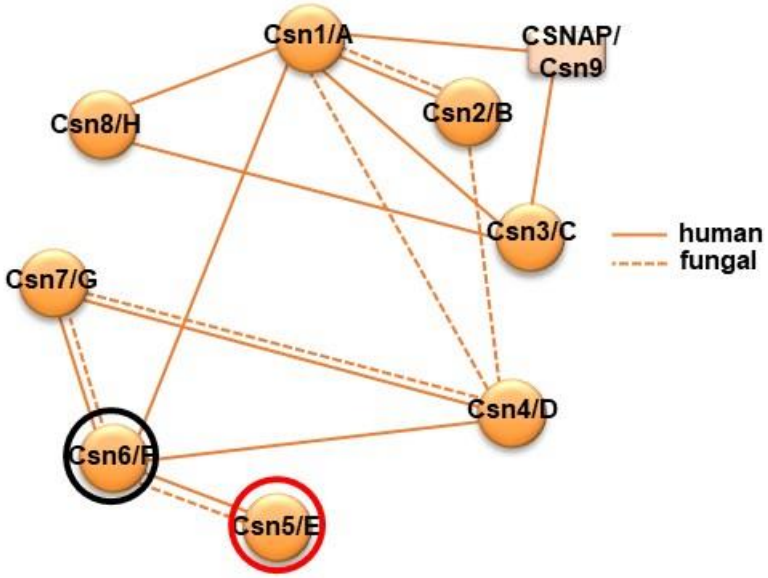

Figure 8. Interconnection of subunits within the COP9 signalosome.
Subunit cohesion within the human COP9 signalosome is indicated with continuous lines (Sharon *et al.*, 2009; Lingaraju *et al.*, 2014; Gutierrez *et al.*, 2020). Clusters of Csn4-Csn5-Csn6-Csn7 and Csn1-Csn3-Csn8-Csn2 were shown, which join through the interaction between Csn1 and Csn6. Binary interactions within the CSN complex observed in *A. nidulans* are indicated with dotted lines (Busch *et al.*, 2007). The MPN domain-containing subunit is highlighted with a black circle and the MPN+ domain subunit is marked with a red circle.

CSN acidic protein (CSNAP alias Csn9), a ninth, auxiliary subunit was discovered in experiments with human CSN complex. CSNAP/Csn9 is similar to Rpn15/Dss1/Sem1 and formed cross-links with Csn5, Csn6 and Csn3 (Rozen *et al.*, 2015) and associates to the Csn1-Csn3 subunit pair (Gutierrez *et al.*, 2020). CSNAP has multiple cellular functions, such as the attenuation of the CSN-SCF CRL complex binding and it is involved in proper cell cycle progression and viability (Füzesi-Levi *et al.*, 2020). Studies on the human and fungal CSN subunit organization reveal two main clusters. These clusters are linked by an association between Csn1/A and Csn6/F in humans, whereas interaction analysis of fungal subunits revealed a connection between Csn1/A and Csn4/D to link these clusters (Figure 8). Yeast-two-hybrid experiments with *A. nidulans* CSN subunits show binary interactions between the Csn1/A-Csn2/B, Csn1/A-Csn4/D, Csn2/B-Csn4/D, Csn4/D-Csn6/G, Csn5/E-Csn6/F, Csn6/F-Csn7/G subunit pairs and cohesion between the PCI domains of the Csn1/A-Csn2/B-Csn4/D-Csn6/G subunits (Figure 8) (Busch *et al.*, 2007). The deletion of the *csn1/A* and *csn4/D* genes abolished the further interactions of TAP-tagged Csn5/E with other subunits in tandem affinity purification (TAP) experiments (Busch *et al*., 2007). Similarly, GFP-affinity purification results show that the deletion of *csnG* diminished the interactions of CsnD-GFP with other CSN subunits (Beckmann *et al*., 2015). These results suggest subcomplexes within the fungal COP9 signalosome. *In vitro* reconstruction studies and GFP-affinity purifications with the CsnD-GFP subunit fusion as bait revealed a stable, seven-subunit pre-assembled COP9 signalosome, short pre-CSN complex, in absence of the deneddylase subunit (Beckmann *et al*., 2015). This present work aimed to provide experimental proof for the existence of subcomplexes as intermediates of the multiprotein CSN complex and to reveal the assembly choreography of the fungal pre-CSN complex.

Formation of two main clusters seems evident in the assembly of the ZOMES, which provides symmetry within these complexes (Figure 5, Figure 7 and Figure 8). Besides the parallels, there are also discrepancies in the subunit organization within these multisubunit complexes (Meister *et al.*, 2016), which might be a result of the adaptation of different functions.

1.3.3.2 Subcellular localization of the COP9 signalosome

Subcellular localization of the COP9 signalosome or its subunits was studied in various organisms during various conditions. In human cell lines, the CSN complex visualized through fluorescent CSN2/B, CSN3/C, CSN5/E, CSN6/F and CSN7/G subunits, was found in cytoplasm and nucleus as well, but this equilibrium was shifted to nuclear localization upon stress (Fuzesi-Levi *et al.*, 2014). The eight subunit CSN holocomplex localized to the nucleus in cauliflower seedlings and this nuclear enrichment required the presence of COP8/Csn4 and COP11/Csn1 (Chamovitz *et al.*, 1996). The CSN complex, visualized by Csn1-GFP, Csn5-GFP, was observed in the nucleus in *A. thaliana* as well (Wang *et al.*, 2009). Studies on the subcellular localization of the fission yeast *S. pombe* CSN complex found the tagged Csn1/A, Csn2/B, Csn4/D and Csn5/E subunits also predominantly in the nucleus, but upon deletion of any of these subunits, this nuclear localization of the CSN complex could not be detected (Mundt *et al.*, 2002). Similarly, the CSN holocomplex was also mainly nuclear when visualized by the Csn4/D-GFP fusion in the multicellular fungus *A. nidulans* (Busch *et al.*, 2003). The CSN holocomplex is mainly described as nuclear, but loss of its subunits diminish the nuclear enrichment, what indicates that at least some degree of CSN complex pre-assembly is required for its nuclear translocation (Chamovitz *et al.*, 1996). So far, no mechanistic evidence was provided for the subcellular localization of the CSN subunits and subcomplexes in relation with CSN complex assembly happenings. This, and the abovementioned observations motivated this work, which also addresses the interplay between CSN subunits and subcomplexes for their location in *A. nidulans*.

1.3.3.3 Overview of the CSN complex functions

The CSN deneddylase complex, albeit indirectly, regulates a wide spectrum of cellular processes by arresting the proteasomal destruction of specific protein substrates. An increasing number of experimental data suggests that the COP9 signalosome is more than a deneddylase (reviewed in Wei *et al.*, 2008 and in Stratmann and Gusmaroli, 2012). The COP9 signalosome interaction partners are involved in direct regulation of biological mechanisms described in more detail in the following chapters.

1.3.3.3.1 Nedd8-specific isopeptidase activity

The only endogenous enzyme activity of the eight-subunit CSN holocomplex is the Nedd8-specific isopeptidase function exerted on SCF CRLs, whereby the SCF CRL assembly-disassembly dynamic is provided (Duda *et al.*, 2008; Mosadeghi *et al.*, 2016). Due to the Csn5 isopeptidase autoinhibition, the SCF CRL neddylation can only be carried out by the CSN holocomplex. The isopeptidase function is not a prerequisite for the CSN complex formation in humans, because Csn5 carrying a mutated version of the catalytic center did not abolish

complex formation (Groisman *et al.*, 2003). The eight-subunit CSN binds to the substrate-free SCF CRL. The CSN-SCF CRL interaction is mediated by the N-terminal domains of Csn2 and Csn4, which go through conformational changes (Figure 9).

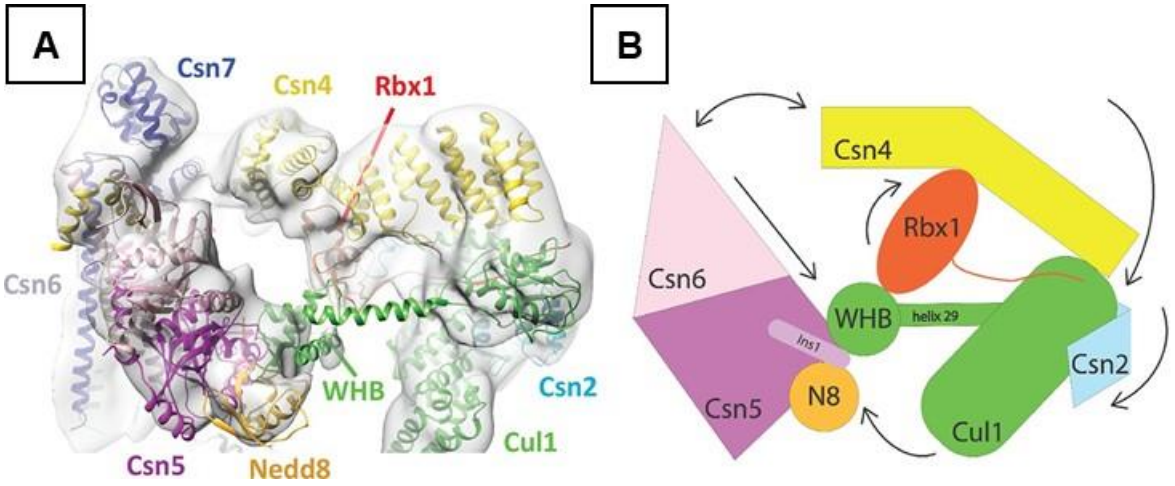

Figure 9. Tertiary structure and model of the conformational changes of the CSN and SCF CRL complexes.
The position of the COP9 signalosome subunits binding the SCF CRL complex, based on cryo-electron microscopy (adapted from Mosadeghi *et al.,* 2016). (**A**) Csn2 binds to cullin 1 (Cul1), and Csn4 interacts with Rbx1, which is the interface of the E2 enzyme, and stretches towards Cul1. These interactions promote a conformational change of the Csn5-Csn6 dimer and thus, the Csn5 catalytic center is activated for Nedd8 (N8) cleavage. (**B**) The simplified schematic model represents the above described motions between the CSN and the SCF CRL complexes (adapted from Mosadeghi *et al.,* 2016).

Thus, Csn2 binds to cullin 1 (Cul1) and Csn4 associates with both, Cul1 and Rbx1 (Lingaraju *et al.*, 2014; Mosadeghi *et al.*, 2016). The elimination of the N-terminal end of Csn2 resulted in drastic reduction of substrate binding capacity. The binding of Csn4 triggers a conformational rearrangement of the Csn5-Csn6 dimer, which moves towards Nedd8 (Mosadeghi *et al.*, 2016). These conformational changes dislocate the Ins-1 from the catalytic site, allowing the Zn^{2+} ion to activate the water molecule for nucleophilic attack on the isopeptide link between Nedd8 and Cul1 (Lingaraju *et al.*, 2014).

1.3.3.3.2 Deubiquitination

The CSN complex was suggested to be a component of the 26S proteasome, because they were co-purified from human erythrocytes (Seeger *et al.*, 1998) and also from plant cells (Kwok *et al.*, 1999; Peng *et al.*, 2003). The striking topological similarities that CSN shares with the deubiquitinase 26S proteasomal lid (Figure 4) (reviewed in Scheel and Hofmann, 2005), and the structural similarities between Ub and Nedd8 (Figure 2A and Figure 2B) lead to the hypothesizes that CSN might act as an additional or alternative proteasomal lid (reviewed in Li, 2003). Purified CSN5 of the CSN complex deriving from human cells possessed ubiquitinase activity towards an artificially polyubiquitinated cullin 4A substrate (Groisman *et al.*, 2003). Physical interactions between the CSN complex and ubiquitin specific proteases were described to contribute to the deubiquitinase activity of these enzymes in yeast, filamentous fungi and human (reviewed in Dubiel *et al.*, 2020). The human Usp15 and

its homologs in *A. nidulans* and in fission yeast (UspA and Ubp12p, respectively) physically interact with CSN subunits (Zhou *et al.*, 2003; Hetfeld *et al*., 2005; Meister *et al.*, 2019). Yeast-two-hybrid experiments revealed the binding UspA to Csn1/A, Csn2/B, Csn4/D, Csn5/E, Csn6/F and Csn8/H in *A. nidulans* (Meister *et al.*, 2019). Moreover, *in vivo* bimolecular fluorescence complementation assay demonstrated physical interactions between UspA and CsnB in the nucleus and between UspA and CsnF in the cytoplasm. It is proposed that the COP9 signalosome is involved in the stabilization or destabilization of transcriptional activators and repressors, which modulate the gene expression of ubiquitin specific proteases during the differentiation of *A. nidulans* (Meister *et al.*, 2019).

1.3.3.3.3 Phosphorylation

The CSN complex is involved in phosphorylation of protein substrates though CSN-interacting kinases, such as the **inositol 1,3,4-triposphate 5/6 kinase**, **protein kinase D, CK2 kinase** and **IκB kinases.** Protein kinase D recruits Csn3 whereby it phosphorylates Csn7. CK2 kinase binds to Csn7 whereby it phosphorylates Csn2 (Uhle *et al.*, 2003). Csn3 is specifically interacting with IκB kinases (IKKs) (Hong *et al.*, 2001). IκB, the inhibitor of nuclear factor kappa B (NFκB) associates with NFκB under normal conditions. NFκB is required for immune response in humans. Upon stress, IκBs are phosphorylated by IKKs resulting in their degradation and thus, NFκB is activated. As a result of the interactions with CSN-associated kinases, CSN subunits are also phosphorylated; phosphorylations were discovered on the human Csn2 and Csn7 subunits (Kapelari *et al.*, 2000).

1.3.3.3.4 Transcriptional regulation

The CSN complex was revealed as a nuclear enriched regulator of light sensing in plants (Wei and Deng, 1992; Wei *et al*., 1994; Chamovitz *et al.*, 1996). Since then, increasing experimental evidence demonstrates that the CSN complex is involved in regulation of gene expression, because it interacts with multiple transcription factors as well as with regulators of the cell cycle, tumor suppressors and hormone receptors (reviewed in Wei and Deng, 2003; in Schwechheimer, 2004 and in Chamovitz, 2009). Transcriptomic profiling of *csn4* an *csn5 D. melanogaster* mutants found CSN as a regulator of gene expression during late embryogenesis (Oron *et al.*, 2007). Also in *A. nidulans*, the *csn5/E* deletion affects the gene expression of 15% of the fungal genome during development (Nahlik *et al.*, 2010), and thereby changes the metabolome through de-repression of the derivate of benzaldehyde (*dba*) secondary metabolite cluster genes (Gerke *et al.*, 2012). A DNA-binding ability of Csn7 was also shown in the fruit fly *D. melanogaster,* which suggests a role of Csn7 in regulation of developmental genes (Singer *et al.*, 2014). The N-terminal splicing variant of Csn2, also called as `Alien´, a putative co-repressor in hormone signaling in fruit flies (Dressel *et al.*, 1999). Alien acts directly on chromatin, promoting the nucleosome formation and thus, contributing to gene silencing in human cell cultures (Eckey *et al.*, 2007). The Csn5 deneddylase subunit can also exist in a CSN complex-free form and it interacts with a number of cellular regulators, for example c-Jun, p53, p27 and IκB kinase complex (IKK) (reviewed in Dubiel *et al.*, 2015). Csn5, also called as Jun activating binding protein (Jab1), binds **c-Jun**, an oncogenic transcription factor what is phosphorylated in CSN-dependent manner at its transactivation domain. This phosphorylation prevents c-Jun form ubiquitination and thus, degradation (Musti *et al.*, 1997). **p53** is a tumor suppressor and is important for G1/S cell cycle arrest upon cellular

stress. Csn5 binds physically to p53, which is phosphorylated by the CSN-associated kinases. This phosphorylation targets p53 for degradation and keeps p53 levels low in unstressed cells (Bech-Otschir *et al*., 2001). Physical interaction between the cyclin-dependent kinase (CDK) inhibitor **p27** protein and Csn5 promotes the CRM1-dependent nuclear export and the subsequent degradation of p27 (Tomoda *et al.*, 2002). Nuclear export of p27 and p53 proteins by the CRM1 exporter pathway was reported (reviewed in Wei *et al.*, 2008). p27 and p53 bind to Csn5, which carries a nuclear export signal that is recognized by CRM1, a nuclear export protein (Shaikhqasem *et al.*, 2021). This facilitates their nuclear export, promoting the degradation of these proteins.

1.4 *Aspergillus nidulans*: a genetic reference organism for *in vivo* studies on the COP9 signalosome

The COP9 signalosome is a key regulator of multicellular development, because the *csn* mutants are arrested in early developmental stages in plants, fruit flies and mice (reviewed in Schwechheimer and Isono, 2010; Freilich *et al.,* 1999; Yan *et al.*, 2003; Lykke-Andersen *et al.*, 2003). Thus, investigation of the highly conserved eight-subunit COP9 signalosome by genetics is extremely challenging in mammalian reference organisms or plants, whereas the *csn* mutant strains of *A. nidulans* are able to propagate vegetatively and can complete asexual life cycle (Busch *et al.*, 2007). Moreover, *A. nidulans* harbors an eight-subunit CSN holocomplex, which is similar to the CSN complex in humans (Table 2 and Figure 10).

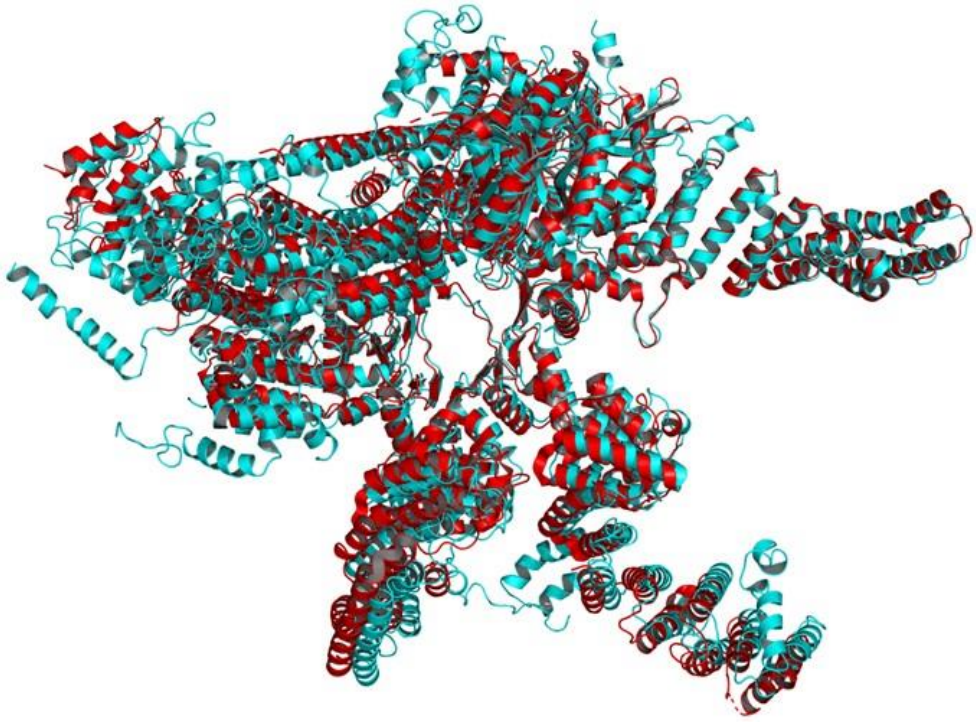

Figure 10. The COP9 signalosome of *Aspergillus nidulans* and in humans are similar.
The models of the human (shown in red, PDB ID: 4D10) and the *A. nidulans* eight-subunit COP9 signalosome (shown in cyan blue) were created as described in chapter 2.10.3 (p.c. Piotr Neumann, Department for Molecular Structural Biology, GZMB, Göttingen) and the structures were drawn and fitted with the PyMOL Molecular Graphics System version 1.7.1.3 (www.pymol.org).

Thus, it is a suitable genetic reference for the COP9 signalosome studies (Busch *et al*., 2003; Beckmann *et al.,* 2015). *A. nidulans* is a soil-borne multicellular filamentous fungus, which is widely used as laboratory model for physiology and developmental studies. This fungus belongs to the phylum Ascomycota and can differentiate through asexual and sexual developmental programs as well, leading to the formation of asexual and sexual tissues (Pöggeler *et al.*, 2018).

1.4.1 Vegetative growth of *A. nidulans*

The vegetative growth of *A. nidulans* starts with the germination of a uninucleate asexual or a binucleate sexual spore, which are resting in G1 phase (Russo *et al.*, 1999). The germination is initiated by swelling of a spore, followed by the formation of a germ tube and polarized growth after approximately 4-6 hours in favored conditions (Pontecorvo *et al.*, 1953). The temperature optimum for spore germination lies between 28°C and 37°C (according to the Fungal Genetics Stock Center), although it was proposed that 37°C causes stress of some heat sensitive fungal mutants (Trinci and Morris, 1979). Cell wall is generated around the germ tube, and as a result of mitosis and nuclear divisions (Russo *et al*., 1999), the newly grown vegetative hypha becomes multinucleate. At the hyphal tip, the Spitzenkörper is a supply hub, which provides the necessary materials for the apical extension and filamentous growth. The apically growing hypha is divided by septae into segments. In submerged cultures, apart from a few cases, like nutrient starvation, *A. nidulans* propagates as a mass of undifferentiated vegetative hyphae, called mycelium. Several cellular factors carry out the regulation and surveillance of internal and external signals and keep the fungus in vegetative growth phase during optimal conditions. Such regulator is the FadA/GanB heterotrimer G-protein pathway (reviewed in Yu, 2006). The vegetative growth continues until the fungus reaches the state of developmental competence, which happens at 36°C approximately 18-20 hours after inoculation into liquid medium (Axelrod *et al.*, 1973). Vegetative growth can be a sufficient way for the fungal propagation, for example in water. On the other hand, building robust asexual or sexual spores is more advantageous for survival when dispersed through air or soil. Apart from internal and external stimuli, the surface contact is necessary for the differentiation of *A. nidulans* (Axelrod *et al.,* 1973). Then, the pluripotent vegetative mycelium enters either the asexual or the sexual developmental program (reviewed in Park *et al.*, 2019).

1.4.2 Asexual development and its regulation

Various environmental and internal conditions shift *A. nidulans* from the phase of developmental competence to differentiate and propagate asexual or sexual structures and tissues (Figure 11) (reviewed in Park *et al.*, 2019). Such environmental conditions are the exposure to light, the availability of nutrients, the O_2/CO_2 ratio or the presence of pheromones. When the fungus grows on surfaces, and illumination and high a concentration of oxygen is provided, *A. nidulans* starts the asexual developmental program as a result of an orchestrated interplay of developmental factors and regulators. The *brlA*-*wetA*-*abaA* pathway initiates the asexual development against repressors. Such repressors are the FadA/GanB heterotrimer G-protein signaling pathway (reviewed in Yu, 2006) and NsdD, which binds to *brlA* and blocks its transcription in favor of vegetative growth (Lee *et al.,* 2014).

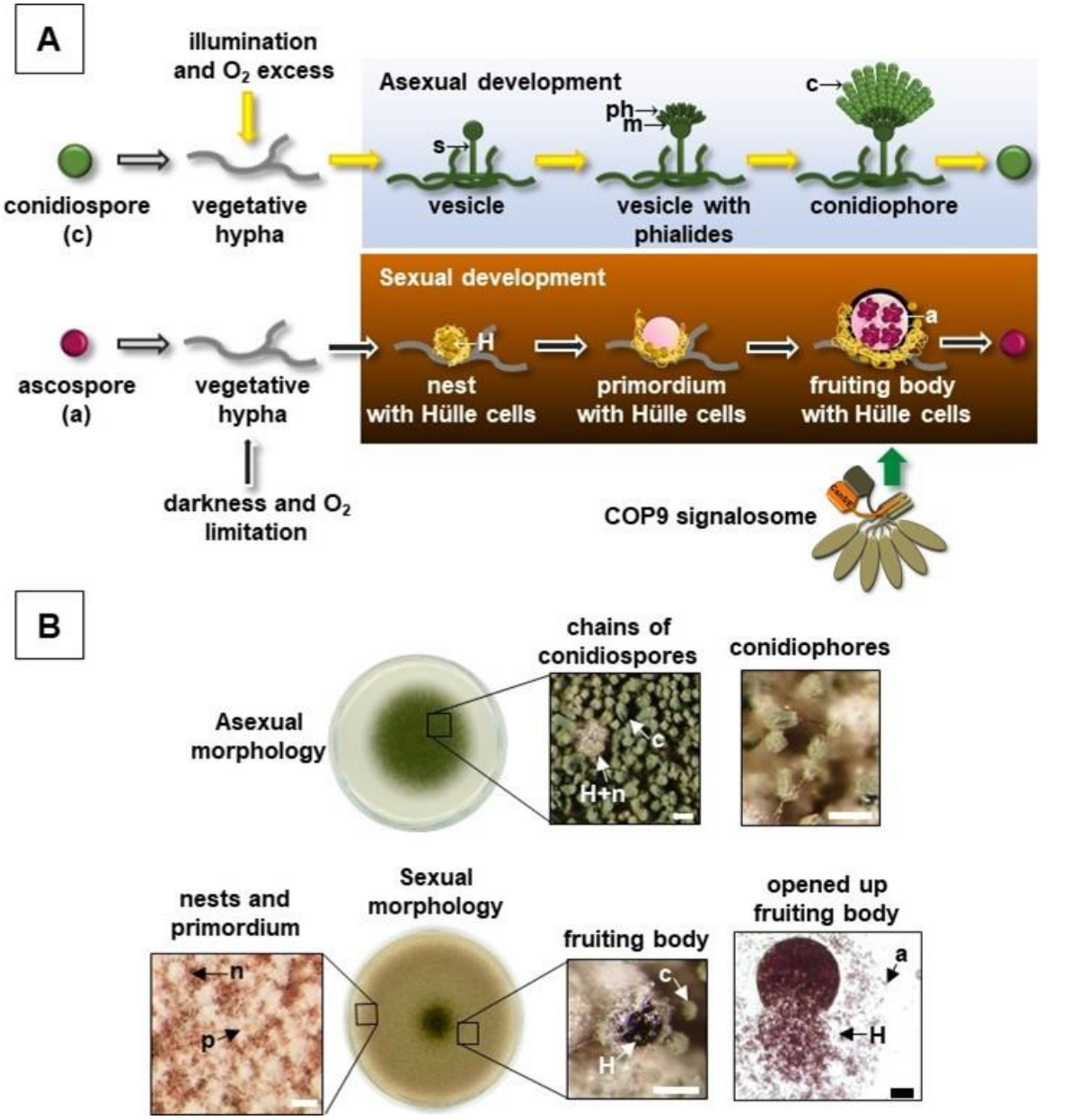

Figure 11. Multicellular life cycle of *Aspergillus nidulans.*
(**A**) Asexual conidiospores or sexual ascospores germinate and propagate vegetative hyphae. As a result of internal and external signals, *A. nidulans* starts the multicellular differentiation. The asexual developmental program is induced by illuminated and aeration is provided. First, a vesicle emerges on a stalk (s) formed of a vegetative hyphae, on which metulae (m) and two rows of phialide (ph) cells emerge. Finally, chains of conidiospores (c) grow creating the conidiophore. When the fungus is grown in dark with limited oxygen access and high CO_2 pressure, for example in soil, it mainly propagates through sexual tissue. The development of sexual structures involves the formation of a nest surrounded by nursing Hülle cells (H), a primordium (p) is formed inside the nest, which matures to a µ-cleistothecium (not shown). A µ-cleistothecium is the precursor of the mature fruiting body called cleistothecium harboring ascospores (a). Development of sexual tissues in the *csn* gene mutation or deletion strains is arrested at the level of nest or primordia production. Thus, the COP9 signalosome is essential for the sexual development in filamentous fungi. (**B**) Asexual and sexual colony morphology of the *A. nidulans* wild type strain and the structures of the asexual and sexual tissues. The engagement to any developmental programs is not an exclusive production of either asexual or sexual structures, but both can be represented during opposite developmental program. White scale bars = 100 µm, black scale bar = 50 µm.

A group of developmental regulators are the multifunctional *velvet* domain family proteins VeA, VelB, VelC and VosA, whose function is light-dependent (reviewed in Bayram and Braus, 2012). They are able to form different homo- and heterodimers or trimers and thus, exert various regulatory roles. For example, VosA either together with NsdD or as a VosA-VelB hetero- or as a VosA-VosA homodimer, represses the *brlA-wetA-abaA* pathway during vegetative growth and sexual development, respectively (Bayram *et al.*, 2010). A VelB-VelB homodimer might also be formed and it is proposed to act as a positive regulator of *brlA* (Park *et al.*, 2012). As part of the tetrameric VeA-FhpA-LreB-LreA complex, VeA plays a role light sensing (Purschwitz *et al.*, 2009; Bayram *et al*., 2010). A proposed positive asexual regulatory effect is also suggested for the VipC-VapB-VeA or the VipC-VapB complexes, comprising the VipC and VapB methyltransferases (reviewed in Sarikaya-Bayram *et al.,* 2015). When the fungus is engaged for asexual development, the repressors are removed and the upstream FluG/SfgA/Flb proteins activate the *brlA-wetA-abaA* pathway, which is responsible for asexual spore formation (reviewed in Yu, 2010). In the initial step of the asexual differentiation, a stalk formed of a vegetative hypha. A vesicle emerges on the stalk and form the vesicle metulae and two rows of phialide cells bud out (Figure 11A). In a later phase, mitotic asexual conidiospores, also called conidia, emerge from the phialides. Conidia are organized in compact chains on the vesicles creating the conidiophore. The air-borne conidiospores are green pigmented and thick walled surviving structures, containing one single nucleus. Thus, the healthy wild type fungus grows green colony when cultivated in asexual development promoting conditions. The engagement for the asexual cycle leads to the production of mainly asexual tissue, although it is not restricted to exclusively asexual structures. Formation of sexual structures can be observed even during asexual growth conditions (Figure 11B).

1.4.3 Sexual development and its regulation- the role of the COP9 signalosome in the development of *A. nidulans*

A. nidulans is a homothallic or self-fertile soil-borne fungus, which mainly propagates via sexual cycle without mating partner, when grown in the dark with limited oxygen access. In early phase a nest-like structure (nest) is formed of vegetative aerial hyphae with nursing Hülle cells (Troppens *et al*., 2020; Liu *et al.*, 2021). Later a primordium and then µ-cleistothecium is formed, which are filled with ascogenous hyphae. These hyphae develop asci and later ascospores within the fruiting body during maturation (reviewed in Pöggeler *et al.*, 2006). The mature and closed fruiting bodies are called cleistothecia. Cleistothecia are dark pigmented and thick-walled overwintering structures, which harbor meiotic, binucleate ascospores (Figure 11B). The initiation and conduction of fungal sexual reproduction requires the concerted interplay of numerous endogenous regulatory factors like transcription factors or pheromone signaling in response to external signals, such as availability of nutrients and light, O_2/CO_2 ratio, osmolarity or environmental pH (reviewed Pöggeler *et al.*, 2006 and in Busch and Braus, 2007). The sexual cycle is favoured and initiated in low O_2-high CO_2 dark conditions by signal transduction pathways like the FadA-SfaD-GpgA heterotrimer G-protein pathway, G-protein associated pheromone sensing receptors and the mitogen-activated protein kinase (MAPK) pathway (reviewed in Pöggeler *et al*., 2006; Yu *et al.*, 2016; Bayram *et al.*, 2012). The MAPK SakA/HogA pathway plays a role not only in osmoadaptation but also in the sexuality of *A. nidulans* (Yu *et al.*, 2016). SteA is a transcription factor, a component of the MAPK pathway, which regulates the fungal sexual cycle (Bayram *et al.*, 2012). The

deletion mutant of the gene encoding SteA (Sterile12-like) is sterile and unable to differentiate ascogenous hyphae, but the formation of Hülle cell is intact (Vallim *et al.*, 2000). Moreover, other transcription factors initiate the sexual cycle. NsdD (never in sexual development D), a repressor of asexual development, is essential for sexual development, because the *nsdD* deletion mutant fails to form cleistothecia (Han *et al.*, 2001). The deletion strains of the genes encoding the StuA, DopA, MedA transcription factors are arrested in their sexual program, though at different stages. StuA and DopA are essential to produce Hülle cells and MedA is important for cleistothecia production (reviewed in Pöggeler *et al*., 2006). The multifunctional developmental regulators, the *velvet* proteins, are involved in both, asexual and sexual development of *A. nidulans* (reviewed in Bayram and Braus, 2012). For example, a VelB-VeA heterodimer is formed and localized to the cytoplasm during illumination. In darkness the dimer is transported to nucleus, where it promotes fruiting body formation (Bayram *et al.,* 2010). The VelB-Vea-LaeA heterotrimer promotes sexual differentiation and coordinates specific secondary metabolite production (Bayram *et al.*, 2008). The UPP, recycling various protein substrates, has a role in the sexual developmental program of *A. nidulans*. The F-box protein GrrA is required for the production of meiotic ascospores in the fungus (Krappmann *et al.*, 2006). The *A. nidulans* strain deleted for the *grrA* gene shows wild type-like asexual sporulation and vegetative growth and is able to produce Hülle cells. Although this fungal strain forms asci-containing cleistothecia, it is unable to produce meiotic ascospores (Krappmann *et al*, 2006). The sensor and SCF CRL inactivating COP9 signalosome is a positive regulator of the sexual program in *A. nidulans* (Figure 11A). Fungal strains with mutated and deleted CSN subunit-encoding genes share a common developmental phenotype: the complete block of mature fruiting body formation (Busch *et al*., 2007; Beckmann *et al.*, 2015). Formation of sexual tissues in these strains is arrested at the level of nest or primordia production. Another characteristic phenotype of the *csn* gene deletion strains is the secretion of reddish-brownish secondary metabolites into the culturing medium (Busch *et al*., 2003; Nahlik *et al*., 2010; Gerke *et al*., 2012). Similarly, deletion of genes encoding the substrate receptor exchange factor CandA proteins result in disturbance in secondary metabolism and arrest in sexual development in *A. nidulans*. This demonstrates the role of the coordinated protein destruction for the sexual program of the filamentous fungus (Köhler *et al.,* 2019).

1.4.4 The production of secondary metabolites is linked to development in *A. nidulans*

The word metabolism is extractable from the Greek word for `change´. Metabolism itself is the set of life-sustaining synthetic processes of the living organisms to gain energy, to synthetize cell components or to provide some sort of advantage in competition with other organisms for survival. Although the production and regulation of the cellular metabolome is interconnected, two main divisions can be defined. Primary metabolism provides the essential energy and cell components from the available nutrients for growth as well as precursor molecules for secondary metabolism. Secondary metabolism is the production of cellular compounds, which play role in intra- and extracellular signaling, communication, protection against harsh environmental factors or confer advantage in the race with other organisms (Gerke *et al*., 2020; Liu *et al.*, 2021). **Signaling metabolites** are required to initiate fungal development. For example, diorcinol and dehydroaustinol are extracellular conidiation factors, whose production is under FluG control (Lee and Adams, 1994; Rodríguez-Urra *et al*., 2012).

The precocious sexual inducers, short psi factors, are hormone-like signaling molecules and are important in establishing the ratio of sexual and asexual development (Mazur *et al.*, 1991; Nahlik *et al*., 2010; reviewed in Busch and Braus, 2007). **Pigments** protect the fungus from environmental factors such as UV radiation, but they can also repel other organisms, such as the yellow pigment of the Hülle cells (Troppens *et al.*, 2020), which is produced by the *mpd/xpt* cluster proteins (Liu *et al.*, 2021). Other developmental structures also contain special pigments. Various pigments color conidiospores greenish (Clutterbuck, 1990) and melanin colors the wall of fruiting bodies black. Accumulation of the asperthecin colors ascospores red (Howard and Raistrick, 1955). There are **mycotoxins** amongst the secondary metabolites, such as the carcinogen compound sterigmatocystin (reviewed in Zingales *et al*., 2020). Production of secondary metabolites is inseparably connected with fungal development, because regulators of the fungal development also coordinate secondary metabolism (reviewed in Bayram and Braus, 2012). The fungal-specific *velvet* protein family regulates secondary metabolism. Deletion of *veA*, *velB* and *laeA* result in the abolishment of sterigmatocystin production (Kato *et al*., 2003; Bayram *et al.,* 2008). Enzyme complexes of the targeted protein degradation system, the UPP, were shown to be required for proper cell progression and multicellular development. Deletions of *csn* genes, encoding COP9 signalosome subunits, cause similar phenotypes, which include the arrest of sexual development as well as aberrant secondary metabolism in *A. nidulans*. A reddish metabolite is secreted by the *csn* mutants, which is identified as orsellinic acid and/or its derivates (Beckmann *et al.*, 2015; Busch *et al*., 2003; Nahlik *et al.*, 2010; Gerke *et al*., 2012). Moreover, the *csn5*/*E* deletion leads to changes in gene expression during development (Nahlik *et al.*, 2010), thereby altering the fungal metabolome (Gerke *et al.*, 2012). The *csn5*/*E* deletion leads to de-repression of the *dba* secondary metabolite cluster of nine genes, which are silenced in wild type strains. These genes encode for proteins (DbaA to DbaI), comprising a polyketide synthase, producing the antibiotic 2,4- dihydroxy-3-methyl-6-(2-oxopropyl)benzaldehyde (DHMBA) (Gerke *et al.*, 2012). Similarly, the deubiquitinase enzyme UspA has a negative effect on the transcription of the *dba* cluster genes (Meister *et al.*, 2019). Moreover, the substrate exchange factor CandA complex plays also a role in secondary metabolism. The fungal CandA complex comprises three proteins, which coordinate the expression of distinct secondary metabolite genes (Köhler *et al*., 2019).

1.5 Aims

Cleavage of Nedd8 from the cullin subunit of the cullin ring E3 ligase is the sole intrinsic enzyme activity of the COP9 signalosome (CSN complex) (Duda *et al.*, 2008; Mosadeghi *et al.*, 2016). This catalytic activity is exerted by the octameric CSN complex, which is formed and activated by the association of the Csn5/E deneddylase subunit into a heptameric pre-assembled COP9 signalosome (pre-CSN complex) (Lingaraju *et al.*, 2014; Beckmann *et al.*, 2015). The Nedd8-specific isopeptidase activity is conferred by the predominantly nuclear CSN holocomplex (Busch *et al.*, 2003; Chamovitz *et al.*, 1996), but probably there are cytoplasmic localized CSN subassemblies, which might perform various cellular functions (reviewed in Dubiel *et al.*, 2015). The observation leads to the assumption that the CSN complex assembly has to be coordinated with the subcellular localization for its nuclear enrichment and function (Chamovitz *et al.*, 1996).

The main goal of this work is to investigate the choreography of the pre-CSN complex formation and to identify CSN subassemblies; as well as to explore cellular functions of the pre-CSN subassemblies, which are independent of the catalytic activity of CsnE. Genetic and protein analytical methods were combined to address these questions, taking advantage of the multicellular fungus *Aspergillus nidulans* as genetic reference organism. Fungal strains deleted for genes encoding COP9 signalosome subunits were constructed using the recyclable marker system (Hartmann *et al.*, 2010), resulting in mutants without retaining any marker genes. The phenotypical analysis of these strains allowed to draw conclusions about the physiological consequences caused by various *csn* gene deletions. GFP-affinity purifications were performed with functional N-terminal fusions of GFP with CSN subunits, which were produced in various pre-CSN complex deficient background strains. This method enabled the reconstruction of the subunit organization within the pre-CSN complex and to gain insights into the interactome pre-CSN complex subassemblies. GFP-CSN subunit fusions produced in different background strains facilitated the investigation of the subcellular localization of CSN subassemblies by confocal microscopy and the measurement of CSN subunit protein amounts by GFP-immunoblotting. This work explores the yet unidentified assembly steps, which build a catalytically active COP9 signalosome. This process is coupled with a choreography between CSN subunits for their correct subcellular localization as well as for their accurate cellular protein amounts. This study also gives insights to possible cellular functions of the CSN complex subassemblies.

2 Materials and Methods

2.1 Chemicals, materials, equipment and software

The solutions, buffers and culture media were prepared with deionized water (ddH_2O). The culture media and their components were autoclaved at 120°C for 20 minutes at 2 bar pressure. Heat sensitive solutions were filter-sterilized. All chemicals materials, equipment and software used for this work are listed in Table 3.

Table 3. Chemicals, materials, equipment and software used for this study.
The chemicals, materials, equipment and software, which were used are listed with their manufacturer or distributor and the country of origin.

Product	Manufacturer or distributor	City, Country
Chemicals		
Amersham™ CDP-Star Detection Reagent	GE Healthcare	Solingen, Germany
Amersham™ Gene Images AlkPhos Direct Labelling and Detection System	GE Healthcare	Solingen, Germany
Ampicillin sodium salt	Carl Roth GmbH and Co KG	Karlsruhe, Germany
Chemicals for general buffers, solutions and culturing media	Applichem GmbH BD Biosciences Biozyme Scientific GmbH Carl Roth GmbH and Co KG Fluka Invitrogen Merck KgaA Oxoid Deutschland GmbH Roche Diagnostics GmbH Sigma-Aldrich Chemie GmbH Serva Electrophoresis GmbH TH Geyer GmbH and Co KG VWR International GmbH	Darmstadt, Germany Heidelberg, Germany Hessisch Oldendorf, Germany Karlsruhe, Germany Neu-Ulm, Germany Carlsbad, CA, USA Darmstadt, Germany Wesel, Germany Mannheim, Germany München, Germany Heidelberg, Germany Renningen, Germany Darmstadt, Germany
clonNat (nourseothricin-dihydrogen-sulphate)	Werner Bioagents	Jena, Germany
cOmplete EDTA-free protease inhibitor cocktail	Roche Diagnostics GmbH	Mannheim, Germany
DAPI (4´,6-diamidin-2-phenylindol)	Carl Roth GmbH and Co KG	Karlsruhe, Germany
GFP-Trap® Agarose beads	Chromotek GmbH	Planegg-Martinsried, Germany
Horseradish peroxidase-coupled mouse antibody (115-035-003)	Jackson ImmunoResearch Laboratories INC.	Newmarket, UK
Invitrogen GeneArt® Seamless Cloning and Assembly Enzyme Mix	Thermo Fisher Scientific	Schwerte, Germany
Invitrogen GeneArt® Seamless PLUS Cloning and Assembly Kit	Thermo Fisher Scientific	Schwerte, Germany
Lysozyme from chicken egg white	Sigma-Aldrich Chemie GmbH	München, Germany
Milk powder Sucofin®	TSI Consumer Goods GmbH	Zeven, Germany
Monoclonal α-GFP antibody (B-2): sc-9996	Santa Cruz Biotechnology	Dallas, TX, USA
NucleoSpin Plasmid Kit	Macherey-Nagel	Düren, Germany

NucleoSpin Gel and PCR Clean Up Kit	Macherey-Nagel	Düren, Germany
Oligonucleotides	Sigma-Aldrich Chemie GmbH	München, Germany
pBluescript KS cloning vector	Fermentas GmbH	St. Leon-Rot, Germany
Phleomycin	InvivoGen	Toulouse, France
Phusion High Fidelity Polymerase	Thermo Fisher Scientific	Schwerte, Germany
Q5® High-Fidelity 2X Master Mix	New England Biolabs GmbH	Frankfurt am Main, Germany
*Rapi*Gest™ SF surfactant solution	Walters GmbH	Eschborn, Germany
Trypsin	Serva Electrophoresis GmbH	Heidelberg, Germany
VinoTaste® Pro	Novozymes	Bagsvaerd, Denmark
1 kb DNA Ladder GeneRuler	Thermo Fisher Scientific	Schwerte, Germany
Materials		
Amersham™ Hybond®-N membrane	GE Healthcare	Solingen, Germany
Amersham™ Hyperfilm™ ECL	GE Healthcare	Solingen, Germany
Amersham™ Protran® 0.45 µm NC	GE Healthcare	Solingen, Germany
Mass spectrometry glass vial	Agilent	Santa Clara, CA, USA
Miracloth filter	Merck KGaA	Darmstadt, Germany
Plastic consumables such as petri dishes, pipette tips, Eppendorf and Falcon tubes, PCR tubes	Eppendorf AG Sarstedt AG and Co Starlab GmbH	Hamburg, Germany Nümbrecht, Germany Hamburg, Germany
Poly-Prep® Chromatography columns	Bio-Rad Laboratories GmbH	Hercules, CA, USA
Protein LoBind Tube	Eppendorf AG	Hamburg, Germany
SS-34 centrifugation tubes	Thermo Fisher Scientific	Schwerte, Germany
µ-Slide 8-well microscopy chamber	Ibidi GmbH	Gräfelfing, Germany
Equipment		
Acclaim PepMap RLSC™ column	Thermo Fisher Scientific	Schwerte, Germany
Biofuge *fresco* cooling and *pico* table-top centrifuge	Heraeus Instruments GmbH	Hanau, Germany
Eppendorf 5804R cooling falcon centrifuge	Thermo Fisher Scientific	Schwerte, Germany
Fusion-SL7 chemiluminescence detection system	PeqLab Biotechnologie GmbH	Erlangen, Germany
LTQ Velos Pro™ linear ion trap	Thermo Fisher Scientific	Schwerte, Germany
Nanospray Flex™ Ion Source	Thermo Fisher Scientific	Schwerte, Germany
NanoDrop® ND-1000 spectrophotometer	PeqLab Biotechnologie GmbH	Erlangen, Germany
Optimax X-ray Film Processor	Protec GmbH and Co. KG	Oberstenfeld, Germany
Orbitrap-FT analyzer	Thermo Fisher Scientific	Schwerte, Germany
Orbitrap Velos Pro™ mass spectrometer	Thermo Fisher Scientific	Schwerte, Germany
Plan-Apochromat 100x/1.4 oil objective	Carl Zeiss Microscopy GmbH	Göttingen, Germany
QuantEM:512SC camera	Photometrics	Tucson, AZ, USA
Retch mixer mill (MM400)	Retsch GmbH	Haan, Germany
Savant™ SPD111V SpeedVac concentrator	Thermo Fisher Scientific	Schwerte, Germany
Sonorex™ Digital 10 P ultrasonic bath	Bandelin Electronics GmbH	Berlin, Germany
Sorvall RC-5B Plus Refrigerated Centrifuge	Thermo Fisher Scientific	Schwerte, Germany
SZX12-ILLB2-200 binocular microscope	Olympus Deutschland GmbH	Hamburg, Germany
UltiMate™ 3000 RLSC nano liquid chromatography system	Thermo Fisher Scientific	Schwerte, Germany
Thoma cell counting chamber	Paul Marienfeld GmbH and Co. KG	Lauda-Königshofen, Germany

T Professional Standard 96/Trio48/96 Gradient thermocyclers	Biometra GmbH	Göttingen, Germany
Zeiss AxioObserver Z.1 inverted confocal microscope	Carl Zeiss Microscopy GmbH	Göttingen, Germany
Software, programmes, tools		
Bio1D software version 15.08	Vilber Lourmat Deutschland GmbH	Eberhardzell, Germany
CellSens dimension software version 1.4	Olympus Deutschland GmbH	Hamburg, Germany
Fusion software version 15.18	Vilber Lourmat Deutschland GmbH	Eberhardzell, Germany
Intas GDS Gel Documentation System	Intas Science Imaging Instruments GmbH	Göttingen, Germany
MaxQuant software version 1.6.0.16	Cox and Mann, 2008	www.maxquant.org
PeptideCutter/ExPasy	Gasteiger *et al.*, 2003	web.expasy.org /peptide_cutter
Perseus software version 1.6.0.7	Tyanova *et al.,* 2016	www.maxquant.org/perseus
PISA (Protein Interfaces, Surfaces and Assemblies)	(Krissinel and Henrick, 2007)	www.ebi.ac.uk/pdbe/pisa
ProtParam/ExPasy	(Gasteiger *et al*, 2003)	web.expasy.org/protparam
DNASTAR Lasergene/SeqBuilder and MegAlign version 7.1.0.44	DNASTAR Inc.	Madison, WI, USA
SlideBook version 6.0	Intelligent Imaging Innovations GmbH	Göttingen, Germany
Xcalibur™ software version 2.2	Thermo Fisher Scientific	Schwerte, Germany
The PyMOL Molecular Graphics System version 1.7.1.3	Schrödinger LLC.	www.pymol.org

2.2 Nucleic acid methods

2.2.1 PCR reactions and agarose gel electrophoresis

AGB552 genomic DNA (gDNA) was used as template for polymerase chain reactions (PCRs) with the Phusion High Fidelity Polymerase (Table 4) or the Q5® High-Fidelity 2x Master Mix in the T Professional Standard 96/Trio48/96 Gradient thermocyclers following the manufacturer's instructions, if not specified otherwise.

Table 4. Steps of a general PCR reaction applied in this study using the Phusion High Fidelity Polymerase.

Cycle step	Temperature	Time (second or minute)/kilo base pair(s)	Cycles
Initial denaturation	98°C	30 sec	1
Denaturation	98°C	10 sec	35
Annealing	x°C	30 sec	
Extension	72°C	30 sec/kbp	
Final extension	72°C	10 min	1
Hold	4-10°C	Hold	Hold

The PCR products or DNA fragments were separated according to size by agarose gel electrophoresis. The agarose gels consisted of 1% (w/v) agarose and 0.001 mg/mL ethidium-

bromide prepared in 1x TAE buffer (40 mM Tris, 20 mM acetic acid, 1 mM EDTA). Prior to loading, the DNA was mixed with 10x DNA loading dye (10% (v/v) Ficoll 400, 200 mM EDTA pH 8.0 and 0.2% (w/v) bromophenol blue and 0.2% (w/v) xylene cyanole FF). The DNA fragments were visualized by UV exposure and documented by the Intas GDS Gel Documentation System. After the agarose gel electrophoresis, the NucleoSpin Gel and PCR Clean Up Kit was used to extract the PCR products from the agarose gel.

2.2.2 Plasmid construction

The gene coding sequences and the 5' upstream and 3' downstream flanking regions were obtained from the Aspergillus Genome Database (AspGD) (Cerqueira *et al.*, 2014). The plasmid constructions and subsequent sequence analyses were done using SeqBuilder and MegAlign version 7.1.0.44 of the DNASTAR Lasergene package. The cloning reactions were carried out using either the Invitrogen GeneArt® Seamless Cloning and Assembly Enzyme Mix or the Invitrogen GeneArt® Seamless PLUS Cloning and Assembly Kit. All plasmids were constructed using the ß-recombinase-six-site self-excisable marker system, which contained either the *nat1* gene of *Saccharomyces cerevisiae* or the *ble* gene from *Streptoalloteichus hindustanus* for selection (Hartmann *et al*., 2010). The *nat1* and the *ble* provide resistance against nourseothricin and phleomycin, respectively (Kück and Hoff, 2006; Drocourt *et al*., 1990). The preparation of different deletion or complementation cassettes for *Aspergillus* transformation occurred by restriction digestion of the plasmids. Therefore, the naturally occurring restriction enzymatic recognition half site was used without changing the native nucleic acid sequence. The other restriction recognition half site was created artificially by co-amplification with the outermost primers. For *gfp* plasmid constructs, the *gfp* fragment with a C-terminal linker and a precision protease cleavage site for N-terminal protein labelling was obtained by PCR amplification with EB10-oAMK95 from pME4716 plasmid. The NucleoSpin Plasmid Kit was used to isolate plasmids from *Escherichia coli* strains. All used oligonucleotides and plasmids are listed in Table 5 and Table 6, respectively. For sequencing of plasmids the KT182, KT183, KT184 and KT339 oligonucleotides were used in addition to oligonucleotides designed for this study. All constructed plasmids were sequenced in SeqLab Sequence Laboratories (Göttingen, Germany).

Table 5. List of oligonucleotides applied in this work for plasmid construction.
The primers were designed using the DNASTAR Lasergene/SeqBuilder package. Glossary: bp: base pair, p.c.: personal communication.

Primer	Sequence 5' to 3'	Size (bp)	Reference
EB10	ATG GTG AGC AAG GGC GAG G	19	Köhler, p.c.
oAMK95	ACC ACC GCT ACC ACC GGG	18	Köhler, 2018
JG1171	CTT TGC CCG GTG TAT GAA ACC	21	Gerke, p.c.
KT182	CAT CAG TGC CAG CTG TCT TCG	21	Thieme, 2017
KT183	GAT GTG CTG CAA GGC GAT TAA GTT G	25	Thieme, 2017
KT184	GGC TTT ACA CTT TAT GCT TCC G	22	Thieme, 2017
KT339	CTT CTG ATA TCT ATA GGT CAA TAG AG	26	Thieme, 2017
FB047	CTG CAG GAA TTC GAT GTT TAA ACT GCA CAG TTC ATT ACA CTG AG	44	This study
FB048	GAC CTA TAG GCC TGA GTG CGT CTA TGC TGG ACA GCT	36	This study
FB049	ATA ATA TGG CCA TCT GTC TGA AGC CAG TCC GTC GG	35	This study
FB050	ATC GAT AAG CTT GAT GTT TAA ACT TAG GCC AAT TCT ATA AGT CGC T	46	This study
FB051	CTG CAG GAA TTC GAT GTT TAA ACG TGC CTC TGC GAG ATT GAA G	43	This study
FB052	ACC TAT AGG CCT GAG TAT GTG CGG CAG TCT TGA GT	35	This study
FB053	ATA ATA TGG CCA TCT GGA GAA GAA ACA TTG AAG GAA	36	This study
FB054	ATC GAT AAG CTT GAT GTT TAA ACA TGC GAG GTA ACT TGC	39	This study
FB055	CTG CAG GAA TTC GAT GTT TAA ACC CTT GCC CAT TGC AAC	39	This study
FB056	ACC TAT AGG CCT GAG TTT GAG AGA TAT GAA GCA AGC AAG	39	This study
FB057	ATA ATA TGG CCA TCT TGC GAA TAT GGT TGT TGG AC	35	This study
FB058	ATC GAT AAG CTT GAT GTT TAA ACT CAG TCC TGA AAT CAG ACT C	43	This study
FB059	CTG CAG GAA TTC GAT GTT TAA ACG CGC CCT GCT CTC C	37	This study
FB060	ACC TAT AGG CCT GAG GGG GAA GGT TTG GTG ATG AG	35	This study
FB061	ATA ATA TGG CCA TCT CCT CCT GAC GTG CTG CAG	33	This study
FB062	ATC GAT AAG CTT GAT GTT TAA ACA AAA GGA GAG TCC GCT	39	This study
FB063	CTG CAG GAA TTC GAT GTT TAA ACT TAA ATC CAC GGG GTC	39	This study
FB064	ACC TAT AGG CCT GAG CTT GCG TGT GTG TAT GCG	33	This study
FB065	ATA ATA TGG CCA TCT TGA CTT AGC TTA TTA AGA CCA ACC	39	This study
FB066	ATC GAT AAG CTT GAT GTT TAA ACC GTA CGC AAT CGG A	37	This study
FB067	CTG CAG GAA TTC GAT GTT TAA ACT CAC GGA GAC TTC ACC	39	This study
FB068	ACC TAT AGG CCT GAG CAG TGC TGA GTG CTG GAG	33	This study
FB069	ATA ATA TGG CCA TCT CAT CTC ATT GTA CGG TTC AG	35	This study
FB070	ATC GAT AAG CTT GAT GTT TAA ACG ATA TCC CAC TCG TG	38	This study

FB071	CTG CAG GAA TTC GAT GTT TAA ACT CCG CGA AGG CCA C	37	This study
FB072	ACC TAT AGG CCT GAG GGC ACA GAG AAC GTA TTA CCA GTA T	40	This study
FB073	ATA ATA TGG CCA TCT AAC CTG TAT GCG AAA CGA CC	35	This study
FB074	ATC GAT AAG CTT GAT GTT TAA ACT CGC GAC AGG AAC TTC	39	This study
FB085	CTG CAG GAA TTC GAT GTT TAA ACA TCT CTG TCG TTG AAA	39	This study
FB088	ACC TAT AGG CCT GAG TTA TCC GAG TGC CAC GCC	33	This study
FB089	ATA ATA TGG CCA TCT TGA CTT AGC TTA TTA AGA CCA AC	38	This study
FB090	ATC GAT AAG CTT GAT GTT TAA ACC CAT CCA CTA GCG A	37	This study
FB091	GTG GCA CTC GGA TAA CTC AGG CCT ATA GGT CAA TA	35	This study
FB092	GCC CTT GCT CAC CAT CTT GCG TGT GTG TAT GC	32	This study
FB093	GGT GGT AGC GGT GGT ATG CCA GAC GAA GCC ATA TC	35	This study
FB111	ATA TGG CCA TCT CAC GTC TGA AGC CAG TCC GTC G	34	This study
FB112	GAT AAG CTT GAT CAC GTT TAA ACT AAT CTG GTG GCC ACG	39	This study
FB113	AGG AAT TCG ATA TTT GTT TAA ACA TGT TTA TAG AGT GAG CGG	42	This study
FB114	GCC CTT GCT CAC CAT TGC GTC TAT GCT GGA CA	32	This study
FB115	GGT GGT AGC GGT GGT ATG GAG CCC ATG TTA CCA GA	35	This study
FB116	ATA GGC CTG AGA TTT TTA TTG CTT CAT CCC CGT CG	35	This study
FB117	AGG AAT TCG ATA TTT AAA TGA AGA CTG CGC CCC AG	35	This study
FB118	GCC CTT GCT CAC CAT TAT GTG CGG CAG TCT TGA GT	35	This study
FB119	GGT GGT AGC GGT GGT ATG TCA GAC GAC GAT GAT TT	35	This study
FB120	ATA GGC CTG AGA TTT TTA GAA CAG GCC CGT CTT CA	35	This study
FB121	ATA TGG CCA TCT CAC GCG GGG GAG GGG GAG G	31	This study
FB122	GAT AAG CTT GAT CAC GTG TTG AGC GTC GAT TTC GAT AGT AAT C	43	This study
FB123	ATA TGG CCA TCT CAC CAT CTC ATT GTA CGG TTC AG	35	This study
FB124	GAT AAG CTT GAT CAC GTT TAA ACG ATA TCC CAC TCG TG	38	This study
FB125	AGG AAT TCG ATA TTT GTT TAA ACT CAC GGA GAC TTC AC	38	This study
FB126	ATA GGC CTG AGA TTT CTA TGA CTT CTT CCC AAG AA	35	This study
FB141	GAA TCG GTG GCC GCT AGA AC	20	This study
FB144	AAA GCA GGA GGA GGG CTT GG	20	This study
FB145	AGG AAT TCG ATA TTT GTT TAA ACA CTT ACT CGT CCA CAA G	40	This study
FB146	GCC CTT GCT CAC CAT GAT GAT TGT CAG GTG GGG AT	35	This study
FB147	GGT GGT AGC GGT GGT ATG CAA GCT GCT CAA CTA TC	35	This study
FB148	ATA GGC CTG AGA TTT CTA AGT AGA CTC TAC CGT CT	35	This study
FB149	ATA TGG CCA TCT CAC CGC ATG ATC AGA TGA TGA GA	35	This study
FB150	GAT AAG CTT GAT CAC GTT TAA ACA CGT GCT AGC GAT ACC	39	This study
FB151	CCC TCC TCC TGC TTT GAA TCG GTG GCC GCT AGA AC	35	This study
FB153	CTC GCA TCT CTG CAA TGA CG	20	This study
FB154	CTG CAT CGA GCC CGC TTC GT	20	This study
FB155	CCG GTG TAT GAA ACC GGA AAG GCC GCT CAG GAG CT	35	This study
FB156	GGT GGT AGC GGT GGT ATG TCA GAC GAC GAT GAT TTC ATG C	40	This study
FB157	TCC TGC TTT GCT GCC AGC CCC CCC AGC TGC GAA TCG GTG GCC GCT AGA AC	50	This study
FB158	GGC AGC AAA GCA GGA GGA GG	20	This study

FB159	CGT CTC CTG CGA GTG GAA GG	20	This study
FB160	CAC TCG CAG GAG ACG ACA CCG TAC ACG ACT GAC CCT CGC ATC TCT GC	47	This study
FB170	ACC TAT AGG CCT GAG TCA GCT GCC TTG ATT GCT GAT TAA AGC	42	This study

Table 6. List of plasmids constructed and applied in this work.
Glossary: *ble*: phleomycin gene, *nat1*: nourseothricin gene, ^{P}promoter, resistance gene^{R}, terminator^{t}, L: linker sequence, PP: precision protease recognition site, p.c.: personal communication.

Plasmid	Description	Reference
pBluescript KS	cloning vector	Fermentas GmbH
pME3173	^{P}*gpdA:mrfp:h2A:hisB*^{t}*:nat1*^{R}	Bayram, 2008
pME4305	*six:*^{P}*xyl:β-rec:trpC*^{t}*:*^{P}*gpdA:ble*^{R}*:six*	Gerke, p.c.
pME4716	^{P}*nedd8:gfp:L:PP:nedd8:*^{P}*gpdA:nat1*^{R}*:nedd8*^{t}	Köhler, 2018
pME4319	*six:*^{P}*xylP:β-rec:trpC*^{t}*: ble*^{R}*:six*	Gerke, p.c.
pME4702	*5´*^{csnD}*:gfp:csnD*$^{1-1227}$*:six:*^{P}*xylP:β-rec:trpC*^{t}*:nat1*^{R}*:3´*^{csnD}	Meister, 2018
pME5430	*5´*^{csnA}*:six:*^{P}*xylP:β-rec:trpC*^{t}*:ble*^{R}*:six:3´*^{csnA}	This study
pME5431	*5´*^{csnB}*:six:*^{P}*xylP:β-rec:trpC*^{t}*:ble*^{R}*:six:3´*^{csnB}	This study
pME5432	*5´*^{csnC}*:six:*^{P}*xylP:β-rec:trpC*^{t}*:ble*^{R}*:six:3´*^{csnC}	This study
pME5433	*5´*^{csnD}*:six:*^{P}*xylP:β-rec:trpC*^{t}*:ble*^{R}*:six:3´*^{csnD}	This study
pME5434	*5´*^{csnF}*:six:*^{P}*xylP:β-rec:trpC*^{t}*:ble*^{R}*:six:3´*^{csnF}	This study
pME5435	*5´*^{csnG}*:six:*^{P}*xylP:β-rec:trpC*^{t}*: ble*^{R}*:six:3´*^{csnG}	This study
pME5436	*5´*^{csnH}*:six:*^{P}*xylP:β-rec:trpC*^{t}*:ble*^{R}*:six:3´*^{csnH}	This study
pME5437	*5´*^{csnF}*:gfp:csnF:six:*^{P}*xylP:β-rec:trpC*^{t}*:ble*^{R}*:six:3*^{csnF}	This study
pME5438	*six:*^{P}*xylP:β-rec:trpC*^{t}*:ble*^{R}*:six:3*^{csnA}	This study
pME5439	*5*^{csnA}*:gfp:csnA:six:*^{P}*xylP:β-rec:trpC*^{t}*:ble*^{R}*:six:3*^{csnA}	This study
pME5440	*six:*^{P}*xylP:β-rec:trpC*^{T}*:ble*^{R}*:six:3*^{csnB}	This study
pME5441	*5*^{csnB}*:gfp:csnB:six:*^{P}*xylP:β-rec:trpC*^{t}*:ble*^{R}*:six:3*^{csnB}	This study
pME5442	*six:*^{P}*xylP::β-rec:trpC*^{t}*:ble*^{R}*:six:3*^{csnG}	This study
pME5443	*5*^{csnG}*:csnG:six:*^{P}*xylP:β-rec:trpC*^{t}*:ble*^{R}*:six:3*^{csnG}	This study
pME5444	*5*^{csnB}*:gfp:csnB*$^{\Delta NLS2}$*:six:*^{P}*xylP:β-rec:trpC*^{t}*:ble*^{R}*:six:3*^{csnB}	This study
pME5445	*six:*^{P}*xylP:β-rec:trpC*^{t}*:ble*^{R}*:six:3*^{csnE}	This study
pME5446	*5*^{csnE}*:gfp:csnE:six:*^{P}*xylP:β-rec:trpC*^{t}*:ble*^{R}*:six:3*^{csnE}	This study
pME5447	*5*^{csnB}*:gfp:csnB*$^{\Delta NLS1}$*:six:*^{P}*xylP:β-rec:trpC*^{t}*:ble*^{R}*:six:3*^{csnB}	This study
pME5448	*5*^{csnB}*:gfp:csnB*$^{NLS2(R739A;R740A;K743A)}$*:six:*^{P}*xylP:β-rec:trpC*^{t}*:ble*^{R}*:six:3*^{csnB}	This study
pME5449	*5*^{csnB}*:gfp:csnB*$^{NLS1(K557T;K560T)}$*:six:*^{P}*xylP:β-rec:trpC*^{t}*: ble*^{R}*:six:3*^{csnB}	This study
pME5452	*six:*^{P}*xylP:β-rec:trpC*^{t}*:ble*^{R}*:six:3*^{csnH}	This study
pME5453	*5*^{csnH}*:csnH:six:*^{P}*xylP:β-rec:trpC*^{t}*:ble*^{R}*:six:3*^{csnH}	This study

2.2.3 Construction of the Δ*csnA* deletion cassette with self-excisable phleomycin marker (pME5430)

For the construction of the Δ*csnA* deletion cassette, the 5' flanking region of *csnA* was amplified with the oligo pair FB047-048 (1720 bp) and the 3' flanking region of *csnA* was amplified with FB049-050 (1476 bp). Both flanking regions and the marker cassette were cloned into the recipient vector backbone (see Figure 12A). For *Aspergillus* transformation, pME5430 was enzymatically digested with *Mss*I resulting in the *csnA* deletion construct of 8077 bp length.

2.2.4 Construction of the Δ*csnB* deletion cassette with self-excisable phleomycin marker (pME5431)

For the construction of the Δ*csnB* deletion cassette, 5' flanking region of *csnB* was amplified with FB051-052 (889 bp). The 3' flanking region of *csnB* was amplified with FB053-054 (1797 bp). Both flanking regions and the marker cassette were cloned into the recipient vector backbone (see Figure 12A). For *Aspergillus* transformation, pME5431 was enzymatically digested with *Mss*I resulting in the *csnB* deletion construct of 7575 bp length.

2.2.5 Construction of the Δ*csnC* deletion cassette with self-excisable phleomycin marker (pME5432)

For the construction of the Δ*csnC* deletion cassette, 5' flanking region of *csnC* was amplified with FB055-056 (1206 bp). The 3' flanking region of *csnC* was amplified with FB057-058 (1517 bp). Both flanking regions and the marker cassette were cloned into the recipient vector backbone (see Figure 12A). For *Aspergillus* transformation, pME5432 was enzymatically digested with *Mss*I resulting in the *csnC* deletion construct of 7608 bp length.

2.2.6 Construction of the Δ*csnD* deletion cassette with self-excisable phleomycin marker (pME5433)

For the construction of the Δ*csnD* deletion cassette, 5' flanking region of *csnD* was amplified with FB059-060 (1524 bp). The 3' flanking region of *csnD* was amplified with FB061-062 (1803 bp). Both flanking regions and the marker cassette were cloned into the recipient vector backbone (see Figure 12A). For *Aspergillus* transformation, pME5433 was enzymatically digested with *Mss*I resulting in the *csnD* deletion construct of 8224 bp length.

2.2.7 Construction of the Δ*csnF* deletion cassette with self-excisable phleomycin marker (pME5434)

For the construction of the Δ*csnF* deletion cassette, 5' flanking region of *csnF* was amplified with FB063-064 (1162 bp). The 3' flanking region of *csnF* was amplified with FB065-066 (1460 bp). Both flanking regions and the marker cassette were cloned into the recipient vector backbone (see Figure 12A). For *Aspergillus* transformation, pME5434 was enzymatically digested with *Mss*I resulting in the *csnF* deletion construct of 7636 bp length.

2.2.8 Construction of the Δ*csnG* deletion cassette with self-excisable phleomycin marker (pME5435)

For the construction of the Δ*csnG* deletion cassette, 5' flanking region of *csnG* was amplified with FB067-068 (1564 bp). The 3' flanking region of *csnG* was amplified with FB069-070 (1320 bp). Both flanking regions and the marker cassette were cloned into the recipient

vector backbone (see Figure 12A). For *Aspergillus* transformation, pME5435 was enzymatically digested with *MssI* resulting in the *csnG* deletion construct of 7769 bp length.

2.2.9 Construction of the Δ*csnH* deletion cassette with self-excisable phleomycin marker (pME5436)

For the construction of the Δ*csnH* deletion cassette, 5' flanking region of *csnH* was amplified with FB071-072 (1510 bp). The 3' flanking region of *csnH* was amplified with FB073-074 (1071 bp). Both flanking regions and the marker cassette were cloned into the recipient vector backbone (see Figure 12A). For *Aspergillus* transformation, pME5436 was enzymatically digested with *Mss*I resulting in the *csnH* deletion construct of 7466 bp length.

2.2.10 Construction of the *gfp:csnF* cassette with self-excisable phleomycin marker (pME5437)

The *gfp:csnF* cassette was created from four fragments cloned into the *Eco*RV cutting site of the pBluescript KS cloning vector. The *csnF* 5' flanking region and the *csnF* coding sequence were amplified with FB085-092 (801 bp) and FB093-088 (1263 bp), respectively. The *csnF* 3' flanking region was amplified with FB089-090 (1100 bp). The recyclable marker cassette and the 3' flanking region were fused by PCR with FB090-091 (6046 bp) and this fusion PCR product was used for cloning, resulting in pME5437. For the fusion PCR amplification the Q5® High-Fidelity 2X Master Mix and for seamless cloning the Invitrogen GeneArt® Seamless PLUS Cloning and Assembly Kit was used. The flanking regions and the marker cassette were cloned into the recipient vector backbone (see Figure 12B). For *Aspergillus* transformation, pME5437 was enzymatically digested with *Mss*I resulting in the *gfp:csnF* construct of 8866 bp length.

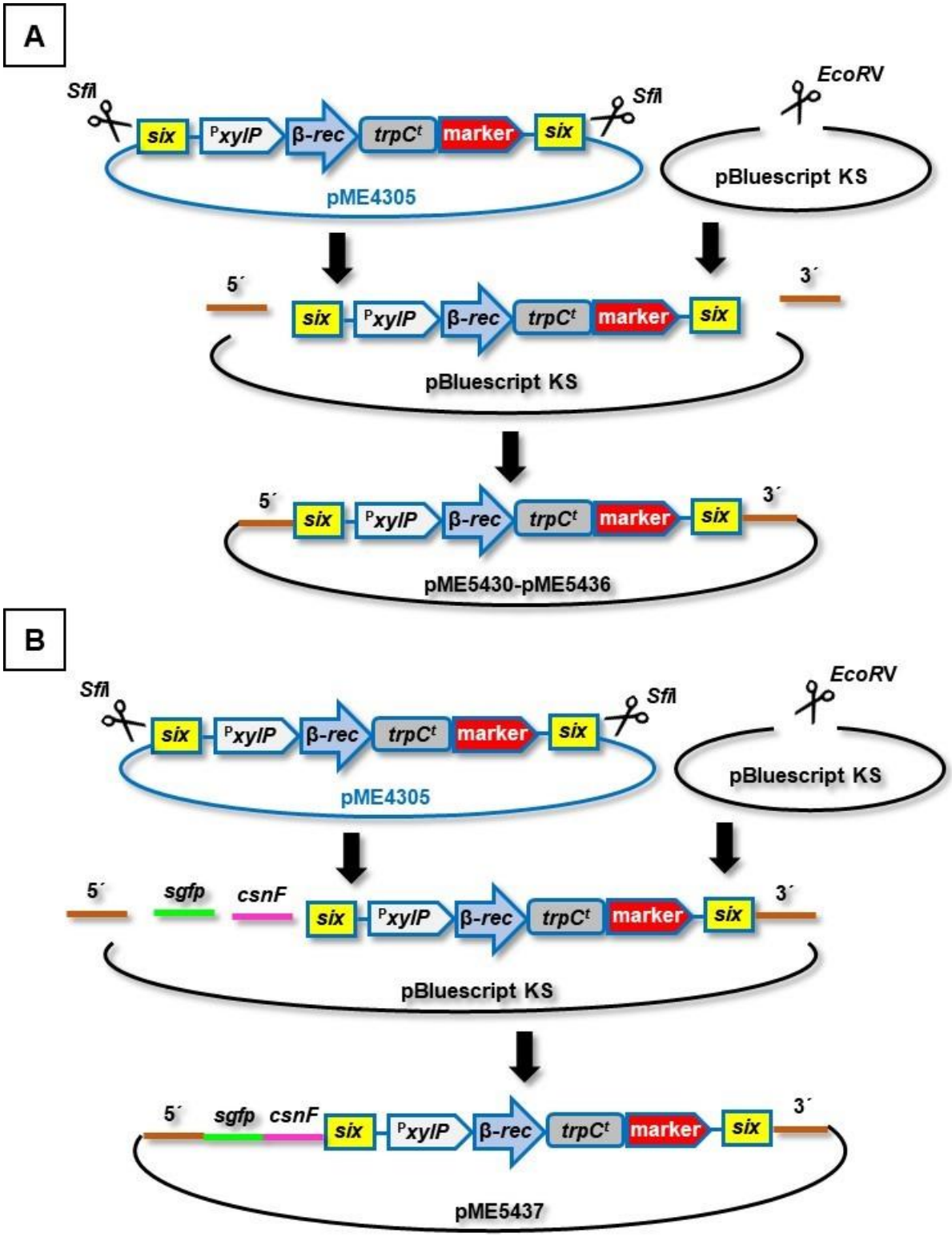

Figure 12. Construction of the pME5430 to pME5436 and pME5437 plasmids.
The pME5430 to pME5436 and pME5437 plasmids were constructed with the recyclable marker cassette accessed from pME4305 by *Sfi*I enzymatic digestion and the pBluescript KS linearized by *Eco*RV was used as cloning vector. (**A**) For the pME5430 to pME5436 plasmids the 5´ and 3´ flanking regions of the gene of interest were cloned together with the marker cassette into the cloning vector. (**B**) For the pME5437 plasmid the 5´ flanking region, the *gfp*, the *csnF* coding sequence and the marker cassette-3´flanking region fusion were cloned into the cloning vector.

2.2.11 Construction of the *gfp:csnA* cassette with self-excisable phleomycin marker (pME5439)

The *gfp:csnA* plasmid was constructed in two cloning steps. In the first step the *csnA* 3' flanking region was amplified with FB111-112 (841 bp) and cloned into the *Pml*I restriction site of pME4319, resulting in pME5438. In the second step the *csnA* 5' flanking was amplified with FB113-114 (894 bp). The *csnA* coding sequence was amplified with FB115-116 (1656 bp). The 5' flanking region, the *gfp* and the *csnA* coding sequence were cloned into the *Swa*I restriction site of pME5438, resulting in pME5439 (see Figure 13). For *Aspergillus* transformation, pME5439 was enzymatically digested with *Mss*I resulting in the *gfp:csnA* construct of 9045 bp length.

2.2.12 Construction of the *gfp:csnB* cassette with self-excisable phleomycin marker (pME5441)

The *gfp:csnB* plasmid was constructed in two cloning steps. In the first step the *csnB* 3' flanking region was amplified with FB121-122 (967 bp) and cloned into the *Pml*I restriction site of pME4319, resulting in pME5440. In the second step the *csnB* 5' flanking was amplified with FB117-118 (854 bp). The *csnB* coding sequence was amplified with FB119-120 (1683 bp). The 5' flanking region, the *gfp* and the *csnB* coding sequence were cloned into the *Swa*I restriction site of pME5440, resulting in pME5441 (see Figure 13). The naturally occurring *Mss*I cutting site in the *csnB* coding sequence did not allow the *Mss*I cassette excision. Therefore, the outermost primers contained a *Swa*I half site on the 5' and a *Pml*I half site on the 3' flanking region. Thus, the 9158 bp *gfp:csnB* cassette for *Aspergillus* transformation was obtained by stepwise *Pml*I/*Swa*I digestion of the pME5441 plasmid.

2.2.13 Construction of the *csnG* complementation cassette with self-excisable phleomycin marker (pME5443)

The *csnG* complementation plasmid was constructed in two cloning steps. In the first step the 3' flanking region of *csnG* was amplified with FB123-124 (1320 bp) and cloned into the *Pml*I restriction site of pME4319, resulting in pME5442. In the second step the 5' flanking of *csnG* were amplified together with the *csnG* coding sequence with FB125-126 (2548 bp). The 5' flanking region and the *csnG* coding sequence were cloned into the *Swa*I restriction site of pME5442, resulting in pME5443 (see Figure 13). For *Aspergillus* transformation, pME5443 was enzymatically digested with *Mss*I resulting in the *csnG* complementation construct of 8766 bp length.

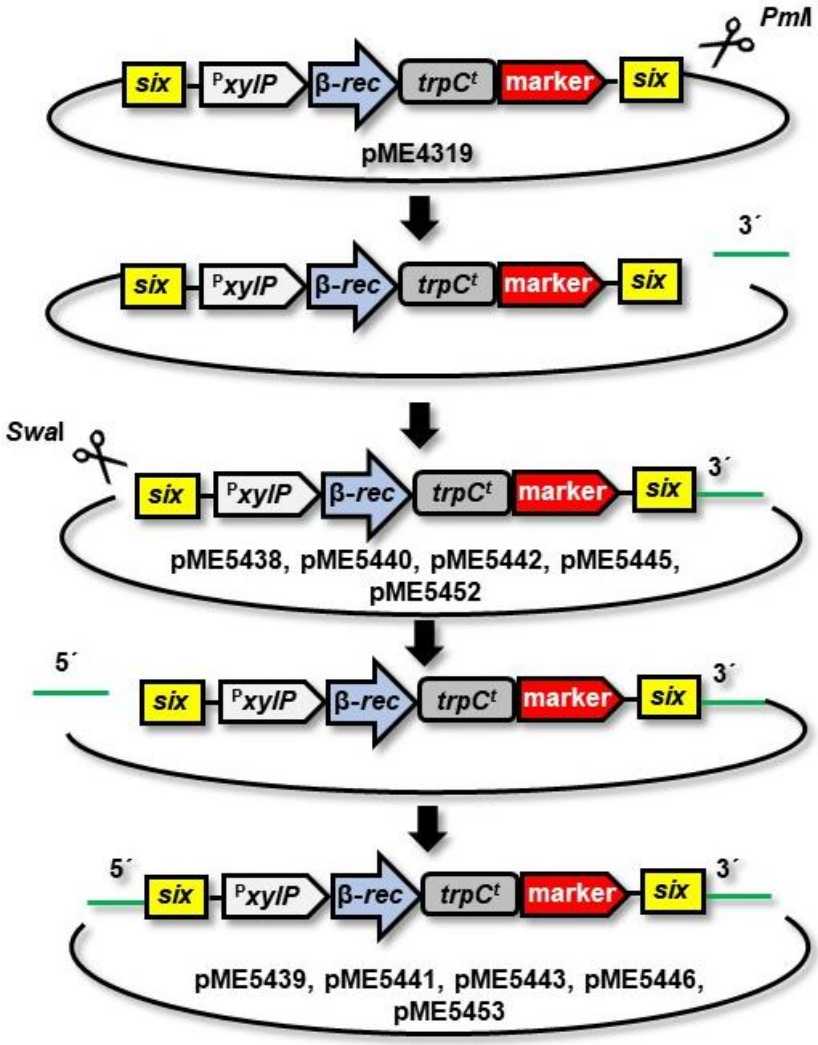

Figure 13. Scheme of the two-step construction of pME5439, pME5441, pME5443, pME5446 and pME5453 plasmids.
First the 3´ flanking region of the gene of interest was cloned into the *Pml*I restriction site of pME4319, resulting in pME5438, pME5440, pME5442, pME5445, pME5452, respectively. Then, the 5´ flanking region of the gene of interest was cloned into the *Swa*I restriction site of either the pME5438, pME5440, pME5442, pME5445 or the pME5452 plasmid, resulting in the pME5439, pME5441, pME5443, pME5446 and pME5453 plasmid, respectively.

2.2.14 Construction of the *gfp:csnB*$^{NLS2\Delta}$ cassette with self-excisable phleomycin marker (pME5444)

The plasmid was constructed in six steps fusing PCR fragments (Figure 14).
Fragment 1: PCR product of FB117-oAMK95 (1610 bp), amplified from pME5441.
Fragment 2: PCR product of FB156-FB141 (1620 bp), amplified from gDNA.
Fragment 3: PCR product of FB156-FB151 (1620 bp), where fragment 2 was used as DNA template. FB151 is a reverse primer located in the *csnB* coding sequence framing and excluding the NLS2 sequence.
Fragment 4: PCR product of FB144-JG1171 (3263 bp), amplified from AnFB97 gDNA.

Fragment 5: PCR product of FB155-FB122 (2644 bp), amplified from pME5441.
Fragment 6: fusion PCR product of fragment 1 and 3, amplified with FB117-FB151 (3220 bp).
The fragments 4, 5 and 6 were cloned into the pBluescript KS *Eco*RV cutting site, resulting in pME5444. The naturally occurring *Mss*I cutting site in the *csnB* coding sequence did not allow the *Mss*I cassette excision. Therefore, the outermost primers contained *Swa*I half site on the 5' and *Pml*I half site on the 3' flanking region. Thus, the 9137 bp *gfp:csnB*$^{NLS2\Delta}$ cassette for *Aspergillus* transformation was obtained by stepwise *Pml*I/*Swa*I digestion of the pME5444 plasmid.

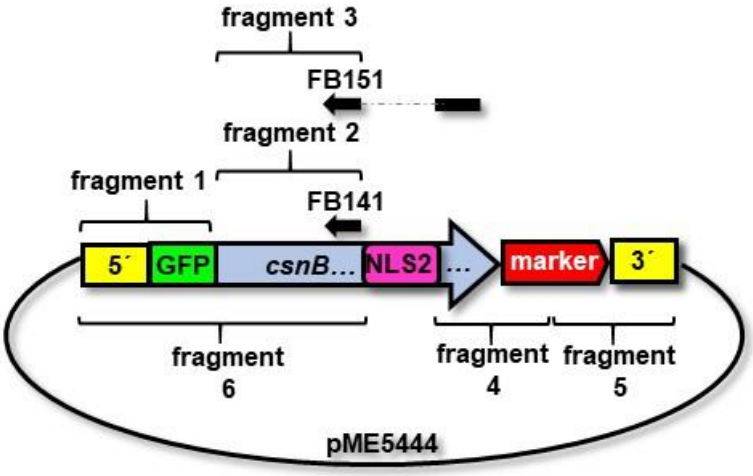

Figure 14. Scheme of the pME5444 plasmid construction.
The pME5444 plasmid was constructed from the six above listed DNA fragments, which were cloned into the *Eco*RV cutting site of the pBluescript KS plasmid backbone.

2.2.15 Construction of the *gfp:csnE* cassette with self-excisable phleomycin marker (pME5446)

The *gfp:csnE* plasmid was constructed in two cloning steps. First, the 3' flanking region of *csnE* was amplified with FB149-150 (1014 bp) and cloned into the *Pml*I restriction site of pME4319, resulting in pME5445. For the second step, the *csnE* 5' flanking region was amplified with FB145-146 (872 bp) and the *csnE* coding sequence was amplified with FB147-148 (1060 bp). The *csnE* 5' flanking region was fused to the *gfp* by PCR using FB145-oAMK95 (1628 bp) prior to cloning. In the second step the 5' flanking:*gfp* fusion fragment and *csnE* coding sequence was cloned into the *Swa*I restriction site of pME5445, resulting in pME5446 (see Figure 13). For *Aspergillus* transformation, pME5446 was enzymatically digested with *Mss*I resulting in the *gfp:csnE* construct of 8596 bp length.

2.2.16 Construction of the *gfp:csnB*$^{NLS1\Delta}$ cassette with self-excisable phleomycin marker (pME5447)

The plasmid was constructed in five steps fusing PCR fragments (Figure 15).
Fragment 1: PCR product of FB117-oAMK95 (1610 bp), amplified from pME5441.
Fragment 2: PCR product of FB156-FB154 (993 bp), amplified from gDNA.

Fragment 3: PCR product of FB156-FB157 (993 bp), where fragment 2 was used as DNA template. FB157 is a reverse primer located in the *csnB* coding sequence framing and excluding the NLS1 sequence.
Fragment 4: PCR product of FB153-FB120 (590 bp), amplified from gDNA.
Fragment 5: fusion PCR product of fragment 3 and 4 amplified with FB119-FB120 (1683 bp).
Fragments 1 and 5 were cloned into the *Swa*I cutting site of pME5440. The naturally occurring *Mss*I cutting site in the *csnB* coding sequence did not allow the *Mss*I cassette excision. Therefore, the outermost primers contained *Swa*I half site on the 5' and *Pml*I half site on the 3' flanking region. Thus, the 9058 bp *gfp:csnB*$^{NLS1\Delta}$ cassette for *Aspergillus* transformation was obtained by a stepwise *Pml*I/*Swa*I digestion of the pME5447 plasmid.

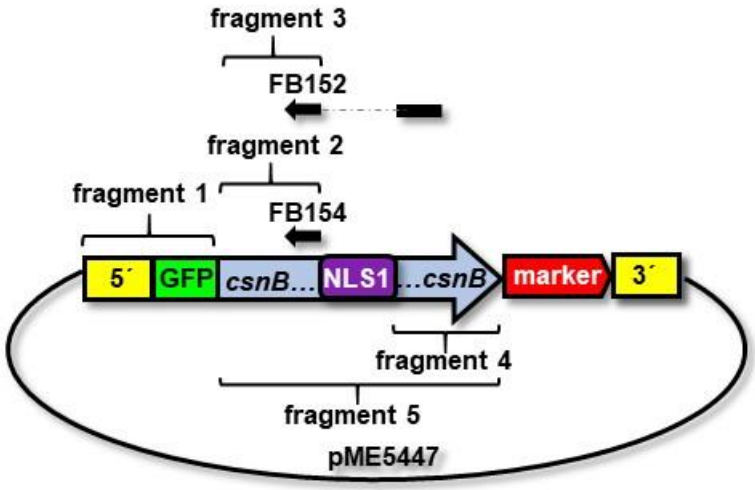

Figure 15. Scheme of the pME5447 plasmid construction.
The pME5447 plasmid was constructed from the five above listed DNA fragments, which were cloned into the *Swa*I cutting site of the pME5440 plasmid.

2.2.17 Construction of the *gfp:csnB*^{NLS2}* cassette with self-excisable phleomycin marker (pME5448)

The plasmid was constructed in five steps fusing PCR fragments (Figure 16).
Fragment 1: PCR product of FB117-oAMK95 (1610 bp), amplified from pME5441.
Fragment 2: PCR product of FB156-FB157 (1620 bp), where FB156-FB141 was used as template (see pME5444 plasmid construction). FB157 is a reverse primer located in the *csnB* coding sequence including the NLS2 sequence carrying the R739A, R740A and K743A amino acid substation mutations.
Fragment 3: PCR product of FB158-JG1171 (3263 bp), amplified from pME5441.
Fragment 5: PCR product of FB155-FB122 (2644 bp), amplified from pME5441.
Fragment 6: fusion PCR product of fragment 1 and 2, amplified with FB117-FB157 (3220 bp).
Fragments 3, 5 and 6 were cloned into the *Eco*RV cutting site of the pBluescript KS plasmid backbone. The naturally occurring *Mss*I cutting site in the *csnB* coding sequence did not allow the *Mss*I cassette excision. Therefore, the outermost primers contained *Swa*I half site on the 5' and *Pml*I half site on the 3' flanking region. Thus, the 9158 bp *gfp:csnB*^{NLS2}* cassette for

Aspergillus transformation was obtained by a stepwise *Pml*I/*Swa*I digestion of the pME5448 plasmid.

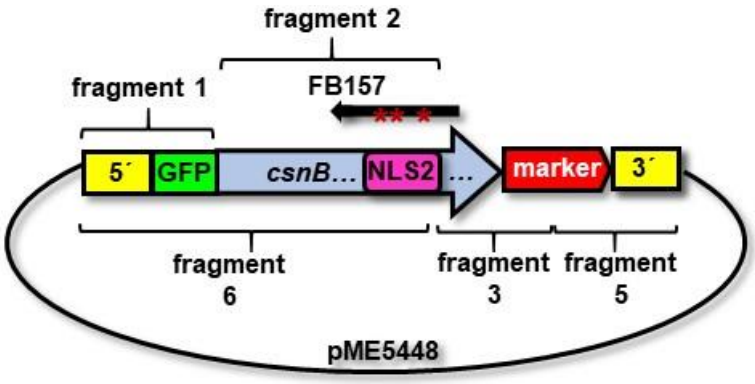

Figure 16. Scheme of pME5448 plasmid construction.
The pME5448 plasmid was constructed from the five above listed DNA fragments, which were cloned into the EcoRV cutting site of the pBluescript KS plasmid backbone.

2.2.18 Construction of the *gfp:csnB*^{NLS1}* cassette with self-excisable phleomycin marker (pME5449)

The plasmid was constructed in four steps fusing PCR fragments (Figure 17).
Fragment 1: PCR product of FB117-oAMK95 (1610 bp), amplified from pME5441.
Fragment 2: PCR product of FB156-FB159 (1074 bp), amplified from gDNA.
Fragment 3: PCR product of FB160-FB120 (597 bp), amplified from gDNA. FB160 is a forward primer located in the *csnB* coding sequence, carrying the K557T and K560T amino acid substitution mutations.
Fragment 4: fusion PCR product of fragment 1 and 2, amplified with FB117-FB159 (2684 bp).

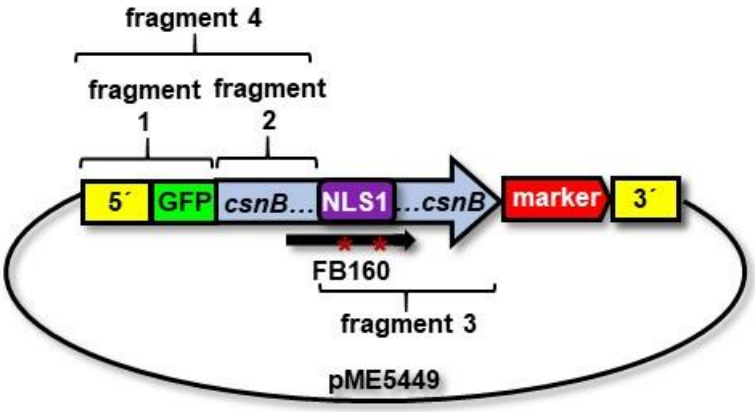

Figure 17. Scheme of the pME5449 plasmid construction.
The pME5449 plasmid was constructed from the four above listed DNA fragments, which were cloned into the *Swa*I cutting site of the pME5440 plasmid.

Fragments 3 and 4 were cloned into the *Swa*I cutting site of pME5440. The naturally occurring *Mss*I cutting site in the *csnB* coding sequence did not allow the *Mss*I cassette excision. Therefore, the outermost primers contained *Swa*I half site on the 5' and *Pml*I half site on the 3' flanking region. Thus, the 9158 bp *gfp:csnB*^{NLS1}* cassette for *Aspergillus* transformation was obtained by a stepwise *Pml*I/*Swa*I digestion of the pME5449 plasmid.

2.2.19 Construction of the *csnH* complementation cassette with self-excisable phleomycin marker (pME5453)

The *csnH* complementation plasmid was constructed in two cloning steps. In the first step the 3' flanking region of *csnH* was amplified with FB073-074 (1071 bp) and cloned into the *Pml*I restriction site of pME4319, resulting in pME5452. In the second step the 5' flanking of *csnH* was amplified together with the *csnH* coding sequence with FB071-170 (2265 bp). The 5' flanking region and the *csnH* coding sequence were cloned into the *Swa*I restriction site of pME5452, resulting in pME5453 (see Figure 13). For *Aspergillus* transformation, pME5453 was enzymatically digested with *Mss*I resulting in the *csnH* complementation construct of 8221 bp length.

2.3 Cultivation and genetic manipulations of bacteria and fungi

2.3.1 Cultivation of *Escherichia coli* strains

The bacterial cultures were cultivated overnight at 37°C in lysogeny broth medium (LB; 1% (w/v) tryptone, 0.5% (w/v) yeast extract, 1% (w/v) NaCl) under agitation or on solid agar plates supplemented with 2% (w/v) agar. For selection, the LB medium was supplemented with 100 µg/mL ampicillin (LB_{AMP} medium).

2.3.2 Transformation and selection of *Escherichia coli* strains

For all cloning events the *Escherichia coli* DH5α strain was used as recipient bacterium. The transformation of the chemical competent bacteria was carried out by following the protocol of Inoue *et al.*, 1990. The purified DNA construct and 200 µL chemical-competent *E. coli* cells were mixed and incubated for 20 minutes on ice followed by a one-minute-heat shock at 42°C. For the regeneration of the bacterial cell wall and the bacterial reproduction 800 µL fresh LB medium was added to the *E. coli* -DNA mixture and it was incubated for one hour at 37°C under agitation (Bertani, 1951). Then, different amounts of the transformed bacteria suspension were plated on LB_{AMP} medium. Approximately 1/4 of the *E. coli* cells was plated on one agar plate and the rest 3/4 of the mixture was plated on another plate and grown overnight at 37°C. The resulting newly transformed *E. coli* clones were screened by colony PCR for either the 5' or the 3' flanking region. Based on the colony PCR results, the plasmids were isolated from the positive *E. coli* clones and restriction digestion of the plasmids was carried out as additional test. Finally, the correct DNA sequence of the new plasmids was verified by Sanger sequencing.

2.3.3 Cultivation of *Aspergillus nidulans* strains

The *A. nidulans* strains were grown and maintained on minimal medium (MM), which consisted of 1% (w/v) D-glucose monohydrate, 1x AspA (7 mM KCl, 70 mM $NaNO_3$, 11.2 mM KH_2PO_4, pH 5.5), 2 mM $MgSO_4$ x 7 H_2O, 0.1% (v/v) trace elements (76 µM $ZnSO_4$, 178 µM H_3BO_4, 18 µM $FeSO_4$, 25 µM $MnCl_2$, 7.1 µM $CoCl_2$, 6.4 µM $CuSO_4$, 6.2 µM Na_2MoO_4, 174 µM EDTA, pH 6.5). All fungal strains were created in AGB552 background (Table 7) (Bayram *et al.*, 2012). Accordingly, the MM was supplemented with 1 µg/mL para-aminobenzoic acid (PABA), resulting in MM_{PABA}. The strains were vegetatively grown in liquid MM_{PABA} under agitation for 20 hours at 37°C. For surface cultures, maintenance and prior to all experiments, conidiospores of the strains were plated and grown for five days in light at 37°C on the MM_{PABA} supplemented with 2% (w/v) agar. The conidiospores were harvested in NaCl-Tween80 solution (0.5% (w/v) NaCl, 0.01% (v/v) Tween80) and for all experiments, these five days old, freshly grown conidiospores were used.

2.3.4 Cultivation of fungal strains for the recyclable marker cassette excision

The excision of the recyclable marker cassette occurred by growing the fungal clones on X/G_{PABA} medium for five days at 37°C. The X/G_{PABA} medium is a modified MM_{PABA} containing 0.5% (w/v) D-xylose and 0.5% (w/v) D-glucose monohydrate. The resulting clones were isolated by colony picking and streaking out on X/G_{PABA} medium and grown for five days at 37°C. After five days, a new colony was picked and isolated from this plate and plated on X/G_{PABA} medium. The procedure was repeated altogether three times for marker excision. The genetic locus of interest of the resulting fungal strains was not interrupted by any resistance genes, only the β-recombinase recognition `six´ site remained after the marker excision

2.3.5 Transformation and selection of *Aspergillus nidulans* strains

The *Aspergillus* transformations were performed according to Punt and van den Hondel with some modifications (Punt and van den Hondel, 1992). An overnight fungal culture of the recipient *A. nidulans* strain was harvested by filtration and the mycelia was washed with citrate buffer (150 mM KCl, 580 mM NaCl, 50 mM Na-citrate, pH 5.5). The protoplastation occurred during incubation of the mycelia in the protoplastation mixture for 120 minutes under gentle agitation at 30°C. The protoplasting enzyme mixture consisted of 30 mg/mL VinoTaste® Pro and 15 mg/mL lysozyme dissolved in 15-50 mL citrate buffer in approximately 1:1 buffer-wet cell mass ratio. The protoplasts were then harvested by filtering and were washed with ice-cold STC1700 buffer containing sorbitol to provide isotonic conditions for the protoplasts (1.2 M D-sorbitol, 10 mM Tris-HCl pH 5.5, 50 mM $CaCl_2$ x 2 H_2O, 35 mM NaCl). The protoplasts were pelleted by centrifugation for 15 minutes at 2700 rpm and the supernatant was discarded. The washing and centrifugation steps were repeated one more time. Then, 2-10 µg DNA resuspended in maximum 30 µL ddH_2O was added to the protoplasts. Protoplasts without addition of DNA served as negative control. The protoplasts were incubated for 25 minutes on ice, then 500 and 800 µL PEG4000 (10 mM Tris-HCl pH 7.5, 50 mM $CaCl_2$, 60% (w/v) polyethylene glycol 4000) was added step-wise to the protoplasts and mixed gently. After 35 minutes incubation above ice, the protoplasts were washed with STC1700 buffer and pelleted by centrifugation for 15 minutes at 2700 rpm. The

resuspended protoplasts were plated and grown on selective, isotonic sorbitol-MM_{PABA} agar plates, where the MM_{PABA} medium was supplemented with 1.2 M D-sorbitol to provide isotonic conditions. The protoplasts were regenerated growing for 5 days at 37°C. The sorbitol-MM_{PABA} was supplemented with either 140 µg/mL nourseothricin or 40 µg/mL phleomycin for selection pressure on the transformed clones. Then, selected clones were isolated by colony picking and repeated streaking and growing on selective MM_{PABA} medium for 5 days at 37°C. The colony picking and isolation was repeated at least three times on selective medium. The genotype of the resulting new fungal strains was verified by Southern hybridization and in several cases by additional PCR reactions and Sanger sequencing.

2.4 General fungal strain construction strategies and excision of the recyclable marker cassette

The excisable marker system containing the phleomycin (*ble*) or the nourseothricin (*nat1*) biosynthesis genes (Drocourt *et al*., 1990; Kück and Hoff, 2006) was used for *A. nidulans* strain construction, and fungal strains after marker recycling were used for all experiments, if not specified otherwise. All fungal strains were created by the integration of the *Aspergillus* transformation cassettes by homologous recombination at the genomic locus of the gene of interest in one single copy (Figure 18). All genes were driven by their native endogenous promoter, if not specified otherwise. For fluorescence microscopy experiments *A. nidulans* strains were constructed, which express RFP-Histone 2A. Therefore, the pME3173 plasmid with the nourseothricin marker was ectopically integrated into the genome. The selective marker cassette of pME3173 is not excisable, thus, the resulting fungal strains used for fluorescence microscopy contained the selective marker. All fungal strains used in this study are listed in Table 7.

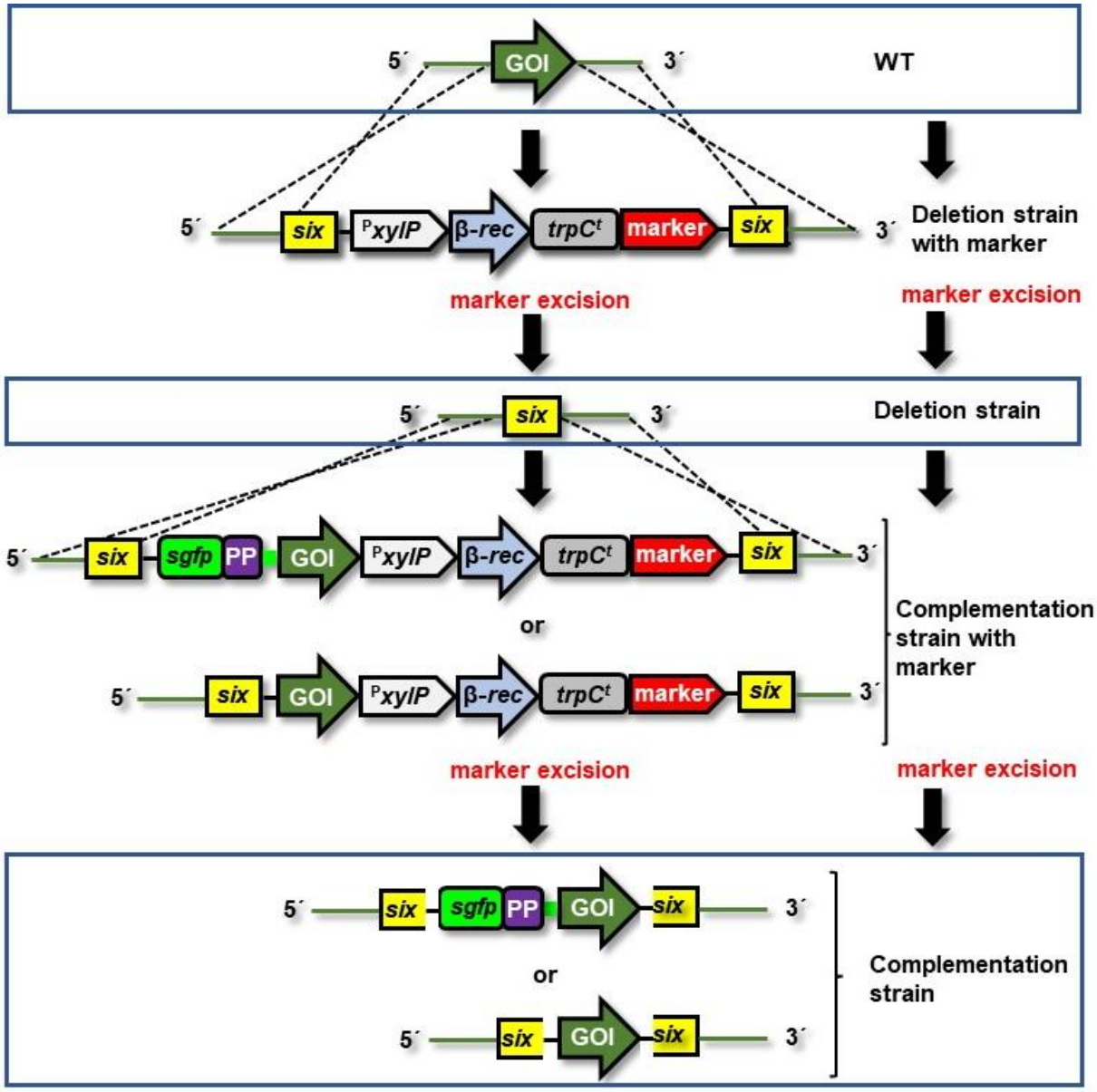

Figure 18. Workflow of fungal deletion and complementation strain construction using the recyclable marker system.
If not specified otherwise, for all fungal strain constructions the recyclable marker cassette was used, which contains two flanking ß-recombinase recognition sites (`six´ sites), a xylose promoter ($^{P}$*xylP*), the ß-recombinase gene (ß-rec), a *trpC* terminator (*trpC*$^{t}$) and the *bleomycin* or *nourseothricin* marker gene (marker) to replace the gene of interest (GOI). After marker recycling, only an approximately 90 bp long `six´ recognition site remained in the genetic locus. In case of strains producing GFP, the *gfp* sequence is fused to a precision protease sequence (PP), which is C-terminally fused to a linker sequence (depicted as thick light green line between PP and GOI), which provides flexibility to the GFP-tag.

Table 7. List of *Aspergillus nidulans* strains constructed and applied in this work.
Glossary: *ble*: phleomycin gene, *nat1*: nourseothricin gene, ^{P}promoter, resistance gene^{R}, terminator^{t}, p.c.: personal communication, cl.: clone. Descriptions are only given for those strains, which were used for experiments. The strains without description served as parental strains for the strain construction.

Strain name (alternative name)	Description	Parental strain+ plasmid	Genotype	Reference
AGB552	wild type		Δ*nkuA::argB;pabaA1;yA2;veA*$^{+}$	Bayram *et al.*, 2012
AGB1111	Δ*csnE*		Δ*nkuA::argB;pabaA1;yA2;veA*$^{+}$ *;*Δ*csnE::six*	(Köhler *et al.*, 2019)
AGB1584 (CM48 cl.8)	WT,*gfp:csnD*	AGB552+ pME4702	Δ*nkuA::argB;pabaA1;yA2;veA*$^{+}$ *;*^{P}*csnD:gfp: csnD:csnD*^{t}*:six*	Meister, p.c.
AGB596	GFP over-expression		Δ*nkuA*::*argB;pabaA1;yA2;veA*$^{+}$ *;*^{P}*gpdA:gfp::phleo*^{R}	Bayram *et al.*, 2012
AnFB35 cl.3		AGB1111+ pME4702	Δ*nkuA::argB;pabaA1;yA2;veA*$^{+}$ *;*Δ*csnE*::*six;* ^{P}*csnD:gfp:csnD:csnD*^{t}*:nat1*^{R}	This study
AnFB36 cl.6		AGB1111+ pME5437	Δ*nkuA::argB;pabaA1;yA2;veA*$^{+}$ *;*Δ*csnE*::*six;* ^{P}*csnF:gfp:csnF:csnF*^{t}*:ble*^{R}	This study
AGB1585 (AnFB37 cl.3)	Δ*csnE, gfp:csnD*	AnFB35	Δ*nkuA::argB;pabaA1;yA2;veA*$^{+}$ *;*Δ*csnE*::*six;* ^{P}*csnD:gfp:csnD:csnD*^{t}*:six*	This study
AGB1586 (AnFB38 cl.6)	Δ*csnE, gfp:csnF*	AnFB36	Δ*nkuA::argB;pabaA1;yA2;veA*$^{+}$ *;*Δ*csnE*::*six;* ^{P}*csnF:gfp:csnF:csnF*^{t}*:six*	This study
AnFB39 cl.1		AGB1585 (AnFB37)+ pME5430	Δ*nkuA::argB;pabaA1;yA2;veA*$^{+}$ *;*Δ*csnE*::*six;* ^{P}*csnD:gfp:csnD:csnD*^{t}*:six;* Δ*csnA*:*ble*^{R}	This study
AnFB40 cl.1		AGB1585 (AnFB37)+ pME5431	Δ*nkuA::argB;pabaA1;yA2;veA*$^{+}$ *;*Δ*csnE*::*six;* ^{P}*csnD:gfp:csnD:csnD*^{t}*:six;* Δ*csnB*:*ble*^{R}	This study
AnFB41 cl.1/1		AGB1585 (AnFB37)+ pME5432	Δ*nkuA::argB;pabaA1;yA2;veA*$^{+}$ *;*Δ*csnE*::*six;* ^{P}*csnD:gfp:csnD:csnD*^{t}*:six;* Δ*csnC*:*ble*^{R}	This study
AnFB42 cl.1		AGB1586 (AnFB38)+ pME5433	Δ*nkuA::argB;pabaA1;yA2;veA*$^{+}$ *;*Δ*csnE*::*six;* ^{P}*csnF:gfp:csnF:csnF*^{t}*:six;* Δ*csnD*:*ble*^{R}	This study
AnFB43 cl.3		AGB1585 (AnFB37)+ pME5434	Δ*nkuA::argB;pabaA1;yA2;veA*$^{+}$ *;*Δ*csnE*::*six;* ^{P}*csnD:gfp:csnD:csnD*^{t}*:six;* Δ*csnF*:*ble*^{R}	This study
AnFB44 cl.1		AGB1585 (AnFB37)+ pME5435	Δ*nkuA::argB;pabaA1;yA2;veA*$^{+}$ *;*Δ*csnE*::*six;* ^{P}*csnD:gfp:csnD:csnD*^{t}*:six;* Δ*csnG*:*ble*^{R}	This study
AnFB45 cl.2		AGB1585 (AnFB37)+ pME5436	Δ*nkuA::argB;pabaA1;yA2;veA*$^{+}$ *;*Δ*csnE*::*six;* ^{P}*csnD:gfp:csnD:csnD*^{t}*:six;* Δ*csnH*:*ble*^{R}	This study
AGB1587 (AnFB46 cl.1)	Δ*csnA*Δ*csnE, gfp:csnD*	AnFB39	Δ*nkuA::argB;pabaA1;yA2;veA*$^{+}$ *;*Δ*csnE*::*six;*	This study

			^{P}csnD:gfp:csnD:csnD^{t}:six; ΔcsnA::six	
AGB1588 (AnFB47 cl.1)	*ΔcsnBΔcsnE, gfp:csnD*	AnFB40	*ΔnkuA::argB;pabaA1;yA2;veA^{+} ;ΔcsnE::six; ^{P}csnD:gfp:csnD:csnD^{t}:six; ΔcsnB::six*	This study
AGB1589 (AnFB48 cl.1/1)	*ΔcsnCΔcsnE, gfp:csnD*	AnFB41	*ΔnkuA::argB;pabaA1;yA2;veA^{+} ;ΔcsnE::six; ^{P}csnD:gfp:csnD:csnD^{t}:six; ΔcsnC::six*	This study
AGB1590 (AnFB49 cl.1)	*ΔcsnDΔcsnE, gfp:csnF*	AnFB42	*ΔnkuA::argB;pabaA1;yA2;veA^{+} ;ΔcsnE::six; ^{P}csnF:gfp:csnF:csnF^{t}:six; ΔcsnD::six*	This study
AGB1591 (AnFB50 cl.3)	*ΔcsnFΔcsnE, gfp:csnD*	AnFB43	*ΔnkuA::argB;pabaA1;yA2;veA^{+} ;ΔcsnE::six; ^{P}csnD:gfp:csnD:csnD^{t}:six; ΔcsnF::six*	This study
AGB1592 (AnFB51 cl.1)	*ΔcsnGΔcsnE, gfp:csnD*	AnFB44	*ΔnkuA::argB;pabaA1;yA2;veA^{+} ;ΔcsnE::six; ^{P}csnD:gfp:csnD:csnD^{t}:six; ΔcsnG::six*	This study
AGB1593 (AnFB52 cl.2)	*ΔcsnHΔcsnE, gfp:csnD*	AnFB45	*ΔnkuA::argB;pabaA1;yA2;veA^{+} ;ΔcsnE::six; ^{P}csnD:gfp:csnD:csnD^{t}:six; ΔcsnH::six*	This study
AnFB53 cl.1		AGB552+ pME5437	*ΔnkuA::argB;pabaA1;yA2;veA^{+} ;^{P}csnF:gfp: csnF:csnF^{t}:ble^{R}*	This study
AGB1594 (AnFB54 cl.1)	WT,*gfp:csnF*	AnFB53	*ΔnkuA::argB;pabaA1;yA2;veA^{+} ;^{P}csnF:gfp: csnF:csnF^{t}:six*	This study
AnFB57 cl.7		AGB552+ pME5430	*ΔnkuA::argB;pabaA1;yA2;veA^{+} ;ΔcsnA:: ble^{R}*	This study
AnFB58 cl.1		AGB552+ pME5431	*ΔnkuA::argB;pabaA1;yA2;veA^{+} ;ΔcsnB:: ble^{R}*	This study
AnFB60 cl.5		AGB552+ pME5433	*ΔnkuA::argB;pabaA1;yA2;veA^{+} ;ΔcsnD:: ble^{R}*	This study
AnFB61 cl.2		AGB552+ pME5434	*ΔnkuA::argB;pabaA1;yA2;veA^{+} ;ΔcsnF:: ble^{R}*	This study
AnFB62 cl.7		AGB552+ pME5435	*ΔnkuA::argB;pabaA1;yA2;veA^{+} ;ΔcsnG:: ble^{R}*	This study
AnFB63 cl.6		AGB552+ pME5436	*ΔnkuA::argB;pabaA1;yA2;veA^{+} ;ΔcsnH:: ble^{R}*	This study
AnFB64 cl.3		AGB1111+ pME5430	*ΔnkuA::argB;pabaA1;yA2;veA^{+} ;ΔcsnE::six;ΔcsnA::ble^{R}*	This study
AnFB65 cl.4		AGB1111+ pME5431	*ΔnkuA::argB;pabaA1;yA2;veA^{+} ;ΔcsnE::six;ΔcsnB::ble^{R}*	This study
AnFB66 cl.3		AGB1111+ pME5432	*ΔnkuA::argB;pabaA1;yA2;veA^{+} ;ΔcsnE::six;ΔcsnC::ble^{R}*	This study
AnFB67 cl.5		AGB1111+ pME5433	*ΔnkuA::argB;pabaA1;yA2;veA^{+} ;ΔcsnE::six;ΔcsnD::ble^{R}*	This study
AnFB68 cl.3		AGB1111+ pME5434	*ΔnkuA::argB;pabaA1;yA2;veA^{+} ;ΔcsnE::six;ΔcsnF::ble^{R}*	This study

AnFB69 cl.2		AGB1111+ pME5435	Δ*nkuA::argB;pabaA1;yA2;veA*$^{+}$ *;ΔcsnE::six;ΔcsnG::ble*^{R}	This study
AnFB70 cl.3		AGB1111+ pME5436	Δ*nkuA::argB;pabaA1;yA2;veA*$^{+}$ *;ΔcsnE::six;ΔcsnH::ble*^{R}	This study
AGB1595 (AnFB71 cl.3)	Δ*csnA*Δ*csnE*	AnFB64	Δ*nkuA::argB;pabaA1;yA2;veA*$^{+}$ *;ΔcsnE::six;ΔcsnA::six*	This study
AGB1596 (AnFB72 cl.4)	Δ*csnB*Δ*csnE*	AnFB65	Δ*nkuA::argB;pabaA1;yA2;veA*$^{+}$ *;ΔcsnE::six;ΔcsnB::six*	This study
AGB1597 (AnFB73 cl.3)	Δ*csnC*Δ*csnE*	AnFB66	Δ*nkuA::argB;pabaA1;yA2;veA*$^{+}$ *;ΔcsnE::six;ΔcsnC::six*	This study
AGB1598 (AnFB74 cl.5)	Δ*csnD*Δ*csnE*	AnFB67	Δ*nkuA::argB;pabaA1;yA2;veA*$^{+}$ *;ΔcsnE::six;ΔcsnD::six*	This study
AGB1599 (AnFB75 cl.3)	Δ*csnF*Δ*csnE*	AnFB68	Δ*nkuA::argB;pabaA1;yA2;veA*$^{+}$ *;ΔcsnE::six;ΔcsnF::six*	This study
AGB1600 (AnFB76 cl.2)	Δ*csnG*Δ*csnE*	AnFB69	Δ*nkuA::argB;pabaA1;yA2;veA*$^{+}$ *;ΔcsnE::six;ΔcsnG::six*	This study
AGB1601 (AnFB77 cl.3)	Δ*csnH*Δ*csnE*	AnFB70	Δ*nkuA::argB;pabaA1;yA2;veA*$^{+}$ *;ΔcsnE::six;ΔcsnH::six*	This study
AnFB78 cl.4		AGB1595 (AnFB71)+ pME5441	Δ*nkuA::argB;pabaA1;yA2;veA*$^{+}$ *;ΔcsnE::six;ΔcsnA::six;*^{P}*csnB:gfp:csnB:csnB*^{t}*:ble*^{R}	This study
AnFB79 cl.2		AGB1596 (AnFB72)+ pME5439	Δ*nkuA::argB;pabaA1;yA2;veA*$^{+}$ *;ΔcsnE::six;ΔcsnB::six;*^{P}*csnA:gfp:csnA:csnA*^{t}*:ble*^{R}	This study
AnFB80 cl.2		AGB1597 (AnFB73)+ pME5439	Δ*nkuA::argB;pabaA1;yA2;veA*$^{+}$ *;ΔcsnE::six;ΔcsnC::six;*^{P}*csnA:gfp:csnA:csnA*^{t}*:ble*^{R}	This study
AnFB81 cl.2		AGB1598 (AnFB74)+ pME5439	Δ*nkuA::argB;pabaA1;yA2;veA*$^{+}$ *;ΔcsnE::six;ΔcsnD::six;*^{P}*csnA:gfp:csnA:csnA*^{t}*:ble*^{R}	This study
AnFB82 cl.3		AGB1599 (AnFB75)+ pME5439	Δ*nkuA::argB;pabaA1;yA2;veA*$^{+}$ *;ΔcsnE::six;ΔcsnF::six;*^{P}*csnA:gfp:csnA:csnA*^{t}*:ble*^{R}	This study
AnFB83 cl.1		AGB1600 (AnFB76)+ pME5439	Δ*nkuA::argB;pabaA1;yA2;veA*$^{+}$ *;ΔcsnE::six;ΔcsnG::six;*^{P}*csnA:gfp:csnA:csnA*^{t}*:ble*^{R}	This study
AnFB84 cl.2		AGB1601 (AnFB77)+ pME5439	Δ*nkuA::argB;pabaA1;yA2;veA*$^{+}$ *;ΔcsnE::six;ΔcsnH::six;*^{P}*csnA:gfp:csnA:csnA*^{t}*:ble*^{R}	This study
AnFB85 cl.1		AGB1111+ pME5439	Δ*nkuA::argB;pabaA1;yA2;veA*$^{+}$ *;ΔcsnE::six;* ^{P}*csnA:gfp:csnA:csnA*^{t}*:ble*^{R}	This study
AnFB86 cl.5		AGB552+ pME5439	Δ*nkuA::argB;pabaA1;yA2;veA*$^{+}$ *;* ^{P}*csnA:gfp:csnA:csnA*^{t}*:ble*^{R}	This study
AGB1602 (AnFB87 cl.4)	Δ*csnA*Δ*csnE*, *gfp:csnB*	AnFB78	Δ*nkuA::argB;pabaA1;yA2;veA*$^{+}$ *;ΔcsnE::six;ΔcsnA::six;*^{P}*csnB:gfp:csnB:csnB*^{t}*:six*	This study
AGB1603 (AnFB88 cl.2)	Δ*csnB*Δ*csnE*, *gfp:csnA*	AnFB79	Δ*nkuA::argB;pabaA1;yA2;veA*$^{+}$ *;ΔcsnE::six;ΔcsnB::six;*^{P}*csnA:gfp:csnA:csnA*^{t}*:six*	This study
AGB1604 (AnFB89 cl.2)	Δ*csnC*Δ*csnE*, *gfp:csnA*	AnFB80	Δ*nkuA::argB;pabaA1;yA2;veA*$^{+}$ *;ΔcsnE::six;ΔcsnC::six;*^{P}*csnA:gfp:csnA:csnA*^{t}*:six*	This study
AGB1605 (AnFB90 cl.2)	Δ*csnD*Δ*csnE*, *gfp:csnA*	AnFB81	Δ*nkuA::argB;pabaA1;yA2;veA*$^{+}$ *;ΔcsnE::six;ΔcsnD::six;*^{P}*csnA:gfp:csnA:csnA*^{t}*:six*	This study
AGB1606 (AnFB91 cl.3)	Δ*csnF*Δ*csnE*, *gfp:csnA*	AnFB82	Δ*nkuA::argB;pabaA1;yA2;veA*$^{+}$ *;ΔcsnE::six;ΔcsnF::six;*^{P}*csnA:gfp:csnA:csnA*^{t}*:six*	This study

AGB1607 (AnFB92 cl.1)	Δ*csnG*Δ*csnE*,*gfp:csnA*	AnFB83	Δ*nkuA::argB;pabaA1;yA2;veA*$^{+}$*;*Δ*csnE*::*six;*Δ*csnG::six;*^{P}*csnA:gfp:csnA:csnA*^{t}*:six*	This study
AGB1608 (AnFB93 cl.2)	Δ*csnH*Δ*csnE*, *gfp:csnA*	AnFB84	Δ*nkuA::argB;pabaA1;yA2;veA*$^{+}$*;*Δ*csnE*::*six;*Δ*csnH::six;*^{P}*csnA:gfp:csnA:csnA*^{t}*:six*	This study
AGB1609 (AnFB94 cl.1)	Δ*csnE*, *gfp:csnA*	AnFB85	Δ*nkuA::argB;pabaA1;yA2;veA*$^{+}$*;*Δ*csnE*::*six;* ^{P}*csnA:gfp:csnA:csnA*^{t}*:six*	This study
AGB1610 (AnFB95 cl.5)	WT, *gfp:csnA*	AnFB86	Δ*nkuA::argB;pabaA1;yA2;veA*$^{+}$*;*^{P}*csnA:gfp:csnA:csnA*^{t}*:six*	This study
AnFB96 cl.6		AGB1111+ pME5441	Δ*nkuA::argB;pabaA1;yA2;veA*$^{+}$*;*Δ*csnE*::*six;* ^{P}*csnB:gfp:csnB:csnB*^{t}*:ble*^{R}	This study
AnFB97 cl.1		AGB552+ pME5441	Δ*nkuA::argB;pabaA1;yA2;veA*$^{+}$*;*^{P}*csnB:gfp:csnB:csnB*^{t}*:ble*^{R}	This study
AGB1611 (AnFB98 cl.6)	Δ*csnE*, *gfp:csnB*	AnFB96	Δ*nkuA::argB;pabaA1;yA2;veA*$^{+}$*;*Δ*csnE*::*six;* ^{P}*csnB:gfp:csnB:csnB*^{t}*:six*	This study
AGB1612 (AnFB99 cl.1)	WT, *gfp:csnB*	AnFB97	Δ*nkuA::argB;pabaA1;yA2;veA*$^{+}$*;*^{P}*csnB:gfp:csnB:csnB*^{t}*:six*	This study
AGB1613 (AnFB101 cl.2)	Δ*csnF*	AnFB61	Δ*nkuA::argB;pabaA1;yA2;veA*$^{+}$*;*Δ*csnF*::*six*	This study
AGB1614 (AnFB105 cl.1)	Δ*csnB*	AnFB58	Δ*nkuA::argB;pabaA1;yA2;veA*$^{+}$*;*Δ*csnB*::*six*	This study
AGB1615 (AnFB106 cl.5)	Δ*csnD*	AnFB60	Δ*nkuA::argB;pabaA1;yA2;veA*$^{+}$*;*Δ*csnD*::*six*	This study
AGB1616 (AnFB107 cl.6)	Δ*csnH*	AnFB63	Δ*nkuA::argB;pabaA1;yA2;veA*$^{+}$*;*Δ*csnH*::*six*	This study
AGB1617 (AnFB109 cl.7)	Δ*csnA*	AnFB57	Δ*nkuA::argB;pabaA1;yA2;veA*$^{+}$*;*Δ*csnA*::*six*	This study
AGB1618 (AnFB111 cl.7)	Δ*csnG*	AnFB62	Δ*nkuA::argB;pabaA1;yA2;veA*$^{+}$*;*Δ*csnG*::*six*	This study
AGB1619 (AnFB115 cl.3)	Δ*csnA*Δ*csnE*, *gfp:csnB, rfp:h2a*	AGB1602 (AnFB87)+ pME3173	Δ*nkuA::argB;pabaA1;yA2;veA*$^{+}$*;*Δ*csnE*::*six;*Δ*csnA::six;*^{P}*csnB:gfp:csnB:csnB*^{t}*:six;*^{P}*gpdA:mrfp:h2A:hisB*^{t}*:nat1*^{R}	This study
AGB1620 (AnFB117 cl.4)	WT, *gfp:csnA, rfp:h2a*	AGB1610 (AnFB95)+ pME3173	Δ*nkuA::argB;pabaA1;yA2;veA*$^{+}$*;*^{P}*csnA:gfp:csnA:csnA*^{t}*:six;*^{P}*gpdA:mrfp:h2A:hisB*^{t}*:nat1*^{R}	This study
AGB1621 (AnFB120 cl.1)	WT, *gfp:csnD, rfp:h2a*	AGB1584 (CM48)+ pME3173	Δ*nkuA::argB;pabaA1;yA2;veA*$^{+}$*;*^{P}*csnD:gfp:csnD:csnD*^{t}*:six;*^{P}*gpdA:mrfp:h2A:hisB*^{t}*:nat1*^{R}	This study
AGB1622 (AnFB136 cl.1)	Δ*csnB*Δ*csnE*, *gfp:csnD, rfp:h2a*	AGB1588 (AnFB47)+ pME3173	Δ*nkuA::argB;pabaA1;yA2;veA*$^{+}$*;*Δ*csnE*::*six;* ^{P}*csnD:gfp:csnD:csnD*^{t}*:six;* Δ*csnB::six;*^{P}*gpdA:mrfp:h2A:hisB*^{t}*:nat1*^{R}	This study
AGB1623 (AnFB137 cl.1)	Δ*csnB*Δ*csnE*, *gfp:csnA, rfp:h2a*	AGB1603 (AnFB88)+ pME3173	Δ*nkuA::argB;pabaA1;yA2;veA*$^{+}$*;*Δ*csnE*::*six;*Δ*csnB::six;*^{P}*csnA:gfp:csnA:csnA*^{t}*:six;*^{P}*gpdA:mrfp:h2A:hisB*^{t}*:nat1*^{R}	This study
AnFB139 cl.3		AGB1614 (AnFB105) + pME5441	Δ*nkuA::argB;pabaA1;yA2;veA*$^{+}$*;*Δ*csnB*::*six::*^{P}*csnB:gfp:csnB:csnB*^{t}*:ble*^{R}	This study

AGB1624 (AnFB140 cl.3)	Δ*csnB:: gfp:csnB*	AnFB139	Δ*nkuA::argB;pabaA1;yA2;veA*$^{+}$ *;ΔcsnB::six::*^{P}*csnB:gfp:csnB:csnB*^{t}*:six*	This study
AnFB141 cl.16		AGB552+pME5446	Δ*nkuA::argB;pabaA1;yA2;veA*$^{+}$ *;* ^{P}*csnE:gfp:csnE:csnE*^{t}*:: ble*^{R}	This study
AGB1625 (AnFB142 cl.16)	WT, *gfp:csnE*	AnFB141	Δ*nkuA::argB;pabaA1;yA2;veA*$^{+}$ *;* ^{P}*csnE:gfp:csnE:csnE*^{t}*:six*	This study
AnFB143 cl.2		AGB1111+pME5446	Δ*nkuA::argB;pabaA1;yA2;veA*$^{+}$ *;ΔcsnE::six::*^{P}*csnE:gfp:csnE:csnE*^{t}*:ble*^{R}	This study
AGB1626 (AnFB144 cl.2)	Δ*csnE:: gfp:csnE*	AnFB143	Δ*nkuA::argB;pabaA1;yA2;veA*$^{+}$ *;ΔcsnE::six::*^{P}*csnE:gfp:csnE:csnE*^{t}*:six*	This study
AnFB145 cl.4		AGB1614 (AnFB105) + pME5446	Δ*nkuA::argB;pabaA1;yA2;veA*$^{+}$ *;ΔcsnB::six;* ^{P}*csnE:gfp:csnE:csnE*^{t}*:ble*^{R}	This study
AGB1627 (AnFB146 cl.4)	Δ*csnB; gfp:csnE*	AnFB145	Δ*nkuA::argB;pabaA1;yA2;veA*$^{+}$ *;ΔcsnB::six;* ^{P}*csnE:gfp:csnE:csnE*^{t}*:six*	This study
AnFB156 cl.1		AGB1617 (AnFB109) + pME5439	Δ*nkuA::argB;pabaA1;yA2;veA*$^{+}$ *;ΔcsnA::six::*^{P}*csnA:gfp:csnA:csnA*^{t}*:ble*^{R}	This study
AGB1628 (AnFB157 cl.1)	Δ*csnA:: gfp:csnA*	AnFB156	Δ*nkuA::argB;pabaA1;yA2;veA*$^{+}$ *;ΔcsnA::six::*^{P}*csnA:gfp:csnA:csnA*^{t}*:six*	This study
AnFB158 cl.21		AGB1613 (AnFB101) + pME5437	Δ*nkuA::argB;pabaA1;yA2;veA*$^{+}$ *;ΔcsnF::six::*^{P}*csnF:gfp:csnF:csnF*^{t}*:ble*^{R}	This study
AGB1629 (AnFB159 cl.21)	Δ*csnF:: gfp:csnF*	AnFB158	Δ*nkuA::argB;pabaA1;yA2;veA*$^{+}$ *;ΔcsnF::six::*^{P}*csnF:gfp:csnF:csnF*^{t}*:six*	This study
AnFB160 cl.1		AGB1615 (AnFB106) + pME4702	Δ*nkuA::argB;pabaA1;yA2;veA*$^{+}$ *;ΔcsnD::six::*^{P}*csnD:gfp:csnD:csnD*^{t}*:ble*^{R}	This study
AGB1630 (AnFB161 cl.1)	Δ*csnD:: gfp:csnD*	AnFB160	Δ*nkuA::argB;pabaA1;yA2;veA*$^{+}$ *;ΔcsnD::six::*^{P}*csnD:gfp:csnD:csnD*^{t}*:six*	This study
AnFB162 cl.5		AGB1614 (AnFB105) + pME5444	Δ*nkuA::argB;pabaA1;yA2;veA*$^{+}$ *;ΔcsnB::six::*^{P}*csnB:gfp:csnB*$^{NLS2\Delta}$*:csnB*^{t}*:ble*^{R}	This study
AGB1631 (AnFB163 cl.5)	Δ*csnB*:: *gfp:csnB*$^{\Delta NLS2}$	AnFB162	Δ*nkuA::argB;pabaA1;yA2;veA*$^{+}$ *;ΔcsnB::six::*^{P}*csnB:gfp:csnB*$^{NLS2\Delta}$*:csnB*^{t}*:six*	This study
AnFB164 cl.1		AGB1614 (AnFB105) + pME5447	Δ*nkuA::argB;pabaA1;yA2;veA*$^{+}$ *;ΔcsnB::six::*^{P}*csnB:gfp:csnB*$^{NLS1\Delta}$*:csnB*^{t}*:ble*^{R}	This study
AGB1632 (AnFB165 cl.1)	Δ*csnB*:: *gfp:csnB*$^{\Delta NLS1}$	AnFB164	Δ*nkuA::argB;pabaA1;yA2;veA*$^{+}$ *;ΔcsnB::six::*^{P}*csnB:gfp:csnB*$^{NLS1\Delta}$*:csnB*^{t}*:six*	This study
AnFB166 cl.5		AGB1614 (AnFB105) + pME5448	Δ*nkuA::argB;pabaA1;yA2;veA*$^{+}$ *;ΔcsnB::six::*^{P}*csnB:gfp:csnB*$^{NLS2(R739A,R740A,K743A)}$*:csnB*^{t}*: ble*^{R}	This study
AGB1633 (AnFB167 cl.5)	Δ*csnB*:: *gfp:csnB*^{*NLS2}	AnFB166	Δ*nkuA::argB;pabaA1;yA2;veA*$^{+}$ *;ΔcsnB::six::*^{P}*csnB:gfp:csnB*$^{NLS2(R739A,R740A,K743A)}$*:csnB*^{t}*: six*	This study

AnFB168 cl.3		AGB1614 (AnFB105) + pME5449	Δ*nkuA::argB;pabaA1;yA2;veA*$^{+}$ *;ΔcsnB::six::*^{P}*csnB:gfp:csnB*$^{NLS\ 1(K557T,K560T)}$*:csnB*^{t}*:ble*^{R}	This study
AGB1634 (AnFB169 cl.3)	Δ*csnB*:: *gfp:csnB*^{*NLS1}	AnFB168	Δ*nkuA::argB;pabaA1;yA2;veA*$^{+}$ *;ΔcsnB::six::*^{P}*csnB:gfp:csnB*$^{NLS\ 1(K557T,K560T)}$*:csnB*^{t}*:six*	This study
AnFB182 cl.14		AGB1616 (AnFB107) + pME5453	Δ*nkuA::argB;pabaA1;yA2;veA*$^{+}$ *;ΔcsnH::six::*^{P}*csnH:csnH:csnH*^{t} *:ble*^{R}	This study
AGB1635 (AnFB183 cl.14)	Δ*csnH:: csnH*	AnFB182	Δ*nkuA::argB;pabaA1;yA2;veA*$^{+}$ *;ΔcsnH::six::*^{P}*csnH:csnH:csnH*^{t} *:six*	This study
AnFB184 cl.5		AGB1618 (AnFB111) + pME5443	Δ*nkuA::argB;pabaA1;yA2;veA*$^{+}$ *;ΔcsnG::six::*^{P}*csnG:csnG:csnG*^{t} *:ble*^{R}	This study
AGB1636 (AnFB185 cl.5)	Δ*csnG:: csnG*	AnFB184	Δ*nkuA::argB;pabaA1;yA2;veA*$^{+}$ *;ΔcsnG::six::*^{P}*csnG:csnG:csnG*^{t} *:six*	This study

2.5 Genomic DNA extraction from the fungal strains

A. nidulans strains were grown vegetatively overnight at 37°C prior to the extraction of genomic DNA. The vegetatively grown fungal mycelium was harvested by filtering and washed with 0.96% saline. After washing the mycelium was shock-frozen in liquid nitrogen. The shock-frozen mycelium was grained either manually in a mortar or in a Retch mixer mill (MM400). 500 µL lysis buffer (200 mM Tris-HCl pH 8.5, 250 mM NaCl, 25 mM EDTA, 0.5% (w/v) SDS) was added to the disrupted mycelium in approximately 1:1 ratio, and the mixture was heated at 65°C for 15-60 minutes. After cooling the samples on ice for 5 minutes, the protein content of the samples was precipitated with 100 µL 8 M potassium-acetate. The cell debris was pelleted by centrifugation at 13 000 rpm for 15 minutes at room temperature. The supernatant containing the nucleic acids was transferred into a new centrifuge tube and the protein precipitation step was repeated for a cleaner gDNA sample. Afterwards, the supernatant was transferred into a new centrifuge tube. For the nucleic acid precipitation approximately 300 µL isopropanol was added to the supernatant in an approximately 1:1 ratio to the sample volume. The samples were centrifuged at 13 000 rpm for 15 minutes at room temperature. The nucleic acid pellet was washed with 1 mL 70% (v/v) ethanol and then dried at 65°C. The nucleic acid pellet was resuspended in 50-100 µL sterile ddH_2O supplemented with 100 µg/mL RNaseA to remove RNA from the samples.

2.6 Southern hybridization

The correct integration of the deletion or the complementation constructs into the genomic locus of the recipient fungal strain was checked by Southern blotting (Figure 19) (Southern, 1975).

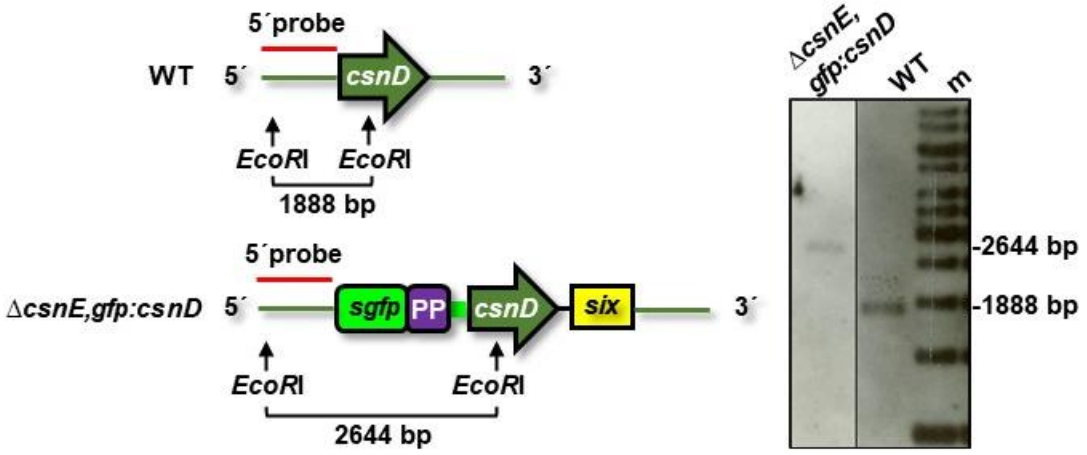

Figure 19. Scheme of an exemplary restriction digestion for Southern hybridization of a *csn* mutant *A. nidulans* strain.
The *EcoR*I restriction digestion of the gDNA resulted in a 1888 bp fragment in the wild type (WT) strain and in a 2644 bp fragment in case of the marker recycled Δ*csnE,gfp:csnD* strain, when hybridized with the labeled *csnD* 5´ flanking probe. m: Gene Ruler 1 kbp DNA Ladder. For the verification of the fungal strains constructed in this work, the applied restriction enzymes and the resulting DNA fragment sizes are listed in Table S11.

Genomic DNA derived from *A. nidulans* clones was restriction digested overnight at 37°C and separated by agarose gel electrophoresis. The agarose gel was treated with gel washing buffer I (0.25 M HCl) under gentle agitation at room temperature for 20 minutes followed washing with gel washing buffer II (0.5 M NaOH, 1.5 M NaCl) for 20 minutes and pH neutralization (1.5 NaCl, 0.5 M Tris-HCl, pH 7.4) for 20 minutes. The DNA was transferred from the agarose gel onto an Amersham™ Hybond®-N membrane via dry blotting for minimum 2 hours at room temperature. Then, the membrane was dried at 75°C for 10 minutes, followed by UV cross-linking of the DNA to the nylon membrane for 5 minutes. Afterwards, the membrane was treated with prehybridization buffer (0.5 M NaCl and 4% (w/v) blocking reagent dissolved in prehybridization buffer) for prehybridization for 30 minutes at 55°C while rotating. The specific DNA probe was labeled with Amersham™ Gene Images AlkPhos Direct Labelling and Detection System according to the manufacturer´s instructions. The labeled DNA probe was added to fresh prehybridization buffer and incubated for hybridization with the membrane overnight at 55°C under rotation. After the hybridization, the membrane was washed with membrane washing buffer I (2 M urea, 0.1% (w/v) SDS, 50 mM Na-phosphate pH 6.88, 150 mM NaCl, 1 mM $MgCl_2$, 0.2% (w/v) blocking reagent) for 10 minutes at 55°C while rotating and with membrane washing buffer II (1 M Tris pH 10, 2 M NaCl and 2 mM $MgCl_2$) for 5 minutes at room temperature under gentle agitation. For detection 100 to 200 µL Amersham™ CDP-Star Detection Reagent was added and evenly distributed on the nylon membrane and incubated for 5 minutes in darkness at room temperature. For the detection of the chemiluminescence signal, an Amersham™ Hyperfilm™ ECL film was placed on the membrane and incubated for 1 hour to overnight in darkness. Afterwards, the ECL film was developed with the Optimax X-ray Film Processor.

2.7 Analyses of the fungal phenotypes

2.7.1 Morphological analyses by spotting assay

The analyses of the fungal phenotypes were carried out by point inoculation of $2x10^3$ conidia in 2 µL NaCl-Tween80 of each *A. nidulans* strains on the center of agar plate containing 30 mL MM_{PABA}, if not specified otherwise. The strains were grown for five days under constant illumination and with aeration at 37°C to analyze the asexual development. The strains were grown for 14 days (if not specified otherwise) in darkness and with low O_2-high CO_2 pressure at 37°C to induce the sexual development. The SZX12-ILLB2-200 binocular microscope was used to analyze the asexual and sexual reproduction structures of the fungus. The close-up pictures were recorded with the CellSens dimension software version 1.4 at 4.8x magnifications of the colony surface.

2.7.2 Quantification of conidiospores

The fungal strains were point inoculated and grown asexually as described in the previous chapter. The colony diameter was measured and conidiospores were harvested from the whole colony into 2 mL NaCl-Tween80 solution and counted in a Thoma chamber. The conidiospore number per colony was determined as follows. The number of conidiospores per colony diameter was determined for all mutants and the wild type (WT). The number of $conidiospores_{mutant}$ per $colony\ diameter_{mutant}$ was determined relative to the WT and is given in percent (%):

$$\left[\frac{conidiospores_{mutant}/colony\ diameter_{mutant}}{number\ of\ conidiospores_{WT}/colony\ diameter_{WT}}\right] *100$$

2.8 Confocal microscopy and visualization of fungal nuclei

For confocal microscopy 1000 conidiospores of each strain were inoculated in Ibidi® µ-Slide 8-well microscopy chambers containing 400 µL liquid MM_{PABA} and were grown for 20 hours at 37°C. To analyze the subcellular localization of GFP-tagged proteins, the Zeiss AxioObserver Z.1 inverted confocal microscope connected with a Plan-Apochromat 100x/1.4 oil objective and a QuantEM:512SC camera were used. The SlideBook version 6.0 software was used with default settings to record and process the pictures. The GFP-fused proteins were detected at around 510 nm. The visualization of fungal nuclei occurred either by DAPI staining or by the expression of RFP-Histone 2A. DAPI was added in 1 µg/mL final concentration to fungal cultures grown vegetatively for 20 hours and were subsequently incubated for additional 30 minutes at room temperature in the darkness prior to microscopy. DAPI signals were detected at around 460 nm. In case of fungal strains expressing RFP-Histone 2A, the RFP was visualized by illumination at around 588 nm. 100 or 1000 millisecond illumination was used to visualize the DIC (differential interference contrast), GFP, RFP and DAPI signals.

2.9 Protein analytical methods

2.9.1 Preparation of protein crude extracts from fungal strains

Total protein crude extracts of the fungal cultures were prepared prior to protein immunoblot analysis (Köhler *et al*., 2016). If not stated otherwise, $1x10^6$/mL conidia of each fungal strains were inoculated in 100 mL MM_{paba} and grown vegetatively for 20 hours at 37°C under agitation. The mycelium deriving from vegetative cultures was harvested, washed with saline-PMSF-DMSO (0.96% (w/v) NaCl, 0.1 mM PMSF and 0.1% (v/v) DMSO). The harvested mycelium was dried and shock-frozen in liquid nitrogen. Then, the mycelium was disrupted in a Retch mixer mill (MM400). Cell lysis occurred by addition of B* lysis buffer to the grinded mycelium in an approximately 1:1 ratio. B* lysis buffer consisted of 300 mM NaCl, 10 mM Tris-HCl pH 7.5, 0.5 mM EDTA, 10% (v/v) glycerol, 0.2% (v/v) NP-40, supplemented freshly with 1 mM PMSF, 2 mM DTT and 10 µL/mL cOmplete™ protease inhibitor cocktail (1.5 tablets/mL dissolved in B* lysis buffer). The mixture was vortexed thoroughly for one minute, followed by centrifugation for 30 minutes at 13 000 rpm at 4°C to pellet cell debris. The centrifugation step was repeated with the supernatant for 10 minutes at 13 000 rpm at 4°C to gain a clear protein crude extract containing the water-soluble proteins. Protein concentration was determined with NanoDrop® ND-1000 spectrophotometer at 280 nm.

2.9.2 Protein immunoblotting

Protein immunoblotting was applied to determine the abundance and stability of the GFP fusion proteins (Köhler *et al*., 2016). For protein immunoblotting experiments 400 µg crude protein extract in 50 µL B* lysis buffer was denatured with 16.6 µL 3x sample buffer (250 mM Tris-HCl pH 6.8, 15% (v/v) β-mercaptoethanol, 30% (v/v) glycerol, 7% (v/v) SDS and 0.3% (w/v) bromophenol blue) for each samples. After denaturing of proteins at 95°C for 5 minutes, approximately 90 µg denatured protein crude extract of each fungal strains was loaded onto a 12% SDS polyacrylamide gel. The SDS gels consisted of an upper stacking gel (1 mL 2x stacking buffer, 250 µL 30% (v/v) acrylamide, 750 µL ddH_2O, 30 µL 10% (w/v) APS and 3.75 µL TEMED) and a bottom resolving gel (2.5 mL 2x resolving buffer, 2 mL 30% (v/v) acrylamide, 500 µL ddH_2O, 75 µL 10% (w/v) APS and 7.5 µL TEMED). The 2x resolving buffer consisted of 0.75 M Tris-HCl pH 8.8 and 0.1% (w/v) SDS. The 2x stacking buffer consisted of 0.25 M Tris-HCl pH 6.8 and 0.1% (w/v) SDS. The proteins were separated by sodium dodecyl sulphate polyacrylamide gel electrophoresis (SDS-PAGE) in 1x running buffer (25 mM Tris-base, 0.25 M glycine, 0.1% (w/v) SDS), then transferred to a nitrocellulose membrane (Amersham™ Protran® 0.45 µm NC) blotting chambers containing 1x transfer buffer (25 mM Tris-base, 192 mM glycine, 0.02% (w/v) SDS). The blotting took place either overnight at room temperature at 35V or for one hour in blotting chambers on ice at 100-110V. Ponceau staining visualized (3% (v/v) trichloroacetic acid, 0.2% (w/v) Ponceau S) the proteins on the membranes and served as loading control for later protein abundance quantifications. Blocking of the membrane occurred in 5% (w/v) Sucofin® milk powder dissolved in 1x TBST buffer (10 mM Tris-HCl pH 8.0, 150 mM NaCl, 0.05% (v/v) Tween20) for 1 hour under agitation. Following the blocking step, the membrane was incubated with the primary monoclonal α-GFP antibody (B-2) sc-9996) prepared in 5% (w/v) milk powder-1x TBST solution overnight at 4°C under agitation. The nitrocellulose membrane was washed three times for 10 minutes with

fresh 1x TBST buffer under agitation the next day. After the washing, the secondary polyclonal α-goat anti-mouse antibody conjugated with horseradish peroxidase (115-035-003) prepared in milk powder-TBST solution was added to the membrane. After incubation for 1 hour under agitation at room temperature, the membrane was washed again three times with TBST solution. Solution A (9 mL ddH_2O, 1 mL 1 M Tris-HCl pH 8.5, 100 µL 250 mM luminol, 44 µL 400 mM p-coumaric acid) and solution B (9 mL ddH_2O, 1 mL 1 M Tris-HCl pH 8.5, 6.14 µL 30% H_2O_2) were prepared and mixed directly before their addition to the membrane for detection of the chemiluminescence signal. The membrane was shaken in solution A and B gently at room temperature for two minutes in darkness. The chemiluminescent signals were recorded with the Fusion-SL7 chemiluminescence detection system and analyzed with the Fusion software version 15.18 and the Bio1D software version 15.08.

2.9.3 Optical density quantification for the determination of protein abundances

The pixel densities of the detected GFP-fusion protein bands were calculated with the Bio1D software version 15.08 for the quantification of the GFP-fusion protein signals. The calculated GFP signal pixel densities were normalized against the Ponceau loading control pixel densities in the mutant and WT strain. The normalized pixel density of the mutant strain´s sample was determined relative to the WT and is given in percent (%):

$$\left[\frac{\text{GFP signal}_{mutant}/\text{Ponceau signal}_{mutant}}{\text{GFP signal}_{WT}/\text{Ponceau signal}_{WT}} \right] *100$$

2.9.4 Protein-protein interaction studies

For determining protein-protein interactions, GFP co-immunoprecipitation assays were carried out (chapter 2.9.4.1). Total protein extracts were prepared from vegetative fungal cultures and incubated with GFP-Trap® Agarose beads for the binding of GFP-tagged proteins. After elution of GFP-tagged proteins from the agarose beads, the protein content of the eluate was precipitated by chloroform-methanol extraction (chapter 2.9.4.2). The precipitated proteins were digested with trypsin (chapter 2.9.4.3) and the resulting peptides were further purified by C18 stage tipping (chapter 2.9.4.4). The peptide content of the samples was analyzed by liquid chromatography coupled with mass spectrometry (LC-MS/MS), described in chapter 2.9.4.5). The raw data deriving from the LC-MS/MS measurements were analyzed as described in chapter 2.9.4.6. The workflow of the protein-protein interaction studies is presented in Figure 20.

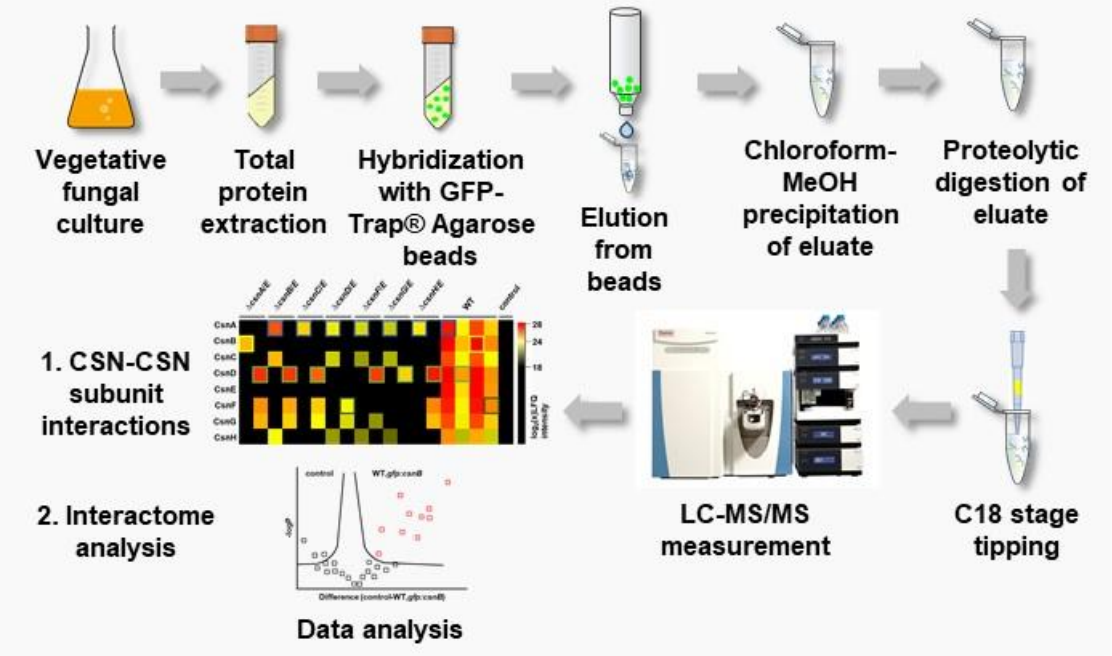

Figure 20. Schematic representation of the protein-protein interaction studies.
Workflow of the GFP co-immunoprecipitation, the downstream proteolytic digestion, the further peptide purification and LC-MS/MS measurements followed by data analyses. `Chloroform-MeOH´: chloroform-methanol.

2.9.4.1 GFP co-immunoprecipitation assay

For the GFP co-immunoprecipitation (also referred to as GFP-affinity purification or GFP-trap experiment) assays $1x10^6$ conidiospores/mL in 500 mL MM_{PABA} were inoculated of each fungal strains and grown for 20 hours at 37°C under agitation. The mycelium was harvested, washed with saline-PMSF-DMSO, then dried and shock-frozen in liquid nitrogen. The frozen mycelium was grinded manually with a pre-cooled pestle and mortar. Equal amounts of grinded mycelium of each fungal strains was filled into pre-cooled SS- 34 centrifugation tubes. Altogether maximum 2 mL B* lysis buffer was added to the grinded mycelia in an approximately 1:1 ratio. The mixture was thoroughly mixed by vortexing for one minute. The grinded mycelium, the cell debris, was pelleted by centrifugation in Sorvall RC-5B Plus Refrigerated Centrifuge for 30 minutes at 15 000 rpm at 4°C. All subsequent procedures were carried out at 4°C and the protein samples were kept on ice in between experimental steps. During the centrifugation, 35 µL GFP-Trap® Agarose beads, which had approximately 42 µg protein binding capacity, were loaded onto a Poly-Prep® Chromatography column and were equilibrated by washing with 5 mL B* lysis buffer. Following the centrifugation, the supernatant containing the crude protein extract was filtered through a Miracloth filter into a 15 mL falcon tube and the crude extract protein concentration was measured at 280 nm with NanoDrop® ND-1000 spectrophotometer. 16 mg total protein in 2 mL final volume was added to the GFP-Trap® Agarose beads and incubated while rotating for 2 hours at 4°C. Afterwards, the unspecific or weakly bound proteins were washed off the GFP-Trap® Agarose beads by applying increasing salt concentration. For that first 5 mL W300 buffer (300 mM sodium chloride, 10 mM Tris-hydrogen chloride pH 7.5, 0.5 mM EDTA) and then 5 mL W500 buffer (500 mM sodium chloride, 10 mM Tris-hydrogen chloride pH 7.5, 0.5

mM EDTA) were applied. The GFP-Trap® Agarose bead-bound proteins were then eluted. The elution occurred by adding 150 µL 0.2 M glycine pH 2.5 to the beads and mixed by pipetting up-and-down for not longer than 30 seconds. The pH of this mixture was immediately neutralized by 15 µL 1 M Tris pH 10.4. The elution fraction was collected in 1.5 mL Eppendorf tubes. The elution was performed two additional times resulting in three elution fractions (e1, e2 and e3). Based on earlier experimental experience (data not shown), the e1 fraction is expected to contain most of the GFP-Trap® Agarose beads bound proteins, while the e3 fraction is expected to contain the least proteins. If not specified otherwise, the complete e1, e2 and e3 fractions (à approximately 150 µL) were used for the precipitation by chloroform/methanol.

2.9.4.2 Chloroform-methanol extraction

The complete e1, e2 and e3 elution fractions deriving from the GFP-CsnA, GFP-CsnB, GFP-CsnD and GFP-CsnF mediated co-immunoprecipitation assays, and 50 µL of both, e1 and e2, fractions combined from the GFP-CsnE mediated pull down assays were used for the chloroform/methanol extraction following the protocol by Wessel and Flügge, 1984. First, 600 µL methanol was added to approximately 150 µL e1, e2 and e3 fractions in a 1:4 ratio and mixed by vortexing for 30 seconds at room temperature. Next, 150 µL chloroform was pipetted to the protein samples in a 5:1 ratio and mixed by vortexing for 30 seconds at room temperature. Afterwards, 450 µL ddH_2O was added to the samples in a 2:1 ratio and mixed by vortexing for 30 seconds at room temperature followed by centrifugation for 3 minutes at 10 000 rpm at 4°C. This step resulted in the separation of the two solution phases. The upper phase was carefully discarded without disturbing the interphase, which contains proteins. The lower phase was then mixed with 450 µL methanol by vortexing for 30 seconds at room temperature and centrifuged for 10 minutes at 13 000 rpm and 4°C. The supernatant was carefully discarded and the protein pellet was dried on air overnight at room temperature in a fume hood. The dried protein pellet was further processed by tryptic in-solution digestion.

2.9.4.3 In-solution tryptic protein digestion

For the in-solution tryptic protein digestion the dried protein pellets of e1, e2 and e3 deriving from the chloroform/methanol extraction were mixed together by stepwise resuspensions as follows. As expected, the e3 fraction has the lowest and the e1 fraction has the highest protein concentration. Therefore, the e3→e2→e1 resuspension order was followed to combine the elution fractions. First, 20 µL 0.1% (w/v) RapiGest™ SF surfactant solution was added to the e3 pellet and resuspended carefully. This resuspended 20 µL RapiGest™-e3 pellet mixture was transferred onto the e2 pellet and was resuspended carefully. This resulting 20 µL RapiGest™-e3 and e2 pellet mixture was transferred onto the e1 pellet and was resuspended carefully. Then, the Eppendorf tube, which contained the e3 pellet was rinsed with 20 µL 0.1% (w/v) RapiGest™ SF surfactant solution. This rinsing solution was also used to rinse the Eppendorf tube which contained the e2 pellet. At last, the e3-e2 rinsing 20 µL 0.1% (w/v) RapiGest™ SF surfactant solution was added to the e1 resuspended pellet. Afterwards, 2 µL of 100 mM DTT in 100 mM ammonium bicarbonate was added to the protein solution and incubated for 30 minutes at 60°C. The protein sample was cooled to room temperature. 15 mM iodoacetamide was added to the protein sample and incubated for 30 minutes at room temperature in darkness. Next, trypsin was dissolved as the

manufacturer suggested and was added to the samples in 1:20 dilution, then, incubated overnight at 37°C. The following day the samples were treated with 0.5% (v/v) trifluoroacetic acid by incubation for 35 minutes at 37°C. The samples were centrifuged for 10 minutes at 13 000 rpm at room temperature to pellet the precipitated RapiGest™ SF surfactant. The supernatant was transferred to a Protein LoBind Tube, and it was vaporized in the Savant™ SPD111V SpeedVac concentrator at 50°C to obtain a dry peptide pellet. The peptide pellet was further processed by the C18 stage tip purification.

2.9.4.4 C18 stage tip purification

The peptide samples resulting from the *Rapi*Gest™ procedure were further purified according to the C18 stage tip protocol (Rappsilber *et al.*, 2007). First, a C18 stage tip was prepared. Three C18 Solid Phase Extraction disks were placed tight, airproof into the bottom of a 200 µL pipette tip, resulting in a C18 stage tip column. The C18 stage tip column was equilibrated with 100 µL 0.1% (v/v) formic acid dissolved in HPLC grade methanol, then centrifuged for 2 minutes at 10 000 rpm. 100 µL elution solution (70% (v/v) acetonitrile, 0.1% (v/v) formic acid) were added to the C18 stage tip column, and it was centrifuged for 2 minutes at 10 000 rpm. Then, 100 µL 0.1% (v/v) formic acid dissolved in water was added to the C18 stage tip column followed by centrifugation for 2 minutes at 10 000 rpm. This step was repeated one more time. Then, the C18 stage tip column was transferred into a fresh Protein LoBind Tube. The peptide pellet from the *Rapi*Gest™ procedure was resuspended in 20 µL sample solution (98% (v/v) HPLC-grade water, 2% (v/v) acetonitrile and 0.1% (v/v) formic acid), loaded onto the equilibrated C18 stage tip column and for peptide binding incubated for 5 minutes at room temperature. The peptide sample was centrifuged for 5 minutes at 4000 rpm. For a higher peptide yield, the flow through was reloaded onto the C18 stage tip column, incubated for 5 minutes at room temperature and centrifuged again for 5 minutes at 4000 rpm. The C18 stage tip column was washed twice with 100 µL 0.1% (v/v) formic acid dissolved in water, followed by centrifugation for 2 minutes at 10 000 rpm. For the elution of the C18 stage tip column-bound peptides, the column was transferred to a fresh Protein LoBind Tube and 30 µL elution solution was loaded onto the C18 stage tip column. After 5 minutes incubation at room temperature, the column was centrifuged for 5 minutes at 4000 rpm. The elution step was repeated one more time for a higher peptide yield. The elution solution was evaporated at 50°C in the Savant™ SPD111V SpeedVac concentrator. The resulting peptide pellet was resuspended in 20 µL sample solution, placed in the Sonorex™ Digital 10 P ultrasonic bath for 3 minutes at 10% performance and transferred to a mass spectrometry glass vial directly prior to the LC-MS/MS analysis.

2.9.4.5 Liquid chromatography coupled with mass spectrometry analysis

Peptide composition of the samples derived from the C18 stage tip purification was analyzed by liquid chromatography coupled with mass spectrometry (LC-MS/MS). The LC-MS/MS analysis was performed with an UltiMate™ 3000 RLSC nano liquid chromatography system coupled with an Orbitrap Velos Pro™ mass spectrometer. The peptide sample was loaded onto an Acclaim PepMap RLSC™ column and was separated via a water-acetonitrile gradient at a flow rate of 300 nL/minute. Then, the vaporization and subsequent ionization of the peptides was carried out by the Nanospray Flex™ Ion Source at 2.4 kV. The ionized peptides entered the Orbitrap Velos Pro™ mass spectrometer and were recorded with the

incorporated Orbitrap-FT analyzer at a resolution of 30 000 within a mass range of 300 to 1850 m/z. Collision-induced dissociation (CID) was performed with the LTQ Velos Pro™ linear ion trap to obtain the data-dependent top ten fragmentation spectra of the ionized peptides. The Xcalibur™ software version 2.2 was applied for data recording and programming. The obtained LC-MS/MS data was analyzed with the MaxQuant software version 1.6.0.16 and the Perseus software version 1.6.0.7.

2.9.4.6 Analysis of the raw data deriving from the LC-MS/MS measurements

The LC-MS/MS raw data was analyzed to identify protein-protein interactions. The raw data deriving from the Xcalibur™ software version 2.2 was searched against *A. nidulans*-specific protein database (UniProt Proteomes, Proteome ID: UP000000560) (Bateman *et al*, 2021) using the MaxQuant software version 1.6.0.16. (Cox and Mann, 2008) as described in Table 8.

Table 8. Analysis of the raw data deriving from the LC-MS/MS measurements using MaxQuant software version 1.6.0.16.

MaxQuant analysis		
Step	**Command**	**Description**
1	Download proteome database	Download and save the *Aspergillus* database from UniProt Proteomes in Fasta format: (*Emericella/Aspergillus nidulans* (strain FGSC A4/ATCC38163/ CBS 112.46/NRRL194/M139), UniProt Proteome ID: UP000000560).
2	Andromeda configuration	Configure proteome sequence database: select and add saved database in Fasta format and confirm changes with “Modify table”.
3	Name parse rule	Unify unique proteome identifier from UniProt and in MaxQuant and confirm changes with “Modify table”.
4	Taxonomy	Unify taxonomy identifier from UniProt and in MaxQuant and confirm changes with “Modify table”.
5	Save changes	Save all changes.
6	Load	Load raw files (.raw) deriving from the Xcalibur™ software version 2.2.
7	Set experiment	Define biological replicates: name replicates as “replicate_1”, “replicate_2” and “replicate_3”.
8	Instrument	Orbitrap.
9	Label-free quantification	Activate label-free quantification by tricking.
10	Global parameters	Add UniProt proteome database.
11	MS/MS-FTMS	Activate FTMS re-calibration by ticking (Fourier transform for smaller standard deviation of masses).
12	Run analysis	Run analysis with 9 number of threads, then start run with “Start”.
13	After analysis	The “combined” folder deriving from the MaxQuant analysis contains a “txt” folder and within this, the “proteinGroups.txt” file. Use this file for “Generic matrix upload” in the Perseus software.

The output data from the MaxQuant analysis was further analyzed with the Perseus version 1.6.0.7 (Tyanova *et al.*, 2016) following an LFQ-based filtering workflow described in Table 9 and a p-value-based workflow presented in Table 10.

Table 9. LFQ-based data analysis with the Perseus software version 1.6.0.7.
The filtering strategy was used to determine protein-protein interaction between CSN subunits was carried out considering the label free quantification (LFQ), the number of the LC-MS/MS (MS/MS) counts and the recognized unique peptides (UP). Only those proteins passed the filtering, which were identified in all biological replicates.

Data analysis based on LFQ, MS/MS counts and number of unique peptides		
Step	**Command**	**Description**
1	Generic matrix upload	Generating matrix upload of LFQ intensities (Expression/Main column), MS/MS counts of all samples, unique peptides of all samples (UP), razor peptides, sequence coverages (Numerical column). Potential contaminants (only identified by site, reverse, potential contaminant) and text (protein IDs) columns.
2	Filter rows based on categorical column	Filter out contaminants in three consecutive steps: only identified by site, reverse, potential contaminant.
3	Rearrange/Remove empty columns	Removal of empty columns deriving from the previous step.
4	Transformation	log2(x) of LFQs. "0" values are replaced with missing values ("NaN").
5	Add annotation	Select and upload "*A. nidulans* FGSC A4 atcc38163.txt".
6	Categorical annotation rows	Create a group of LFQs of samples including WT. Name replicates identically.
7	Categorical annotation rows	Create a group of LFQs of OE GFP negative control. Name replicates identically.
8	Categorical annotation rows	Create groups of replicates, name replicates identically.
9	Rearrange/Change column type	Source type: numerical (select MS/MS counts) to target type: main. Now grouping and filtering is allowed for MS/MS counts.
10	Categorical annotation rows	Create a group of MS/MS counts of samples including WT. Name replicates identically.
11	Categorical annotation rows	Create a group of MS/MS counts of OE GFP negative control. Name replicates identically.
12	Rearrange/Change column type	Source type: numerical (select unique peptides (UPs)) to target type: main. Now grouping and filtering is allowed for UPs.
13	Categorical annotation rows	Create a group of UPs of samples including WT. Name replicates identically.
14	Categorical annotation rows	Create a group of UPs of OE GFP negative control. Name replicates identically.
15	Imputation/Replace missing values by constant	Replace missing values with constant: 1.
16	Filter rows based on valid values	Min. number of values: **3**. Mode: in at least one group: LFQ of samples, then values should be: greater or equal than 18.
17	Filter rows based on valid values	Min. number of values: **3**. Mode: in at least one group: LFQ of the OE GFP negative control, then values should be: less or equal than 18.
18	Filter rows based on valid values	Min. number of values: **3**. Mode: in at least one group: MS/MS count of samples, values should be: greater or equal than 4. Repeat with MS/MS count of OE GFP negative control and less or equal than 4.
19	Filter rows based on valid values	Min. number of values: **3**. Mode: in at least one group: UPs of samples, values should be: greater or equal than 3. Repeat with UPs of OE GFP negative control and less or equal than 3.
20	Average groups	Average LFQs of groups. Average type: mean. Min. valid values per group: 3. Keep original data.
21	Average groups	Average LFQs of OE GFP negative control. Average type: mean. Min. valid values per group: 3. Keep original data.
22	Hierarchical clustering	Visualization of the mean of the LFQs of protein hits as a heat map (only row tree).

Table 10. Significance-based data analysis in Perseus software version 1.6.0.7.
In this filtering strategy, the significance was calculated with two-sided t-tests, where the default settings for false discovery rate (FDR) 0.05 and s0=0.1 were used. The value s0 defines the artificial within groups' variance. This means, in case of s0=0 only the p-value will be considered, whereas if s0 is higher than 0, also the mean value differences, the level of regulation, will be considered in the calculations. Only those proteins passed the filtering, which were identified in all biological replicates.

Data analysis based on p-value		
Step	**Command**	**Description**
1	Generic matrix upload	Generating matrix of LFQ intensities (Expression/Main column), MS/MS counts, unique peptides (UP), razor peptides, sequence coverages (Numerical column), Potential contaminants (only identified by site, reverse, potential contaminant) and text (protein IDs) columns.
2	Filter rows based on categorical column	Filter out contaminants in three following steps: only identified by site, reverse, potential contaminant.
3	Rearrange/Remove empty columns	Removal of empty columns deriving from the previous step.
4	Transformation	log2(x) of LFQs. "0" values are replaced with missing values ("NaN").
5	Add annotation	Select and upload "*A. nidulans* FGSC A4 atcc38163.txt".
6	Rearrange/Rearrange remove columns	Choose columns of interest for pairwise comparison, for example: WT,*gfp:csn* vs control.
7	Rearrange/Rename columns	(Reg-ex-column/ Pattern: LFQ intensity): shortens column descriptions.
8	Categorical annotation rows	Create a group of LFQs of samples including WT, same as for pairwise comparison (name replicates identically): group1.
9	Filter rows based on valid values	Min. number of values: **3**. Mode: in at least one group: group1.
10	Analysis	Numeric Venn diagram.
11	Imputation/Replace missing values by normal distribution	Mode: whole matrix.
12	Analysis	Multiscatter plot: compare all replicates based on R squared R=1
13	Analysis	Volcano plot pairwise
14	Repeat "step 13" four more times.	
15	Load significant interacting partners in http://bioinformatics.psb.ugent.be/webtools/Venn/ from all five volcano plots.	

2.10 *In silico* methods

2.10.1 Databases and online tools

The AspGD (Cerqueira *et al.*, 2014), FungiDB (Basenko *et al.*, 2018), PomBase (Lock *et al.*, 2019) and *Saccharomyces* Genome Database (Cherry *et al.*, 2012) databases were used to gather information about fungal genetic loci and gene products. The UniProt, UniProt Proteomes, (Bateman *et al.*, 2021) and Protein Data Bank (PDB) (www.rcsb.org/) as well as the ExPASy/ProtParam and ExPASy/PeptideCutter (Gasteiger *et al.*, 2005) online tools were used to gather information about proteins. For sequence alignments the National Institutes of Health/Blast and for multiple sequence alignments the ClustalW/Muscle (Madeira *et al.*, 2019) was used. National Institutes of Health/PubMed was used for the literature search for this work.

2.10.2 Sequence search engines for NLS and NES prediction

The cNLS Mapper online tool (Kosugi *et al.*, 2009), where the maximum score is 10 and the NLStradamus online tool (Nguyen Ba *et al.*, 2009), where the prediction cutoff is 0.6 were used to predict NLS signals. The NetNes 1.1 tool (La Cour *et al.*, 2004), wherein the threshold was set to minimum 0.5 and maximum 2.0 as default was used to search for NES signals.

2.10.3 The atomic modeling of the *Aspergillus nidulans* COP9 signalosome

Homology modeling of the *A. nidulans* COP9 signalosome was performed using the comparative modeling (CM) protocol as implemented in Rosetta software suite (RosettaCM) (Song *et al.*, 2013) (p.c. Piotr Neumann, Department for Molecular Structural Biology, GZMB, Göttingen). The chosen protocol yields models with accurate side-chain and backbone conformations due to optimization of a physically realistic all-atom energy function over the conformational space defined by the structurally related template. The sequence similarity search was performed using the advanced search option available at the PDB and yielded the human COP9 signalosome crystal structure (PDB ID: 4D10) as the best suited template for comparative modelling approach (overall sequence identity 35.1%). For individual components: Csn1/A, Csn2/B, Csn3/C, Csn4/D, Csn5/E, Csn6/F, Csn7/G, Csn8/H, the following pairs of sequence identity/similarity values [%] have been calculated using HHPRED server (Gabler *et al.*, 2020): 36/62, 50/89.9, 23/37.7, 39/64.5, 54/92.9, 30/53.7, 31/54.1, 20/31.8, respectively. The HHPRED server provided also sequence alignments for each individual CSN subunit domain, which were used for modelling purposes. Initial model was calculated using a density guided homology modeling protocol utilizing a low resolution (3.8 Å) electron density map calculated for one COP9 signalosome molecule (chains Csn1/A to Csn8/H) used as template. These additional spatial restraints were employed in order to maintain high similarity between aligned, and most likely structurally related regions of the COP9 signalosome. Gaps modeling or *ab-initio* generation of missing N- or C-termini were not performed. The calculated decoys (2600) were energetically scored in Rosetta and subsequently clustered. The best decoy, selected as the centroid model from the lowest energy cluster, was used for the model completion and refinement using native CM protocol. During this step, harmonic constraints for main chain atoms were used during relax protocol (Conway *et al.*, 2014). The utilized CM protocol performed gaps modeling and generation of missing N- or C-termini, based on fragment libraries obtained for each component (Csn1/A to Csn8/H) from Robetta server (robetta.bakerlab.org). The calculated decoys (500) were energetically scored using Rosetta's internal score and subsequently clustered. The final model has been selected based on its lowest score among the decoys forming the lowest energy cluster. Analysis of macromolecular interactions between individual CSN components of the modeled *A. nidulans* COP9 signalosome was performed with Protein Interfaces, Surfaces and Assemblies (PISA) (www.ebi.ac.uk/pdbe/pisa) (Krissinel and Henrick, 2007). Figures were drawn using the PyMOL Molecular Graphics System version 1.7.1.3 (www.pymol.org).

2.10.4 Statistical analysis

Significance was determined by one way ANOVA tests (Simple Interactive Statistical Analysis, www.quantitativeskills.com/sisa/index.htm) based on the standard deviation (SD). Not significant (ns): p>0.05, *: p≤0.05, **: p≤0.01, ***: p≤0.001, ****: p≤0.0001. Significances of pairwise comparisons were depicted with matrices using the following color code:

Significance: p > 0.05 p ≤ 0.05 p ≤ 0.01 p ≤ 0.001 p ≤ 0.0001

The error is given in standard error of mean (SEM), which was calculated considering the number of the technical replicates.

3 Results

3.1 The seven subunit pre-COP9 signalosome contributes to growth and development of *Aspergillus nidulans*

The COP9 signalosome (CSN complex) is an evolutionary conserved eight-subunit complex with deneddylase activity. This Nedd8-specific isopeptidase activity is provided by CsnE, the only intrinsic catalytic subunit of the holocomplex. For catalysis, CsnE binds to a pre-assembled seven-subunit pre-COP9 signalosome, also called the pre-CSN complex (Beckmann *et al.*, 2015). The questions addressed in this work are: (i) what are the CSN complex assembly steps prior to CsnE incorporation and subsequent activation, and (ii) are there cellular pre-CSN complex functions, which are independent of the catalytic subunit CsnE in the fungus. *A. nidulans* strains with COP9 signalosome subunit gene deletions were constructed (Table 7) to analyze the cellular consequences caused by the impairment of the CSN and the pre-CSN complex formation. The fungal strains were constructed using the β-recombinase/six self-excisable marker system (Hartmann *et al.*, 2010) and therefore, these strains do not retain any resistance marker cassette (Figure 18). Surface growth, conidiospore (conidia) production during asexual development and mature fruiting body formation as a result of the complete sexual program were monitored in the Δ*csn* strains in comparison to the wild type strain. Since fungal development and production of secondary metabolites are strongly interconnected and coordinated (Braus *et al.*, 2010), the secondary metabolite secretion was also assessed for phenotypical changes.

The wild type strain carrying an intact, eight-subunit COP9 signalosome formed green pigmented conidia and developed mature fruiting bodies during asexual and sexual development, respectively (Figure 21, close-ups). The Δ*csnE* strain, harboring a seven-subunit pre-CSN complex, formed colonies of similar size of the wild type and produced green pigmented conidiospores during asexual development. The Δ*csnE* strain was unable to form mature fruiting bodies and its sexual development was blocked at early precursor stages of nest and primordia formation, when it was cultivated under sexual development inducing conditions (Busch *et al.*, 2007; Beckmann *et al.*, 2015; and Figure 21). Another typical feature of the Δ*csnE* strain was the secretion of reddish-brownish secondary metabolites into the cultivating agar medium during both, asexual and sexual, developmental programs (Nahlik *et al.*, 2010; Beckmann *et al.*, 2015; and Figure 21, bottom view). Re-integration of a single copy the *gfp:csnE* construct to the native chromosomal *csnE* locus complemented the phenotypes of the Δ*csnE* strain and restored the wild type behavior (Figure 21).

Deletion of genes encoding any of the seven subunits of the pre-CSN complex caused the failure of primordia maturation and the formation of fruiting bodies as well as they produced reddish secondary metabolites, similarly to the Δ*csnE* strain (Figure 21). In addition, deletion of any pre-CSN complex subunit genes resulted in severe growth reduction and drastic decrease in conidiospore production. The pre-CSN subunit gene deletion (Δ*pre-CSN*) strains formed stunted conidiophores, with only a few conidiospores compared to the wild type strain (Figure 21, close-ups). Loss of any of the analyzed pre-CSN subunit genes caused a severe growth defect with hardly any conidia production combined with the block in the formation of mature fruiting bodies. An N-terminal region of CsnA is involved in conidiospores formation and with that, also the Δ*csnA* strain barely forms asexual spores (Figure 21) (Beckmann *et al.*,

2015). The Δ*pre-CSN* phenotype could be rescued in the respective complementation strains (Figure 21). In case of the Δ*csnG* and Δ*csnH* strains, the single copy re-integration of the respective genes to the native chromosomal locus in the respective deletion background restored the wild type-like phenotype. In case of the complementation of the Δ*csnA,* Δ*csnB,* Δ*csnD,* Δ*csnE* and Δ*csnF* strains, the re-integration of the respective genes occurred by a single copy of the *gfp:csn* construct for N-terminal GFP labeling of the CSN subunits. This resulted in GFP-CsnA, GFP-CsnB, GFP-CsnD, GFP-CsnE or GFP-CsnF fusion proteins, which were functional in the fungal strains and had nearly wild type-like abundance (Figure S1). Based on the differences in phenotype and physiology between the Δ*csnE* and the Δ*pre-CSN* strains, an additional cellular function in growth and asexual development can be deduced for the pre-CSN complex subunit genes.

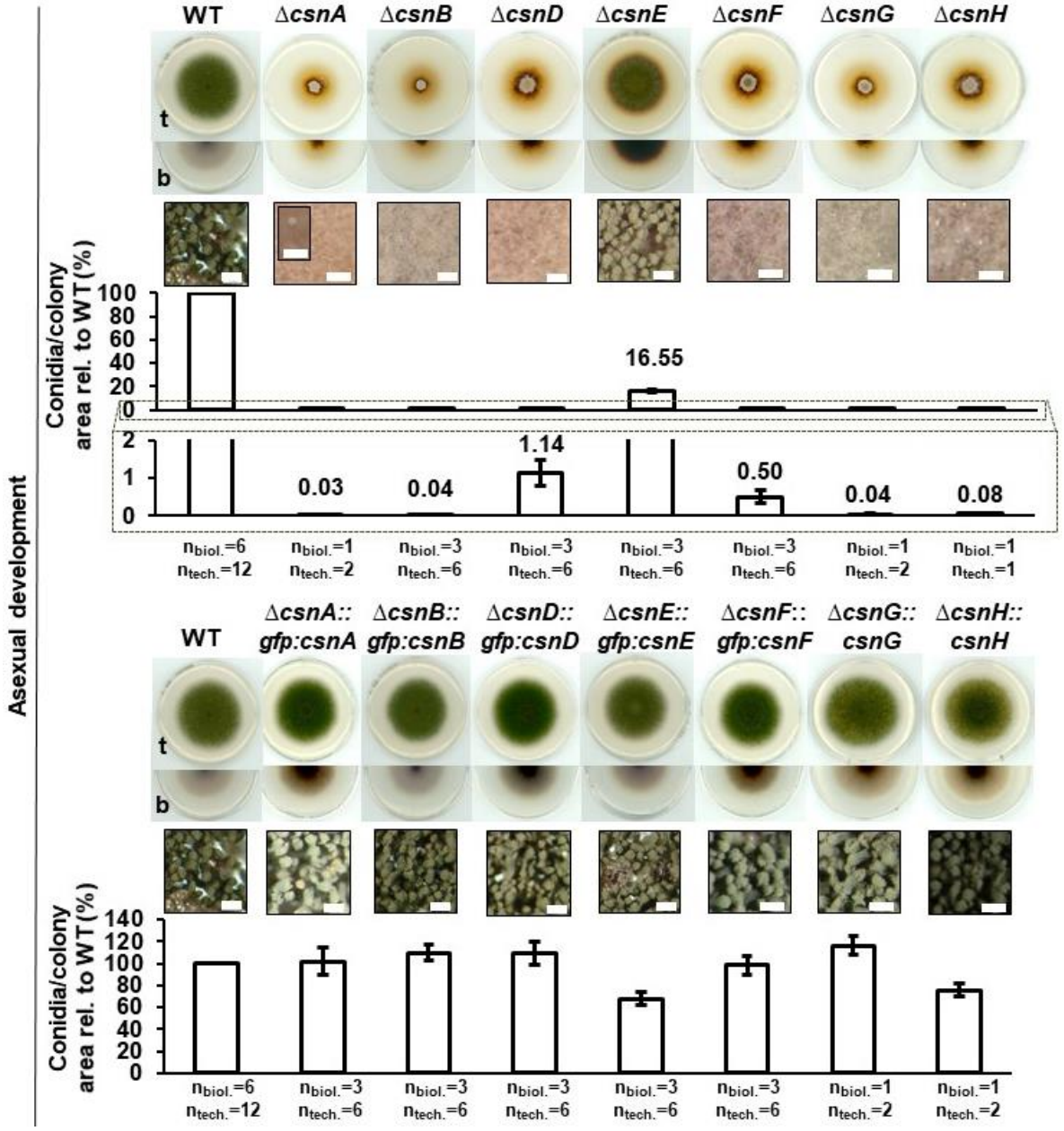

Figure 21. The figure is continued on the next page.

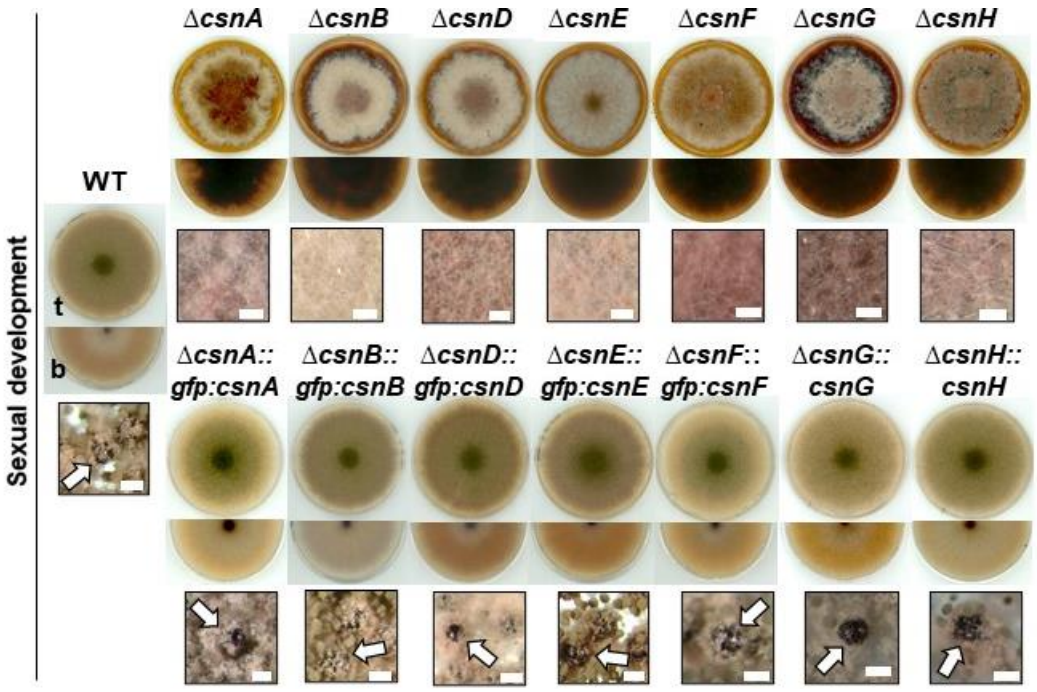

Figure 21. Loss of pre-CSN subunit encoding genes leads to more severe phenotypes than loss of the *csnE* deneddylase gene.
Growth, as well as asexual and sexual development of *A. nidulans* Δ*csn* strains (Table 7) were analyzed in spotting assays. 10^3 conidia of the Δ*csnA* strain and $2x10^3$ conidia of the other strains were point inoculated on MM_{PABA} agar plates. The strains were grown at 37°C either for five days under constant illumination and with aeration to induce asexual development or for 14 days in darkness and with low O_2-high CO_2 pressure to promote sexual differentiation. The figure shows the top (t) and the bottom (b) views of the colonies. An example for the conidiophores of the Δ*csn* strains is presented on the close-up picture of the Δ*csnA* strain. The arrows point to mature fruiting bodies. Scale bars represent 100 µm. The charts display the mean of the conidia number per colony area and the error bars display the SEM. The charts display the means of the conidia number per colony of independent biological (biol.) experiments carried out with technical (tech.) replicates. The conidia counts per colony area of each strain were relative (rel.) to the mean value of the wild type strain (WT).

3.2 The *csnE* deneddylase encoding gene is epistatic towards the pre-CSN subunit encoding genes

Deletions of *csnE* or pre-CSN subunit genes resulted in distinct fungal appearances, when the respective strains were grown in asexual development promoting conditions (Figure 21). This has risen the question whether there is a hierarchical relationship between *csnE* gene and the pre-CSN subunit genes. To address this question, fungal strains were constructed, which are deleted for a pre-CSN subunit gene in addition to the *csnE* deneddylase gene, resulting in the following strains: Δ*csnA*Δ*csnE*, Δ*csnB*Δ*csnE*, Δ*csnC*Δ*csnE*, Δ*csnD*Δ*csnE*, Δ*csnF*Δ*csnE*, Δ*csnG*Δ*csnE* and Δ*csnH*Δ*csnE* strains (Table 7). These are referred to as `Δ*pre-csn*Δ*csnE*´ double deletion strains. Growth, asexual and sexual development as well as the development-linked secondary metabolism of the Δ*pre-csn*Δ*csnE* strains were analyzed in comparison to the wild type and the Δ*csnE* strains. The Δ*pre-csn*Δ*csnE* strains resemble the Δ*csnE* strain in all tested features (Figure 22). These findings suggest that there is a hierarchical relationship between *csnE* and the pre-CSN subunit genes,

where the *csnE* deneddylase gene is a prerequisite and epistatic towards the pre-CSN subunit genes.

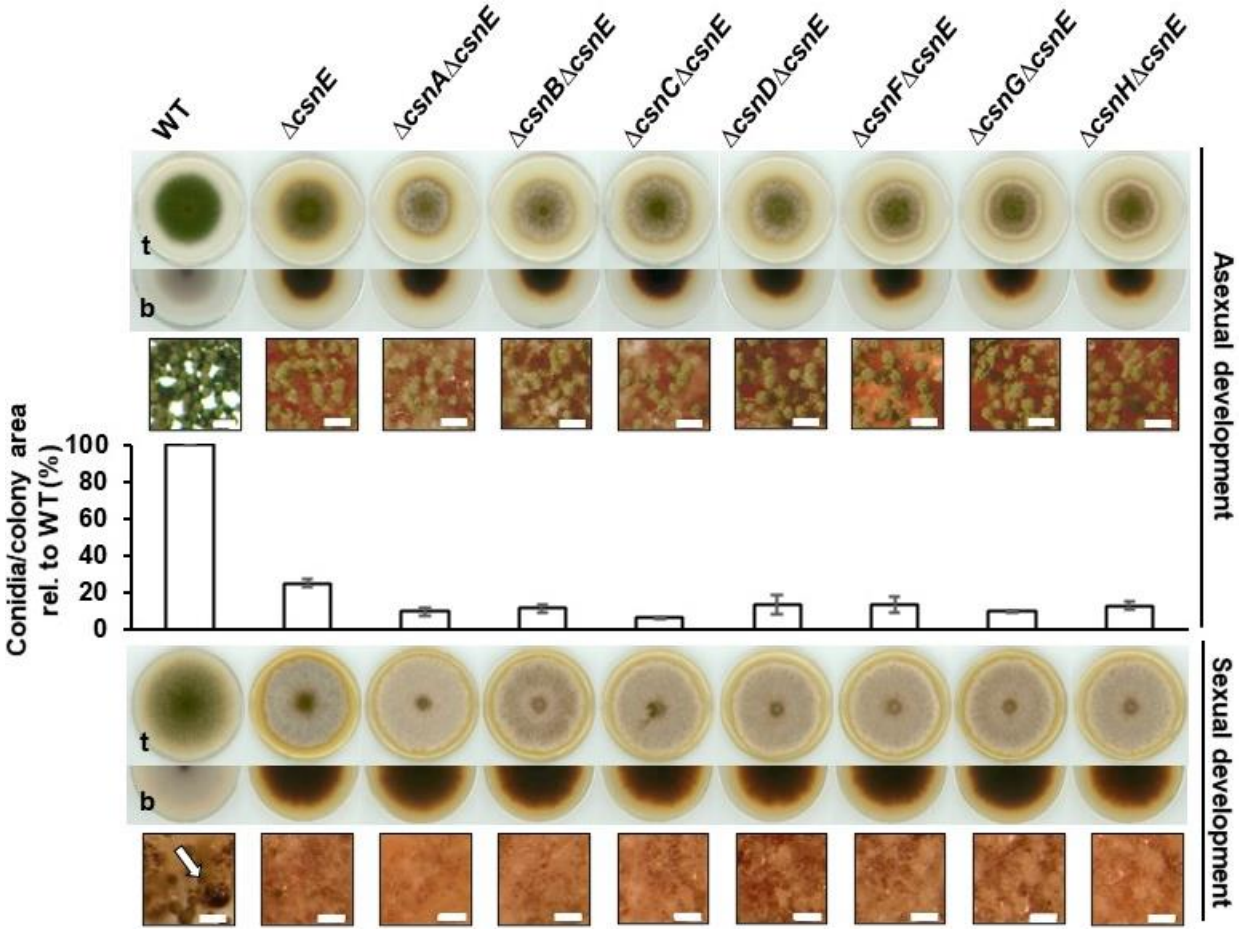

Figure 22. The *csnE* gene is epistatic towards the pre-CSN subunit encoding genes.
Growth, asexual and sexual development of the *A. nidulans* Δ*pre-csn*Δ*csnE* strains (Table 7) were analyzed in spotting assays. 2x10^3 conidia of each strain were point inoculated on MM_{PABA} agar plates. The fungal strains were grown at 37°C either for five days under constant illumination and with aeration to induce asexual development or for 14 days in darkness and with low O_2-high CO_2 pressure to promote sexual differentiation. The figure shows the top (t) and the bottom (b) views of the colonies. Scale bars represent 100 µm. The arrow points to a mature fruiting body. The charts display the mean of the conidia number per colony area of one biological replicate performed in duplicates and the error bars display the SEM. The conidia number per colony area of each strain is relative (rel.) to the mean value of the wild type strain (WT).

3.3 The pre-COP9 signalosome assembly includes two trimeric subcomplexes, CsnD-CsnF-CsnG and CsnA-CsnC-CsnH, which are linked by CsnB

A stable pre-CSN complex comprising seven subunits is activated by the incorporation of the catalytic CsnE subunit (Beckmann *et al.*, 2015). Various *A. nidulans* Δ*pre-csn*Δ*csnE* double deletion strains carrying a *gfp:csn* construct were prepared and analyzed to unveil the choreography of the heptameric pre-CSN complex assembly and to identify possible CSN subcomplexes. The Δ*pre-csn*Δ*csnE,gfp:csn* strains (Table 7) lack the *csnE* and a pre-CSN

subunit gene, as well as they additionally produce either functional GFP-CsnA, GFP-CsnB, GFP-CsnD or GFP-CsnF fusions (Figure 21 and Figure S1). These Δ*pre-csn*Δ*csnE,gfp:csn* strains resemble the Δ*csnE* phenotype in growth and development on surface cultures (Figure 23).

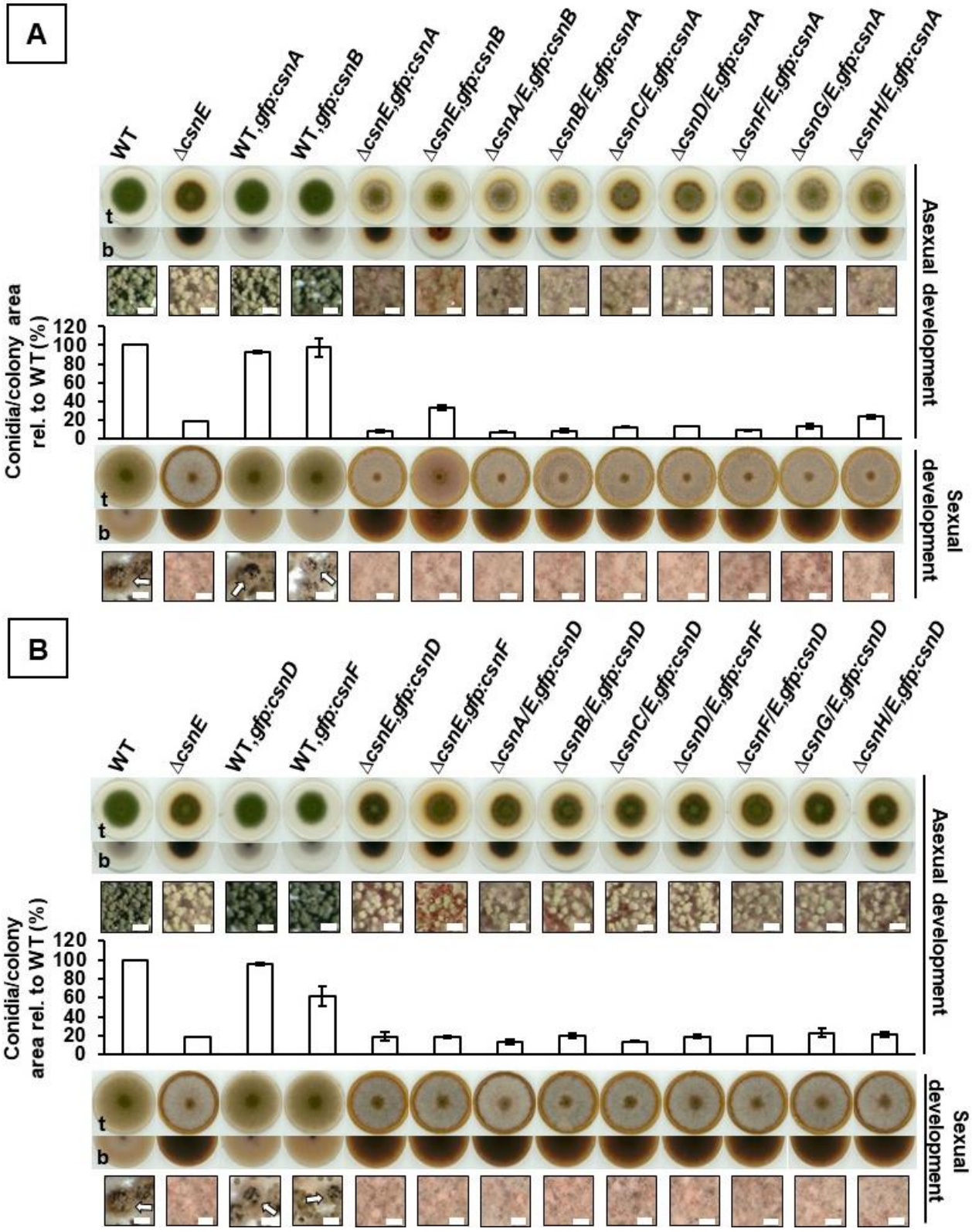

Figure 23. The figure legend is on the next page.

Figure 23. The phenotypes of the Δ*pre-csn*Δ*csnE,gfp:csn* strains producing either GFP-CsnA, GFP-CsnB, GFP-CsnD or GFP-CsnF are similar to the phenotype of the Δ*csnE* strain.
Growth and development of the *A. nidulans* Δ*pre-csn*Δ*csnE,gfp:csn* strains (Table 7) (shortened Δ*csnA*/*E,gfp:csn* to Δ*csnH*/*E,gfp:csn*), producing functional (**A**) GFP-CsnA or GFP-CsnB, or (**B**) GFP-CsnD or GFP-CsnF, were analyzed in spotting assays. $2x10^3$ conidia of each fungal strains were point inoculated on MM_{PABA} agar plates. The strains were grown at 37°C either for five days under constant illumination and with aeration to induce asexual development or for 14 days in darkness and with low O_2-high CO_2 pressure to promote sexual differentiation. The figure shows the top (t) and bottom (b) view of the colonies. Size bars represent 100 µm. The mature fruiting bodies are indicated with arrows. The spotting assay was carried out in two to four biological replicates. The charts display the mean of the conidia number per colony of one biological replicate performed in duplicates and the error bars display the SEM. The conidia counts per colony area of each strain were relative (rel.) to the mean value of the wild type strain (WT).

Interactions between the CSN subunits were studied with GFP co-immunoprecipitation experiments followed by LC-MS/MS measurements using the Δ*pre-csn*Δ*csnE,gfp:csn* double deletion strains introduced on Figure 23. An *A. nidulans* strain was included in all GFP-affinity purifications as negative control to filter out unspecific interactions between solely GFP tags, in which a *gfp* construct, encoding for free cytoplasmic GFP, was overexpressed (Table 7). This control strain did not recruit any CSN subunits in any of the GFP co-purification assays, thus, the later observed interactions exclusively relied on CSN-CSN subunit interactions (Figure 24A). Strains producing either GFP-CsnD, GFP-CsnF, GFP-CsnA or GFP-CsnB in wild type background were used as positive references in GFP-trap experiments. All applied GFP-CSN fusion as bait, produced in the wild type strain, were co-purified with all CSN subunits and with that, these baits recruited the eight-subunit holocomplex (Figure 24A). The seven-subunit pre-CSN complex was found in three biological experiments in the Δ*csnE,gfp:csnB* and Δ*csnE,gfp:csnD* strains producing functional GFP-CsnB and GFP-CsnD subunits, respectively (data not shown). The seven-subunit pre-CSN complex could not be identified in Δ*csnE,gfp:csnA* and in Δ*csnE,gfp:csnF* background due to ambiguous results of the GFP-trap replicates (data not shown).

Combined deletions of *csnE* with one of the heptameric pre-CSN complex subunit encoding genes resulted in defined specific interactions between CSN subunits. A strong interaction was observed between CsnD-CsnF-CsnG in GFP-CsnD mediated GFP-traps, when the isopeptidase CsnE and additionally, either CsnA, CsnB, CsnC or CsnH were absent (Figure 24A). GFP-CsnD was co-purified with CsnG upon combined loss of CsnE and CsnF, suggesting a CsnD-CsnG heterodimer. GFP-CsnF also recruited CsnG in absence of both CsnE and CsnD subunits, suggesting a CsnF-CsnG heterodimer. The recruitment of CSN subunits by GFP-CsnD was abolished by the combined loss of CsnE and CsnG. This leads to the conclusion that CsnG functions as anchor for the heterotrimeric CsnD-CsnF-CsnG subcomplex. GFP-CsnD was never able to recruit CsnA, CsnB, CsnC or CsnH in a strain, where the formation of the pre-CSN complex was abolished by a corresponding *csn* deletion.

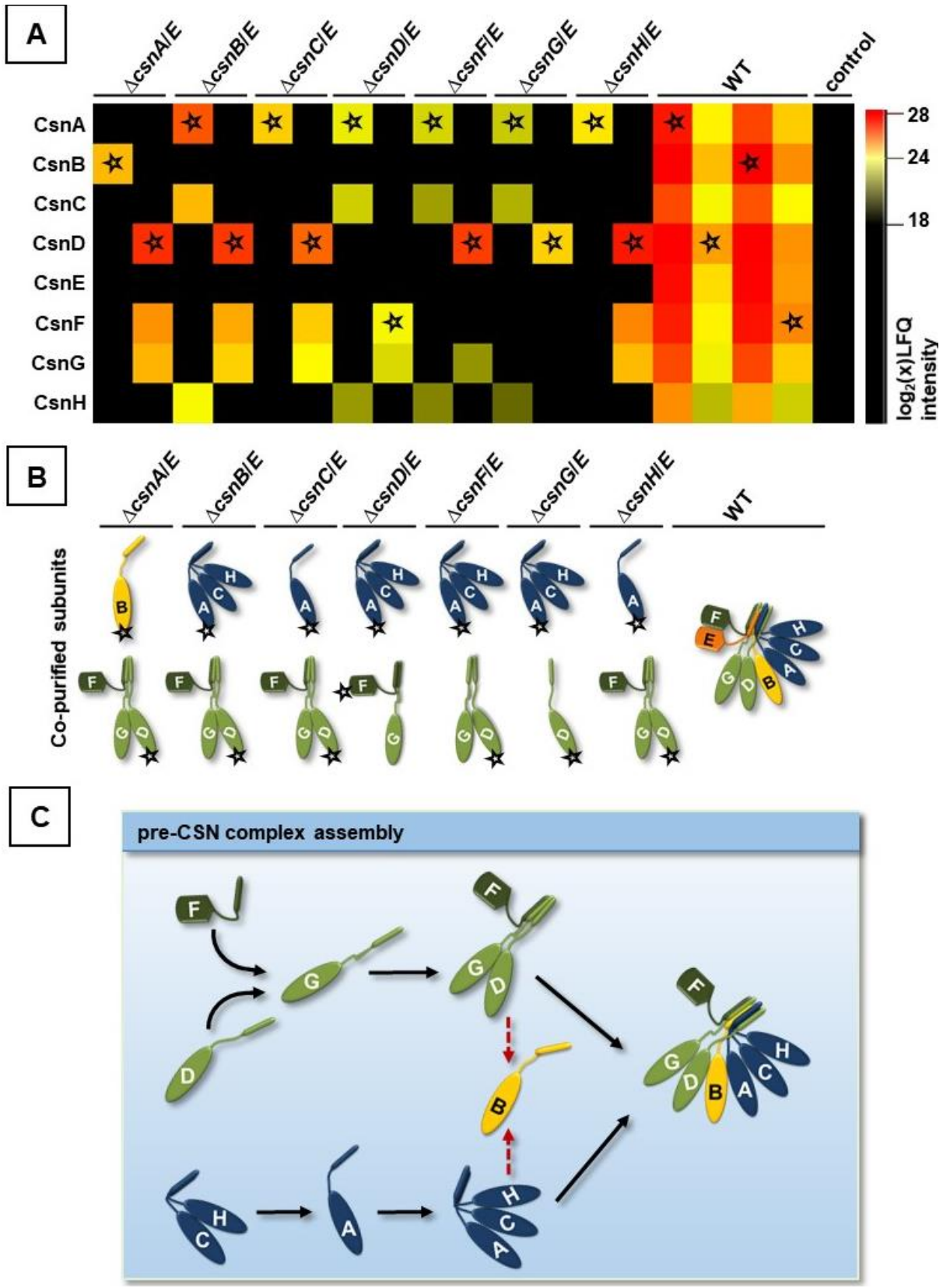

Figure 24. The figure legend is on the next page.

Figure 24. Formation of the two heterotrimeric subcomplexes, CsnD-CsnF-CsnG and CsnA-CsnC-CsnH, is hallmark in the COP9 signalosome assembly pathway in *A. nidulans*.
(**A**) GFP co-purifications from protein extracts of the Δ*pre-csn*Δ*csnE,gfp:csn* mutant strains, producing GFP-CsnA, GFP-CsnB, GFP-CsnD or GFP-CsnF fusion proteins, were carried out (shortened Δ*csnA*/*E,gfp:csn* to Δ*csnH*/*E,gfp:csn*) (Table 7). Protein eluates were further processed and analyzed by LC-MS/MS. The LC-MS/MS data were analyzed with MaxQuant and the heat map was generated with Perseus executing an abundance-based filtering strategy summarized in Table 8 and Table 9. The heat map summarizes the results of the GFP-CsnA, GFP-CsnB, GFP-CsnD and GFP-CsnF mediated affinity purifications represented together and including the results of the control for the GFP-CsnA pull-down experiments. Stars indicate the CSN subunits used as molecular bait for the GFP co-purifications. The heat map was generated on the basis of mean $\log_2$(x)label-free quantification values (LFQ intensities) derived from three to six independent biological replicates for the GFP-CsnD and three to four independent biological replicates for the GFP-CsnA co-purifications. Only those proteins that were enriched in all biological replicates, were further considered as potential interaction partners. The identified proteins were further filtered as follows: $\log_2$(x)LFQ intensity ≤ 18, number of unique peptides ≤ 3 and MS/MS counts ≤ 4. The heat map depicts proteins under $\log_2$(x)LFQ intensity 18 as `not identified´ (shown in black), between $\log_2$(x)LFQ intensity 18 and 24 as `identified´ (shown in a black to yellow gradient) and as `identified with high abundance´ between 24 and 28 (shown in a yellow to red gradient). (**B**) The pictograms summarize the identified CSN subunits in the Δ*pre-csn*Δ*csnE,gfp:csn* strains producing GFP-CsnA or GFP-CsnB and GFP-CsnD or GFP-CsnF fusion proteins as bait. (**C**) Proposed model of the heptameric pre-CSN complex assembly. A CsnD-CsnF-CsnG is formed, where CsnG presumably plays anchoring roles for the interacting CsnD and CsnF. Another trimeric subcomplex, CsnA-CsnC-CsnH assembles, where probably CsnA joins with a CsnC-CsnH dimer. The two trimeric subcomplexes are presumably linked by CsnB to form the seven-subunit pre-CSN complex.

GFP-affinity purification assays using GFP-CsnA as molecular bait were carried out to gather information on the incorporation of CsnA, CsnB, CsnC and CsnH subunits into the pre-CSN complex (Figure 24A). In absence of CsnE and either CsnB, CsnD, CsnF or CsnG, GFP-CsnA was co-eluted with CsnC and CsnH. Thus, an intermediate trimeric CsnA-CsnC-CsnH subcomplex seems evident during COP9 signalosome assembly. GFP-CsnA was unable to bind any further CSN subunit in the absence of CsnE and either CsnC or CsnH. This hints to a potential CsnC-CsnH heterodimer that binds to CsnA, thereby establishing the CsnA-CsnC-CsnH subcomplex. Without CsnA and CsnE subunits, GFP-CsnB as bait was unable to recruit any CSN subunits, although, in this fungal background, the CsnD-CsnF-CsnG trimer was also present. Both, the CsnD-CsnF-CsnG and the CsnA-CsnC-CsnH, subcomplexes were identified upon the absence of CsnE and CsnB, thus, the formation of the two trimers is independent of these subunits (Figure 24B). GFP-CsnA as bait was unable to recruit CsnB, CsnD, CsnF or CsnG, when the pre-CSN complex formation was abolished. This biochemical analysis of CSN subunit deletion strains provides two trimeric subcomplexes as intermediates of the COP9 signalosome assembly pathway in the multicellular filamentous fungus *A. nidulans*. Further assembly of these two heterotrimeric complexes, CsnD-CsnF-CsnG and CsnA-CsnC-CsnH, requires attachment by CsnB subunit to form the stable, but inactive heptameric pre-CSN complex prior to the final integration of the CsnE deneddylase subunit to yield a functional CSN complex with a deneddylase activity (Figure 24C).

3.4 CsnB is required to connect the two trimeric CSN subcomplexes and for the subsequent incorporation of the CsnE deneddylase

The interactions between the remaining two subunits CsnB and the CsnE deneddylase as well as the newly discovered two trimeric CSN-subcomplexes were explored by the genetic and biochemical approach described previously (Figure 24). *In vitro* interaction studies with recombinantly expressed CSN subunits supported COP9 signalosome subcomplexes containing CsnE (Kotiguda *et al.*, 2012). An *A. nidulans csnB* deletion strain was constructed, which produced a functional GFP-CsnE fusion protein to analyze whether CsnE can associate to any of the CSN subcomplexes or subunits. The morphology of the constructed Δ*csnB,gfp:csnE* and the corresponding control Δ*csnE::gfp:csnE* complementation strain (Table 7) was compared by spotting assay. The GFP-CsnE fusion protein was functional, because the Δ*csnE::gfp:csnE* showed wild type-like asexual (Figure 21 and Figure 25A and Figure S1) and sexual development (Figure S2). Moreover, the expression of *gfp:csnE* in the Δ*csnB* strain did not alter its phenotype (Figure 21, Figure 25A and Figure S2).

GFP-immunoblotting revealed similar cellular abundances for the GFP-CsnE fusion protein in the Δ*csnB,gfp:csnE* and its Δ*csnE::gfp:csnE* control strain, suggesting that the GFP-CsnE amount is independent of the absence of CsnB (Figure 25B). GFP-CsnE-based affinity purification experiments were carried out using crude protein extracts of the Δ*csnB,gfp:csnE* and the Δ*csnE::gfp:csnE* control strains to analyze the binding ability of CsnE to any CSN subunits and/or to the identified subcomplexes, in the absence of CsnB linker subunit. As introduced in the previous chapter, an *A. nidulans* strain was included as negative control for the GFP-affinity purifications, which overexpressed a *gfp* construct coding for free, cytoplasmic GFP (Table 7). This control was used to filter out unspecific interactions conferred solely by GFP. Figure 25C shows that free, cytoplasmic GFP alone was not sufficient to recruit CSN subunits in the control strain. In contrast, the wild type-like Δ*csnE::gfp:csnE* complementation strain was applied as reference, in which GFP-CsnE recruited all eight subunits of the CSN holocomplex (Figure 25C). The CsnB subunit assembles with the CsnA-CsnC-CsnH and the CsnD-CsnF-CsnG heterotrimer and does not require the presence of CsnE (Figure 24). This suggests that CsnB has presumably the function of a molecular clamp connecting both heterotrimers (Figure 24C). The relationship between CsnB and CsnE for CSN complex assembly was further examined. Loss of CsnB abolished any interactions between GFP-CsnE and any CSN subunits in the Δ*csnB,gfp:csnE* strain (Figure 25C), showing that CsnB is not only required for connecting both heterotrimeric subcomplexes, but also to incorporate the deneddylase CsnE as final step in the COP9 signalosome assembly (Beckmann *et al.*, 2015). These results demonstrate a novel assembly pathway for the COP9 signalosome in *A. nidulans*, which choreography includes the parallel formation of the CsnA-CsnC-CsnH and the CsnD-CsnF-CsnG heterotrimeric subcomplexes clamped by CsnB to form the heptameric pre-CSN complex. CsnB is required for the subsequent incorporation of the deneddylase subunit to build the catalytically active CSN complex.

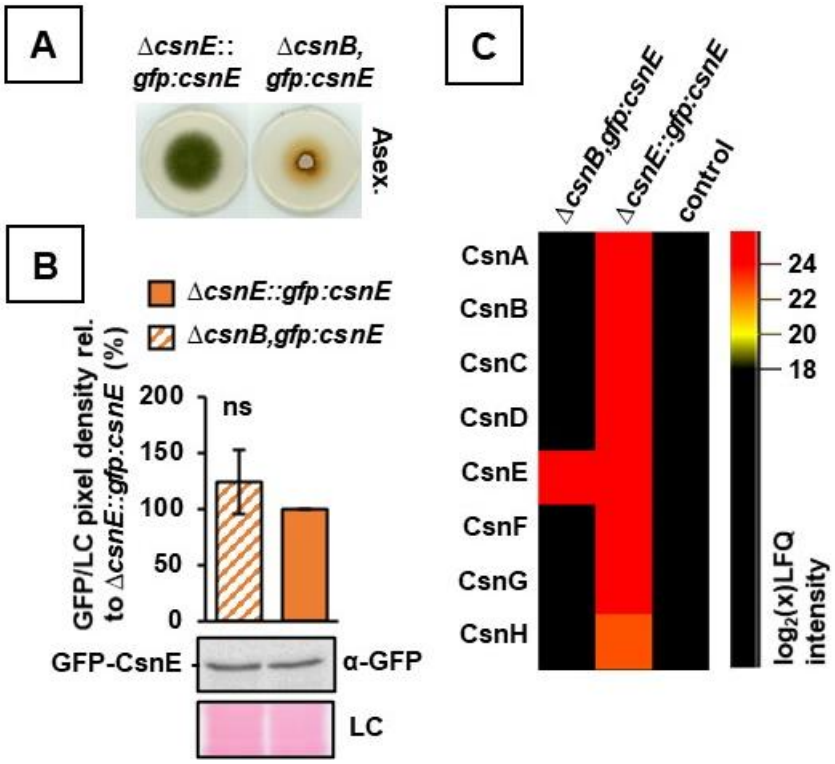

Figure 25. Loss of CsnB abolishes the interactions of CsnE with other CSN subunits.
(**A**) Surface growth and asexual (asex.) development of the Δ*csnB,gfp:csnE* and Δ*csnE::gfp:csnE* complementation strains (Table 7) were analyzed in spotting assays. $2x10^3$ conidia of each fungal strains were point inoculated on MM_{PABA} agar plates. The strains were grown for five days at 37°C under constant illumination and with aeration to induce asexual development. (**B**) The cellular GFP-CsnE abundance in the abovementioned strains was determined with α-GFP immunoblotting experiments. Relative protein amounts were corresponding to the GFP signal/loading control pixel density ratios. The GFP signal/loading control pixel density ratio of the Δ*csnB,gfp:csnE* strain was relative (rel.) to the mean value of the Δ*csnE::gfp:csnE* control strain. Ponceau staining served as loading control (LC). The presented cropped membrane region was used for the pixel density quantification. The charts represent the mean values of five independent biological replicates performed in duplicates and the error bars display SEM. Not significant (ns):p>0.05. (**C**) GFP co-purifications with protein extracts of the Δ*csnB,gfp:csnE* and its control Δ*csnE::gfp:csnE* strain were carried out. 50 µL of both eluate 1 and eluate 2 were combined, further processed and analyzed with LC-MS/MS. The LC-MS/MS data were analyzed with MaxQuant and the heat map was generated with Perseus executing an abundance-based filtering strategy summarized in Table 8 and Table 9. The heat map was generated on the basis of mean log_2(x)label-free quantification values (LFQ intensities) derived from three independent biological experiments. Only those proteins that were enriched in all biological replicates, were further considered as potential interaction partners. The identified proteins were further filtered as follows: log_2(x)LFQ ≤ 18, number of unique peptides ≤ 3, MS/MS counts ≤ 4. The heat map depicts protein candidates under log_2(x)LFQ intensity 18 as `not identified´ (shown in black), between $log_2$(x)LFQ intensity 18 and 20 as `identified´ (shown in a black to yellow gradient) and above 20 as `identified with high abundance´ (shown in a yellow to red gradient).

3.5 Abolishment of the fungal pre-CSN complex formation leads to the disturbance of the remaining CSN subunit abundances

Meticulous surveillance mechanisms are required to maintain the CSN subunit levels, because the CSN complex is part of the specific protein degradation control, which is essential for developmental programs. In plants, some CSN proteins could be stable without interactions, whereas other CSN subunits might require protective interactions with other CSN subunits for stability (Gusmaroli *et al.*, 2007). A genetic approach was applied to explore whether and how the loss of CSN subunit genes and thus, inability to form the pre-CSN and/or CSN complex, affects the protein levels and, therefore, presumably the stability of other CSN subunits in *A. nidulans*. Transcriptional control of the fungal *csn* genes has not been found, not even under intensive stress conditions as the presence of DNA-damaging agents (Lima *et al.*, 2005).

The relative steady state protein levels of selected CSN subunits of the CsnD-CsnF-CsnG and CsnA-CsnC-CsnH subcomplexes as well as of the CsnB linker subunit (Figure 26A) were chosen and monitored by α-GFP immunoblotting following pixel density measurements (Figure 26B to Figure 26E) in different fungal background strains producing respective GFP-CSN fusions. The Δ*pre-csn*Δ*csnE,gfp:csn* double deletion strains were used for these measurements, which were also applied for the GFP-CsnA-, GFP-CsnB-, GFP-CsnD-, GFP-CsnE- and GFP-CsnF-mediated affinity purifications (Table 7; Figure 24). The abundance of the selected GFP-CSN fusion proteins was measured in the Δ*pre-csn*Δ*csnE,gfp:csn* and Δ*csnE,gfp:csn* strains compared to respective wild type controls. The GFP-CSN protein amounts were also monitored in the light of the CSN complex assembly mechanisms (Figure 24, Table S1).

Pixel density measurements corresponding to the steady state protein levels of the various GFP-CSN subunit fusions in wild type background did not reveal significant difference between the analyzed GFP-CSN protein amounts (Figure 26B). The CsnD and CsnF subunits, which shared similar low steady states as GFP fusions in the wild type background (Figure 26B), represent two subunits of the CsnD-CsnF-CsnG heterotrimer (Figure 26A). *csn* subunit gene deletions had mostly strong effects on CsnD or CsnF protein levels as GFP fusions compared to the respective wild type controls, which were set as 100% (Figure 26C). Loss of the gene encoding for the CsnE deneddylase, whose incorporation to the pre-CSN complex represents the final assembly step, caused no significant change for CsnD, but an even five-fold reduction in CsnF protein levels. The relative amounts of GFP-CsnD, as part of the CsnD-CsnF-CsnG subcomplex, also remained wild type-like upon the combined loss of the CsnE and CsnG subunits. GFP-trap assays showed in this genetic background that GFP-CsnD subunit as bait was unable to recruit any CSN subunits (Figure 24 and Table S1) and might therefore be an unprotected target for protein stability control, when the formation of the CsnD-CsnG heterodimer or the CsnD-CsnF-CsnG heterotrimer is abolished. The inability to form the CsnA-CsnC-CsnH subcomplex had a strong impact on the CsnD abundance. Loss of any subunits of this heterotrimer in addition to the loss of CsnE increased the CsnD protein level by a factor of four- to five-fold. The relative cellular GFP-CsnD level was found three-fold elevated in absence of CsnE in combination with either CsnB or CsnF. When CsnE and CsnD were missing, GFP-CsnF as bait was co-purified with CsnG (Figure 24) and had a 3.5-fold elevated amount compared to the wild type control (Figure 26C). This might be, because CsnF is protected and stable in a form of the CsnF-CsnG heterodimer.

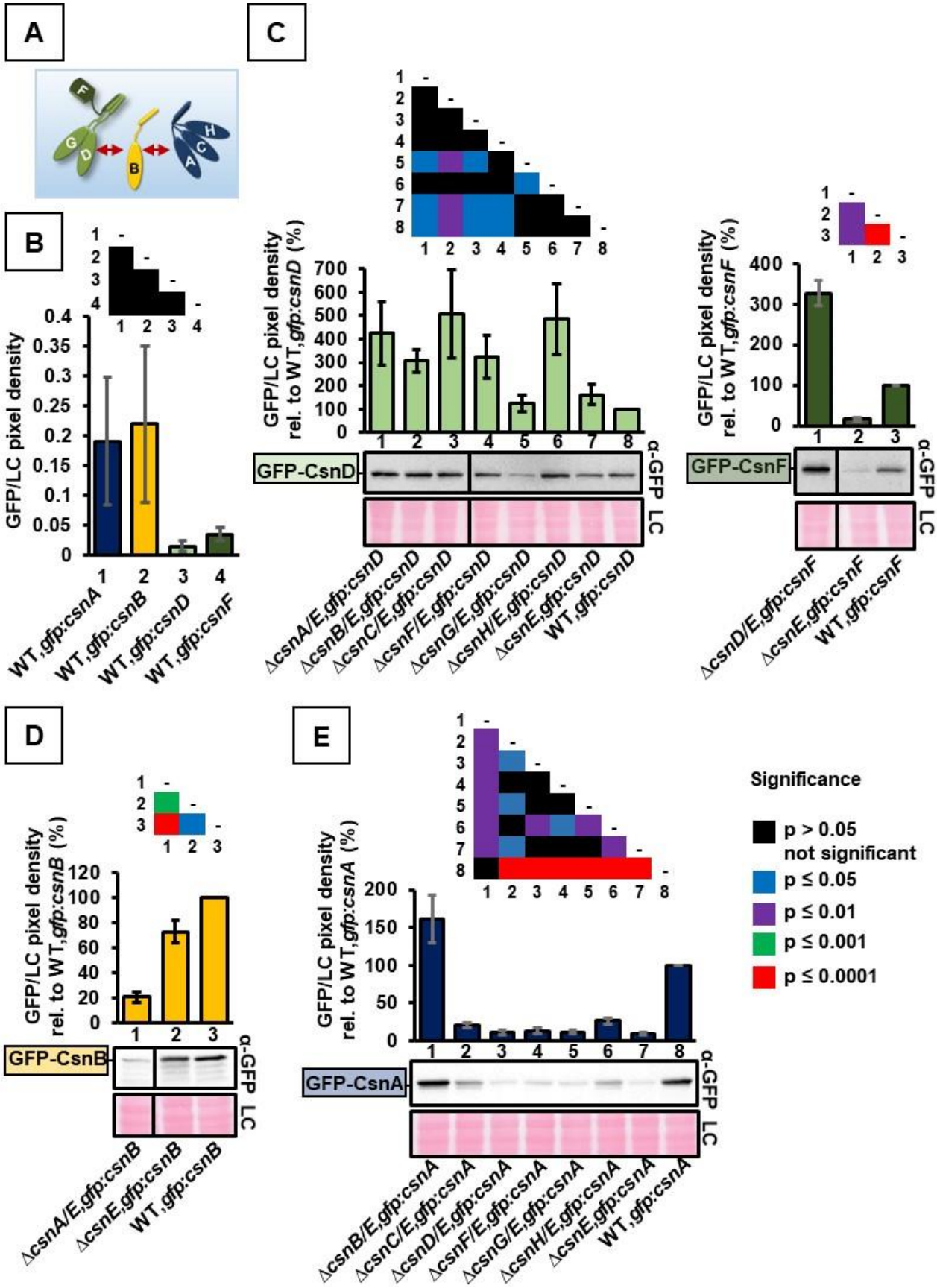

Figure 26. The figure legend is on the next page.

Figure 26. The relative abundance of GFP-CsnA, GFP-CsnB, GFP-CsnD and GFP-CsnF in the Δ*pre-csn*Δ*csnE*,*gfp:csn* strains compared to respective wild type controls.
The cellular protein abundance of the GFP fusion proteins was determined by α-GFP immunoblotting in the Δ*pre-csn*Δ*csnE,gfp:csn* double deletion strains, shortened Δ*csnA*/*E,gfp:csn* to Δ*csnH*/*E,gfp:csn*. The presented cropped region of the western blot was used for the pixel density quantification. Relative protein amounts were corresponding to the GFP signal/loading control pixel density ratios. The GFP signal/loading control pixel density ratio of each strain was relative (rel.) to the mean value of the respective wild type strain (WT,*gfp:csn*). Ponceau staining was used as loading control (LC). The charts represent the mean of three independent biological replicates, each performed in duplicates, and the error bars display SEM. The matrices above the chart area represent the significance of pairwise comparisons between protein amounts (marked with numbers) expressed in the different fungal strains. (**A**) Schematic model of the seven subunit pre-CSN complex assembly steps. (**B**) The absolute amount of the GFP fusion proteins was determined in wild type background. The figure depicts the (**C**) GFP-CsnD and GFP-CsnF, (**D**) GFP-CsnB, (**E**) GFP-CsnA abundance relative to the respective wild type control. (**D**) Lower migrating and fainter bands can be observed on the immunoblot of GFP-CsnB produced in Δ*csnA*Δ*csnE,* in Δ*csnE* and in wild type background as well, which probably correspond to degradation products of GFP-CsnB.

CsnB is the linker between the two heterotrimeric complexes (Figure 26A). The relative GFP-CsnB amount showed a slight, 1.25-fold reduction upon loss of CsnE (Figure 26D), whereas cellular GFP-CsnE levels were unaffected by the absence of CsnB (Figure 25B). In contrast, the additional loss of CsnA in a CsnE-deficient background strain resulted in five-fold reduction of the relative cellular GFP-CsnB amount. This suggests that the cellular CsnB levels strongly depend on the presence of CsnA and/or the intact CsnA-CsnC-CsnH subcomplex rather than on the CsnE deneddylase.

CsnA was chosen as representative of the CsnA-CsnC-CsnH heterotrimeric subcomplex for stability analysis (Figure 26E). The GFP-CsnA abundance was wild type-like in a strain with the combined loss of the deneddylase CsnE and clamp factor CsnB, probably because the formation of the CsnA-CsnC-CsnH subcomplex occurs independently of the these subunits (Figure 24 and Table S1). In contrast, when compared to the wild type control, GFP-CsnA was by a factor of five to 10-fold less abundant without CsnE alone, as well as upon the combined loss of CsnE and subunits of both heterotrimeric subcomplexes (Figure 26E). Noteworthy, the inability to form the CsnD-CsnF-CsnG subcomplex had a stronger negative effect on the cellular GFP-CsnA amount than the inability to form the CsnA-CsnC-CsnH trimer. Upon the combined loss CsnE and either CsnC or CsnH, the CsnD-CsnF-CsnG trimer could form, what had a slight positive effect on the relative CsnA level. This suggests that either the intact CSN holocomplex or at least both, the CsnA-CsnC-CsnH and the CsnD-CsnF-CsnG, trimers are required to reach wild type-like GFP-CsnA levels.

Taken together, there are a variety of distinct responses of the cellular steady state levels of different CSN subunits when the genes for other subunits are missing. Relative protein levels of CsnA, a component of the trimeric CsnA-CsnC-CsnH complex, remain unaffected by the loss of the linker CsnB and the deneddylase CsnE, but are decreased when subunits of one of the two heterotrimeric CSN subcomplexes are missing. The steady state level of the clamp protein CsnB is reduced when the CsnE deneddylase and CsnA are absent. In contrast, relative protein levels of CsnD, a subunit of the CsnD-CsnF-CsnG subcomplex, are rather increased by the pre-CSN complex deficiency. This suggests that the CSN assembly choreography is monitored by cellular surveillance systems, which specifically control the correct CSN subunit levels for the assembly.

3.6 CsnE promotes nuclear accumulation of CSN subunits from both heterotrimeric complexes

A number of studies, which investigated the subcellular localization of the CSN complex and the CSN subunits revealed substantial differences between organisms in various conditions (Chamovitz *et al*., 1996; Mundt *et al.,* 2002). For example, the human CSN complex is found in the cytoplasm and nuclei, but upon stress, the localization shifts to mainly nuclear (Fuzesi-Levi *et al.*, 2014). It was suggested that the nuclear accumulation of CSN subunits is connected to the CSN complex formation (Chamovitz *et al*., 1996). The *in vivo* COP9 signalosome assembly pathway in *A. nidulans*, including the formation of two heterotrimers, their connection by CsnB (Figure 24) and finally the CsnE deneddylase integration probably also has to be coordinated with cellular localization of the GFP-CSN fusion proteins.

The subcellular location of the CSN holocomplex and subunits of the heterotrimers of the *in vivo* assembly pathway was addressed in *A. nidulans.* Confocal microscopy was carried out with fungal strains producing CsnA, CsnD or CsnF as GFP fusions in the wild type or in the *csnE* deletion strain. The GFP-CsnA, GFP-CsnD and GFP-CsnF signals were observed throughout the fungal hyphae, but a stronger GFP signal overlapping the DAPI-stained nuclei was detected in the wild type background (Figure 27A). The same result was observed, when the fungal strains were cultivated at lower temperatures to reduce the possibility of heat stress-induced nuclear localization (Figure S3). These results show that the intact eight-subunit COP9 signalosome is mainly localized in the nuclei of the wild type cells at 37°C as well as 30°C. Nuclear co-localization of the DAPI-stained nuclei and the GFP-CsnA, GFP-CsnD or GFP-CsnF signals could not be observed upon loss of CsnE (Figure 27A). Nevertheless, existance of smaller nuclear subpopulations of GFP-CsnA, GFP-CsnD or GFP-CsnF cannot be excluded. The GFP signal may be under the detection treshold due to the decreased relative amount of GFP-CsnF and GFP-CsnA in absence of CsnE (Figure 26C and Figure 26E). Since the cellular GFP-CsnD level is wild type-like in absense of CsnE, it should be expected that the GFP-CsnD level is above the confocal microscopy detection treshold (Figure 26C). Loss of CsnE diminished the nuclear accumulation of the GFP-CsnA, GFP-CsnD and GFP-CsnF fusion proteins, but the subcellular location of the pre-CSN complex is yet open (Figure 27B). A stable seven-subunit pre-CSN complex was identified in a *csnE*-deficient strain by CsnD-GFP mediated pulldown assays (Beckmann *et al.*, 2015) and by GFP-CsnD (data not shown), whereas there is no such experimental information available using GFP-CsnA or GFP-CsnF as molecular bait for the purification (data not shown). Thus, it is yet unclear whether GFP-CsnA or GFP-CsnF recruits the pre-CSN complex in the absence of CsnE. Through this, it is also unclear whether the confocal microscopy visualizes the pre-CSN complex or complex-unbound populations of GFP-CsnA and GFP-CsnF, but it might visualize a mainly cytoplasmic pre-CSN complex by GFP-CsnD.

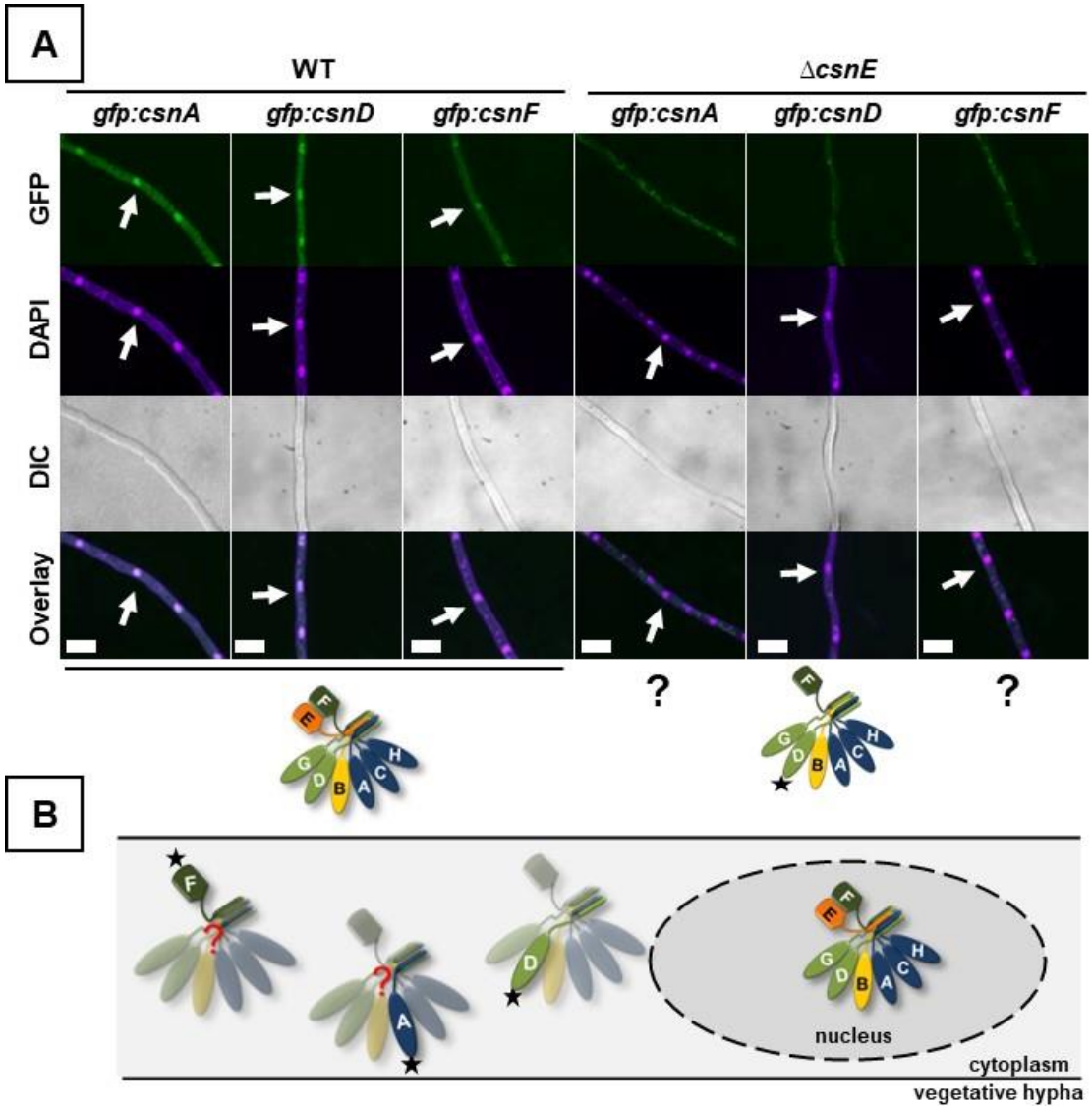

Figure 27. The presence of CsnE and/or the CSN holocomplex is necessary for the nuclear accumulation of CsnA, CsnD and CsnF.
(**A**) The GFP signal co-localizes with the DAPI-stained nuclei in wild type strains producing either GFP-CsnA, GFP-CsnD or GFP-CsnF, whereas such nuclear accumulation of either GFP-CsnA, GFP-CsnD or GFP-CsnF could not be observed in the absence of CsnE. The nuclei are indicated with white arrows. The GFP and the DAPI signals are merged in the overlay pictures. The confocal microscopy was carried out with fungal cultures grown vegetatively for 20 hours at 37°C. The experiment was performed in three independent biological replicates. The autofluorescence of each analyzed strains was subtracted against the background signal of the wild type strain (not shown). Scale bars represent 10 µm. The pictograms depict the CSN subunits or subcomplexes, which were identified by GFP-affinity purifications in the analyzed background strains (Figure 24). The stars label the GFP-tagged CSN subunits. (**B**) Proposed model of the interplay between CsnE and GFP-CsnA, GFP-CsnD and GFP-CsnF for the nuclear accumulation. In the wild type strains, which harbor the eight subunit CSN complex (Figure 24), all analyzed GFP-CSN subunit fusions were detected in the nuclei, thus, the CSN holocomplex is nuclear in *A. nidulans*. In absence of CsnE, in the GFP-CsnD-mediated GFP-trap experiments the seven-subunit pre-CSN complex was identified (data not shown), which is mainly cytoplasmic. The pre-CSN complex could not be identified in the GFP-trap experiments with GFP-CsnA or GFP-CsnF as baits (data not shown), which fusion proteins could not accumulate in the nuclei. Therefore, it is not clear whether these fusion proteins visualize the pre-CSN complex. The stars label the GFP-tagged CSN subunits.

3.7 CsnA together with CsnE is required for nuclear accumulation of CsnB in *Aspergillus nidulans*

Loss of CsnE and/or the CSN holocomplex integrity diminishes the nuclear localization of CsnA, CsnD and CsnF (Figure 27), which are part of the heterotrimeric pre-CSN assembly intermediates (Figure 24). CsnB plays an important role in connecting these complexes into the heptameric pre-CSN complex and to allow the incorporation of the catalytic CsnE deneddylase subunit. The subcellular localization of GFP-CsnB was compared between wild type, the Δ*csnE* and the Δ*csnA*Δ*csnE*,*gfp:csnB,rfp:h2a* strains to elaborate whether CsnB also requires CsnE for nuclear location, as it was shown for CsnA, CsnD and CsnF. The GFP signal of GFP-CsnB was present throughout the fungal cell, but the largest GFP-CsnB population was detected in the nuclei in the wild type background (Figure 28A). The nuclear accumulation of GFP-CsnB remained in the Δ*csnE* strain. Thus, the nuclear accumulation of CsnB did not require CsnE, which was different to the other analyzed subunits CsnA, CsnD or CsnF, which were promoted into the nuclei by CsnE. Combined loss of the CsnA and CsnE subunits changed the cellular localization of the GFP-CsnB fusion protein, because the GFP signal was evenly distributed in the entire fungal hyphae without concentration in the nuclei (Figure 28). Accordingly, CsnB can shuttle to or persist in the nuclei independently of the deneddylase CsnE, what had slightly increased the cellular CsnB levels (Figure 26D). In contrast, the nuclear accumulation of CsnB depends on the presence of CsnA and CsnE subunits (Figure 28B). GFP-CsnB could not recruit any of the remaining CSN subunits upon the combined loss of CsnA and CsnE (Figure 24). The complex-unbound free GFP-CsnB was evenly distributed within the fungal cell, without accumulation in the nuclei. The relative CsnB amount was strongly reduced in absence of CsnA and/or the CsnA-CsnC-CsnH subcomplex, which might be under the detection threshold of confocal microscopy (Figure 26D). The visualization by fluorescent microscopy does not distinguish between CsnB, as a complex-unbound, free protein and as a subunit of the pre-CSN complex. Therefore, it is yet unclear whether free or pre-CSN complex-bound GFP-CsnB was detected in the nuclei in absence of CsnE. In absence of CsnE, GFP-CsnD as bait recruited the pre-CSN complex in GFP-trap experiments (data not shown), and in this background GFP-CsnD was mainly cytoplasmic localized (Figure 27). These observations suggest a discrepancy for the pre-CSN complex localization, when analyzed via GFP-CsnB or GFP-CsnD.

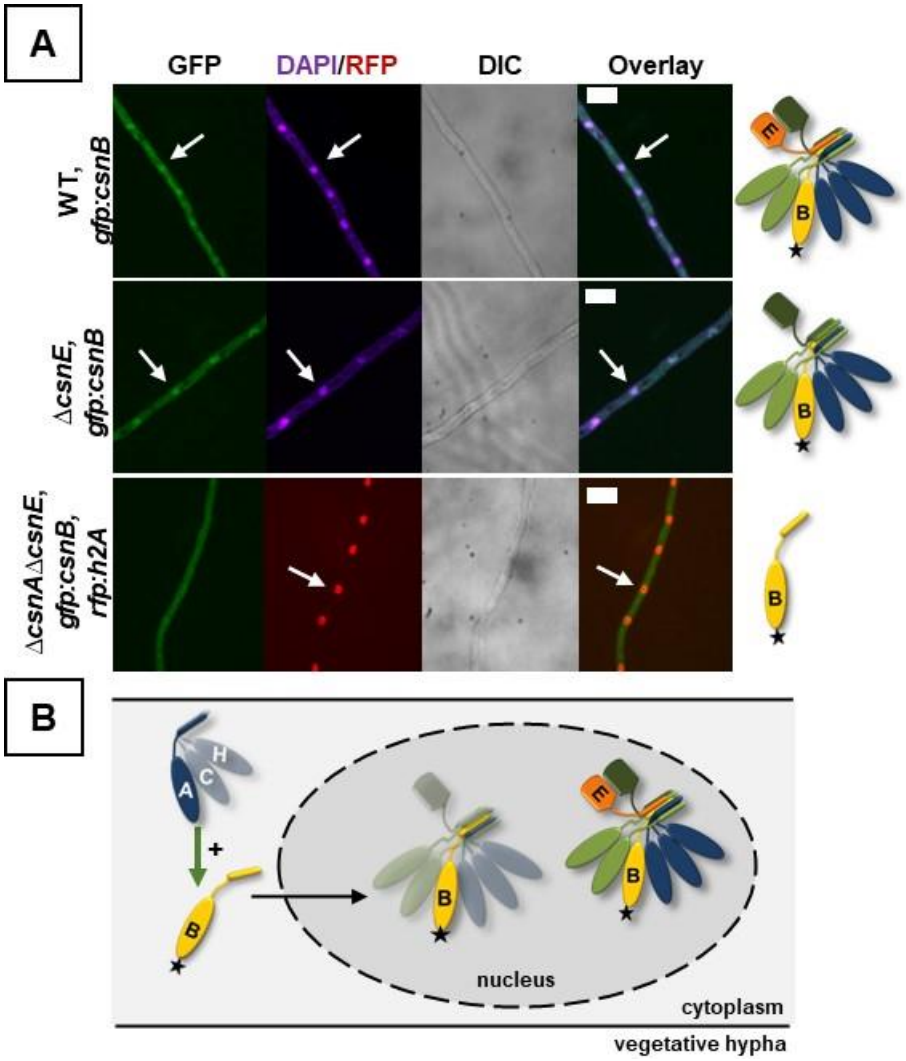

Figure 28. CsnE in combination with CsnA promoted the nuclear accumulation of CsnB.
(**A**) Confocal microscopy reveals the co-localization of the nuclear DAPI and the GFP-CsnB signal in the Δ*csnE,gfp:csnB* strain, such as in the WT,*gfp:csnB* strain. Nuclear co-localization of the GFP-CsnB and the nuclear RFP signal could not be observed in the Δ*csnA*Δ*csnE*,*gfp:csnB,rfp:h2a* strain. The nuclei, indicated with white arrows, were visualized by DAPI staining or through expressing RFP-H2A. The GFP and the DAPI or RFP signals are merged in the overlay pictures. The confocal microscopy was carried out with fungal cultures grown vegetatively for 20 hours at 37°C. The experiment was performed in at least three independent biological replicates. The autofluorescence of each analyzed strains was subtracted against the background signal of the wild type strain (not shown). Scale bars represent 10 µm. The pictograms depict the CSN subunits or subcomplexes, which were identified by GFP-affinity purifications in the analyzed background strains (Figure 24). The star labels the GFP-tagged CSN subunits. (**B**) Proposed model of the interplay of CsnE and CsnA with GFP-CsnB. In the wild type strain, which harbors the eight subunit CSN complex (Figure 24), GFP-CsnB was detected in the nuclei. In absence of CsnE, in the GFP-CsnB-mediated GFP-trap experiments the seven-subunit pre-CSN complex was identified (data not shown), which is mainly nuclear enriched. The nuclear accumulation of GFP-CsnB is diminished in absence of CsnA and CsnE, in which background GFP-CsnB was identified as free, CSN complex-unbound fusion protein (Figure 24). From this, a role of CsnA or the CsnA-CsnC-CsnH subcomplex in the nuclear localization of CsnB is concluded, which is supposedly linked with CSN complex assembly steps. The stars label the GFP-tagged CSN subunits.

3.8 CsnB promotes the nuclear accumulation of the CsnE deneddylase

The nuclear accumulation of CsnB is independent of CsnE (Figure 28). It was analyzed whether *vice versa*, the CsnE localization depends on CsnB. Therefore, the subcellular localization of GFP-CsnE was examined by confocal microscopy in the Δ*csnB,gfp:csnE* strain compared to the wild type-like control Δ*csnE::gfp:csnE* complementation strain. The GFP-CsnE signal was co-localized and predominantly found in the nuclei in the Δ*csnE::gfp:csnE* complementation strain and it was distributed throughout the hyphae in the absence of CsnB (Figure 29).

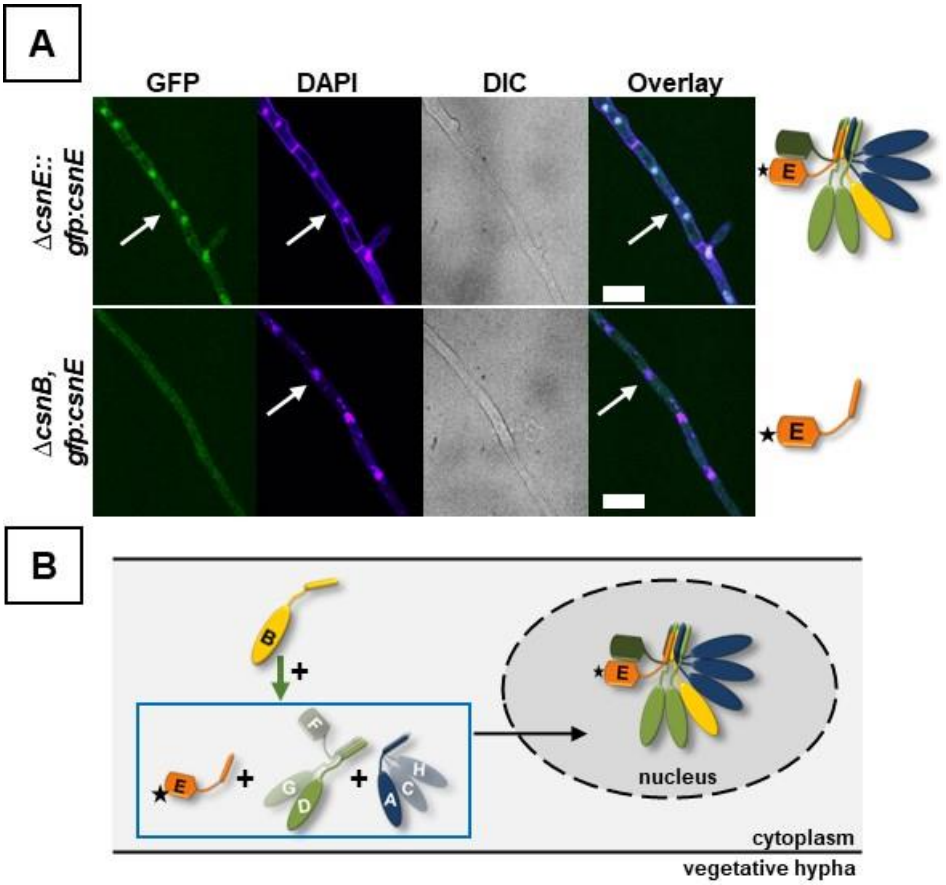

Figure 29. CsnB is required for the nuclear accumulation of GFP-CsnE.
(**A**) A larger GFP-CsnE subpopulation was enriched in the nuclei in the Δ*csnE::gfp:csnE* control strain, but not in the Δ*csnB,gfp:csnE* strain. The nuclei, indicated with white arrows, were visualized by DAPI staining. The GFP and the DAPI signals are merged in the overlay pictures. The confocal microscopy was carried out with fungal cultures grown vegetatively for 20 hours at 37°C. The experiment was performed with three to six independent biological replicates. The autofluorescence of each analyzed strains was subtracted against the background signal of the wild type strain (not shown). Scale bars represent 10 µm. The pictograms depict the CSN subunits or subcomplexes, which were identified by GFP-affinity purifications in the analyzed background strains (Figure 24). The stars label the GFP-tagged CSN subunits. (**B**) Proposed model of the interplay between CsnB and GFP-CsnE. In the wild type strain, which harbors the eight subunit CSN complex (Figure 24), GFP-CsnE was detected in the nucleus. In absence of CsnB, interactions of GFP-CsnE with any CSN subunits were diminished in GFP-trap experiments (Figure 25). Thus, probably the free, CSN complex-unbound GFP-CsnE is visualized, which is distributed between cytoplasm and nuclei without nuclear enrichment. Taken together, CsnB is required for the nuclear accumulation of CsnE and to bind the deneddylase subunit with other CSN subunits. The stars label the GFP-tagged CSN subunits.

The cellular CsnE protein amount was wild type-like upon the loss of CsnB (Figure 25B) and the CsnB abundance was only slightly reduced in the absence of CsnE (Figure 26D). Thus, the cellular GFP-CsnE level probably cannot account for the diminished nuclear accumulation of GFP-CsnE in the absence of CsnB. GFP-CsnE was unable to associate to CSN subunits or subcomplexes without CsnB (Figure 25C), so confocal microscopy visualize the stable and free, complex-unbound CsnE, which is evenly distributed between cytoplasm and nuclei. Supposedly, CsnB connects the two trimeric subcomplexes, thus enable the CsnE incorporation, which processes are coupled with nuclear accumulation of CsnE. As result, an eight-subunit nuclear CSN holocomplex is formed (Figure 29B).

3.9 The CsnA-CsnC-CsnH subcomplex is distributed between the nuclei and the cytoplasm, whereas the CsnD-CsnF-CsnG heterotrimer localized predominantly in the nuclei

The subcellular location of the two heterotrimeric subcomplexes CsnA-CsnC-CsnH and CsnD-CsnF-CsnG was examined in Δ*csnB*Δ*csnE,gfp:csn* strains by confocal microscopy (Figure 30). The Δ*csnB*Δ*csnE,gfp:csn* strains, such as the wild type controls produce either GFP-CsnA or GFP-CsnD and an RFP-fused histone 2A protein to visualize the nuclei, resulting in the Δ*csnB*Δ*csnE,gfp:csnA,rfp:h2a*, Δ*csnB*Δ*csnE,gfp:csnD,rfp:h2a*, WT,*gfp:csnA,rfp:h2a* and the WT,*gfp:csnA,rfp:h2a* strains. GFP-CsnA and GFP-CsnD fusion proteins exhibit wild type-like steady state amounts in these backgrounds (Figure 26C and Figure 26E) and were found as members of the CsnA-CsnC-CsnH and the CsnD-CsnF-CsnG heterotrimers, which are formed and co-exist independently of CsnB and CsnE (Figure 24). The GFP-CsnA signal is evenly distributed between cytoplasm and nuclei, whereas the GFP-CsnD signal was predominantly localized in the nuclei of the vegetative hyphae upon loss of CsnB and CsnE (Figure 30A). Similar observations were made in a preliminary experiment, where the subcellular localization of the CsnA-CsnC-CsnH and the CsnD-CsnF-CsnG heterotrimers was examined in a Δ*csnD*Δ*csnE,gfp:csnA* and a Δ*csnA*Δ*csnE,gfp:csnD* strain, respectively (Figure S4). Subcomplex-unbound subpopulations of CsnA and CsnD might persist in the nuclei or that they might shuttle between nuclei and cytoplasm. Nuclear import or export signals were not predicted for CsnA and CsnD (Table S2), which suggests that these proteins rely on either their trimeric CSN subunit interactions or on other, yet unidentified transport proteins for their nucleocytoplasmic shuttle. These results propose that in absence of CsnB and CsnE, the CsnD-CsnF-CsnG subcomplex is predominantly localized in the nuclei. In contrast, the CsnA-CsnC-CsnH subcomplex is distributed between the nuclei and cytoplasm of the vegetative hyphae (Figure 30B). This localization is independent of the presence or absence of the other heterotrimeric subcomplex. The GFP and the nuclear RFP signals co-localize in the wild type control strains producing either of the abovementioned GFP-CSN fusion proteins (Figure 30).

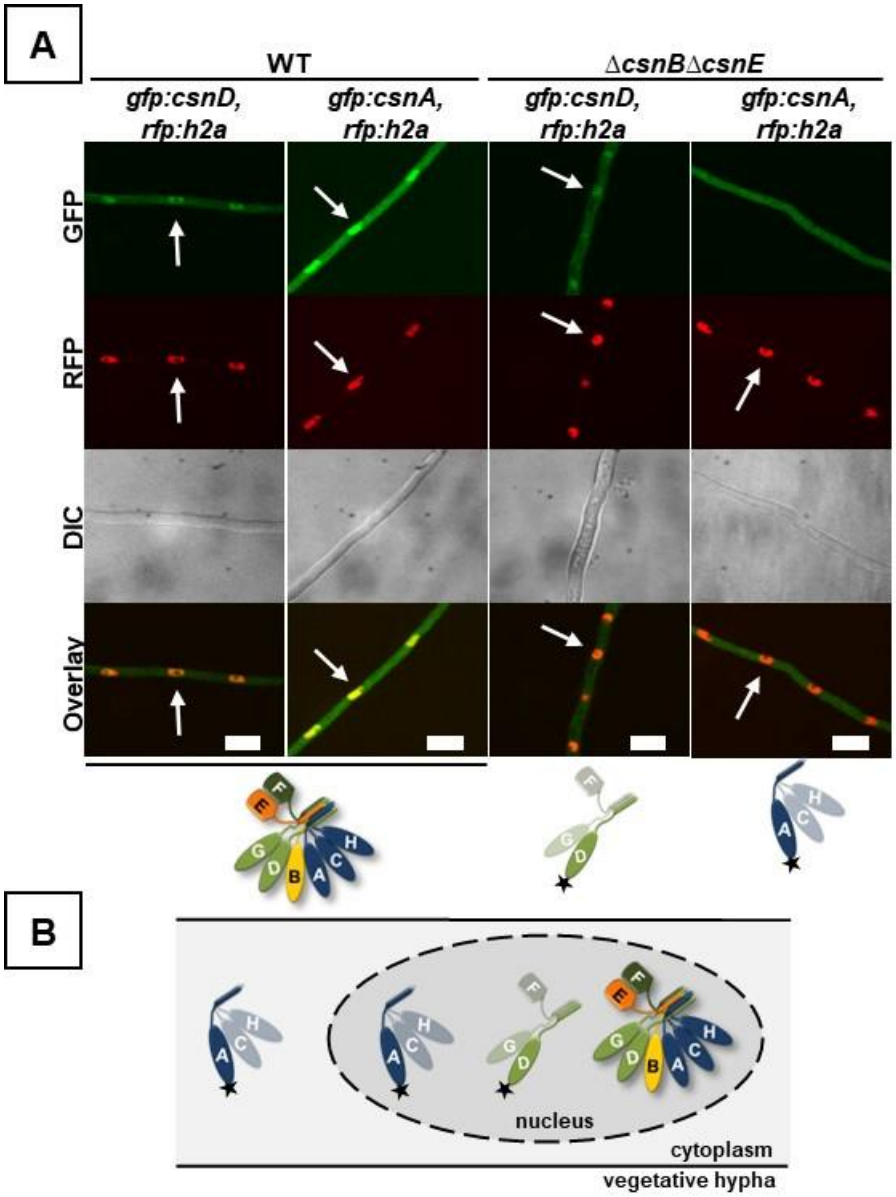

Figure 30. A larger subpopulation of GFP-CsnD and/or the CsnD-CsnF-CsnG subcomplex localized predominantly in the nuclei, whereas GFP-CsnA and/or the CsnA-CsnC-CsnH subcomplex was equally distributed between cytoplasm and nuclei in the vegetative hyphae.
(**A**) In the wild type control strains, the GFP and the RFP-tagged histone 2A signals co-localize. The GFP-CsnA signal was evenly distributed between cytoplasm and nuclei, whereas the GFP-CsnD signal accumulated in the nuclei of the vegetative hyphae in absence of both, CsnB and CsnE. The confocal microscopy was carried out with fungal cultures grown for 20 hours vegetatively at 37°C. The experiment was performed in six independent biological replicates. The autofluorescence of each analyzed strain was subtracted against the wild type strain (not shown). The nuclei, indicated with white arrows, were visualized through producing RFP-histone 2A. The GFP and the RFP signals are merged in the overlay pictures. Scale bars represent 10 µm. The pictograms represent the eight subunit CSN holocomplex identified in the wild type strain and the CsnA-CsnC-CsnH and the CsnD-CsnF-CsnG heterotrimeric complexes identified upon loss of both, CsnB and CsnE, in the GFP-affinity purification experiments (Figure 24). The stars label the GFP-tagged CSN subunits. (**B**) The proposed model depicts the mainly nuclear CsnD-CsnF-CsnG subcomplex and the CsnA-CsnC-CsnH subcomplex, which is distributed between cytoplasm and nuclei in the vegetative hyphae. The stars label the GFP-tagged CSN subunits.

In summary, there is a complex interplay between the subcellular localization of functional, fluorescently tagged GFP-CSN subunits. The CSN holocomplex was localized predominantly to the nuclei (Figure 27A, Figure 28A and Figure 29A). In contrast, in absence of CsnE such nuclear accumulation could not be shown for GFP-CsnA, GFP-CsnF and GFP-CsnD or the pre-CSN visualized by GFP-CsnD, which are primarily cytoplasmic (Figure 27A). GFP-CsnB remained predominantly nuclear upon loss of CsnE (Figure 28A). Nuclear accumulation could neither be shown for the CSN complex-unbound GFP-CsnE in the *csnB*-deficient strain (Figure 29A) nor for the CSN complex-unbound GFP-CsnB in the Δ*csnA*Δ*csnE* strain (Figure 28A). In the absence of CsnB and CsnE, mainly nuclear localization was shown for the CsnD-CsnF-CsnG, but not for the CsnA-CsnC-CsnH subcomplex, which was evenly distributed between nuclei and cytoplasm in the fungal cell (Figure 30).

3.10 Impact of CsnB nuclear localization sequences NLS1 and NLS2 on fungal growth and abundance, stability and subcellular localization of the protein

3.10.1 *Aspergillus nidulans* CsnB possesses two predicted nuclear target sequences and a predicted nuclear export signal

A larger subpopulation of CsnB co-localizes to the nuclei in the absence of CsnE, whereas similar accumulation could not be observed for CsnA, CsnD or CsnF (Figure 27 and Figure 28). *In silico* analyses of the CsnB amino acid sequence and protein structure were carried out to search for nuclear localization signals (NLSs), which might promote the nuclear transport of this linker subunit (Figure 31). Computational search with different search engines revealed two potential NLSs of *A. nidulans* CsnB, similarly to its human ortholog CSN2 (Figure 31A). The 33 amino acid long NLS1 (R278 to D310) of CsnB is located in the PCI domain, which represents the interaction surface with other CSN subunits. The NLS2 is a seven amino acid (R487 to S493) long fungal specific sequence, which is not present in the human CSN2 subunit. The *A. nidulans* NLS1 sequence shows high similarity to the predicted HsNLS2 of the human CSN2 with conserved regions such as `KPYK´ (Figure 31A and Figure 31B). The `KPYK´ sequence of the predicted NLS1 is potentially sufficient to bind importins. In a structural model of CsnB, NLS1 lies in a hidden conformation, whereas NLS2 is supposedly accessible for importin proteins (Figure 31C). Nevertheless, the structural arrangement of CsnB might differ in a CSN complex-bound and an unbound state, which might influence the importin binding efficiency. The *in silico* sequence search was carried out for CsnA, CsnC, CsnD, CsnE, CsnF, CsnG and CsnH as well, but none of the applied search engines revealed any NLS (Table S2). *In silico* search identified potential nuclear export signals (NES) in CsnB (Figure 31A), but NESs were also predicted for other CSN subunits, except for CsnA and CsnD (Table S2).

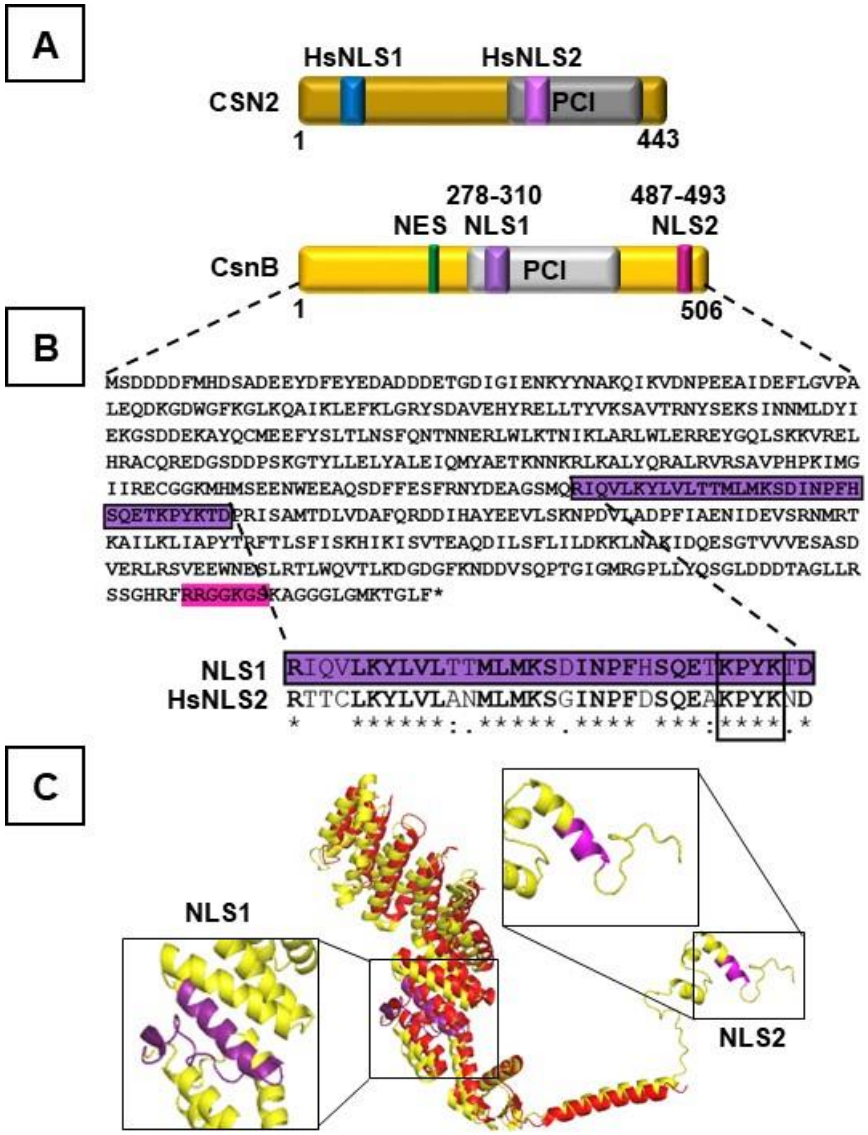

Figure 31. Computational analysis revealed two potential NLSs of *A. nidulans* CsnB similarly to the human ortholog subunit CSN2.
(**A**) Schematic depiction shows the position of NLS1 and NLS2 in *A. nidulans* CsnB as well as HsNLS1 and HsNLS2 in human CSN2. The *in silico* search for NLS sequences was carried out with different search engines for higher confidence. The cNLS Mapper tool predicted NLS1 with the score 5.1/10. NLS1, highlighted with purple, is a bipartide NLS spanning from R278 to D310 in the deduced CsnB amino acid sequence. The CsnB NLS2, highlighted with magenta, located between R487 and S493 and it was predicted with NLStradamus. The cNLS Mapper search revealed HsNLS1 and HsNLS2 of human CSN2, spanning from E44 to K74 and R272 to D305, with the scores 5.9/10 and 6/10, respectively. The NetNes 1.1 tool revealed potential CsnB NES sequence spanning from L202 to I207 (shown in green). (**B**) The multiple sequence alignment revealed similarity between NLS1 and HsNLS2 and conserved regions such as `KPYK´ (shown in box). `*´ conserved residues, `:´ strong similarity between the residues, `.´ weak similarity between the residues. The multiple sequence alignment between *A. nidulans* CsnB and the human CSN2 was carried out with ClustalW/Muscle. (**C**) The complex-bound human CSN2 structure (drawn in red, UniProt ID: P61201, PDB ID: 4D10) was used as template for the structural alignments with *A. nidulans* CsnB, shown in yellow (p.c. Achim Dickmanns and Piotr Neumann, Department for Molecular Structural Biology, GZMB, Göttingen).

3.10.2 NLS1 is required for the accurate function and wild type-like protein abundance of *A. nidulans* CsnB

The predicted CsnB NLSs were examined using mutant versions (deletions and amino acid substitutions) of the CsnB NLS1 and NLS2 sequences to investigate their impact on growth and development as well as abundance and subcellular localization of CsnB (Figure 32). In the GFP-CsnB$^{\Delta NLS1}$ and GFP-CsnB$^{\Delta NLS2}$ versions the complete NLS1 (R278 to D310) and NLS2 (R487 to S493) sequence of CsnB were deleted. In the GFP-CsnB*^{NLS1} and GFP-CsnB*^{NLS2} amino acid substituted mutant versions the hypothetical importin binding lysine residues of CsnB NLS1 and NLS2 were replaced with neutral amino acids in expectation to maintain the correct folding, but to prevent the binding of importin proteins (Figure 31A). The lysine residues K305 and K308 of the conserved `KPYK´ NLS1 sequence were exchanged with threonine, resulting in `TPYT´ in the GFP-CsnB*^{NLS1} version. The arginine residues R487, R488 and lysine residue K491 of the `RRGGKGS´ NLS2 sequence were replaced with alanine, resulting in `AAGGAGS´ in the GFP-CsnB*^{NLS2} version. The CsnB NLS mutant constructs were re-introduced in the native *csnB* locus as a single copy in the Δ*csnB* strain. A wild type strain was used as a control for the experiments, which produces GFP-CsnB (WT,*gfp:csnB*) (Figure 32B). Growth, asexual and sexual development of the resulting *A. nidulans* NLS mutant strains were examined and compared to the parental Δ*csnB* strain, the WT,*gfp:csnB* and the wild type strain. The re-integration of the *csnB* gene deleted for the NLS2 sequence and mutated for the NLS1 and NLS2 in the Δ*csnB* strain could restore the wild type-like fungal growth and development. In contrast, the re-integration of the *csnB* gene deleted for the NLS1 sequence resulted in a fungal strain, whose phenotype remained Δ*csnB*-like. This suggests that the 33 amino acid NLS1 sequence, located in the PCI domain is essential for cellular CsnB function.

The phenotypical analysis demonstrated that the NLS1 sequence of CsnB is essential for normal fungal growth and development (Figure 32B). Protein amounts were analyzed by α-GFP immunoblotting to investigate, if the growth reduction and the asexual developmental defects caused by the NLS1 deletion are due to the change of the GFP-CsnB amount (Figure 32C). The wild type GFP-CsnB and the GFP-CsnB$^{\Delta NLS2}$, GFP-CsnB*^{NLS1} and GFP-CsnB*^{NLS2} migrated in the gel at the predicted molecular weight of around 91 kDa and the relative amount of GFP-CsnB*^{NLS1}, GFP-CsnB$^{\Delta NLS2}$, GFP-CsnB*^{NLS2} was approximately 120%, 130% and 150% of the wild type GFP-CsnB, respectively. The immunoblot experiments revealed a truncated GFP-CsnB in the Δ*csnB::gfp:csnB*$^{\Delta NLS1}$ strain. Although the predicted molecular weight of the GFP-CsnB$^{\Delta NLS1}$ is 85 kDa, the specific α-GFP antibody visualized a GFP signal at around 62 kDa on the immunoblot, which might correspond to a truncated version or a degradation product of CsnB. The detected GFP signal, which is respective to GFP-CsnB$^{\Delta NLS1}$, was strongly reduced compared to the wild type GFP-CsnB. This suggests decreased protein production and/or decreased CsnB protein stability without the NLS1 sequence. This indicates that the NLS1 sequence is essential for wild type-like CsnB stability and thus, abundance, which manifests in growth reduction and asexual developmental defects.

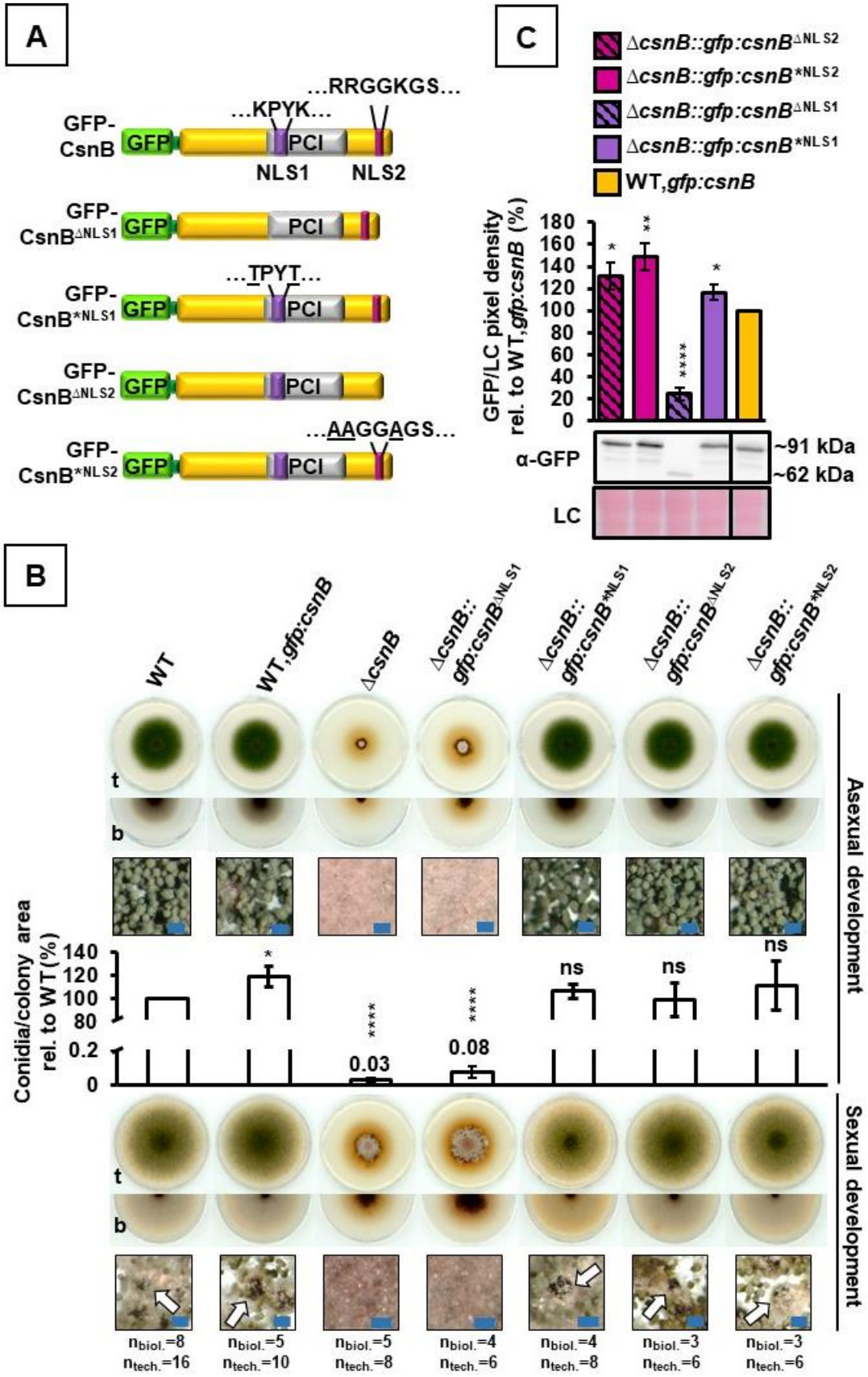

Figure 32. The figure legend is on the next page.

Figure 32. The CsnB NLS1 sequence is important for CsnB stability and abundance as well as for fungal growth and development.
(**A**) Schemes of the CsnB NLS1 and NLS2 knock-out and amino acid substitution constructs prepared in this study. (**B**) Growth and development of the *A. nidulans* strains were examined in spotting assay. $2x10^3$ conidia of each fungal strains were point inoculated on MM_{PABA} agar plates. The fungal strains were grown at 37°C for five days under constant illumination and with aeration to induce asexual development and for seven days in darkness and with low O_2-high CO_2 pressure to promote sexual differentiation. The figure shows the top (t) and the bottom (b) views of the colonies. The arrows point to mature fruiting bodies. Scale bars represent 100 µm. The charts display the mean of the conidia number per colony of three to eight independent biological experiments (biol.) carried out in two technical replicates (tech.). The conidia counts per colony area of each strain were relative (rel.) to the mean value of the WT. The error bars display SEM. Not significant (ns):p>0.05, *:p≤0.05, ****:p≤0.0001. (**C**) $0.25x10^6$/mL conidia of each fungal strains were inoculated in 100 mL MM_{paba} and grown vegetatively for 20 hours at 37°C under agitation for the immunoblotting. The relative amount of the GFP-CsnB NLS mutant and deletion versions was determined by α-GFP immunoblotting. The presented cropped region of the immunoblot was used for the pixel density quantification. Relative protein amounts were corresponding to the GFP signal/loading control pixel density ratios. The GFP signal/loading control pixel density ratio of each strain was relative (rel.) to the mean value of the GFP signal/loading control ratio of the WT,*gfp:csnB* strain. Ponceau staining was used as loading control (LC). The charts represent the mean of three independent biological replicates performed in duplicates and the error bars display SEM. *:p≤0.05, **:p≤0.01, ****:p≤0.0001.

3.10.3 CsnB versions with mutated NLS1 or NLS2 are still able to enter the nuclei

Uniquely among the examined GFP-CSN subunit fusions, only GFP-CsnB co-localizes to the nuclei in absence of CsnE (Figure 28). Therefore, it was investigated by confocal microscopy whether the predicted potential NLS1 and NLS2 sequences (Figure 31) are essential for the nuclear transport of CsnB. The subcellular localization of the GFP-$CsnB^{\Delta NLS1}$, $CsnB^{*NLS1}$, GFP-$CsnB^{\Delta NLS2}$, GFP-$CsnB^{*NLS2}$ produced in Δ*csnB* background was monitored by confocal microscopy (Figure 33). Larger amount of GFP signal respective to GFP-$CsnB^{*NLS1}$, GFP-$CsnB^{\Delta NLS2}$ and GFP-$CsnB^{*NLS2}$ overlapped with the DAPI-stained nuclei in the vegetative hyphae of *A. nidulans*, showing predominantly nuclear localization of these versions of CsnB. In contrast, nuclear localization of the GFP-$CsnB^{\Delta NLS1}$ could not be verified, probably due to the reduction of CsnB amount or the truncation of CsnB as the result of the NLS1 sequence deletion (Figure 32C). These findings imply that the putative NLS1 and NLS2 sequences are not involved in the nuclear localization of CsnB, when the eight subunit CSN holocomplex can be formed. Nevertheless, it cannot be excluded that these NLSs are masked and their function is suppressed in wild type fungal cells and are unmasked only in yet untested specific conditions. The NLS1 sequence is essential for the wild type-like stability, and thus, cellular levels (Figure 32C) as well as the normal cellular function of CsnB (Figure 32B). CsnB is a linker between the trimeric CsnA-CsnC-CsnH and CsnD-CsnF-CsnG subcomplexes (Figure 24) and is probably degraded if this function cannot be fulfilled due to the deletion of the NLS1 sequence.

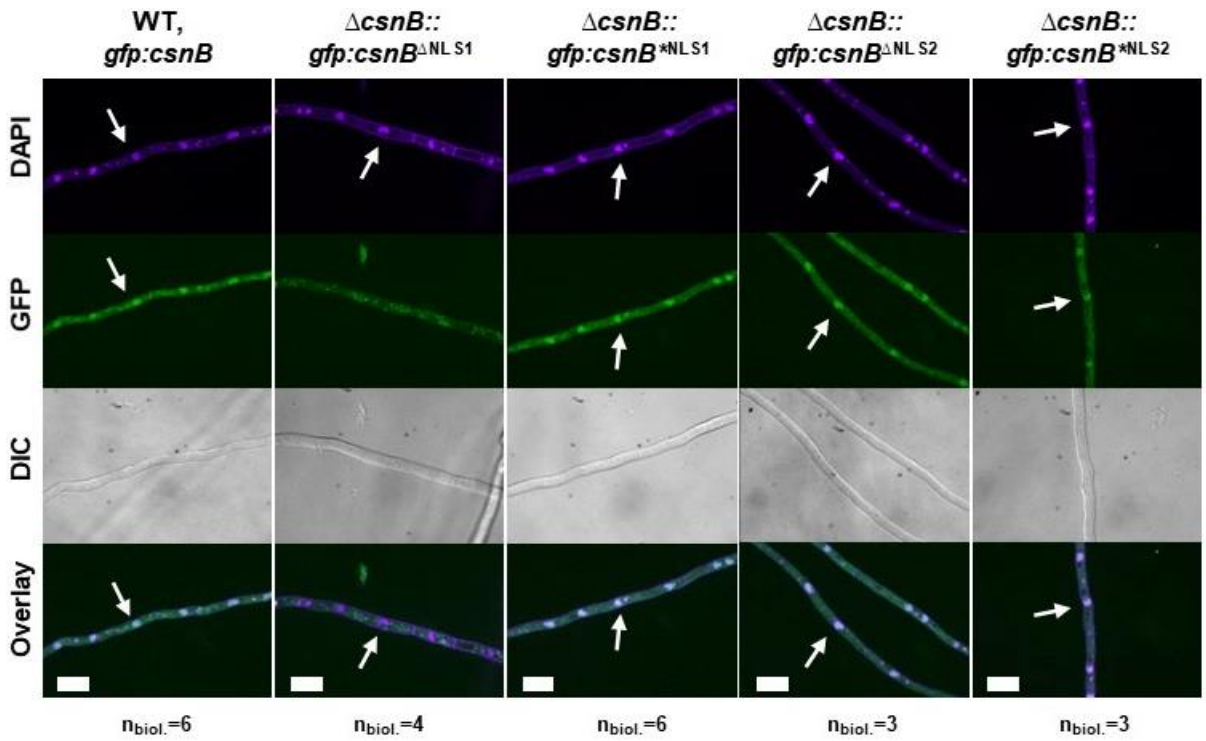

Figure 33. The nuclear localization of CsnB does not rely solely on either NLS1 or NLS2.
The subcellular localization of the NLS mutated GFP-CsnB versions was followed by confocal microscopy. The CsnB*^{NLS1}, GFP-CsnB*^{NLS2} and GFP-CsnB$^{\Delta NLS2}$ versions co-localize to the DAPI-stained nuclei, whereas nuclear localization of the GFP-CsnB$^{\Delta NLS1}$ version could not be shown. The confocal microscopy was carried out with fungal cultures grown for 20 hours vegetatively at 37°C. The experiment was performed with three to six independent biological replicates (biol.). The autofluorescence of each analyzed strain was subtracted against the wild type strain (not shown). The nuclei (indicated with white arrows) were visualized by DAPI staining. The GFP and the DAPI signal are merged in the overlay pictures. Scale bars represent 10 µm.

3.11 The cellular proteome is changed upon the abolishment of the pre-CSN complex formation in *A. nidulans*

An imbalance in CSN subunit occurrence was observed upon the abolishment of the pre-CSN complex formation (Figure 26). This raised the question whether CSN subunits endure instability and targeted break-down by the 26S proteasome. The CSN holocomplex in wild type background and the CsnD-CsnF-CsnG heterotrimeric subcomplex localize predominantly in the nucleus, but some CSN subunits and the CsnA-CsnC-CsnH subcomplex are rather cytoplasmic (Figure 27 to Figure 30; Figure S3 and Figure S4). Only CsnB has predicted nuclear localization signals among all CSN subunits (Figure 31), though CsnB with mutated or deleted NLS sequences still localize to the nuclei (Figure 33). Nuclear export signals were predicted for several CSN subunits, but not for CsnA and CsnD (Table S2), which suggests nucleocytoplasmic and intracytoplasmic shuttling, likely by interactions with trafficking proteins. Yet, no shuttle proteins were identified, which facilitate the translocation of CSN subunits and subcomplexes. Moreover, the question emerged whether the nuclear subunits and subcomplexes have a role in transcriptional regulation in *A. nidulans*, as it was described in plants (Wei and Deng, 1992). In order to address these questions, the protein

interactome of selected CSN subunits was analyzed in pre-CSN complex deficient *A. nidulans* strains.

Therefore, the LC-MS/MS data deriving from the GFP co-purifications of the Δ*pre-csn*Δ*csnE,gfp:csn* strains (Table 7 and Figure 23) was analyzed by significance-based filtering and compared to the respective wild type controls. Figure 34 depicts the applied workflow through the example of the WT,*gfp:csnD* and a Δ*pre-csn*Δ*csnE,gfp:csnD* mutant strain. In the first step, the potential interaction partners of GFP-CsnD in the WT,*gfp:csnD* and the Δ*pre-csn*Δ*csnE,gfp:csnD* strains were compared and subtracted against the cytoplasmic, free GFP overproducing control strain (Table 7). Significantly enriched proteins, the putative interaction partners, of the respective bait lie above the black curve (Figure 34, steps 1 and 4). These calculations were carried out altogether five times for higher confidence (Figure 34, steps 2 and 5). Common potential interacting candidates from all calculations were compared and only the common candidates were further considered (Figure 34, steps 3 and 6). Then, these potential interacting candidates of GFP-CsnD in the WT,*gfp:csnD* and Δ*pre-csn*Δ*csnE,gfp:csnD* mutant strains were compared (Figure 34, step 7). The same procedure was followed to analyze the interactome changes in all pre-CSN deficient Δ*pre-csn*Δ*csnE,gfp:csn* mutant strains producing either GFP-CsnA, GFP-CsnB, GFP-CsnD or GFP-CsnF as well as GFP-CsnE in the Δ*csnB,gfp:csnE* strain (Table 7 and Figure 23 and Figure S2). Significantly enriched proteins, which interacted specifically with GFP-CSN subunit fusions either in wild type background (Table S10) or in pre-CSN complex deficient strains were identified as a result of this filtering method (Table S3 to Table S9). An exemplary result of the interaction studies is presented in Figure 35. The CSN subunits were significantly enriched in the experimental samples as expected, but were not found in any samples of the control. Albeit the CSN subunits were amongst the most enriched proteins in the abundance-based filtering, some CSN subunits were slightly under the used threshold in some cases using the significance-based filtering method (Text S1).

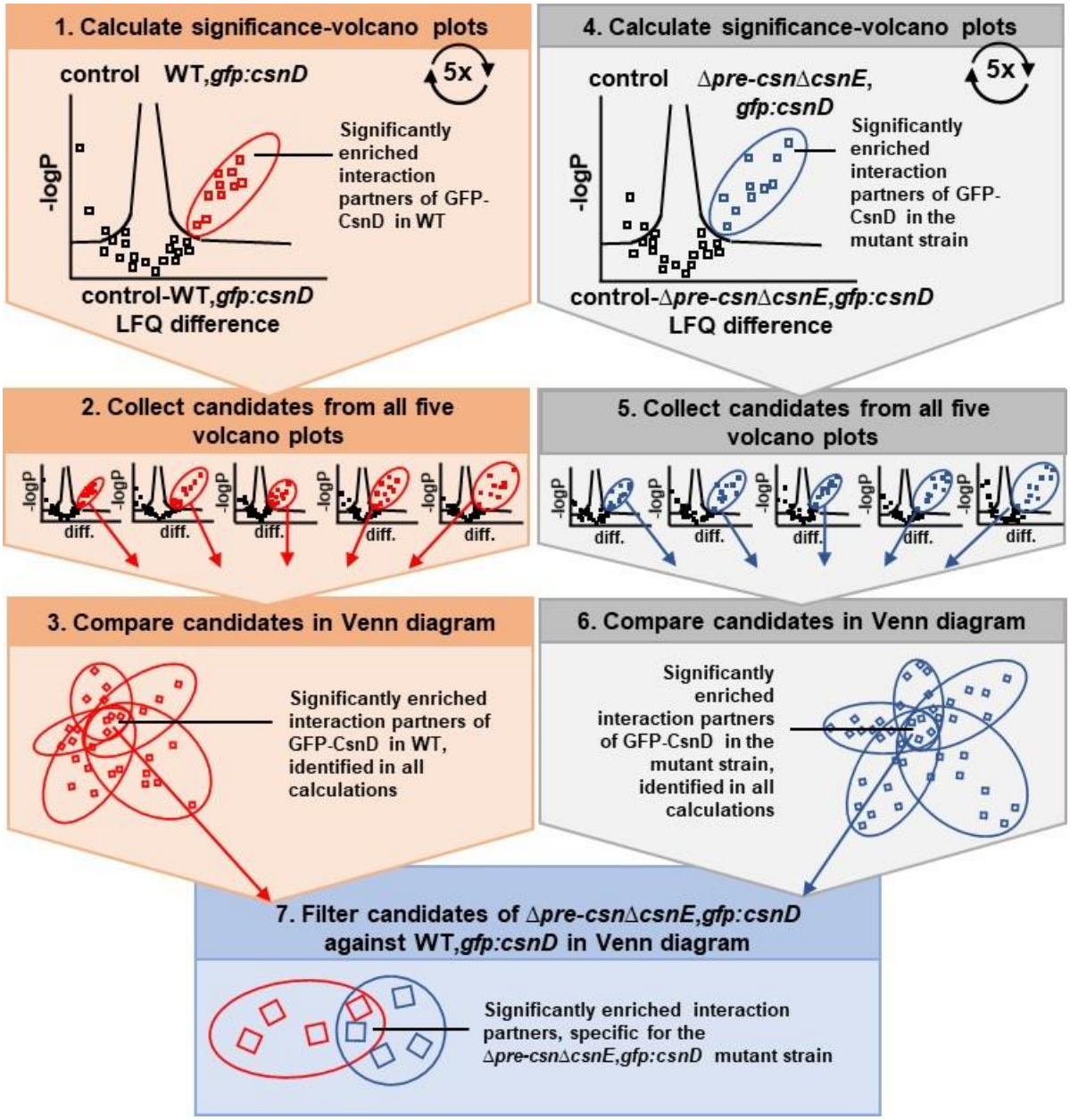

Figure 34. Scheme of the filtering workflow applied to analyze the interactome in pre-CSN complex deficient strains.
The raw data was analyzed and filtered as described in Table 8 and Table 10. Subsequently, the identified potential interaction partners of GFP-CsnD in WT,*gfp:csnD* as well as in *Δpre-csnΔcsnE;gfp:csnD* strain were compared and subtracted against the control strain with two sample t-tests, that were illustrated as volcano plots (step 1 and 4). Potential interaction partners of GFP-CsnD were identified based on label-free quantification (LFQ) of proteins and a two sample t-test was performed to identify significantly enriched proteins. The results of the t-test were illustrated with volcano plots, displaying the t-test difference of averaged LFQ-intensities on the x-axes and the -log10 (p-value) on the y-axes. To obtain meaningful results from the t-test, missing values need to be imputed from the normal distribution. This calculation was performed five times for higher confidence, resulting in five volcano plots for the wild type and the mutant strains. Potential interaction partners deriving from all five volcano plots were collected (step 2 and 5) and compared (step 3 and 6) for the wild type and for the mutant strains using Venn diagrams (step 7).

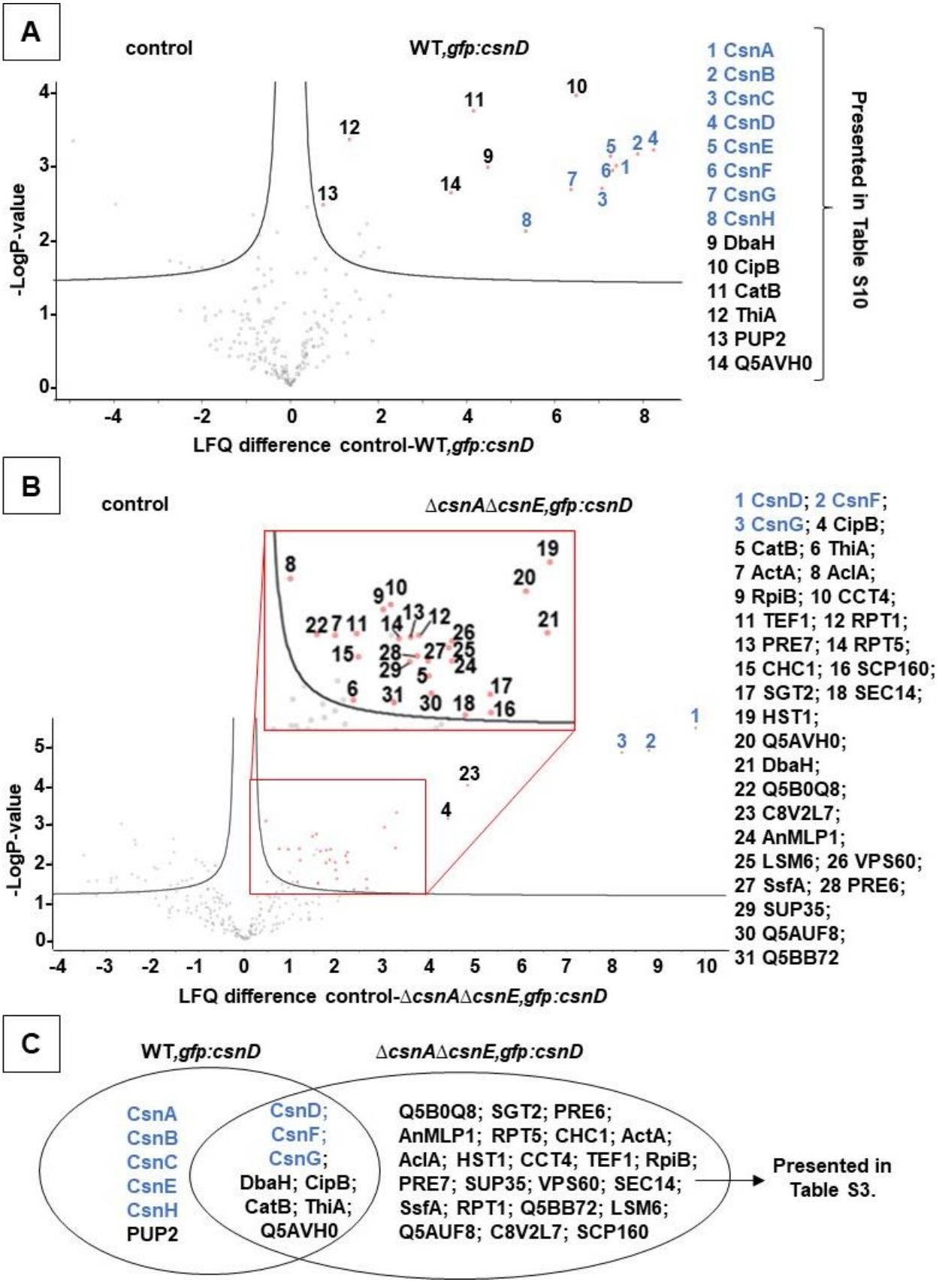

Figure 35. The figure legend is on the next page.

Figure 35. Comparison of the potential significantly enriched interacting partners of GFP-CsnD in the wild type strain and upon the combined loss of CsnA and CsnE.
The volcano plot depicts the LFQ differences in relation with the -LogP values of the pairwise comparisons between the control and the wild type strain as well as between the control and the Δ*csnA*Δ*csnE*,*gfp:csnD* strain. The first volcano plots of the two pairwise comparisons are presented as examples. The protein candidates, which were found in all five volcano plots as significant GFP-CsnD interacting proteins are indicated with the red squares. The proteins are listed with names or UniProt IDs. The identified CSN subunits are shown in blue. (**A**) Potential interaction partners of GFP-CsnD in the WT,*gfp:csnD* strain were compared und subtracted against the control strain (Table S10). (**B**) Potential interaction partners of GFP-CsnD in the Δ*csnA*Δ*csnE*,*gfp:csnD* strain were compared und subtracted against the control strain. (**C**) The significantly enriched potential interaction partners of GFP-CsnD in the Δ*csnA*Δ*csnE*,*gfp:csnD* strain were compared with the protein candidates in the WT,*gfp:csnD* strain. The potential interaction partners, which were found only in the Δ*csnA*Δ*csnE*,*gfp:csnD* strain are listed in Table S3.

3.11.1 The pre-CSN complex subassemblies recruited proteins involved in protein quality control and degradation machinery

3.11.1.1 CSN complex assembly intermediates were co-eluted with chaperons

It was analyzed if the CSN subunits and subcomplexes rely on the assistance of chaperons or chaperonins for their assembly or stabilization. Chaperons assist the self-assembly of nascent proteins to avoid non-functional structure. Chaperonins are oligomeric protein complexes, which use energy to assist the correct folding of protein substrates (Anfinsen, 1973; Ellis, 1991). The CCT/TriC complex is a chaperonin, which consists of two stacked octameric rings providing a hidden cavity to fold protein substrates using energy. The CSN subunits and subcomplexes recruited chaperons and chaperonins in the GFP-pulldown experiments in strains, where the pre-CSN complex cannot form (Table 11, Table S3 Table S4, Table S6, Table S8 and Table S9). Six of eight CCT/TriC complex subunits, orthologs of the yeast CCT2, CCT3, CCT4, CCT5, CCT7 and CCT8 were pulled out by GFP-CsnD as free standing protein and also as part of the CsnD-CsnF-CsnG subcomplex (Table 11). Similarly, these chaperonin orthologs were also identified as potential interaction partners of GFP-CsnF as part of the CsnF-CsnG dimer as well as of free GFP-CsnA and GFP-CsnB proteins (Table 11). Moreover, CSN subunits and subcomplexes were co-purified with heat shock proteins, such as SgdE, and orthologs of the yeast YDJ1 and SGT2 (Table 11). CSN subunits and subcomplexes in pre-CSN complex deficient backgrounds were identified as substrates of chaperones and chaperonins, which presumably facilitate their proper folding. In these experimental set-up, chaperons were not identified as interacting partners of the GFP-CSN fusion proteins in wild type background. This is probably because the eight subunit CSN holocomplex is stable or it can self-assemble without the assistance of chaperons.

Table 11. CSN subunits and subcomplexes were co-purified with chaperons and chaperonins. Several CCT/TriC complex subunits as well as heat shock proteins were recruited by pre-CSN complex assembly intermediates. The free standing, complex-unbound CsnA, CsnD and CsnB subunits required the assistance of the chaperonin and heat shock proteins.

interaction partner	recruited by	CSN subunits or subcomplex	background strain
CCT/TriC complex			
CCT2	GFP-CsnA	CsnA	Δ*csnH*Δ*csnE,gfp:csnA*
CCT3	GFP-CsnB	CsnB	Δ*csnA*Δ*csnE,gfp:csnB*
	GFP-CsnD	CsnD	Δ*csnG*Δ*csnE,gfp:csnD*
CCT4	GFP-CsnD	CsnD-CsnF-CsnG	Δ*csnA*Δ*csnE,gfp:csnD*
	GFP-CsnD	CsnD	Δ*csnG*Δ*csnE,gfp:csnD*
CCT5	GFP-CsnF	CsnF-CsnG	Δ*csnD*Δ*csnE,gfp:csnF*
CCT7	GFP-CsnD	CsnD	Δ*csnG*Δ*csnE,gfp:csnD*
CCT8	GFP-CsnF	CsnF-CsnG	Δ*csnD*Δ*csnE,gfp:csnF*
	GFP-CsnD	CsnD	Δ*csnG*Δ*csnE,gfp:csnD*
	GFP-CsnD	CsnD-CsnF-CsnG	Δ*csnH*Δ*csnE,gfp:csnD*
Heat shock proteins			
SGT2	GFP-CsnD	CsnD-CsnF-CsnG	Δ*csnA*Δ*csnE,gfp:csnD*
	GFP-CsnD	CsnD	Δ*csnG*Δ*csnE,gfp:csnD*
	GFP-CsnA	CsnA	Δ*csnH*Δ*csnE,gfp:csnA*
	GFP-CsnF	CsnF-CsnG	Δ*csnD*Δ*csnE,gfp:csnF*
SgdE	GFP-CsnA	CsnA-CsnC-CsnH	Δ*csnB*Δ*csnE,gfp:csnA*
	GFP-CsnA	CsnA	Δ*csnH*Δ*csnE,gfp:csnA*
YDJ1	GFP-CsnB	CsnB	Δ*csnA*Δ*csnE,gfp:csnB*
	GFP-CsnA	CsnA-CsnC-CsnH	Δ*csnB*Δ*csnE,gfp:csnA*

3.11.1.2 CSN subunits were co-purified with intracytoplasmic transport proteins

The interactome specific for the pre-CSN complex defective fungal Δ*pre-csn*Δ*csnE,gfp:csn* strains was examined in attempt to identify shuttle proteins, which traffic CSN subunits and pre-CSN assembly intermediate subcomplexes between different cell compartments for the assembly. In wild type cells producing either GFP-CsnA, GFP-CsnB, GFP-CsnD or GFP-CsnE, a predominantly nuclear CSN holocomplex was observed (Figure 27A, Figure 28A and Figure 29A) and intracellular shuttle proteins were not identified as interaction partners of these GFP-CSN subunit fusions (Table S10 and Figure S7). Different GFP-CSN fusion proteins and CSN subcomplexes were co-purified with proteins involved in intracytoplasmic transport in various pre-CSN complex deficient strains. Such potential interacting partners were the VPS60, CHC1, SEC14, SEC26 and SEC31 orthologs as well as the RabE/SrgE, CopA, AbpA, ActA and An-Sec13 intracellular transport proteins as well as an ortholog of the yeast BRE5, which is a regulator of cellular transport between the ER and Golgi (Table 12, and Table S3 to Table S9). In wild type backgrounds with a stable and mainly nuclear CSN holocomplex, intracellular transport proteins were not recruited by GFP-CSN fusions. In various pre-CSN complex deficient backgrounds, the CSN subunits and pre-CSN complex intermediates are intensively shuttled in the cytoplasm between Golgi, ER, endosome and cytoskeleton. The intensive trafficking of these CSN subunits and subcomplexes might be a result of protein quality surveillance to maintain the correct folding of these intermediates or even transport into compartments of protein break-down.

Table 12. CSN subunits and subcomplexes recruited proteins involved in intracellular transport. Free, complex-unbound GFP-CsnB and GFP-CsnA, as well as GFP-CsnA, as part of the CsnA-CsnC-CsnH subcomplex, were co-purified with subunits of the COPI and COPII coatomer protein complexes. Cytoskeletal and other transport proteins were recruited by GFP-CsnD and GFP-CsnF in various pre-CSN complex deficient background strains. The asterisk highlight the An-Sec13 protein, which is an ortholog of the yeast SEC13. SEC13 is a component of different protein complexes with distinct cellular locations, including COPII and the nuclear pore complex.

interaction partner	recruited by	CSN subunits or subcomplex	background strain
COPI coatomer			
CopA	GFP-CsnA	CsnA-CsnC-CsnH	Δ*csnF*Δ*csnE,gfp:csnA*
SEC26	GFP-CsnB	CsnB	Δ*csnA*Δ*csnE,gfp:csnB*
COPII coatomer			
An-Sec13*	GFP-CsnA	CsnA-CsnC-CsnH	Δ*csnD*Δ*csnE,gfp:csnA*
		CsnA	Δ*csnH*Δ*csnE,gfp:csnA*
SEC31	GFP-CsnF	CsnF-CsnG	Δ*csnD*Δ*csnE,gfp:csnF*
BRE5	GFP-CsnF	CsnF-CsnG	Δ*csnD*Δ*csnE,gfp:csnF*
Cytoskeleton			
ActA	GFP-CsnD	CsnD-CsnF-CsnG	Δ*csnA*Δ*csnE,gfp:csnD*
		CsnD-CsnF-CsnG	Δ*csnH*Δ*csnE,gfp:csnD*
	GFP-CsnF	CsnF-CsnG	Δ*csnD*Δ*csnE,gfp:csnF*
AbpA	GFP-CsnD	CsnD	Δ*csnG*Δ*csnE,gfp:csnD*
Other cytoplasmic transport proteins			
RabE/SrgE	GFP-CsnD	CsnD-CsnF-CsnG	Δ*csnB*Δ*csnE,gfp:csnD*
		CsnD-CsnG	Δ*csnF*Δ*csnE,gfp:csnD*
		CsnD	Δ*csnG*Δ*csnE,gfp:csnD*
		CsnD-CsnF-CsnG	Δ*csnH*Δ*csnE,gfp:csnD*
VPS60	GFP-CsnD	CsnD-CsnF-CsnG	Δ*csnA*Δ*csnE,gfp:csnD*
SEC14	GFP-CsnD	CsnD-CsnF-CsnG	Δ*csnA*Δ*csnE,gfp:csnD*
		CsnD-CsnG	Δ*csnF*Δ*csnE,gfp:csnD*
CHC1	GFP-CsnD	CsnD-CsnF-CsnG	Δ*csnA*Δ*csnE,gfp:csnD*
		CsnD-CsnF-CsnG	Δ*csnB*Δ*csnE,gfp:csnD*
		CsnD-CsnG	Δ*csnF*Δ*csnE,gfp:csnD*
		CsnD-CsnF-CsnG	Δ*csnH*Δ*csnE,gfp:csnD*

3.11.1.3 The CSN subunits and pre-CSN assembly intermediates were co-purified with the 26S proteasome

Ubiquitin modifications govern various cellular functions, among them monoubiquitination, which can be a signal for the intracellular translocation of a protein as well as polyubiquitination, which targets its substrate for break-down by the proteasome (reviewed in Oh *et al*., 2018). The analysis of the interactome, specific for the pre-CSN complex deficient *A. nidulans* strains, revealed ubiquitin (Ubi1; Noventa-Jordão *et al*., 2000) and an ortholog of the yeast RAD23 protein (Elsasser *et al*, 2004) as potential interaction partners of GFP-CSN subunit fusions. GFP-CsnD, as part of the CsnD-CsnF-CsnG heterotrimeric- as well as the CsnD-CsnG heterodimeric subcomplex, was co-purified with ubiquitin (Table S4, Table S7). The complex-unbound, free GFP-CsnD interacted with an ortholog of the yeast extra-proteasomal ubiquitin receptor, RAD23 (Table S8). Not only ubiquitin and the proteasomal receptor, but subunits of all proteasomal particles were identified as potential significant interacting partners of various CSN subunits and subcomplexes (Table 13).

Table 13. CSN subunits and pre-CSN complex intermediates recruited proteasomal subunits. Subunits from each main 26S proteasomal particles were represented as interaction partners of CSN subunits in different *A. nidulans* strains.

interaction partner	recruited by	CSN subunits or subcomplex	background strain
19S lid			
Rpn11	GFP-CsnA	CsnA-CsnC-CsnH	Δ*csnG*Δ*csnE,gfp:csnA*
	GFP-CsnF	CsnF-CsnG	Δ*csnD*Δ*csnE,gfp:csnF*
Rpn7	GFP-CsnA	CsnA-CsnC-CsnH	Δ*csnG*Δ*csnE,gfp:csnA*
Rpn8	GFP-CsnF	CSN holocomplex	WT,*gfp:csnF*
Rpn12	GFP-CsnF	CSN holocomplex	WT,*gfp:csnF*
19S base			
Rpn2	GFP-CsnA	CsnA-CsnC-CsnH	Δ*csnD*Δ*csnE,gfp:csnA*
Rpn13	GFP-CsnD	CsnD-CsnF-CsnG	Δ*csnH*Δ*csnE,gfp:csnD*
	GFP-CsnF	CSN holocomplex	WT,*gfp:csnF*
Rpt1	GFP-CsnD	CsnD-CsnF-CsnG	Δ*csnA*Δ*csnE,gfp:csnD*
	GFP-CsnD	CsnD-CsnF-CsnG	Δ*csnC*Δ*csnE,gfp:csnD*
	GFP-CsnD	CsnD	Δ*csnG*Δ*csnE,gfp:csnD*
	GFP-CsnD	CsnD-CsnF-CsnG	Δ*csnH*Δ*csnE,gfp:csnD*
	GFP-CsnF	CsnF-CsnG	Δ*csnD*Δ*csnE,gfp:csnF*
Rpt2	GFP-CsnD	CsnD	Δ*csnG*Δ*csnE,gfp:csnD*
Rpt3	GFP-CsnB	CsnB	Δ*csnA*Δ*csnE,gfp:csnB*
	GFP-CsnA	CsnA-CsnC-CsnH	Δ*csnG*Δ*csnE,gfp:csnA*
Rpt5	GFP-CsnD	CsnD-CsnF-CsnG	Δ*csnA*Δ*csnE,gfp:csnD*
	GFP-CsnD	CsnD-CsnF-CsnG	Δ*csnC*Δ*csnE,gfp:csnD*
	GFP-CsnD	CsnD-CsnG	Δ*csnF*Δ*csnE,gfp:csnD*
	GFP-CsnD	CsnD	Δ*csnG*Δ*csnE,gfp:csnD*
	GFP-CsnD	CsnD-CsnF-CsnG	Δ*csnH*Δ*csnE,gfp:csnD*
20S core			
SsfA	GFP-CsnD	CsnD-CsnF-CsnG	Δ*csnA*Δ*csnE,gfp:csnD*
	GFP-CsnD	CsnD-CsnF-CsnG	Δ*csnB*Δ*csnE,gfp:csnD*
	GFP-CsnD	CsnD-CsnF-CsnG	Δ*csnH*Δ*csnE,gfp:csnD*
SCL1	GFP-CsnA	CsnA	Δ*csnH*Δ*csnE,gfp:csnA*
PRE6	GFP-CsnD	CsnD-CsnF-CsnG	Δ*csnA*Δ*csnE,gfp:csnD*
	GFP-CsnD	CsnD-CsnF-CsnG	Δ*csnB*Δ*csnE,gfp:csnD*
	GFP-CsnD	CsnD-CsnF-CsnG	Δ*csnC*Δ*csnE,gfp:csnD*
	GFP-CsnD	CsnD	Δ*csnG*Δ*csnE,gfp:csnD*
	GFP-CsnA	CsnA	Δ*csnH*Δ*csnE,gfp:csnA*
PUP2	GFP-CsnD	CSN holocomplex	WT,*gfp:csnD*
PRE7	GFP-CsnD	CsnD-CsnF-CsnG	Δ*csnA*Δ*csnE,gfp:csnD*
	GFP-CsnD	CsnD-CsnF-CsnG	Δ*csnC*Δ*csnE,gfp:csnD*
	GFP-CsnD	CsnD	Δ*csnG*Δ*csnE,gfp:csnD*
	GFP-CsnF	CSN holocomplex	WT,*gfp:csnF*

GFP-CsnA, as component of the CsnA-CsnC-CsnH trimer, and GFP-CsnF, as part of the CsnF-CsnG dimer, were co-purified with Rpn11 (Table 13, Table S6 and Table S8). GFP-CsnA, as part of CsnA-CsnC-CsnH, pulled out Rpn7/RpnG proteasomal 19S RP lid subunit (Table 13, Table S8). GFP-CSN subunit fusions mediated interactions with non-ATPase 19S proteasomal base subunits (Table 13, Table S6 and Table S9). GFP-CsnA, as component of the CsnA-CsnC-CsnH subcomplex, recruited a yeast Rpn2 ortholog protein. GFP-CsnD as member of the CsnD-CsnF-CsnG trimeric subcomplex mediated interaction with the yeast ubiquitin receptor ortholog Rpn13. Moreover, four of the six proteasomal 19S ATPases (Table 13, Table S3, Table S5 and Table S7 to Table S9) as well as 20S core subunits (Table 13,

Table S3 to Table S5 and Table S8 and Table S9) were amongst the significant potential interacting partners of CSN subunits and subcomplexes. These interactions were not specific to pre-CSN complex deficient strains. GFP-CsnF pulled out the CsnF equivalent Rpn8, the CsnH equivalent Rpn12, as well as the orthologs of the core ß-6 subunit PRE7 and the base subunit Rpn13 in wild type background (Table 13 and Table S10). Moreover, the ortholog of the α-5 subunit of the 20S proteasomal core PUP2 was co-purified with GFP-CsnD (Table 13 and Table S10). These results suggest the intensive and targeted break-down of instable or outdated CSN subunits and/or subcomplexes by the 26S proteasome also in mutant strains, where the pre-CSN complex cannot form. The interactions of GFP-CSN fusions in pre-CSN complex deficient strains with elements of the protein quality control system and degradation machinery might account for the observed differences in GFP-CSN subunit fusion protein abundances (Figure 26).

3.11.2 The two trimeric subcomplexes interacted with proteins located at the nuclear pore

The CSN subunits and subcomplexes are able to shuttle between cytoplasm and nuclei in Δ*pre-csn*Δ*csnE,gfp:csn* strains, where the pre-CSN complex cannot be formed (Figure 27 to Figure 30). The interactome of the pre-CSN complex deficient fungal strains were analyzed to unveil, if CSN subunits interact with any importin or exportin proteins, which facilitate the nucleocytoplasmic trafficking. Such transport proteins were not found, but nuclear pore complex (NPC) proteins were identified by GFP-affinity purification as potential interaction partners of CSN subunits and subcomplexes in pre-CSN complex deficient background strains (Figure 36B and Table S3, Table S6 and Table S9). A NPC protein, An-Mlp1 was recruited by GFP-CsnD in the Δ*csnA*Δ*csnE,gfp:csnD* strain, in which the CsnA-CsnC-CsnH complex cannot be built (Figure 36B). In this background strain the GFP-CsnD fusion protein was identified as component of the CsnD-CsnF-CsnG subcomplex, which was mainly nuclear enriched (Figure 36A and Figure S4). Formation of the CsnD-CsnF-CsnG subcomplex is abolished in the Δ*csnD*Δ*csnE,gfp:csnA* strain, in which the GFP-CsnA fusion protein was a subunit of the CsnA-CsnC-CsnH subcomplex. In this background strain the GFP-CsnA fusion protein was distributed between cytoplasm and nuclei and it interacted with SonA, which is located at the NPC (Figure 36A and Figure S4). Moreover, the CSN complex-unbound, free GFP-CsnA interacted with An-Sec13 (Table 12 and Figure 36B). The An-Sec13 is a yeast SEC13 ortholog and it is a structural component of three protein complexes, which inhabit different subcellular compartments. As an NPC component, An-Sec13 contributes to nucleocytoplasmic transport and NPC biogenesis (Osmani *et al.*, 2007). Taken together, CsnA or CsnA-CsnC-CsnH interacted with SonA, which is a NPC protein (Osmani *et al.*, 2007) and CsnD or CsnD-CsnG-CsnF interacted with An-Mlp1, an integral NPC protein, which stretches into the nucleoplasm (Osmani *et al.*, 2007). In wild type strain, carrying the eight-subunit nuclear CSN complex, neither importins or exportins, nor NPC proteins were identified as interaction partners of the GFP-CSN subunit fusions (Table S10). As the nuclear enriched CSN holocomplex did not recruit nuclear exportins or importins, it can be hypothesized that the CSN subcomplexes assemble in the nucleus to a holocomplex or that the CSN holocomplex is backpacked into the nucleus with other proteins, which could not be detected in these experimental settings.

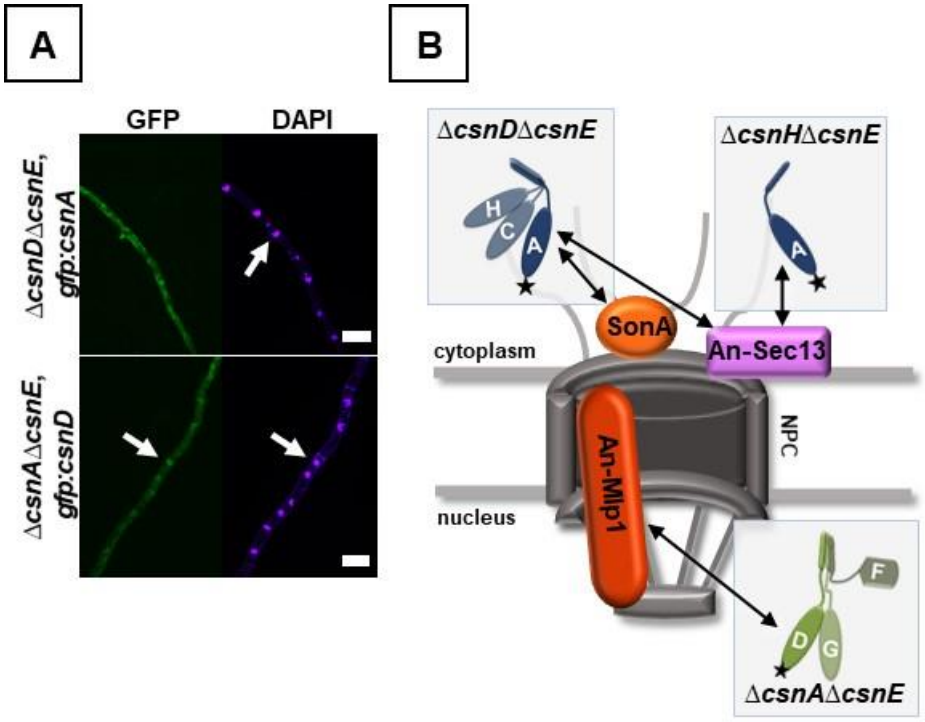

Figure 36. GFP-CsnA in the CsnA-CsnC-CsnH subcomplex and GFP-CsnD in the CsnD-CsnF-CsnG subcomplex were co-purified with nuclear pore proteins.
(**A**) Fluorescence microscopy showed nuclear accumulation of the CsnD-CsnF-CsnG trimer visualized by GFP-CsnD in the Δ*csnA*Δ*csnE,gfp:csnD* strain. In contrast, the GFP-CsnA signal is evenly distributed within the fungal hyphae without nuclear enrichment in the Δ*csnD*Δ*csnE,gfp:csnA* strain. The confocal microscopy was carried out with fungal cultures grown vegetatively for 20 hours at 37°C. The experiment was performed once. The complete figure, including controls, is presented in Figure S4. Scale bars represent 10 µm. (**B**) Both, the CsnA-CsnC-CsnH and the CsnD-CsnF-CsnG, heterotrimeric CSN subcomplexes interacted with proteins located at the nuclear pore complex (NPC), independently of the other trimeric subcomplex. The stars label the GFP-tagged CSN subunits used as molecular bait and the boxes mark the fungal background, in which the interaction was shown in GFP-trap experiments.

3.11.3 CSN subunits and trimeric subcomplexes mediate interactions with proteins involved in transcriptional regulation upon the abolishment of the pre-CSN complex formation

A possible function of the nuclear COP9 signalosome subcomplexes might be gene expression control. It was analyzed whether CSN subunits and assembly intermediates play role in transcriptional regulation by physically binding to proteins involved in gene expression control in *A. nidulans*, as it was shown in other organisms (reviewed in Chamovitz, 2009). Therefore, the interactome of GFP-CSN subunit fusions was analyzed in pre-CSN complex defective strains and compared to wild type controls. In cells harboring the eight-subunit CSN holocomplex, the CSN subunits were unable to recruit any proteins involved in gene expression regulation (Table S10). The CSN assembly intermediates in pre-CSN complex deficient strains were co-purified with proteins playing a role in transcriptional regulation (Table 14 and Table S3 to Table S5 and Table S7 to Table S9).

Table 14. CSN subunits and subcomplexes were co-purified with proteins involved in gene expression regulation.
CSN subunits and subcomplexes interacted with the RcoA gene expression regulator, RVB2 DNA helicase ortholog and with the HST1 histone deacetylase ortholog proteins.

interaction partner	pulled out by	CSN subunits or subcomplex	background strain
HST1	GFP-CsnD	CsnD-CsnF-CsnG	Δ*csnA*Δ*csnE,gfp:csnD*
		CsnD-CsnF-CsnG	Δ*csnB*Δ*csnE,gfp:csnD*
		CsnD-CsnF-CsnG	Δ*csnC*Δ*csnE,gfp:csnD*
		CsnD-CsnF-CsnG	Δ*csnH*Δ*csnE,gfp:csnD*
		CsnD-CsnG	Δ*csnF*Δ*csnE,gfp:csnD*
RcoA	GFP-CsnD	CsnD	Δ*csnG*Δ*csnE,gfp:csnD*
RVB2	GFP-CsnA	CsnA-CsnC-CsnH	Δ*csnG*Δ*csnE,gfp:csnA*

RcoA is a yeast Tup1p ortholog and repressor of stress induced secondary metabolite genes (Hicks *et al.*, 2001; Todd *et al.*, 2006) and it was recruited by the free, complex-unbound GFP-CsnD. The yeast HST1 histone deacetylase ortholog was recruited by the GFP-CsnD fusion protein in all fungal strains, in which the CsnD-CsnF-CsnG subcomplex or the CsnD-CsnG dimer was identified. The ortholog of the yeast RVB2 DNA helicase (Torreira *et al*, 2009) was identified as potential interaction partner of the GFP-CsnA fusion protein, which was also shown to form the CsnA-CsnC-CsnH subcomplex in the analyzed fungal background. The pre-CSN complex assembly intermediates physically bind to gene expression regulators, but such interactions could not be found in the wild type background with the applied experimental settings, probably because they are suppressed in cells containing the eight-subunit CSN holocomplex.

In summary, the comparative analysis of the proteome in pre-CSN complex deficient strains revealed intensive shuttling of pre-CSN complex assembly intermediates between cellular compartments of protein sorting and quality control. Proteasomal degradation of unstable assembly intermediates can be concluded based on the interactions mediated by COP9 signalosome subassemblies with elements of the ubiquitin-proteasome pathway, which might account for the perturbance of the subunit abundances upon the abolishment of the CSN complex formation. The CSN subcomplexes interact with nuclear pore proteins during their transport into the nucleus, where they might mediate interactions with proteins involved in transcriptional regulation.

4 Discussion

A pre-assembled heptameric subcomplex is an intermediate of the COP9 signalosome formation in *Aspergillus nidulans* (Beckmann *et al*, 2015). This work represents novel experimental evidence on the formation of the native pre-CSN complex. It shows that the CSN subunits are organized parallel into two heterotrimeric clusters, rather than following a successive order during the COP9 signalosome assembly. These heterotrimeric clusters, the CsnA-CsnC-CsnH and CsnD-CsnF-CsnG subcomplexes, are bound by the CsnB linker subunit thereby establishing the heptameric pre-CSN complex. This process is coordinated on different levels by meticulous surveillance mechanisms. These provide sufficient amounts of properly folded subunits and subassemblies as well as their required subcellular localization to enable the complex formation.

4.1 The seven-subunit pre-COP9 signalosome is necessary for growth and development of *Aspergillus nidulans*

COP9 signalosome is a regulator of the sexual life cycle in *A. nidulans*. Deficiency of any of its eight subunits caused the complete block of fruiting body formation, accompanied with alterations in secondary metabolite production (Busch *et al*, 2007; Beckmann *et al*, 2015). All *csn* mutants share these common features, but loss of the deneddylase CsnE and loss of any pre-CSN subunits led to additional and distinct morphologies during asexual development promoting conditions. Physiological analyses of fungal mutants showed that the pre-CSN subunits are necessary for the wild type-like surface growth and asexual development, while the effect of CsnE on these is more moderate than those of the pre-CSN subunits. As it was shown in other organisms, these results demonstrate a role of CSN subunits in fungal physiology as well (Figure 37). Orthologous COP9 signalosome subunits from different organisms have functions in cell cycle progression and multicellular development. The mouse Csn8 subunit maintains the G1 phase duration, as the decreased expression of Csn8 shortens the G1 phase (Liu *et al.*, 2013) and *D. melanogaster* CSN7 subunit is essential for the wing disc development and G1-S cell cycle progression (Singer *et al*, 2014). The COP9 signalosome of the fission yeast *S. pombe* plays a role in S-phase control, as deletions of *csn1* and *csn2* subunit genes result in a delay of the S-phase progression (Mundt *et al*, 1999). *A. thaliana csn4* and *csn5* mutants undergo G2-arrest, which propose a role of these subunits in the G2 checkpoint control (Dohmann *et al*, 2008). Necessity of an N-terminal end of CsnA for conidiospore formation in *A. nidulans* was shown, because a strain with a truncated version of CsnA hardly formed conidia (Beckmann *et al*, 2015). Moreover, CSN subunits also provide an interaction platform with various proteins. An interplay between the two cellular deneddylases Den1/A and the CSN complex, coordinate multicellular development in *A. nidulans* (Figure 37) (Christmann *et al*, 2013; Schinke *et al*, 2016). Fungal Den1 ortholog, DenA is required for light-dependent conidia formation and the inhibition of the sexual development pathway, because the Δ*denA* strain could hardly form any asexual spores (Christmann *et al*, 2013). Albeit, this Δ*denA* phenotype was a pyridoxin auxotrophy-dependent synthetic phenotype, since it could not be confirmed in another, pyridoxin prototroph Δ*denA* strain without any retaining marker cassette (Köhler, 2018). Asexual development of this pyridoxin prototroph Δ*denA* strain was similar to that in wild type strain (Köhler, 2018).

Production of conidiospores was observed for the Δ*denA* strain even during sexual development promoting conditions, thus, DenA is involved in the inhibition the asexual pathway in sexual development promoting conditions (Köhler, 2018). An interaction between CsnG and DenA and weaker interactions with CsnA, CsnE and CsnF were shown *in vitro* (Christmann *et al*, 2013). *In vivo* bimolecular fluorescence assay verified the DenA-CsnG interaction, which took place in the nuclei. This interaction was also observed in case of the human Den1 and CSN subunits (Christmann *et al*, 2013). The physiological role of the interaction between CsnG and DenA is the regulation of the cellular DenA amount (Christmann *et al*, 2013). Further COP9 signalosome subunits are involved in the destabilization of DenA. CsnE, CsnG, CsnF, CsnH and CsnC provide an interaction surface for DenA, which, as a result of the interaction is destabilized (Schinke *et al*, 2016). DenA was stable during vegetative growth, suggesting that it is required to maintain vegetative growth (Schinke *et al*, 2016).

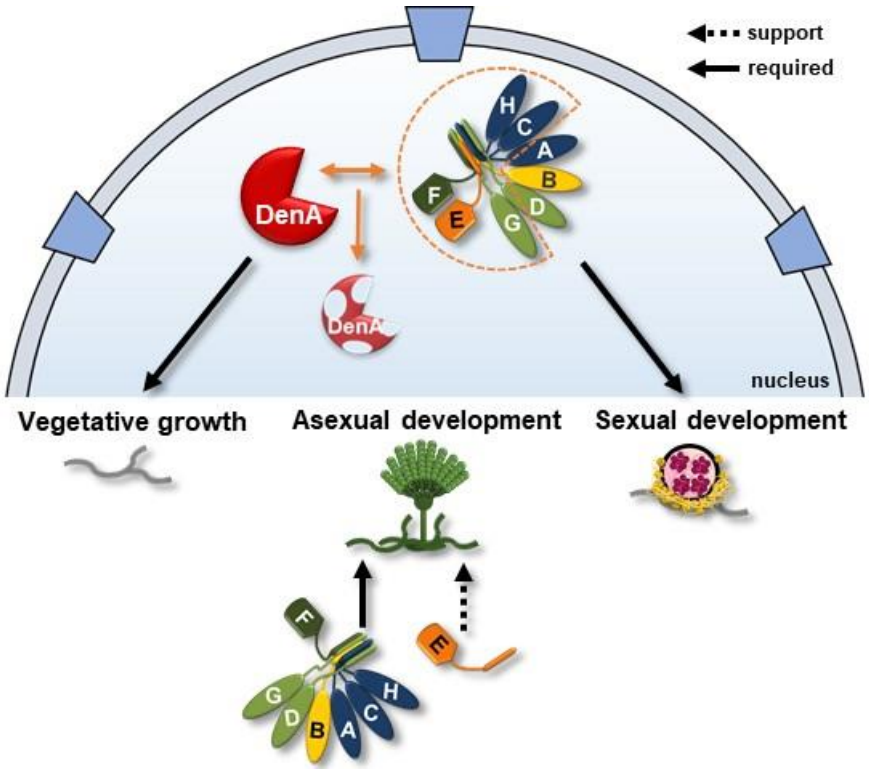

Figure 37. The COP9 signalosome is a regulator of fungal development.
CsnE supports and the seven-subunit pre-CSN complex is required for growth and asexual life cycle of *A. nidulans*. An eight-subunit CSN holocomplex is required for fruiting body formation. Stable DenA is required to maintain vegetative growth. DenA is destabilized as a consequence of the nuclear interaction (orange double-end arrow) with CSN subunits (framed with orange dotted line).

4.2 Assembly of the eight-subunit COP9 signalosome in *A. nidulans*

The assembly of multisubunit complexes is a well-regulated, orchestrated process. Formation of pre-assembled subcomplexes and subassemblies is energetically favorable and it provides a rapid and efficient holocomplex assembly (Marsh *et al*, 2013). On the other hand, these subassemblies might have distinct roles compared to the fully assembled holocomplex

(Marsh *et al*, 2013). It is an interesting question whether the formation of the two main clusters, Csn1/A-Csn3/C-Csn8/H and the Csn4/D-Csn6/F-Csn7/G, is a conserved step of the COP9 signalosome assembly. This work, conducted *in vivo* using a fungal reference system, verifies the results of *in vitro* studies on the assembly of the yeast or human CSN complex (Sharon *et al.*, 2009; Lingaraju *et al.*, 2014; Gutierrez *et al.*, 2020; Kotiguda *et al*, 2012). Formation of two heterotrimeric subcomplexes seems to be an evolutionary conserved process, but there is divergent data about how are these intermediates linked with each other. The *in vitro* human CSN complex assembly studies suggested a link between Csn1/A and Csn6/F (Sharon *et al.*, 2009). In contrast, this work based on *in vivo* results show Csn2/B as clamp connecting the two clusters through interactions with Csn1/A and, according to the structural properties of the subunits, presumably with Csn6/F in a fungal system. The assembly of the CSN complex equivalent 26S proteasomal lid complex also includes two main modules (reviewed in Meister *et al.*, 2016). One of the modules in the lid complex is the Rpn5-Rpn8-Rpn9, which is the equivalent subcomplex to the Csn4/D-Csn6/F-Csn7/G in the CSN complex. The other lid module is the Rpn7-Rpn3-Rpn12 subcomplex, whose equivalent is the Csn1/A-Csn3/C-Csn8/H subcomplex. The lid Rpn5-Rpn8-Rpn9 subcomplex is completed with the ubiquitin-specific isopeptidase Rpn11 and connected to the other subcomplex through an interaction between Rpn6 and Rpn8. The last lid assembly step is the integration of Rpn12 to the Rpn7-Rpn3 dimeric module (Isono *et al.*, 2005; Sharon *et al.,* 2006; Fukunaga *et al*., 2010; Bai *et al.*, 2019). In contrast, the fungal CSN complex assembles through a different pathway, where the two trimeric complexes are bound by the Rpn6 equivalent Csn2/B, forming a heptamer. The heptameric pre-CSN complex is activated by the integration of the Nedd8-specific isopeptidase Csn5/E (Beckmann *et al.*, 2015). A ninth subunit of both multiprotein complexes was implied (Kragelund *et al*, 2016; Rozen *et al*, 2015). CSNAP/Csn9 is a disordered protein, what makes the homology search-based identification challenging. The data deriving from the GFP-affinity purifications was not analyzed for possible interactions between CSN subunits and CSNAP/Csn9-like fungal protein, thus, the question remains open, whether the CSN complex also comprises a ninth, auxiliary subunit in *A. nidulans*.

4.2.1 Formation of the CsnD-CsnF-CsnG heterotrimeric subcomplex

CsnG mediated interactions with CsnD or CsnF in *A. nidulans*, thereby forming the CsnD-CsnG or CsnF-CsnG heterodimers. CsnG has a prominent role to initiate the CsnD-CsnF-CsnG heterotrimer formation *in vivo*, because loss of CsnG abolished this process. This finding verified *in vitro* analyses, which revealed binary interactions between fungal CsnD-CsnG and CsnF-CsnG subunits (Busch *et al*, 2007). Analysis of the quaternary structure model of the CSN complex assembly intermediates (Figure 38) and *in silico* interaction analysis performed with the Protein Interfaces, Surfaces and Assemblies (PISA) (Krissinel and Henrick, 2007) found sufficient binding interface between CsnF and CsnG for a stable dimeric interaction (Figure S6F).

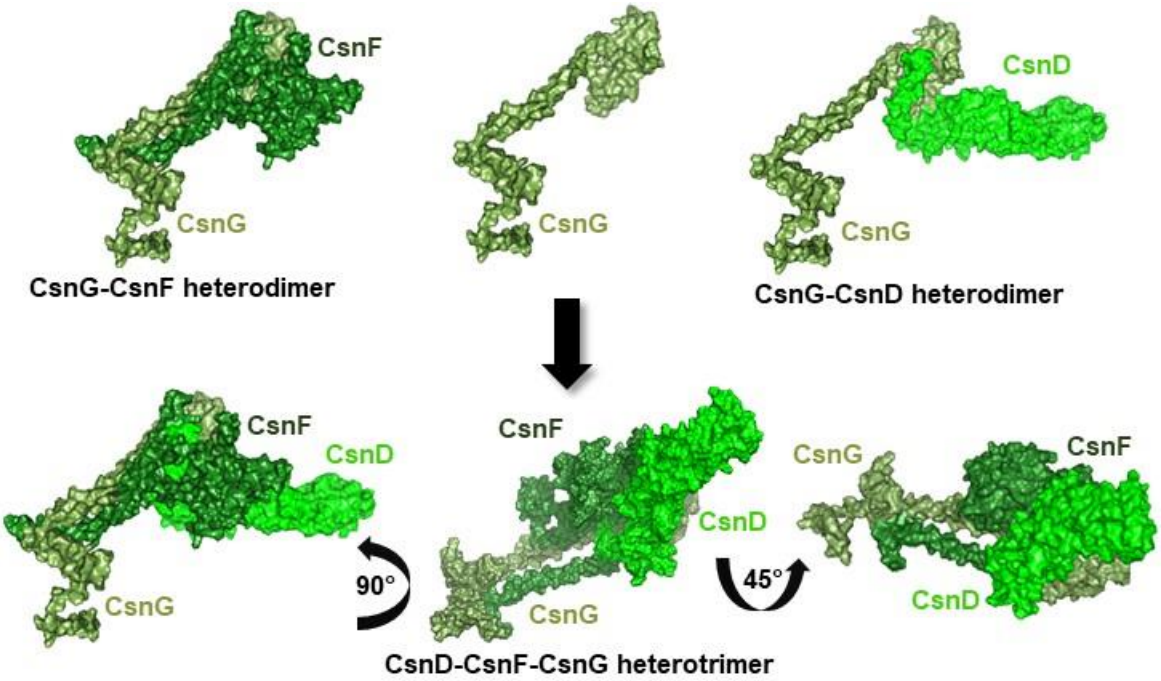

Figure 38. Homology model of the CsnD-CsnF-CsnG subcomplex.
Surface view of the predicted quaternary structure of the CsnD-CsnF-CsnG heterotrimeric subcomplex and two models depict the CsnD-CsnG and CsnF-CsnG heterodimeric interactions. CsnG provides a long stretching surface for joining subunits. The homology modelling was carried out as described in chapter 2.10.3 and the figure was drawn with the PyMOL Molecular Graphics System version 1.7.1.3 (www.pymol.org) using the human CSN complex (PDB ID: 4D10) as template for the alignments (not shown).

A binary interaction was reported in other species between the MPN domain and the PCI domain subunits Csn6/F and Csn7/G, respectively. The cohesion between the recombinantly expressed *A. thaliana* Csn6 and Csn7 subunits is mediated by the C-terminal part of Csn7 (Kotiguda *et al*, 2012). The interaction between Csn6 and Csn7 is described in yeast as well (Pick *et al*, 2012). Interestingly, the PCI domain of Csn7 was not necessary for this interaction. Csn7 and Csn6 were connected through the S6CD domain of Csn6, which domain has conserved residues (Pick *et al*, 2012). A C-terminal S6CD domain carrying conserved amino acid residues was also predicted for *A. nidulans* CsnF, which might be involved in the association to CsnG (Figure 39).

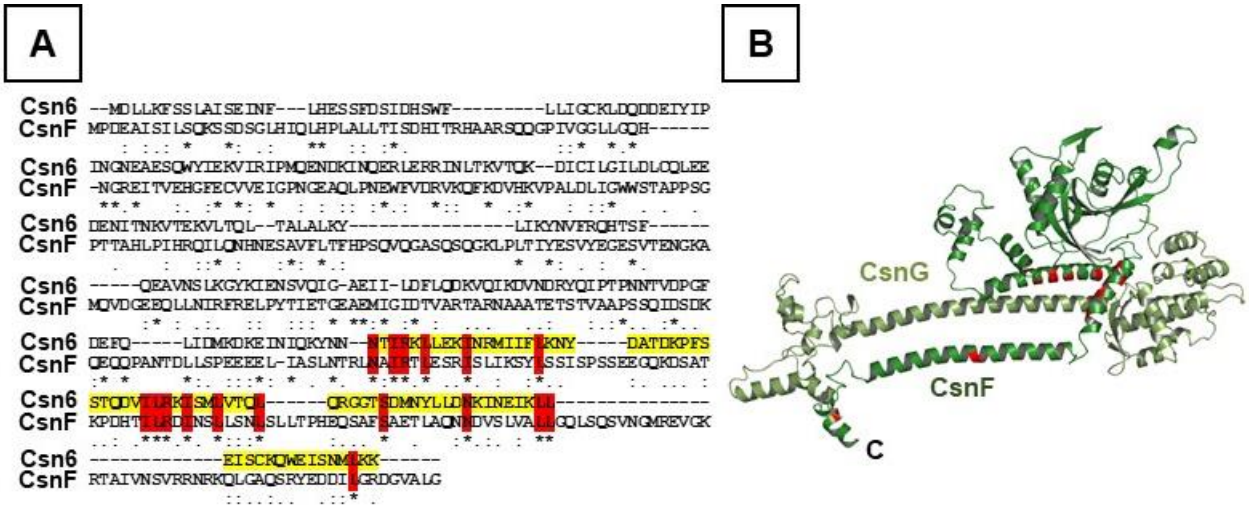

Figure 39. *A. nidulans* CsnF carries conserved residues of the S6CD domain, similar to *S. cerevisiae* Csn6.
(**A**) Comparison of the amino acid sequence of *S. cerevisiae* Csn6 and *A. nidulans* CsnF. The conserved S6CD domain of Csn6, spanning from N213-K295, is highlighted with yellow. The conserved residues between Csn6 and CsnF are highlighted with red. (**B**) Position of the conserved residues in the C-terminal (C) S6CD domain in the CsnF homology model are highlighted with red.

4.2.2 Formation of the CsnA-CsnC-CsnH heterotrimeric subcomplex

The CsnA-CsnC-CsnH heterotrimeric subcomplex is formed by the binding of CsnA to CsnC and CsnH. CsnC and CsnH probably form a heterodimer, because loss of either CsnC or CsnH subunits abolished the binding of CsnA to the remaining subunit. In a preliminary experiment, the co-expression of the fungal GST-CsnC and GST-CsnH fusions in bacterial system resulted more robust expression than the single subunits expressed individually (data not shown), which further supports a CsnC-CsnH heterodimeric subcomplex.

Homology model of the CsnA-CsnC-CsnH heterotrimer quaternary structure (Figure 40), alongside the PISA analysis, show CsnC-CsnH as a compact entity (Figure S6A). There is no direct binding surface between CsnA and CsnH subunits, based on the homology model; CsnA is associated directly to CsnC. The α-helices of CsnA are positioned by a flexible linker arm, which allows its movement, facilitating the complex formation. The prediction of the quaternary structure of the fungal CsnA-CsnC-CsnH revealed a cleft in the CsnC surface, which likely provides sufficient binding surface for the C-terminal α-helices of CsnA to attach bind and form a stable complex (Figure S6B) (Figure 40).

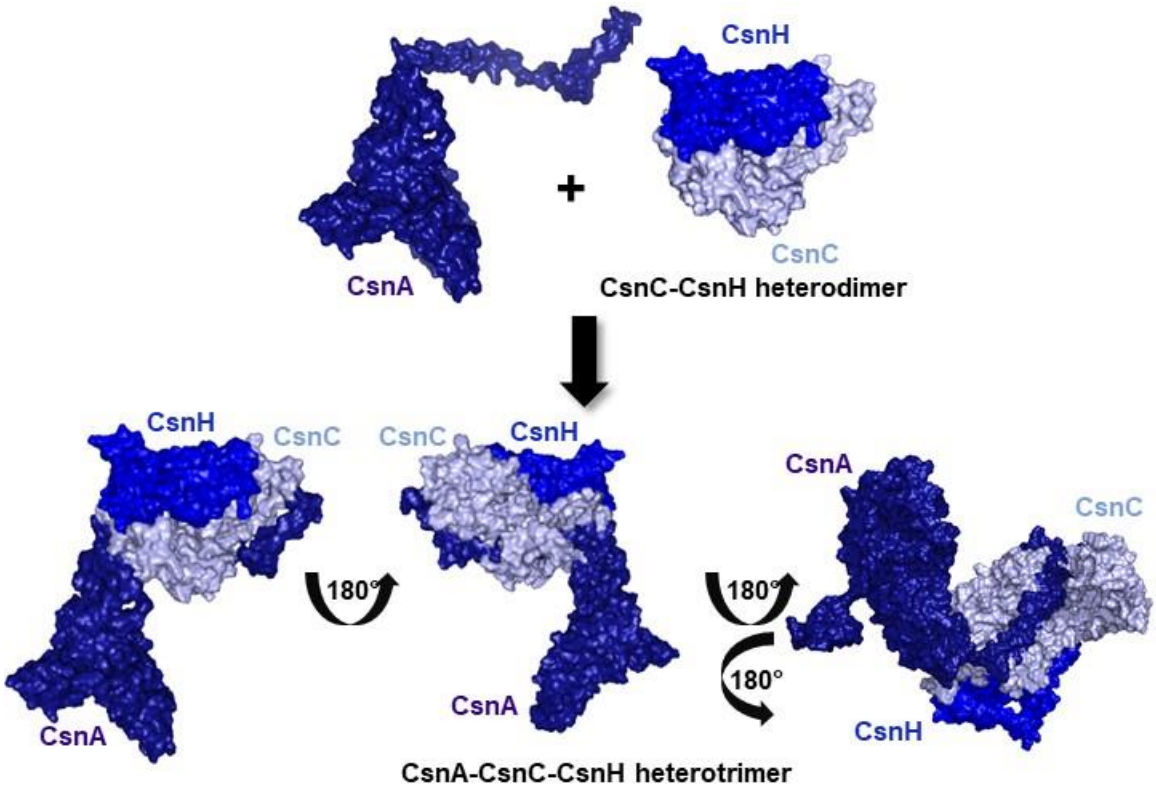

Figure 40. Homology model of the CsnA-CsnC-CsnH subcomplex of *A. nidulans*.
Surface view of the predicted quaternary structure of the CsnA-CsnC-CsnH heterotrimeric subcomplex. The homology modelling was carried out as described in chapter 2.10.3 and the figure was drawn with the PyMOL Molecular Graphics System version 1.7.1.3 (www.pymol.org) using the human CSN complex (PDB ID: 4D10) as template for the alignments (not shown). CsnH is connected to CsnC and CsnC shares binding surface with CsnA. The CsnA C-terminal part composed of α-helices fits well in a cleft of the CsnC surface. CsnA is attached to CsnH through CsnC according to the analysis of the predicted quaternary structure.

4.2.3 The role of CsnB in CSN complex assembly: a molecular clamp binding two timers and enabling of the deneddylase incorporation

The assembly of the two trimeric subcomplexes happens probably simultaneously and independently of the CsnB and CsnE subunits, because the two trimers co-exist in a fungal background lacking these subunits. Although a connection between human Csn1 and Csn6 joins the two clusters, in *A. nidulans* the linker is CsnB mediates ternary interactions with the components of the heterotrimeric subcomplexes. CsnB presumably binds to CsnA, because these subunits interact with each other *in vitro* (Busch *et al*, 2007). CSN subunit binding of CsnB was abolished when the CsnA-CsnC-CsnH subcomplex could not form, albeit the CsnD-CsnF-CsnG trimer was present in this background. Likewise, the linker CsnB was unable to recruit any subunits of the CsnA-CsnC-CsnH subcomplex in absence of the MPN domain subunits CsnF and CsnE *in vivo* (preliminary data, not shown). These result imply that CsnB can only bind to fully assembled trimeric subcomplexes. Formation of heterotrimeric subcomplexes is in good agreement with the studies determining the structure and subunit

organization of the CSN complex *in vitro* (Busch *et al*, 2007; Lingaraju *et al*, 2014; Sharon *et al*, 2009; Gutierrez *et al*, 2020).

Homology modelling (Figure 41) and surface interference analysis between CsnA and CsnB revealed sufficient interaction surface allowing a stable CsnA-CsnB association (Figure S6C). In contrast, CsnB has weaker affinity to bind to CsnD (Figure S6D), but CsnB might have sufficient binding surface with CsnF, based on a structural model (Figure 42). It is possible that CsnB connects to CsnA first enabling the binding of the CsnD-CsnF-CsnG subcomplex. An essential role of the PCI domain of the human CSN2 for the CSN complex assembly was demonstrated (Huang *et al*, 2005). Similarly, the Csn2 paralogous proteasomal subunit Rpn6 was also a prerequisite for the proteasomal lid formation in *S. cerevisiae* and in *D. melanogaster*, where Rpn6 is a molecular clamp between subunits of the proteasomal lid and core and confers binary interaction with the Csn1/A paralog Rpn7 (Santamaría *et al*., 2003; Pathare *et al.*, 2012).

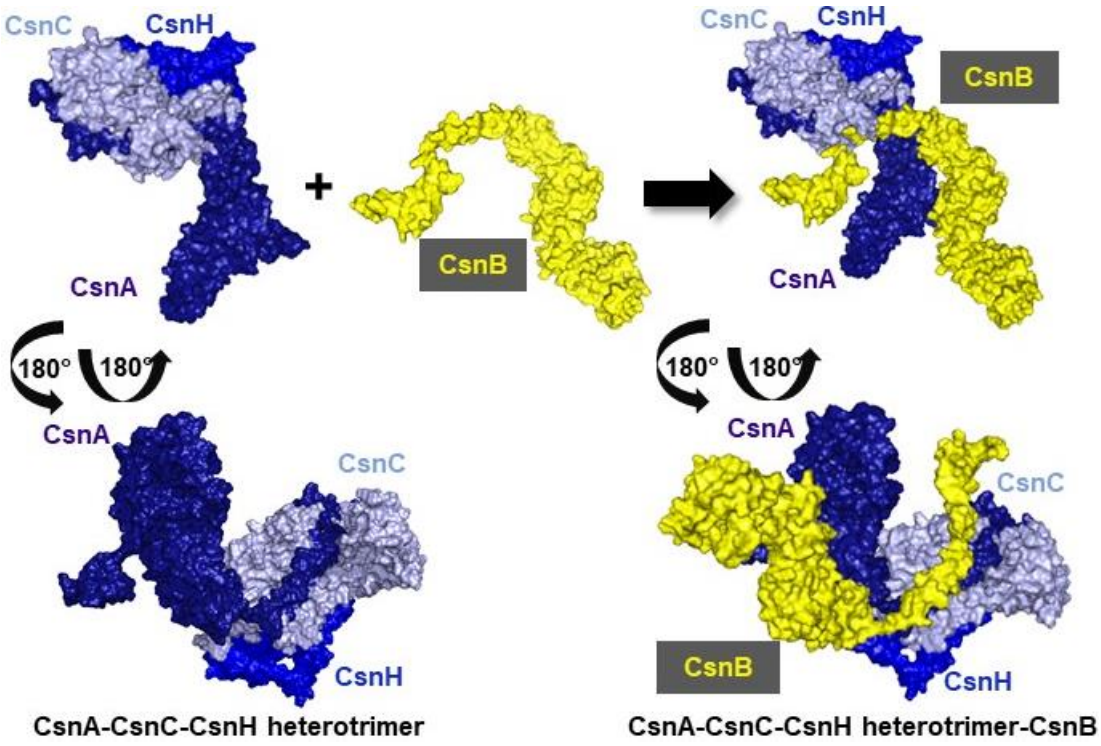

Figure 41. Position of CsnB on the homology model of the CsnA-CsnC-CsnH trimeric subcomplex.
Surface view of the predicted quaternary structure of the CsnA-CsnC-CsnH heterotrimeric subcomplex with the predicted CsnB binding surface. The modelling was carried out as described in chapter 2.10.3 and the figure was drawn with the PyMOL Molecular Graphics System version 1.7.1.3 (www.pymol.org) using the human CSN complex (PDB ID: 4D10) as template for the alignments (not shown). CsnB has a common interface with CsnA, which presumably confers the interaction of CsnB to CsnA-CsnC-CsnH first, allowing the association of the CsnD-CsnF-CsnG trimeric subcomplex.

The fungal CsnB is required to connect the two trimeric CSN subcomplexes and for the subsequent incorporation of the CsnE deneddylase. Similarly to this, the association of the CsnB equivalent lid subunit Rpn6 enhanced the complex-binding ability of the CsnE equivalent Rpn11 in humans (Bai *et al*, 2019). CsnB together with CsnA and CsnD are a prerequisite for the CSN binding of the TAP-tagged CsnE, as in a CsnA-CsnC-CsnH deficient Δ*csnA* and in a

CsnD-CsnF-CsnG deficient Δ*csnD* fungal strain CsnE was unable to connect to CSN subunits (Busch *et al*, 2007). With the binding of CsnB, a heptameric pre-CSN complex assembles, which is activated by the integration of CsnE (Figure 42) (Beckmann *et al.*, 2015).

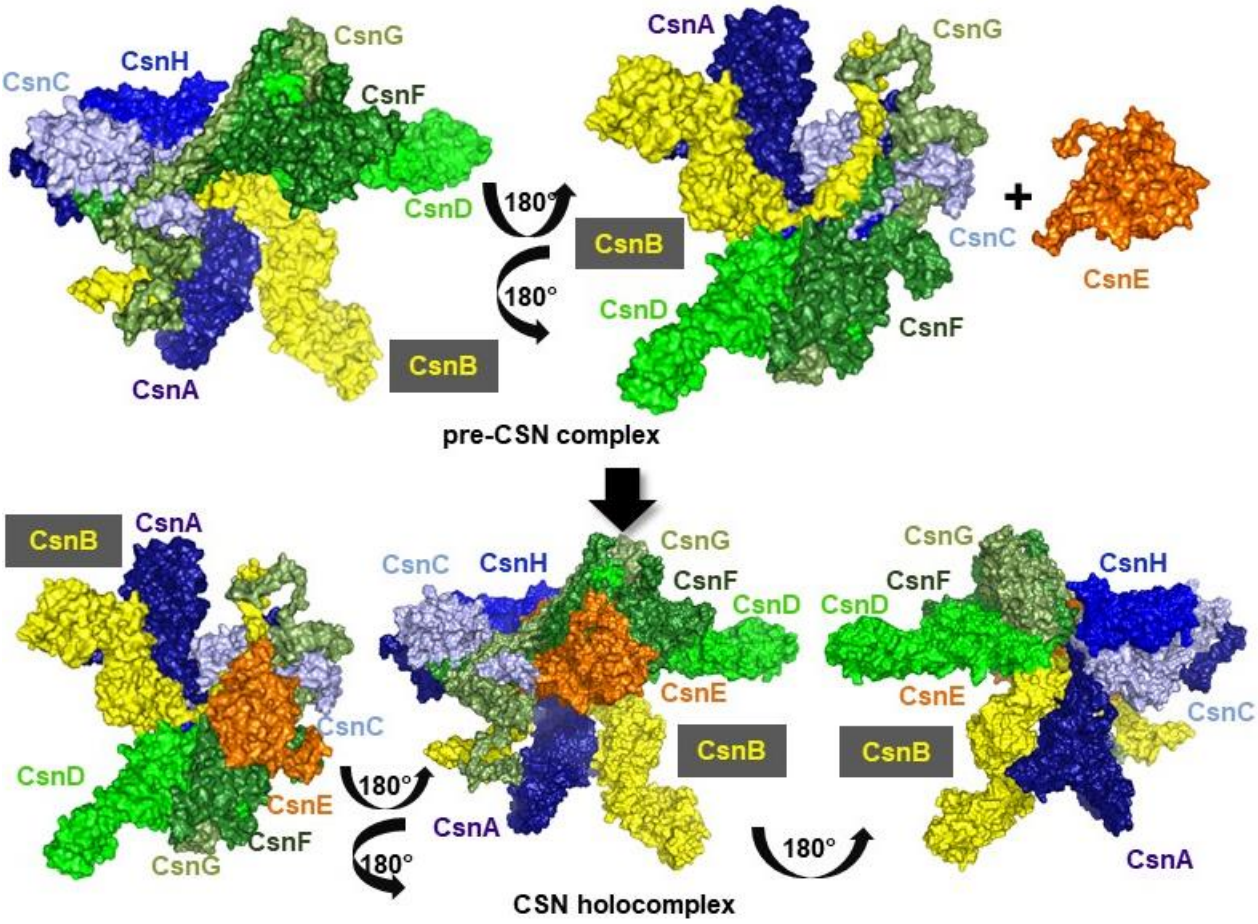

Figure 42. Homology model of the fungal seven-subunit pre-CSN complex and the eight-subunit COP9 signalosome holocomplex.
The homology modelling was carried out as described in chapter 2.10.3 and the figure was drawn with the PyMOL Molecular Graphics System version 1.7.1.3 (www.pymol.org) using the human CSN complex (PDB ID: 4D10) as template for the alignments (not shown).

It would be interesting to specify the factors, which initiate and promote the CSN complex assembly. Such triggers might be posttranslational modifications, for example phosphorylation, or possible conformational changes of the tertiary structure of the CSN complex subassemblies. Phosphorylations were discovered on the human subunits (Kapelari *et al.*, 2000) and also on the Csn1/A and Csn5/E subunits of the COP9 signalosome *in fungi* (preliminary data, not shown).

4.3 Abolishment of the fungal pre-CSN complex formation leads to the disturbance of the remaining CSN subunit abundances

Abolishment of the pre-CSN complex formation led to different GFP-CSN fusion protein levels, which suggest a control mechanism between CSN subunits for their cellular abundances either at transcriptional, translational level or by the regulation of their stability. The interconnections of CSN subunits for their cellular abundance was also shown in *Arabidopsis thaliana*, where loss of function mutations of selected CSN subunits triggered the destabilization of other subunits (Gusmaroli *et al*, 2007). For example, the cellular CSN1, CSN6, CSN7 and CSN8 levels were strongly reduced in absence of CSN5, meanwhile the CSN4 level suffered a slight reduction and the CSN2 amount remained unaffected. A coordinated downregulation of CSN subunits was observed in human cell lines as well, in which the downregulation of Csn1 resulted in reduced Csn3 amounts and *vice versa* (Peth, Boettcher, *et al.,* 2007). In similar experimental settings the downregulation of Csn1 and Csn3 resulted in simultaneous decrease in the Csn5 and Csn8 amounts, whereas the downregulation of Csn5 led to a negligible reduction in the Csn8 levels (Peth, Berndt, *et al.*, 2007).

CsnA is a component of the CsnA-CsnC-CsnH heterotrimeric subcomplex. In response to the loss of CsnE or the inability to form either of the trimeric subcomplexes, the relative cellular CsnA amount is decreased. Also in plants, the CSN5 deficiency also resulted in the strong reduction of CSN1 (Gusmaroli *et al*, 2007). The CsnA abundance was wild type-like in case the eight-subunit CSN holocomplex was formed and in the presence of the components of both heterotrimeric subcomplexes. Interestingly, the capacity to form the CsnD-CsnF-CsnG subcomplex had stronger positive effect on the cellular levels, than capacity to form the CsnA-CsnC-CsnH subcomplex (Figure 43A). This implies that the CsnD-CsnF-CsnG subcomplex plays a role in the surveillance of the cellular amount of CsnA or its heterotrimeric CsnA-CsnC-CsnH subcomplex. This surveillance system probably recognizes the presence of CsnD-CsnF-CsnG and in response the cellular CsnA or CsnA-CsnC-CsnH concentration increases, may be as preparation for the assembly.

The relative cellular amount of CsnD, which is a component of the CsnD-CsnF-CsnG heterotrimeric subcomplex, remained wild type-like in CsnE deficient fungal strains. This result is in good agreement with the observations that CSN5-deficiency has no influence on the cellular CSN4 levels in plants (Gusmaroli *et al*, 2007). Cellular levels of CsnD as complex-unbound, free subunit also remained unaffected in the fungal system, but the ability to form the CsnG-CsnD dimer increased the relative CsnD amount. Similarly, the capacity to form the CsnF-CsnG dimeric subcomplex raised the cellular CsnF level (Figure 43C). The capacity to form at least either the CsnD-CsnG or the CsnF-CsnG dimers is probably recognized by a cellular surveillance system and as result of a control mechanism, CsnD and CsnF are produced in a higher concentration and/or they are stabilized. It is possible that the presence of CsnG, which probably serves as basis in the trimeric CsnD-CsnF-CsnG interaction, stimulates the increase of the remaining CsnD-CsnF-CsnG components. Neither the ability nor the inability to form the CsnA-CsnC-CsnH trimer had an obvious influence on the relative CsnD amount. This indicates that the CsnD-CsnF-CsnG subcomplex promotes higher CsnA or CsnA-CsnC-CsnH concentrations, but not the other way around.

CsnB functions as linker between the two trimeric subcomplexes. Consequently, upon the abolishment of the CsnA-CsnC-CsnH formation, the free and complex-unbound linker

CsnB is produced in a lower amount and/or it is destabilized. The presence of the CsnD-CsnF-CsnG trimer alone is not sufficient to rescue the wild type-like CsnB levels. In conclusion, CsnA or its subcomplex are prerequisite to maintain the sufficient CsnB amounts (Figure 43B). It will be interesting to examine whether overproduction of CsnD in a CsnA-CsnC-CsnH subcomplex deficient strain could restore the wild type-like CsnB concentration. Cellular amount of CsnB is only slightly affected by CsnE. Similarly, a CSN5-independent regulation of the CSN2 amounts was observed in *A. thaliana* (Gusmaroli *et al*, 2007). These imply that the cellular levels of two most conserved CSN subunits are regulated by distinct, yet unexplored mechanism.

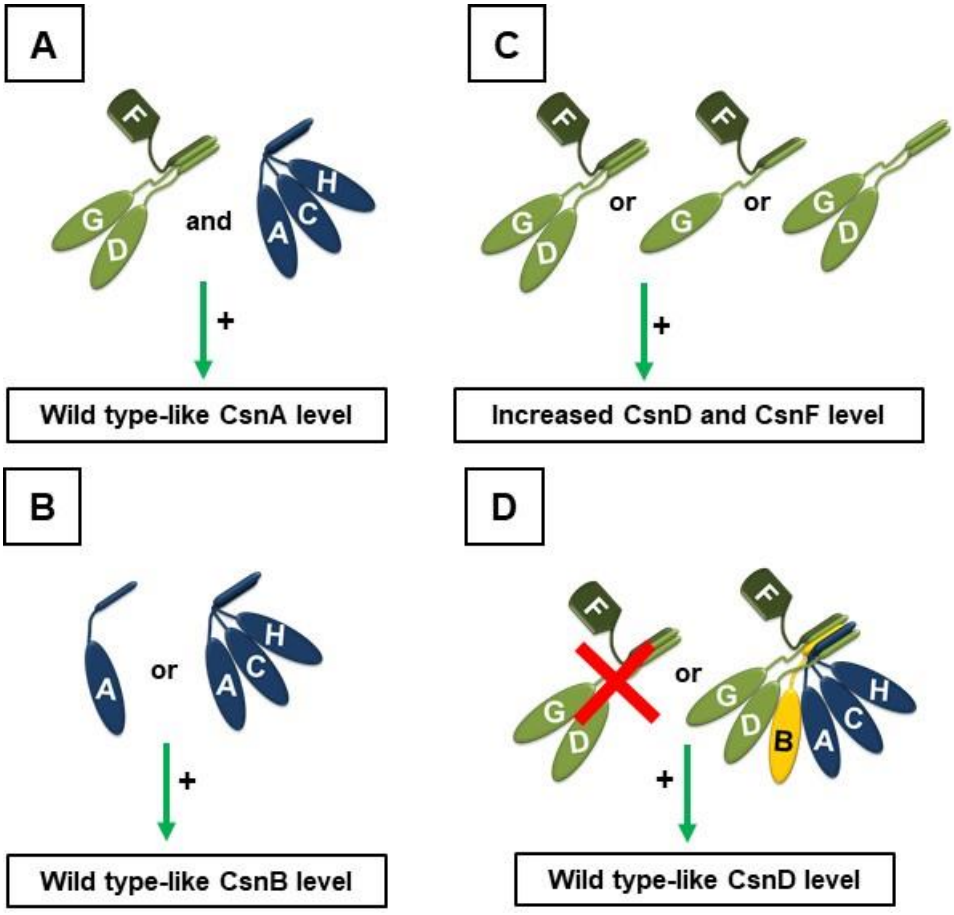

Figure 43. Interdependence between the protein abundances of CSN subunits during CSN complex formation.
(**A**) Presence of both heterotrimeric subcomplex is a prerequisite for the relative CsnA amounts to reach wild type protein levels. (**B**) Presence of CsnA or its heterotrimeric subcomplex, CsnA-CsnC-CsnH is required for CsnB to reach wild type cellular protein levels. (**C**) In presence of CsnG and thus, the capacity to form either of the CsnD-CsnG or the CsnF-CsnG heterodimers or the CsnD-CsnF-CsnG heterotrimer, the cellular CsnD and CsnF is increased compared to the wild type control in a pre-CSN complex deficient background. (**D**) Relative CsnD protein levels remined wild type-like, when the potential to form the CsnD-CsnF-CsnG trimer is lost or if the pre-CSN complex can assemble.

Loss of CsnB abolished the interactions between CsnE and the remaining CSN subunits, but it did not affect the cellular levels of the free CsnE. This observation implies that the regulation of the cellular CsnE amounts is independent of the CSN complex, probably

because CsnE it is a multifunctional protein, which can function even when it is isolated from the complex.

The absolute GFP-CsnE amount is increased in comparison to the GFP-CsnD and GFP-CsnF amount in fungal strains harboring the CSN holocomplex (Figure S5). Quantitative analysis of tandem affinity purifications combined with cross-linking of human CSN complex also revealed elevated levels of the Csn1 and Csn5 subunits, which suggests complex-unbound, free subpopulations of these proteins (Fang *et al*, 2012). There are two possible scenarios, which might explain the discrepancy between the expected stoichiometries and the observed cellular amounts of a subunit belonging to a multiprotein complex (Matalon *et al*, 2014). According to these, CsnE might have additional biological functions in *A. nidulans*, or the affinity of CsnE to bind the complex is weak, which is compensated by elevated cellular amounts. The human Csn5, which exists in stable complex-unbound form, is a protein with multiple functions, like it is suggested for the Csn5 equivalent lid subunit, Rpn11 (reviewed in Pick and Bramasole, 2014). Various cellular functions are attributed by CsnE in *A. nidulans* as well, because loss of this subunit strongly affected the transcription of 15% of the fungal genome (Nahlik *et al*, 2010). Most changes were observed in the regulation of genes encoding proteins, which are involved in redox reactions and secondary metabolism. These changes affected the orsellinic acid synthesis genes, which were upregulated during development upon loss of *csnE*, resulting in the production of orsellinic acid derivates as well as sterigmatocystin intermediates. *csnE* acts as repressor of the *dba* cluster genes, because these genes are silenced in wild type background and are upregulated in response to the loss of *csnE* (Gerke *et al*, 2012). The *dba* gene cluster products, the DbaA-DbaI proteins, produce the DHMBA compound possessing antibiotic properties (Gerke *et al*, 2012; Gerke *et al*, 2021). Interestingly, not only members of the *dba* cluster DbaI and DbaH proteins (Figure S7; Table S5; Table S7; Table S9; Table S10), but also OrsE, a member of the orsellinic acid producing cluster (Sanchez *et al*, 2010) was amongst the specific interaction partners of CSN subassemblies. The purpose of these potential physical interactions is yet elusive and to unveil their biological relevance, further research will be required. CsnE has also a function in stress responses, because deletion of *csnE* led to the increase of proteins of the redox regulation (Nahlik *et al*, 2010), as well as *csnE* and *csnD* genes are involved in DNA damage response (Lima *et al*, 2005). As conclusion, various cellular functions are attributed to CsnE and also to other CSN subunits.

4.4 The interactome of CSN subunits involves elements of the protein quality control and degradation machinery

Synthesis of proteins is a cytoplasmic process, conducted on ribosomes. The newly synthetized nascent polypeptide chain is released from the ribosome and will be modified, folded and translocated for its proper function simultaneously or subsequent translation (Lodish *et al*, 2008). Chaperones and chaperonins, such as the TRiC/CCT complex and heat shock proteins, assist the correct folding of substrate proteins or multisubunit complexes and thereby maintain the proteostasis (reviewed in Yébenes *et al.,* 2011; and in Horianopoulos and Kronstad, 2021). Posttranslational modifications of proteins can occur during or subsequent to translation which can modify the function, activity, localization or lifespan (Wang *et al.,* 2010) takes place in the endoplasmic reticulum (ER). The polypeptide chains synthetized on the ER-bound ribosomes are transported back and forth in coat protein

complex I (COPI), coat protein complex II (COPII) and clathrin-coated vesicles to the Golgi-apparatus for further modifications (reviewed in Duden, 2003 and in McMahon and Mills, 2004). The proteins are sorted and transported to their cellular site of function, and as a part of a quality control mechanism, not properly folded proteins are bound and escorted by chaperons for their refolding or for their targeted break-down (reviewed in Amm *et al.*, 2014). Interactions between proteins involved vesicular transport and the CSN subunits or subassemblies suggest their intensive trafficking to cellular compartments of protein sorting. CSN assembly intermediates were co-purified with COPII vesicle proteins, such as An-Sec13. The COPII-coated vesicle mediated transport targets newly synthesized proteins from the ER to the Golgi apparatus, where sorting of the proteins takes place (reviewed in Pantazopoulou, 2016; and in Duden, 2003). The An-Sec13 and the SEC31 ortholog (Salama *et al.*,1997) form a heterotetramer and together with other SEC proteins they form the COPII vesicle coat (Lederkremer *et al.*, 2001). An-Sec13 is an ortholog of SEC13, which is a WD40 domain containing protein in *S. cerevisiae.* It is a structural component of three protein complexes, including the COPII-coat and the nuclear pore complex (Enninga *et al*, 2003). The retrograde protein transport from the Golgi to the ER occurs mainly by COPI-coated vesicles (reviewed in Duden, 2003). Coatomer proteins, such as CopA and a yeast SEC26 orthologs form the COPI vesicles and they are potential interaction partners of CSN subassemblies. CopA, alias $Sod^{VI}C$, is an alpha coatomer subunit of the COPI complex (Breakspear *et al*, 2007) and it is an ortholog of the yeast COP1/RET1. CopA is essential for establishing and the maintenance of the polarized fungal growth (Whittaker *et al*, 1999). The SEC26 coatomer β-subunit is a subunit of the coatomer COPI complex in *bakers´yeast* (Duden *et al.*, 1994) and it is essential for the retrograde Golgi-to-ER transport of cargo proteins (Ma and Goldberg, 2013). Further elements of the vesicle-mediated transport were identified as potential interaction partners of COP9 signalosome subunits and subassemblies, such as an ortholog of the yeast CHC1, of the yeast VPS60 and SEC14. CHC1 is a clathrin heavy chain protein in *S. cerevisiae* (Payne and Schekman, 1985), which protein forms clathrin-coated vesicle by self-polymerization and it is involved in trans-Golgi mediated trafficking (reviewed in McMahon and Mills, 2004). Vacuolar protein sorting 60 (VPS60) alias MOS10, is an Snf7 protein family member with a coiled-coil domain in *S. cerevisiae* (Kranz *et al.*, 2001). It acts at the late endosome, which is a cellular compartment for protein sorting. The yeast SEC14 is a phospholipid transport protein and is required for proper trans-Golgi-endosome dynamics (Mousley *et al*., 2008). Microtubules are components of the cytoskeleton and take part in the migration of nuclei and vesicles (Lodish *et al*, 2008). CSN assembly intermediates were co-purified with microtubule-associated proteins, such as NudC, RabE, ActA and AbpA. NudC was identified as potential interaction partner of the CSN complex-unbound CsnE (Figure S7). NudC, together with NudF, is a regulator of the microtubule element dynein, which are responsible for the nuclear migration within the fungal hyphae (Helmstaedt *et al*, 2008). Noteworthy that a relationship between *csnE* and NudC was found, which effects the cellular NudC levels, because loss of *csnE* resulted in elevated levels of NudC (Meister, 2018). RabE is a yeast RAB11 ortholog (Pinar *et al*, 2015), which is a small GTPase, a component of secretory vesicles from the trans-Golgi to the plasma membrane during apical extension of fungal hyphae (Pinar and Peñalva, 2017). ActA, or gamma-actin, is a structural component of cytoskeleton located predominantly in the cytoplasm of the hyphal tip (Fidel *et al.,* 1988) and AbpA is an actin-binding protein involved in endocytosis, acts at the site of polarized growth (Araujo-Bazán *et al*, 2008). A nuclear subpopulation of actin supports transcription by assisting in chromatin remodeling in humans (Dopie *et al.*, 2012; reviewed in Kloc *et al.*, 2021). Thus, it cannot be excluded that

there is nuclear subpopulation of actin in fungal cells as well, which might interact with the nuclear subpopulations of CSN subassemblies.

In summary, the CSN subassemblies are targeted by intracellular transport proteins to cellular organelles of protein sorting, as part of a quality control mechanism. Similarly, the interactome of the human COP9 signalosome includes proteins of the intracellular trafficking system among the most enriched CSN complex interacting candidates (Fang *et al*, 2012). It is possible that shuttling between cellular compartments and protein sorting provides the correct folding, modifications of the CSN subassemblies and subunits, which might facilitate the subcellular localization and their subsequent assembly.

4.4.1 Pre-CSN complex intermediates interact with proteins with chaperoning functions

Various intermediates of the pre-CSN complex formation associate with chaperons as potential interaction partners. Six of the eight CCT/TriC complex subunits were co-purified with diverse CSN subassemblies. The CCT/TriC is a chaperonin complex and it has a cylindrical structure formed of two identical rings, each compassing eight subunits (Zang *et al*, 2016). The CCT/TriC complex enclose the substrate within its cavity and facilitates its folding at cost of ATP energy. This multiprotein complex folds approximately 10% of all newly produced cytoplasmic proteins, including elements of the cytoskeleton and proteins involved in cell cycle progression (Zang *et al*, 2016). Demonstrating the biological relevance of the CCT/TriC complex, its subunits are essential in yeast and have supposedly other physiological roles, because identical mutations in a conserved region responsible for the chaperoning function led to distinct phenotypes of each CCT/TriC subunit mutant strains (Amit *et al*, 2010). It can be suggested that the CCT/TriC complex primes the CSN complex assembly intermediates for complex formation by assisting the correct three-dimensional folding of the proteins. The interactome of CSN subunits in pre-CSN complex deficient strains not only involved chaperonins, but also heat shock proteins (HSPs) (Figure 44). Interactions between pre-CSN complex intermediates and HSPs, such as SgdE, and orthologs of the yeast YDJ1 and SGT2, propose that these subassemblies are HSP substrates. SgdE is a heat shock 70 family protein (Hsp70), which is also involved in conidia germination of *A. nidulans* (Osherov and May, 2000). The yeast YDJ1 protein is a DnaJ-like Hsp40 co-chaperone and it works together with Hsp70 proteins for polypeptide folding (Caplan and Douglas, 1991). It is suggested that YDJ1 protects protein kinases from early degradation (Mandal *et al*, 2008), however it is also involved in the ubiquitin-linked clearance of other proteins (Lee *et al.*, 1996). YDJ1 in association with Hsp70 proteins facilitates the translocation of proteins through intracellular membranes of mitochondrion and ER, but also into the nucleus (Figure 44) (Deshaies *et al.*, 1988; Caplan *et al.,* 1992; Heck *et al.*, 2010). A physical interaction between YDJ1 and SGT2 was shown (Liou *et al.,* 2007). SGT2 is a glutamine-rich scaffolding protein in yeast, which binds HSPs in the TRC complex, which sorts proteins to the endoplasmic reticulum (Figure 44) (Wang *et al.*, 2010).

In conclusion, supposedly a quality control mechanism is alerted, which recognizes the accumulated and probably instable assembly intermediates. As a consequence, chaperons are mobilized to support the correct folding, and thus, probably stability of these subassemblies. It is also possible that these assembly intermediates are escorted by chaperons into various cell organelles, such as the endoplasmic reticulum or the nucleus.

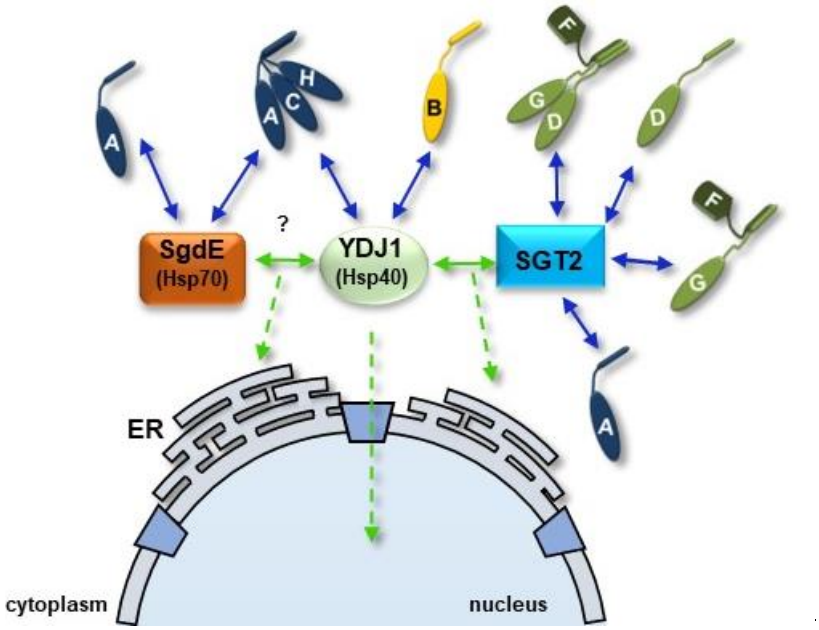

Figure 44. The heterotrimeric subcomplexes and free-standing CSN subunits are potential substrates of heat shock proteins.
Interactions between heat shock proteins were described in yeast (arrows with green continuous line) which are potential interaction partners of CSN subassemblies in *A. nidulans in vivo* (indicated with blue arrows). The interplay of heat shock proteins can also escort substrate proteins into the endoplasmic reticulum or into the nucleus (Heck *et al*, 2010).

4.4.2 The CSN complex and its assembly intermediates associate with the 26S proteasome

Ubiquitination is a powerful tool to label proteins for different purposes (reviewed in Oh *et al.*, 2018; and in French *et al*., 2021). It can contribute to ribosome function, DNA repair and subcellular transport, as well as it targets proteins to endocytosis (Asimaki *et al*, 2021) or break-down by the 26S proteasome (reviewed in Swatek and Komander, 2016). CsnD-CsnG heterodimer and CsnD-CsnF-CsnG subcomplex potentially interact with ubiquitin (Ubi1). The *ubi1* gene encodes a fusion of N-terminal ubiquitin and C-terminal extension protein of the small ribosomal subunit, therefore, the *ubi1* gene products are ubiquitin and a ribosomal protein in *A. nidulans* (Noventa-Jordão *et al*., 2000). In the UPP, ubiquitinated proteins are recognized, bound and escorted to the proteasome by extra-proteasomal ubiquitin receptors (Elsasser *et al*, 2004). The CSN complex-unbound CsnD protein was co-purified with RAD23, which is a ubiquitin-like and ubiquitin-associated domain containing protein and functions as an extra-proteasomal ubiquitin receptor (Elsasser *et al.*, 2004; and reviewed in Livneh *et al*., 2016). Supposedly, the free CsnD subunit suffers instability, when it is isolated from the complex. Physical interaction between the ZOMES, including the 26S proteasome and the COP9 signalosome, were described in various reference organisms (Seeger *et al.,* 1998; Kwok *et al.*, 1999; Peng *et al.*, 2003; Sha *et al.,* 2010). It is hypothesized that CSN might act as an additional or alternative proteasomal lid (reviewed in Li, 2003). As an example, a dual proteasomal-CSN function of the human Rpn5 subunit (Csn4/D equivalent) was suggested (Yu *et al.*, 2011). CSN subunits and subassemblies also mediated interactions with the 26S

proteasome in *A. nidulans*. The proteasome enrichment with these subassemblies may confer their targeted clearance, if their correct tertiary structure cannot be provided by chaperons or chaperonins. These interactions were not exclusive in for CSN assembly intermediates, because CSN subunits mediated interactions with the 26S proteasome even in wild type cells harboring the CSN holocomplex. This phenomenon was described in various organisms with an octameric CSN complex. Interactions between COP9 signalosome and proteasome subunits were determined in human cells, in fruit flies and in plants as well (Huang *et al.*, 2005; Peng *et al.*, 2003; Lier and Paululat, 2002), albeit, up to date there is no precise understanding of the physiological relevance of these interactions. A profane explanation is that the 26S proteasome regulates the CSN complex abundance by targeted degradation of excess or outdated CSN complex populations. But it is also possible that nuclear localized eight-subunit CSN complex and the nuclear 26S proteasome possess other biological roles, such as transcriptional regulation (reviewed in Wei *et al.*, 2008; in Chamovitz, 2009; and in DeMartino and Gillette, 2007). Active contribution of these multisubunit complexes in gene expression regulation was shown: they can regulate transcription by contributing to the clearance of transcriptional modulators, by physical and functional association with the RNA polymerase II (Sun *et al.,* 2002; Gillette *et al.*, 2004) or by chromatin remodeling (reviewed in Bhat and Greer, 2011; in McCann and Tansey, 2014; and in Shmueli *et al.,* 2021), but also by their DNA-binding ability (Gonzalez *et al*., 2002; Singer *et al.,* 2014). A possible explanation of the CSN complex-proteasome interaction is therefore that these together, as super complexes, are part of a translational regulation machinery (Figure 45). Neddylated substrates co-fractionated with the 26S proteasome in mammalian cells (Kamitani *et al*, 2001), furthermore, neddylation on the proteasome itself was reported in human cell lines (Lobato-Gil *et al*, 2021). In both cases, the biological purpose of the Nedd8-modifications remains elusive. Another realizable scenario for the association of the octameric CSN complex with the proteasome is the deneddylation of neddylated proteasomal subunits or proteasome-associated neddylated substrates (Figure 45).

In summary, depletion of either the pre-CSN complex or the CSN holocomplex occurring by deletions of CSN subunit genes causes the accumulation of CSN assembly intermediates. These intermediates are probably quickly connected to each other to proceed to the next assembly step in healthy cells. Accumulation of the subassemblies might alert a quality control system with involvement of intracellular transport proteins and chaperons, which may lead to their clearance (reviewed in Amm *et al.*, 2014). A system might eliminate of the error prone or old subunits, while, simultaneously initiate the production of new ones. According to another possible explanation for the COP9 signalosome-26S proteasome co-enrichment, there is a complex interplay between multiprotein complexes, which regulate not only proteolysis, but presumably other processes as gene expression.

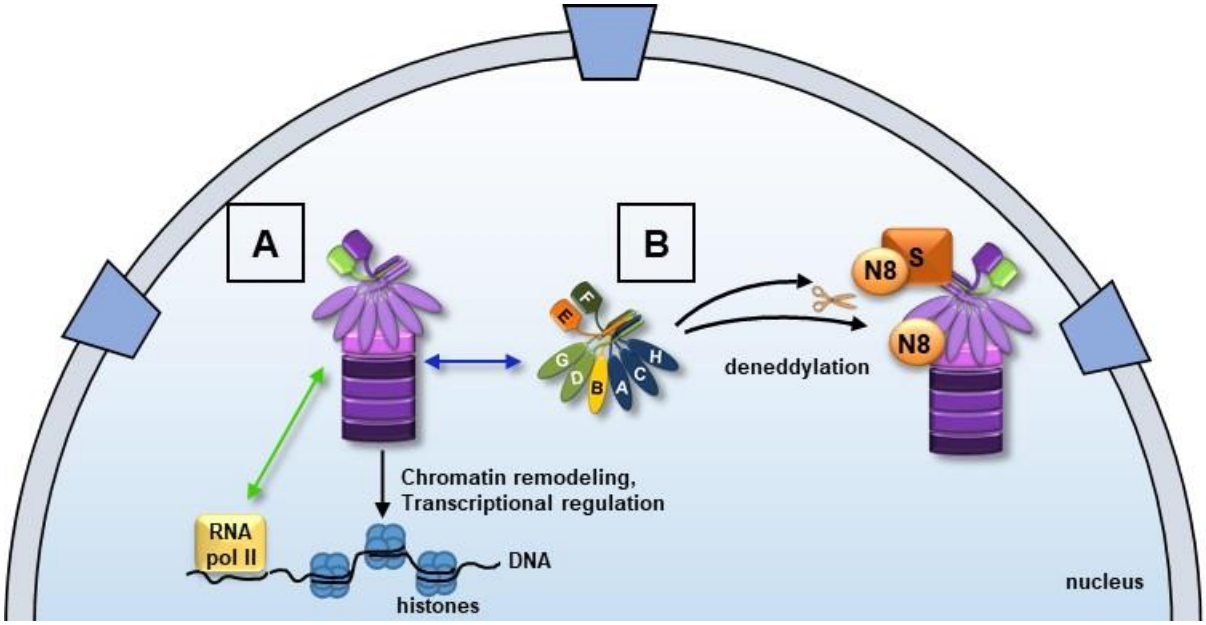

Figure 45. Possible scenarios for the biological function of the CSN complex-proteasome interactions.
The models present two possible scenarios for the interaction between the 26S proteasome and the COP9 signalosome. (**A**) The interplay of the fungal CSN complex and the proteasome (indicated with a blue double-end arrow), which was shown to directly interact with RNA polymerase II in yeast (RNA pol II, indicated with a green double-end arrow) and might contribute to transcriptional regulation. (**B**) Binding of neddylated substrates as well as neddylation of the 26S proteasome itself was reported. Thus, it can be hypostatized that the biological function of the CSN complex-proteasome interplay is the removal of Nedd8 from these substrates by the COP9 signalosome.

4.5 Interplay between the fungal CSN subunits for subcellular localization

It was long suggested that at least some degree of pre-assembly is required for the nuclear localization of the CSN complex (Chamovitz *et al*, 1996). Yet, till now there was no experimental evidence for the interconnection of the CSN complex assembly and the subcellular localization of its subunits and subassemblies. Here, novel insights into this interplay are provided. This recent study, along with earlier works, report that the intact, eight subunit COP9 signalosome inhabits both cellular niches, cytoplasm and nuclei, though it is concentrated in the nuclei (Chamovitz *et al.*, 1996; Busch *et al.*, 2003; Fuzesi-Levi *et al*., 2014). The inability to form either the octameric CSN complex or the heptameric pre-CSN complex is accompanied with perturbation of the nuclear localization of the remaining CSN subunits in *A. nidulans*. CsnE deneddylase or the ability to form the octameric CSN complex promote the nuclear accumulation of GFP-CsnA, GFP-CsnF and GFP-CsnD. GFP-CsnD, produced in a *csnE* deletion strain, recruited a heptameric pre-CSN complex (data not shown), which was mainly cytoplasmic. Without CsnE, the nuclear accumulation of GFP-CsnA and GFP-CsnF was also abolished. Uniquely amongst the analyzed COP9 signalosome subunits, the subcellular localization of the linker GFP-CsnB subunit was independent of the CsnE deneddylase. GFP-CsnB persisted in the nuclei in a *csnE*-deficient strain, in which background the pre-CSN complex was recruited by GFP-CsnB. It cannot be excluded that free, complex-unbound subpopulations of GFP-CsnB persist in the nuclei, as the fluorescence microscopy

is not able to differentiate the free and CSN complex-bound subpopulations of the GFP-CSN fusion proteins. Although *A. nidulans* CsnB possesses two predicted nuclear localization sequences, their single deletion or mutation did not inhibit the nuclear accumulation of CsnB in fungal strains harboring the octameric CSN complex. Yet, it cannot be excluded that the potential NLSs are recognized and bound by importins in other, not examined conditions or upon a possible conformational change of the CsnB. It can be also speculated that CsnB relies on an interacting protein, which binds to CsnB and shuttles it to the nucleus. For example, an interaction between the ubiquitin specific protease UspA and CsnB in the nuclei and nuclear periphery was reported (Meister *et al*, 2019). The CsnB-interacting UspA was also co-eluted with KapB and KapF karyopherins (Meister *et al*, 2019). KapB and KapF are importin proteins, which facilitate the nuclear translocation of their cargo proteins (Markina-Iñarrairaegui *et al*, 2011).

Loss of the capacity to form CsnA-CsnC-CsnH subcomplex had consequences on the cellular abundance, CSN subunit binding ability as well as location of GFP-CsnB. The free, complex-unbound GFP-CsnB is detected mainly outside of the nuclei. In conclusion, CsnA or the CsnA-CsnC-CsnH subcomplex promotes the nuclear accumulation of CsnB (Figure 46). Noteworthy that although the CsnD-CsnF-CsnG subcomplex is present in the examined fungal background, yet, it has no effect on either the abundance or localization of CsnB. In a fungal background, in which the two subcomplexes co-exist, the GFP-CsnD signal, corresponding to the CsnD-CsnF-CsnG subcomplex, is predominantly is enriched in the nuclei. In contrast, the GFP-CsnA signal, corresponding to the CsnA-CsnC-CsnH subcomplex, is equally distributed between cytoplasm and nuclei. The subcellular localization of the GFP-CsnD/CsnD-CsnF-CsnG and the GFP-CsnA/CsnA-CsnC-CsnH subcomplex is probably independent of the opposite trimeric subcomplex. As the nuclear localization of GFP-CsnB is diminished without CsnA/CsnA-CsnC-CsnH and *vice versa*, an interplay between these subunits for their nuclear localization can be concluded. The localization of mainly cytoplasmic CsnB and CsnA/CsnA-CsnC-CsnH subcomplex is independent of the CsnD-CsnF-CsnG heterotrimeric subcomplex, probably because the latter already resides mainly in the nuclei (Figure 46). The precise choreography of the subcellular movements of the CsnD-CsnF-CsnG subcomplex is yet elusive. Experimental data deriving from the GFP-trap experiments propose that the An-Mlp1 nuclear pore complex subunit is involved in the nuclear translocation of this subcomplex (Figure 46). An-Mlp1 is very similar to the yeast Mlp1p protein, which is a coiled coil repeat containing filamentous protein of the nuclear basket stretching from the NPC into the nucleoplasm (Strambio-de-Castillia *et al*, 1999). While Mlp1p is a non-essential protein, An-Mlp1 is essential for viability in *A. nidulans*, as its Δ*An-mlp1* strains could germinate, but failed to form viable colonies (De Souza *et al*., 2009). Consistent with the nuclear accumulation of the CsnD-CsnF-CsnG subcomplex, interactions with the nuclear localized proteasome were shown. Interestingly, Mlp1p also recruited the 26S proteasome and this interaction supposedly contributes to chromatin remodeling (Niepel *et al*, 2013). Thus, there might be a trimeric interaction between the CsnD-CsnF-CsnG subcomplex, the proteasome and An-Mlp1, which might also be involved in the translational regulation.

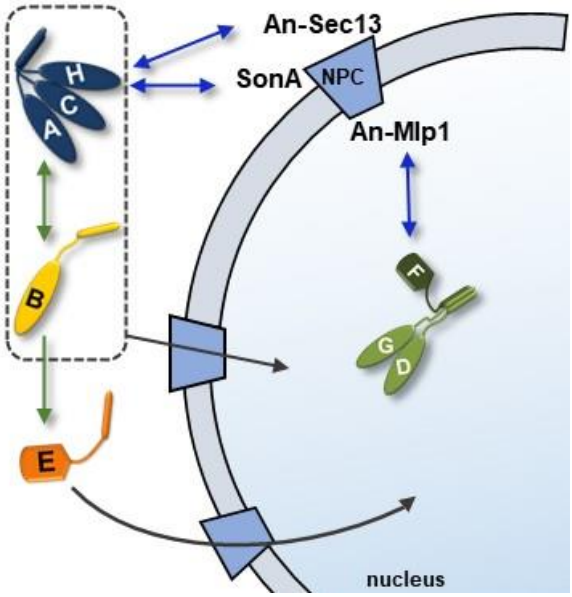

Figure 46. Interconnection of CSN subunits for subcellular localization.
The CsnD-CsnF-CsnG subcomplex is located predominantly in the nuclei, whereas the CsnA-CsnC-CsnH subcomplex is evenly distributed between cytoplasm and nuclei. Both subcomplexes mediated interactions with nuclear pore complex (NPC) proteins. An interplay (green double-end arrow) between CsnB and CsnA or the CsnA-CsnC-CsnH subcomplex is a prerequisite for their nuclear enrichment. Presence of CsnB promotes the nuclear translocation of CsnE.

Nuclear enrichment cannot be observed for the CsnA-CsnC-CsnH subcomplex, which is distributed within the cellular compartments in the vegetative hyphae of *A. nidulans*. Similarly to the fungal CsnA, the human Flag-tagged Csn1 is found in nuclear and cytoplasmic compartments and it is frequently found enriched around the nuclear periphery (Tsuge *et al*, 2001). A truncated version of Csn1, which excludes the PCI domain and thus, is unable to stably associate to the complex, is able to translocate to the nucleus (Tsuge *et al*, 2001). It can be assumed that the N-terminal part of CsnA mediates interaction with proteins, which support its nuclear transport. CsnA, as subunit of the CsnA-CsnC-CsnH subcomplex was co-enriched with NPC proteins, such as SonA and An-Sec13. SonA is an ortholog of the yeast GLE2, which is a WD40 domain containing protein (Murphy *et al*, 1996). SonA is the product of an essential gene in *A. nidulans* and it is a component of the nuclear pore complex (Osmani *et al.*, 2007). The An-Sec13 is a yeast SEC13 ortholog and it is an essential structural component of three protein complexes. An-Sec13 inhabits two locations within the cell (Hernández-González *et al*, 2019), such as its yeast ortholog SEC13 (Enninga *et al*, 2003). As an NPC component, it contributes to nucleocytoplasmic transport and NPC biogenesis (Osmani *et al.*, 2007).

CsnB is crucial for the pre-CSN complex assembly and the subsequent integration of the CsnE, because CsnE deneddylase catalytic subunit is unable to associate to CSN subunits upon loss of the CsnB. The linker CsnB also effects the subcellular localization of the catalytic subunit. CsnE cannot concentrate in the nuclei without the linker. The free, complex-unbound CsnE inhabits the cytoplasm (Figure 46). These results show that the CSN complex assembly steps are coupled with translocation events of the CSN assembly intermediates, where the identified interaction partners probably contribute to complex assembly by shuttling CSN subunits and subassemblies together.

4.6 CSN subunits and trimeric subcomplexes mediate interactions with proteins involved in transcriptional regulation

It is described that the protein degradation machinery elements, as the 26S proteasome, are involved in transcriptional control mechanisms (reviewed in Bhat and Greer, 2011; in McCann and Tansey, 2014; and in Shmueli *et al.,* 2021). Components of the protein degradation machinery and several complexes involved in transcriptional control are represented in the interactome of the human CSN complex (Fang *et al*, 2012). Protein complexes, which contribute to chromatin remodeling and histone deacetylation, like the H2AX, MTA2 and the BRM-SIN3A-histone deacetylase complex were co-enriched with the CSN complex in humans (Fang *et al*, 2012). H2AX is a histone protein, that mediates DNA repair and cell cycle control (reviewed in Fernandez-Capetillo *et al.*, 2004). MTA2 belongs to the metastatic tumor antigen family proteins, which modulate gene expression by chromatin remodeling (Sen *et al*, 2014). Similarly, the BRM-SIN3A-histone deacetylase complex consists of 15 proteins with chromatin remodeling function (Tiana *et al.*, 2018; Giurgiu *et al.,* 2019).

The fungal COP9 signalosome subcomplexes were also co-purified with regulators of gene expression, like an ortholog of the yeast HST1 and a RVB2 as well as RcoA (Figure 47). The *S. cerevisiae* HST1 (homolog of SIR two) belongs to the conserved family of sirtuin protein deacetylases, which are involved in gene silencing (Brachmann *et al.*, 1995; Derbyshire *et al*., 1996; Wierman and Smith, 2014). It is involved in the repression of meiotic processes linked to sporulation in yeast (Pijnappel *et al.*, 2001; McCord *et al.*, 2003).

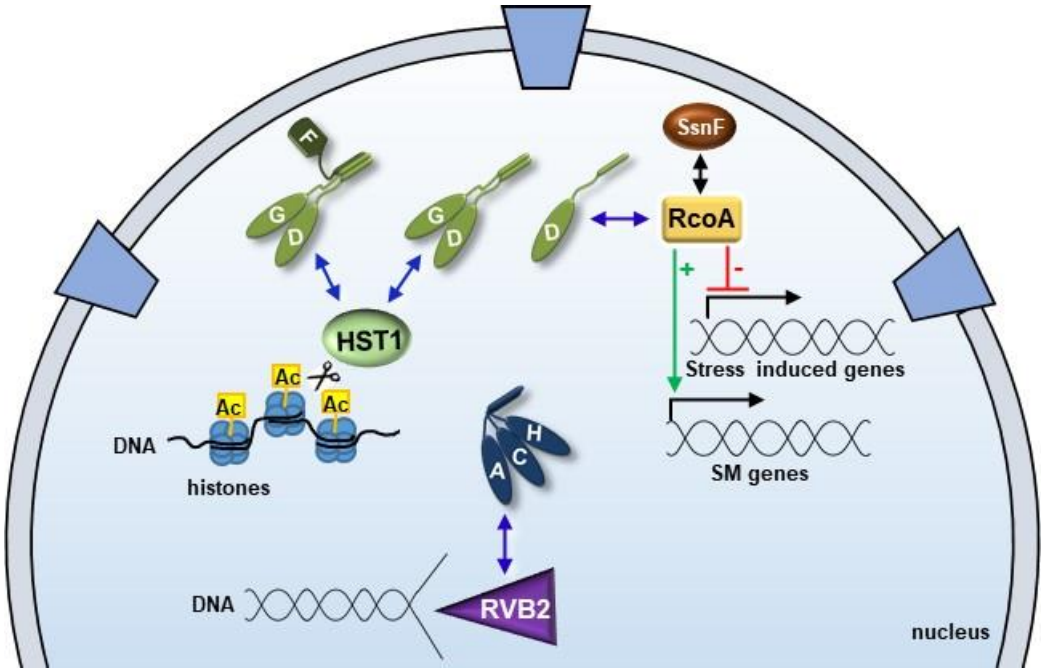

Figure 47. COP9 signalosome subcomplexes mediate interactions with transcriptional regulators.
Both heterotrimeric subcomplex recruited transcriptional regulators (interactions are indicated with blue double-end arrows): the CsnD-CsnF-CsnG subcomplex and its subunits were co-purified with an ortholog of the nuclear HST1 histone deacetylase and RcoA, which is, together with SsnF (interaction indicated with black double-end arrow) involved in repression of stress induced and activation of secondary metabolite (SM) genes. The CsnA-CsnC-CsnH trimeric subcomplex was co-eluted with a nuclear-enriched ortholog of RVB2, what is involved in chromatin remodeling.

The yeast RVB2 is an ortholog of the human reptin and the bacterial RuvB DNA helicase (Torreira *et al.*, 2009). It is a AAA-domain containing chromatin remodeling enzyme, which supposedly serves as platform for protein-protein and nucleic acid-protein interactions and thus, regulates transcription and the cell cycle at multiple levels (reviewed in Mao and Houry, 2017). RcoA is the ortholog of the *S. cerevisiae* Tup1p. Tup1p together with Ssn6p, alias Cyc8p, form a co-repressor complex, which does not possess DNA-binding domains, but it is associated to gene expression regulators, such as histone deacetylases (Watson *et al.*, 2000; Davie *et al.*, 2002; Davie *et al.*, 2003). As co-repressor complex, Ssn6p-Tup1p connects to various DNA-binding proteins, transcription factors and deacetylated histones, preventing the association of RNA polymerase II (Zaman *et al*, 2001). Repression by the Ssn6p-Tup1p complex is achieved by either direct interference with the activator, or altering the local chromatin structure, or by interaction with the general transcription machinery (reviewed in Smith and Johnson, 2000). The Ssn6p-Tup1p regulates gene classes, among them are glucose-repressible genes and genes involved in various stress responses, such as hypoxia and DNA damage, which are repressed in non-stress conditions (reviewed in Smith and Johnson, 2000). Tup1p-Ssn6p is a Janus-faced complex, because it does not only act as repressor, but also as activator of transcription (Conlan *et al*, 1999). The Tup1 ortholog RcoA is a WD40 repeat protein of *A. nidulans*, which is required for fungal growth and is involved in both developmental programs as well as in secondary metabolism (Hicks *et al.*, 2001; Todd *et al.*, 2006). It is required for vegetative growth and asexual spore formation (Hicks *et al.*, 2001), but also for sexual development (Todd *et al.*, 2006). RcoA binds SsnF, which is an ortholog of the yeast Ssn6p/Cyc8p (García *et al*, 2008). SsnF is essential for both, *Aspergillus nidulans* (García *et al*, 2008) and its human pathogenic relative *Aspergillus fumigatus* (Jöhnk *et al*, 2016). An interaction between RcoA-SsnF complex and the F-box protein Fbx15 was demonstrated (Jöhnk *et al*, 2016). Fbx15 is indispensable for oxidative stress response and virulence of *A. fumigatus* and it controls the nuclear localization of SsnF, presumably for an appropriate stress response (Jöhnk *et al*, 2016). Fbx15 was co-enriched with CsnD, CsnF and CsnG subunits of the COP9 signalosome, assumably for the correct function of Fbx15 during oxidative stress (Jöhnk *et al*, 2016).

The interactions with proteins involved in gene expression are specific to CSN complex subassemblies. Probably, they are transient and exist in unfavorable conditions to control stress response, which is possibly provoked by the accumulation of CSN assembly intermediates. It is also possible that these specific interactions are enabled by a conformational change of the CSN subcomplexes or subunits, which might occur when they are not inserted into the CSN holocomplex.

5 Conclusions

This work gives insights into the interconnections of the COP9 signalosome subunits, which regulate their cellular abundance, localization, complex formation and possible additional functions. The fungal COP9 signalosome assembles via the novel CsnD-CsnG-CsnF and the CsnA-CsnC-CsnH heterotrimeric subcomplexes, which were identified in this study. These are linked together by CsnB, presumably through its primary association to the CsnA-CsnC-CsnH subcomplex enabling the binding of the CsnD-CsnF-CsnG subcomplex. As a consequence, a stable, but inactive heptameric subcomplex is formed. The heptameric pre-CSN complex gains its catalytic activity towards the neddylated SCF CRL complex by the association of the CsnE deneddylase subunit to this pre-assembled complex (Lingaraju *et al*, 2014; Beckmann *et al*, 2015). This catalytic activity is conferred by the mainly nuclear localized CSN holocomplex (Busch *et al*, 2003; Chamovitz *et al*, 1996). It was suggested that various CSN complex subassemblies exist and localize to the cytoplasm in eukaryotic cells, where they might be involved in various cellular functions (Dubiel *et al*, 2015; Chamovitz *et al*, 1996). This work links the cellular localization of CSN subunits and subcomplexes with the steps of complex formation and possible further functions of the CSN subunits. The novel heterotrimeric subcomplexes reside both in the cytoplasm and nuclei. The CsnA-CsnC-CsnH subcomplex inhabits both cellular compartments, whereas a larger nuclear subpopulation of CsnD-CsnG-CsnF persists in the nuclei (Figure 48, part 1). Nuclear subpopulations of these subcomplexes might be involved in various cellular functions performed directly or indirectly through interacting proteins. Such a function might be transcriptional regulation. An interconnection between the linker CsnB subunit and CsnA, as part of the CsnA-CsnC-CsnH subcomplex, promote their nuclear enrichment (Figure 48, part 2). There is also an interdependency between the linker subunit CsnB and the deneddylase CsnE for their nuclear transport, where CsnB promotes the nuclear translocation of CsnE, probably coupled to the complex formation (Figure 48, part 3). Apart from nuclear pore proteins, import or export proteins, which would facilitate the nucleocytoplasmic shuttle of the CSN subunits and subcomplexes were so far not identified. It is therefore possible that these CSN assembly intermediates are cargos of interacting proteins or a protein complex, which escort them into the nucleus where the COP9 signalosome holocomplex resides. Cytoplasm-to-nuclei transport capacity was described for chaperons (Heck *et al*, 2010), which were identified as interaction partners of CSN subassemblies. The physical interaction of CsnB with UspA takes place inside or in the close proximity of the nuclei (Meister *et al*, 2019). This fosters the hypothesis that CsnB and/or its associated CSN subassemblies are cargos of UspA, which interacts with nuclear import proteins (Meister *et al*, 2019). The nuclear co-localization of the heterotrimeric CSN subcomplexes, the linker CsnB and CsnE results in the assembly of the catalytically active COP9 signalosome (Figure 48, part 4 and 5).

The CSN holocomplex is an interaction platform for various proteins (reviewed in Wei and Deng, 2003; in Schwechheimer, 2004 and in Chamovitz, 2009), including the other cellular deneddylase, Den1/A (Christmann *et al*, 2013; Schinke *et al*, 2016). These two deneddylases physically interact with each other and they are both required for fungal development (Christmann *et al*, 2013; Schinke *et al*, 2016; Köhler, 2018). The octameric CSN complex is a prerequisite for the orchestration of the sexual developmental pathway (Beckmann *et al*, 2015) and the pre-CSN complex subunits and CsnE are involved in surface growth and in orchestration of the asexual life cycle (Figure 48, part 6).

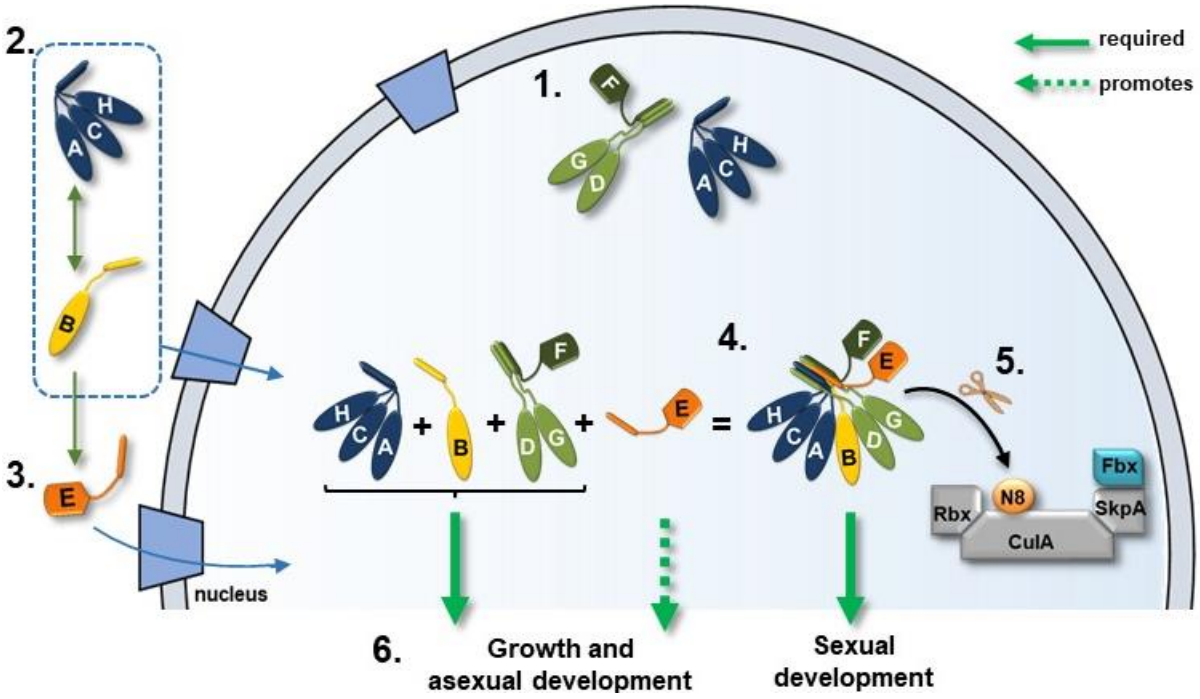

Figure 48. Choreography of the COP9 signalosome assembly.
There is a complex interplay between the CSN subunits and subcomplexes regulate their cellular abundance, location and assembly. **1.** CsnD-CsnG-CsnF subcomplex inhabits predominantly the nuclei and the CsnA-CsnC-CsnH subcomplex is distributed between nuclei and cytoplasm. Nuclear subpopulations of these subcomplexes might be involved in various cellular function, such as transcriptional regulation. **2.** An interplay between CsnB and the CsnA/CsnA-CsnC-CsnH subcomplex governs their nuclear accumulation. **3.** A CsnB-CsnE interplay targets CsnE to the nucleus, **4**. where the fully assembled COP9 signalosome localizes. **5.** The CSN holocomplex acts as sensor of the substrate free and neddylated CRL and catalyzes the Nedd8 cleavage, allowing the binding of a new protein substrate. **6.** As a consequence of this, or maybe through a distinct and yet undiscovered function, the CSN holocomplex is required for the sexual pathway. CsnE promotes the orchestration of the asexual life cycle. The pre-CSN complex subunits are required for this developmental pathway as well as for surface growth.

This work summarizes findings on various cellular mechanisms leading to the formation of the fungal COP9 signalosome and provides a basis for further studies of this developmental regulator complex in other eukaryotic organisms. Future investigations on the human CSN complex can take advantages of these findings made in a fungal reference system, because their orthologous complexes are similar. A great number of publications describe the COP9 signalosome as potential oncogene, because overproduction of CSN subunits promoted many cancer types (reviewed in Richardson and Zundel, 2005; in Wang *et al*, 2016; and in Lee *et al*, 2011a). Thus, this work, describing the assembly pathway and the role of the COP9 signalosome in the fungal physiology, might also have a possible medical relevance in humans.

6 Supporting information

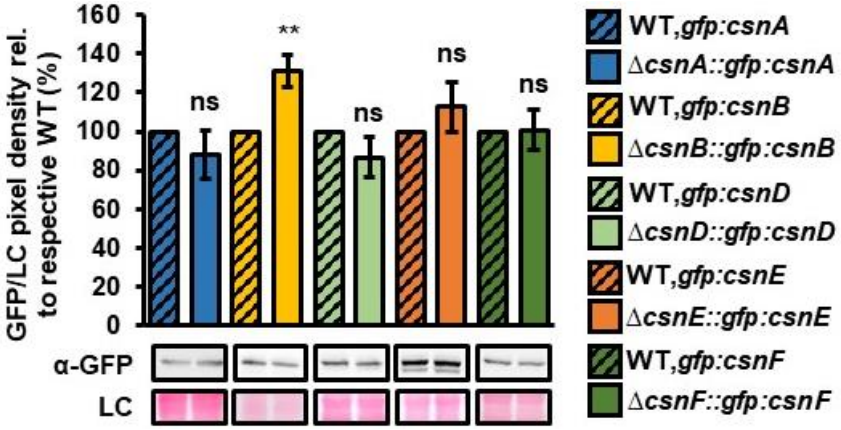

Figure S1. The GFP fusions of CsnA, CsnB, CsnD, CsnE or CsnF are produced at nearly wild type levels in the complementation strains.
The relative amount of GFP-CsnA, GFP-CsnB, GFP-CsnD, GFP-CsnE and GFP-CsnF was determined by α-GFP immunoblot in respective complementation strains compared to respective WT strains. The GFP signal/loading control pixel density ratio of each strain was relative (rel.) to the mean value of the respective WT,*gfp:csn* strain. Ponceau staining was used as loading control (LC). The presented cropped region of the immunoblot was used for the pixel density quantification. The charts represent the mean of three to five independent biological replicates performed in duplicates and the error bars display SEM. Not significant (ns):$p>0.05$, **:$p\leq0.01$.

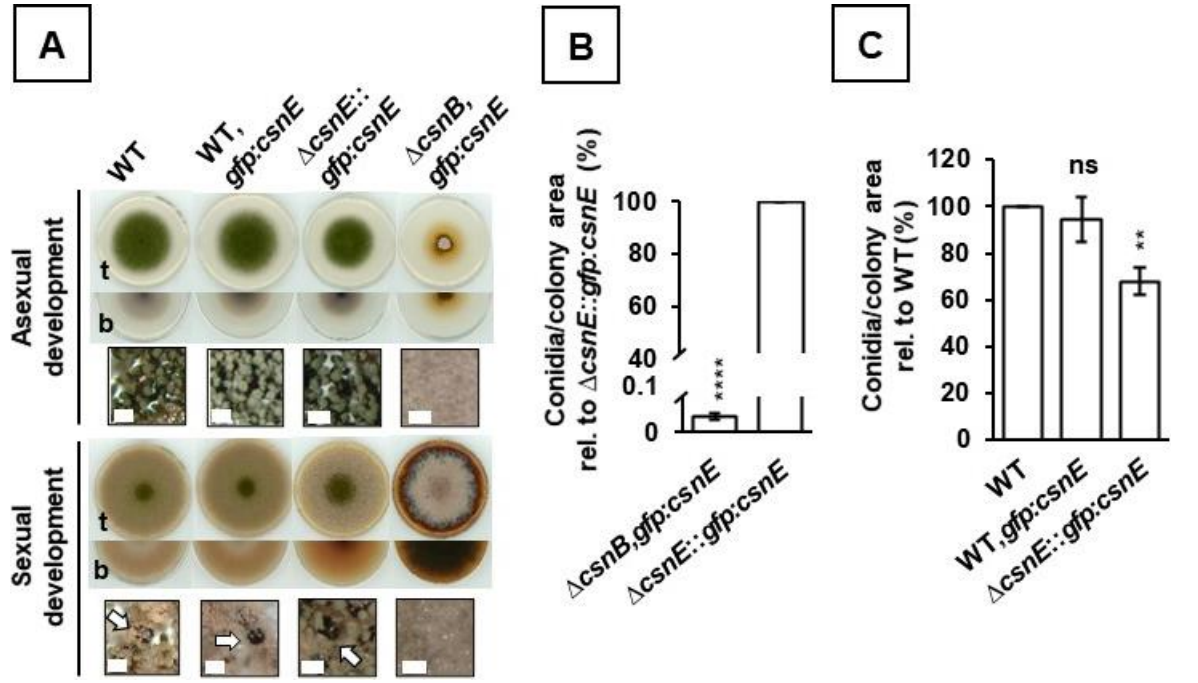

Figure S2. Growth and development of fungal strains producing the GFP-CsnE fusion protein. (**A**) Growth and development of the *A. nidulans* Δ*csnB,gfp:csnE*, Δ*csnE::gfp:csnE* complementation and WT,*gfp:csnE* strains were analyzed in spotting assays. 2x10^3 conidia of each strains were point inoculated on MM$_{PABA}$ agar plates. The fungal strains were grown at 37°C either for five days under constant illumination and with aeration to induce asexual development or for 14 days in darkness and with low O_2-high CO_2 pressure to promote sexual differentiation. The figure shows the top (t) and bottom (b) views of the colonies. Size bars represent 100 µm. The arrows point to mature fruiting bodies. (**B**) The charts represent the mean values of the conidia number per colony area of three independent biological replicates performed in duplicates for the Δ*csnE::gfp:csnE* complementation strain and in five technical replicates of Δ*csnB,gfp:csnE*. The conidia number per colony area of the Δ*csnB,gfp:csnE* strain was relative (rel.) against the mean value of the Δ*csnE::gfp:csnE* complementation strain. The error bars display SEM. ****:p≤0.0001. (**C**) The charts represent the mean of the conidia number per colony area of three independent biological replicates performed in duplicates. The conidia counts per colony area of each strains were relative (rel.) to the mean value of the wild type (WT) strain. The error bars display SEM. Not significant (ns):p>0.05, **:p ≤ 0.01.

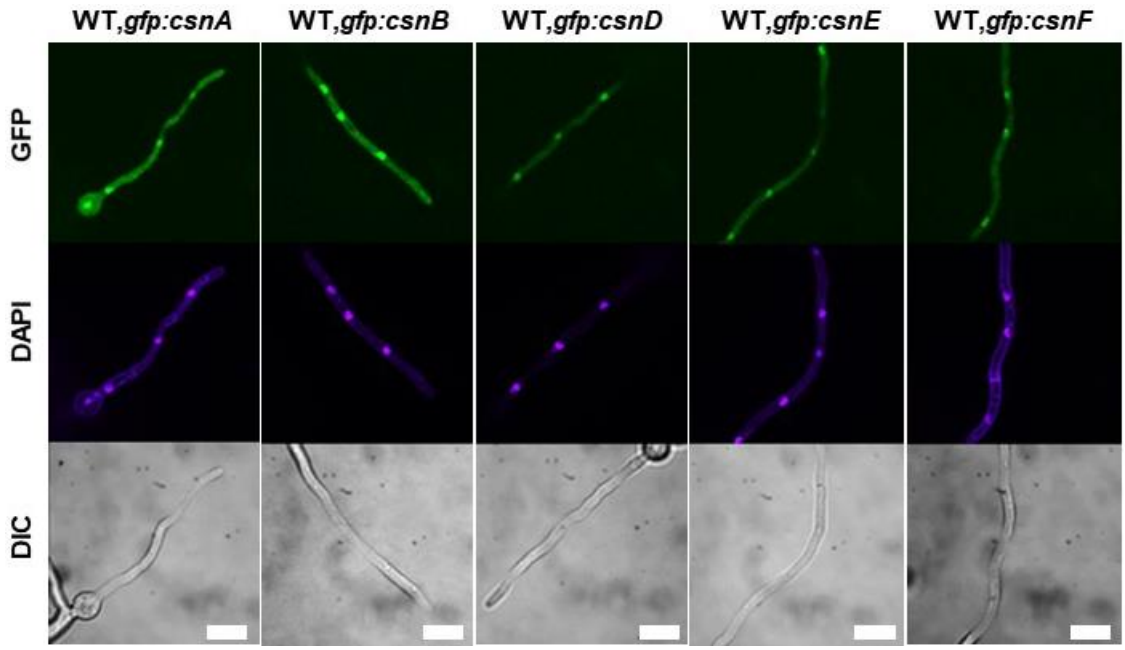

Figure S3. The COP9 signalosome is mainly nuclear localized at lower temperatures.
The fungal CSN holocomplex, visualized by GFP-CsnA, GFP-CsnB, GFP-CsnD, GFP-CsnE and GFP-CsnF produced in the wild type background, co-localized with the DAPI stained nuclei. The confocal microscopy was carried out with fungal cultures grown for 20 hours vegetatively at 30°C. The experiment was performed once. Scale bars represent 10 µm.

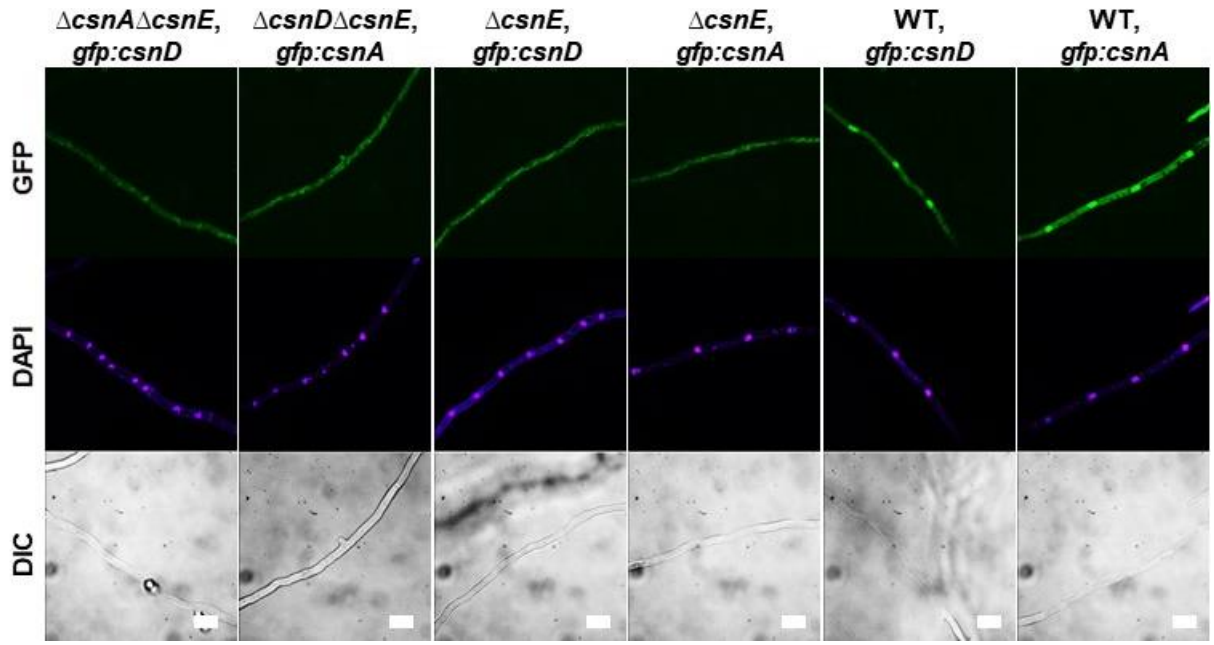

Figure S4. The predominantly nuclear localization of the CsnD-CsnF-CsnG is independent from the CsnA-CsnC-CsnH subcomplex, which is mainly cytoplasmic.
Nuclear accumulation of the CsnD-CsnF-CsnG subcomplex, visualized by GFP-CsnD in the Δ*csnA*Δ*csnE,gfp:csnD* strain, could be shown, when the CsnA-CsnC-CsnH subcomplex formation is abolished. Such nuclear accumulation of the CsnA-CsnC-CsnH subcomplex, visualized by GFP-CsnA in the Δ*csnD*Δ*csnE,gfp:csnA* strain, could not be shown, when the CsnD-CsnF-CsnG subcomplex cannot be formed. The confocal microscopy was with fungal cultures grown for 20 hours vegetatively at 37°C. The experiment was performed once. Scale bars represent 10 µm.

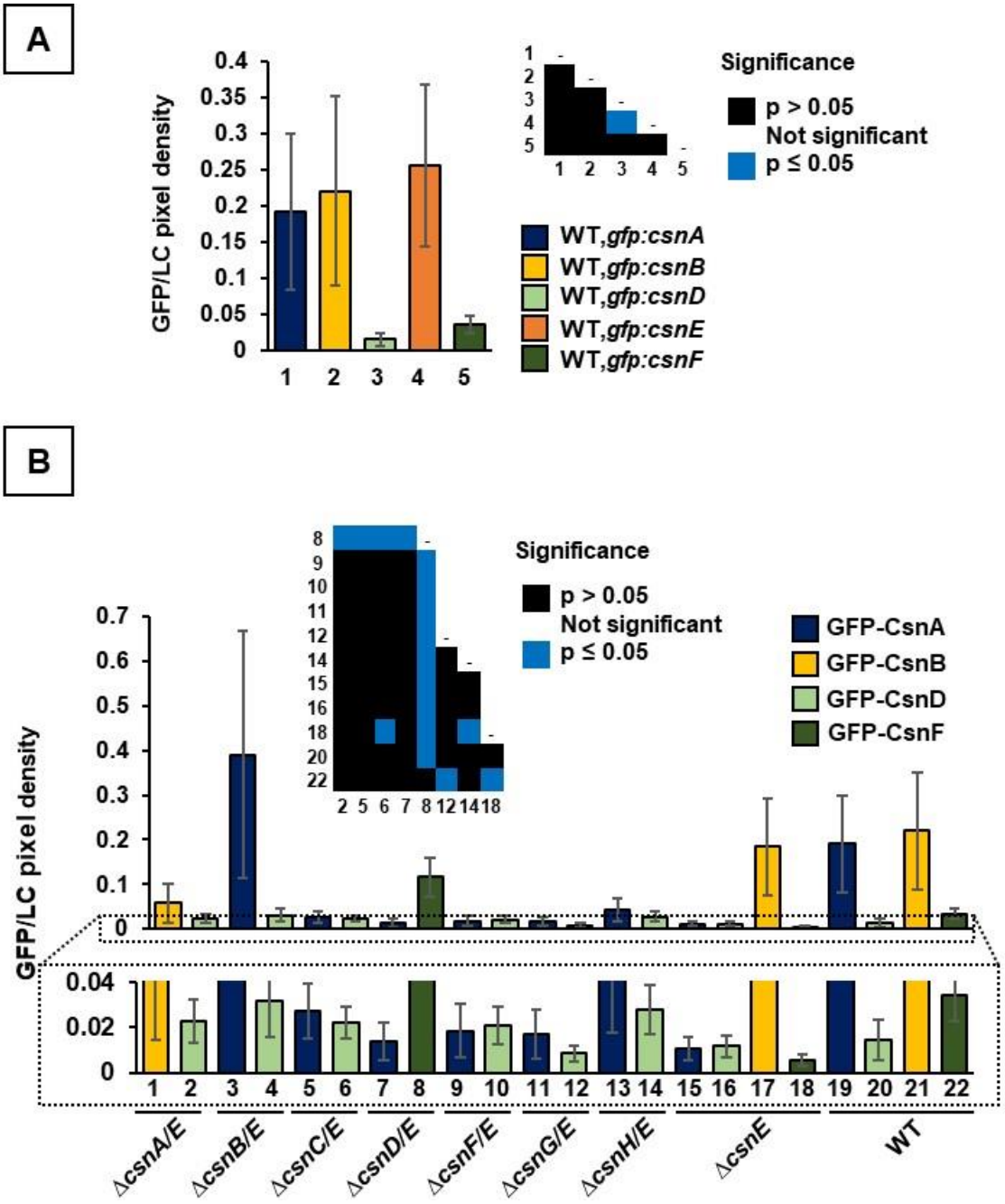

Figure S5. The absolute abundance of GFP-CsnA, GFP-CsnB, GFP-CsnD, GFP-CsnE and GFP-CsnF in the wild type and in the pre-CSN complex deficient strains.
The cellular protein abundances of GFP-CSN subunit fusion proteins were determined by α-GFP immunoblotting in (**A**) wild type and in (**B**) Δ*pre-csn*Δ*csnE,gfp:csn* double deletion strains (shortened Δ*csnA*/*E,gfp:csn* to Δ*csnH*/*E*) producing CSN-GFP fusion proteins. The charts show the absolute GFP signal/loading control (Ponceau staining) pixel density ratio measured in different strains. The charts represent the mean of three independent biological replicates performed in duplicates and the error bars display SEM. The matrices in the chart area display the significance of pairwise comparisons between protein amounts (marked with numbers) produced in different wild type background strains. In case of (**B**) the matrix shows only the significant pairs.

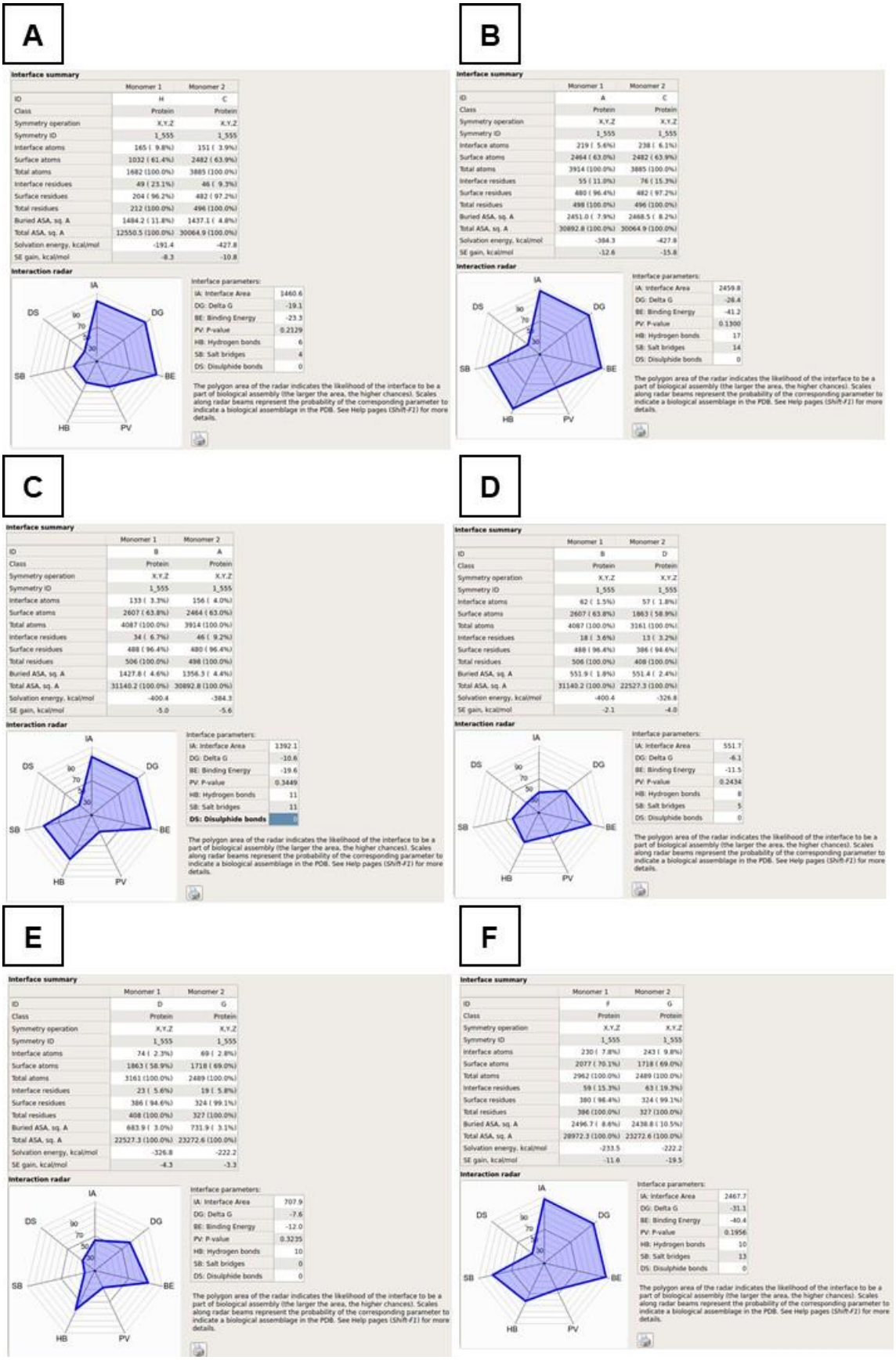

Figure S6. The figure legend is on the next page.

Figure S6. Analysis of the protein interfaces between CSN subunits.
Protein Interfaces, Surfaces and Assemblies (PISA) (described in chapter 2.10.3) (Krissinel and Henrick, 2007; www.ebi.ac.uk/pdbe/pisa) calculations were carried out to examine whether the interacting surfaces between two CSN subunits are sufficient large to result in a stable complex. The screenshots present the pairwise comparison results conducted with the online tool. The radar plot area depicts the likelihood whether the interface between proteins is sufficient to be part in the same biological assembly. The larger the area is, the higher is the probability that the proteins form a complex in solutions. The common interface between the (**A**) CsnC-CsnH, (**B**) CsnA-CsnC, (**C**) CsnA-CsnB and (**F**) CsnF-CsnG subunits suggests that these form a stable dimeric subcomplex. In case of the (**D**) CsnB-CsnD and (**E**) CsnD-CsnG subunit pairs the common interface is not large enough for a stable interaction.

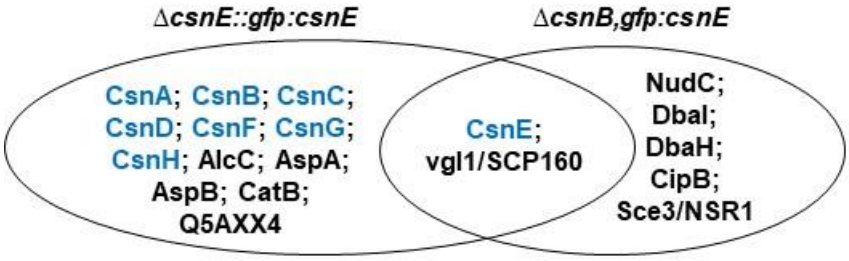

Figure S7. Interacting proteins of the complex-unbound CsnE.
Significant interacting proteins of GFP-CsnE were determined via GFP-trap experimental carried out with the Δ*csnB*,*gfp:csnE* and the wild type-like Δ*csnE::gfp:csnE* complementation control strain. The Venn diagram represents data deriving from GFP-trap experiment followed by LC-MS/MS analyses and subsequent data analyses described in Table 8; Table 10 and Figure 34. The significant, normalized protein candidates of GFP-CsnE in the Δ*csnB*,*gfp:csnE* strain were compared to the normalized protein candidates in the Δ*csnE::gfp:csnE* complementation strain. In the Δ*csnE::gfp:csnE* complementation strain all subunits of the COP9 signalosome were identified as significantly enriched interaction partners, whereas upon loss of CsnB only the bait GFP-CsnE was identified, which was not able to recruit any CSN subunits (written in blue). AlcC, AspA and AspB, involved in primary metabolism, CatB catalase involved in stress response and a protein of unknown function (Q5AXX4) were significantly enriched in the Δ*csnE::gfp:csnE* complementation strain. Vgl1/SCP160, a putative RNA binding effector protein ortholog was pulled out by GFP-CsnE in both the mutant and the Δ*csnE::gfp:csnE* control strain. Loss of CsnB enabled interactions between GFP-CsnE and NudC, DbaI, DbaH, CipB and Sce3/NSR1 ortholog. NudC is involved in the migration of nuclei within the fungal hyphae, what is important for asexual spore formation (Helmstaedt *et al*, 2008). DbaI polyketide synthase and DbaH monooxygenase of the *dba* secondary metabolite gene cluster and CipB is a cytoplasmic zinc-binding alcohol dehydrogenase. The Sce3 protein is an eIF4B-like protein in *S. pombe* (Schmidt, 1997) and NSR1 is a nucleolin localized in the nucleoli that binds to NLSs in *baker´s yeast* (Lee *et al.*, 1991).

Table S1. Summary of the GFP-CSN fusion protein abundances, relative to the respective wild type control strains producing GFP-CSN fusions.
The table summarizes the results of the α-GFP immunoblot measurements in the Δ*pre-csn*Δ*csnE,gfp:csn* double deletion strains in comparison to the respective wild type controls producing GFP-CSN fusion proteins (Figure 26). It depicts the CSN subunits identified in the GFP-co-purification assays (Figure 24) in the respective genetic background. The CSN subunits and/or subcomplexes identified by GFP co-immunoprecipitations in the respective fungal background strain are written in brackets. The stars label the CSN subunit tagged with GFP. Glossary: ↑↑↑: high relative abundance, ↑: elevated relative abundance, ↓↓↓: low relative abundance, ↓: decreased relative abundance, n.d.: no data, n.ch.: no change, -: not analyzed, *: data not shown.

Table S1. Summary of the GFP-CSN fusion protein abundances, relative to the respective wild type control strains producing GFP-CSN fusions.

Fungal strains	Produced GFP-CSN fusion protein			
	GFP-CsnA	**GFP-CsnB**	**GFP-CsnD**	**GFP-CsnF**
Δ*csnA*Δ*csnE*	-	↓↓↓ (CsnB)	↑↑↑ (CsnD-CsnF-CsnG)	-
Δ*csnB*Δ*csnE*	n.ch. (CsnA-CsnC-CsnH)	-	↑↑↑ (CsnD-CsnF-CsnG)	-
Δ*csnC*Δ*csnE*	↓↓↓ (CsnA)	-	↑↑↑ (CsnD-CsnF-CsnG)	-
Δ*csnD*Δ*csnE*	↓↓↓ (CsnA-CsnC-CsnH)	-	-	↑↑↑ (CsnF-CsnG)
Δ*csnF*Δ*csnE*	↓↓↓ (CsnA-CsnC-CsnH)	-	↑↑↑ (CsnD-CsnG)	-
Δ*csnG*Δ*csnE*	↓↓↓ (CsnA-CsnC-CsnH)	-	n.ch. (CsnD)	-
Δ*csnH*Δ*csnE*	↓↓↓ (CsnA)	-	↑↑↑ (CsnD-CsnF-CsnG)	-
Δ*csnE*	↓↓↓ n.d.	↓ (pre-CSN*)	n.ch. (pre-CSN*)	↓↓↓ n.d.

Table S2. Predicted nuclear export signals of the CSN subunits.

The NetNes 1.1 tool was used to search for nuclear export signal sequences in the CSN subunits. The position of amino acids predicted as potential NES are shown in the table and the scores are shown in brackets (maximal score is 2.0). Nuclear export signals were predicted in all CSN subunits with exception of CsnA and CsnD. Updated: 2021.05.04.

Position in aa sequence (score)	**CsnB**	**CsnC**	**CsnE**	**CsnF**	**CsnG**	**CsnH**
	L202(0.613)	I71(0.561)	L230(0.506)	Q11(0.54)	L104(0.875)	L3(0.838)
	I207(0.842)	I73(0.689)	I234(0.562)	L27(0.825)	L107(0.934)	L6(0.549)
		L166(0.729)	L235(0.601)	I30(0.659)	S109(0.685)	S7(0.546)
			L237(0.582)		L110(0.707)	L8(1.093)
			L322(0.67)			D9(0.628)
						Q10(1.141)
						L11(0.766)

Text S1. CSN subunits served as additional controls for the significance-based interactome analyses.

CSN subunits served as additional controls using the significance-based filtering method for the interactome analyses, however, in some fungal deletion background strains CsnH, CsnF and CsnG were slightly under the applied threshold. CsnH was slightly under the significance threshold in the Δ*csnD*Δ*csnE,gfp:csnA,* Δ*csnF*Δ*csnE,gfp:csnA* and the Δ*csnG*Δ*csnE,gfp:csnA* strains. In the Δ*csnD*Δ*csnE,gfp:csnA* strain CsnH was identified in three, in the Δ*csnF*Δ*csnE,gfp:csnA* strain two of five volcano plots, respectively and in the Δ*csnG*Δ*csnE,gfp:csnA* strain CsnH was under the identification threshold in all five volcano plots. This is may be due to the small size of CsnH, whose tryptic digestion results in 19 peptide fragments, but only a few are ideal for the identification by LC-MS/MS measurements (data not shown). CsnF was identified as significantly enriched in three of five volcano plots, whereas CsnG was in all cases under the threshold in the Δ*csnD*Δ*csnE,gfp:csnF* strain.

Table S3. Interaction partners of GFP-CsnB and GFP-CsnD in the Δ*csnA*Δ*csnE* strain.
Source of information: [1]UniProt, where [A]Automatic annotation and [M]Manual annotation, [2]AspGD, [3]FungiDB, [4]PubMed. ND: no data, ER: endoplasmic reticulum, Acc.no.: Accession number. The gene names of the orthologs are written in color, where blue: *Saccharomyces cerevisiae,* green: *Schizosaccharomyces pombe*, purple: *Aspergillus niger*. Protein of unknown function: neither data, nor characterized ortholog was found up to date. Updated: 2021.05.04.

	Acc. no./ UniProt ID	Gene name/ alias	Molecular function	Intracellular localization
GFP-CsnB interacting proteins	**Primary metabolism and development**			
	AN3223/ Q5B8A7	*pfkA*	ATP-dependent 6-phosphofructokinase[1]	cytoplasm[1A],mitochondria[2]
	AN10492 /G5EAZ2	*thiA*	Thiamine thiazole synthase[1]	cytoplasm[1M],nucleus[1M]
	AN7895/ Q5AUY5	*cipB*	Zinc-binding alcohol dehydrogenase[1]	cytoplasm[1M]
	AN10626 /C8V7Z2; AN1523/ C8VMQ7	ATP-1	Putative proton-transporting ATP synthase subunit alpha catalytic core F(1)[1]	plasma membrane[1M2]
	AN5790/ C8VFD8	idh1	Putative isocitrate dehydrogenase (NAD+) with predicted role in TCA cycle[2]	mitochondria[1A2]
	Intracellular transport			
	AN1177/ Q5BE53	SEC26	Putative coatomer subunit beta[1]	cytoplasm[1A], Golgi apparatus[1A], plasma membrane[2]
	Protein biosynthesis and folding			
	AN2068/ Q5BBL2	vgl1 or SCP160	Putative RNA binding effector protein[1]	cytoplasm[1M], nucleus[1M2], ER[2]
	AN4218/ C8V4B4	tef101 or TEF1	Putative translational elongation factor 1-alpha[1]	cytoplasm[2], vacuole membrane[2], mitochondria[2]
	AN3134/ Q5B8J6	cct3	Putative chaperonin-containing T-complex 1 subunit gamma[12] predicted role in unfolded protein binding[2]	cytoplasm[1A]
	AN2731/ C8VJZ5	mas5 or YDJ1	Putative CR-type zinc finger containing protein with function in unfolded protein binding[12] Hsp40 protein family member[4]	cytoplasm[1M], nucleus[1M]
	Ubiquitin-proteasome pathway			
	AN2904/ C8VJ79	RPT3	Putative ATPase of the 19S regulatory base particle of the 26S proteasome[2], AAA domain-containing protein[123] subunit 3	cytoplasm[1M], nucleus[1A] nuclear periphery[2]
	Protein of unknown function			
	AN8072/ Q5AUF8	ND	Uncharacterized disordered protein[1]	cytoplasm[1]
GFP-CsnD interacting proteins	**Primary metabolism and development**			
	AN5907/ Q5B0M3	*rpiB*	Putative ribose-5-phosphate isomerase[123]	ND
	AN2435/ Q5BAJ5	*aclA*	ATP citrate synthase[123]	cytoplasm[1M]
	Intracellular transport			
	AN4463/ Q5B4R7	CHC1	Putative clathrin heavy chain, intracellular transport[12]	cytoplasm[1A]/cytoskeleton[1],Golgi apparatus[1A]
	AN6542/ P20359	*actA*[4]	Gamma-actin[12]	cytoplasm/cytoskeleton[1M]

	AN4997/ Q5B383	spo20 or SEC14	Putative phosphatidylinositol/ phosphatidylcholine transporter[123]	cytoplasm[2],nucleus[12A], Golgi apparatus[2]
GFP-CsnD interacting proteins	AN5499/ Q5B1T1	*an-mlp1*	Nuclear pore complex protein[12]	nucleus[1M], nuclear pore[2]
	AN5632/ Q5B1E8	VPS60	Putative, protein involved in late endosome to vacuole transport[1]	Golgi apparatus[1M], vacuole[1A]
	Transcription and transcriptional regulation			
	AN1782/ Q5BCE8	hst2 or HST1	Putative sirtuin 2-type histone deacetylase domain containing protein[1]	nucleus[1]
	Protein biosynthesis and folding			
	AN2068/ Q5BBL2	vgl1 or SCP160	Putative RNA binding effector protein[1]	cytoplasm[1M],nucleus[12M], ER[2]
	AN10719 /C8VFC9	LSM6	Putative RNA binding protein with a role in RNA splicing[1]	nucleolus[12M]
	AN2080/ Q5BBK0	ERF-3[1] or SUP35	Putative translation termination factor eRF3[123]	cytoplasm[1A2]
	AN4218/ C8V4B4	tef101 or TEF1	Putative translational elongation factor 1-alpha[1]	cytoplasm[2], vacuole membrane[2], mitochondria[2]
	AN2918/ C8VJ63	CCT4	Putative chaperonin-containing T-complex 1 subunit delta[1] predicted role in unfolded protein binding[2]	cytoplasm[1AM2]
	AN1282/ Q5BDU8	SGT2	Putative co-chaperone, glutamine-rich protein[1]	cytoplasm[1M], ER[1M2] nucleus[3]
	Ubiquitin-proteasome pathway			
	AN2917/ Q5B963	RPT1	Putative ATPase of the 19S regulatory base particle of the 26S proteasome[2], AAA domain-containing protein[1] subunit 1	cytoplasm[1A]
	AN4236/ Q5B5E4	RPT5	Putative ATPase of the 19S regulatory base particle of the 26S proteasome[2], AAA domain-containing protein[1], subunit 5	cytoplasm[1A], nucleus[1A]
	AN8054/ C8V668	PRE6	Putative 20S proteasome core component of the 26S proteasome, alpha 4 subunit[12]	cytoplasm[1M],mitochondria[1A] nuclear periphery[1A], nucleus[1M]
	AN5784/ Q5B0Z6	pam1 or PRE7	Putative 20S proteasome core component of the 26S proteasome, beta 6 subunit[1]	cytoplasm[1M], nucleus[1A]
	AN1757/ Q5BCH3	*ssfA*[4]	20S proteasome core component of the 26S proteasome, alpha 3 subunit[123]	cytoplasm[1A], nucleus[1A]
	Protein of unknown function			
	AN2208/ Q5BB72	ND	Putative galactose 1-dehydrogenase[23] NAD-binding oxidoreductase[1]	ND
	AN8072/ Q5AUF8	ND	Disordered domain containing uncharacterized protein[1]	cytoplasm[1]
	AN11499 /C8V2L7	ND	Putative ATP synthase epsilon chain domain-containing protein[1A]	mitochondria[1AM]

Table S4. Interaction partners of GFP-CsnA and GFP-CsnD in the Δ*csnB*Δ*csnE* strain.
Source of information: [1]UniProt, where [A]Automatic annotation and [M]Manual annotation, [2]AspGD, [3]FungiDB, [4]PubMed. ND: no data, Acc.no.: Accession number. The gene names of the orthologs are written in color, where blue: *Saccharomyces cerevisiae,* green: *Schizosaccharomyces pombe*, purple: *Aspergillus niger*. Protein of unknown function: neither data, nor characterized ortholog was found up to date. Updated: 2021.05.04.

	Acc.no./ UniProt ID	Gene name/ alias	Molecular function	Intracellular localization
GFP-CsnA interacting proteins	**Primary metabolism and development**			
	AN2286/ P07754	*alcC*/ *adh3*	Alcohol dehydrogenase 3[12]	cytoplasm[1M]
	AN7895/ Q5AUY5	*cipB*	Zinc-binding alcohol dehydrogenase[1]	cytoplasm[1M]
	Protein folding			
	AN6010/ Q5B0C0	*sgdE*	Heat shock protein 70[123]	cytoplasm[1M], mitochondria[1AM]
	AN2731/ C8VJZ5	mas5 or YDJ1	Putative CR-type zinc finger containing protein with function in unfolded protein binding[12] Hsp40 protein family member[4]	cytoplasm[1M], nucleus[1M]
	Protein of unknown function			
	AN7710/ Q5AVH0	ND	Putative HAD-superfamily hydrolase[1]	ND
GFP-CsnD interacting proteins	**Primary metabolism and development**			
	AN4888/ P87208	*pdcA*	Pyruvate decarboxylase[1]	cytoplasm[1M]
	AN5907/ Q5B0M3	*rpiB*	Putative ribose-5-phosphate isomerase[123]	ND
	AN7657/ Q5AVM3	*gelA*	1,3-beta-transglycosidase[23]	cell wall[1M], plasma membrane[1A2]
	Intracellular transport			
	AN0347/ C8VTZ0	*rabE*/ *srgE*	GTPase with a predicted role in intra-Golgi transport[123]	cytoplasm[2], Golgi apparatus[1M]
	AN4463/ Q5B4R7	CHC1	Putative clathrin heavy chain, intracellular transport[12]	cytoplasm[1A]/cytoskeleton 1, Golgi apparatus[1A]
	Transcription and transcriptional regulation			
	AN1782/ Q5BCE8	hst2 or HST1	Putative sirtuin 2-type histone deacetylase domain containing protein[1]	nucleus[1]
	Protein biosynthesis			
	AN4218/ C8V4B4	tef101 or TEF1	Putative translational elongation factor 1-alpha[1]	cytoplasm[2], vacuole membrane[2], mitochondria[2]
	Ubiquitin-proteasome pathway			
	AN8054/ C8V668	PRE6	Putative 20S proteasome core component of the 26S proteasome, alpha 4 subunit[12]	cytoplasm[1M], mitochondria[1A], nuclear periphery[1A], nucleus[1M]
	AN1757/ Q5BCH3	*ssfA*[4]	20S proteasome core component of the 26S proteasome, alpha 3 subunit[123]	cytoplasm[1A], nucleus[1A]
	AN4872/ G5EB17	*ubi1*[2]	Putative fusion of N-terminal ubiquitin and C-terminal extension protein of the small ribosomal subunit[1]	cytoplasm[1M], nucleus[1M], ribosome[1A]
	Protein of unknown function			
	AN11499 /C8V2L7	ND	Putative ATP synthase epsilon chain domain-containing protein[1A]	mitochondria[1AM]

Table S5. Interaction partners of GFP-CsnA and GFP-CsnD in the Δ*csnC*Δ*csnE* strain.
Source of information: [1]UniProt, where [A]Automatic annotation and [M]Manual annotation, [2]AspGD, [3]FungiDB, [4]PubMed. ND: no data, Acc.no.: Accession number. The gene names of the orthologs are written in color, where blue: *Saccharomyces cerevisiae,* green: *Schizosaccharomyces pombe*, purple: *Aspergillus niger*. Protein of unknown function: neither data, nor characterized ortholog was found up to date. Updated: 2021.05.05.

	Acc.no./ UniProt ID	Gene name/ alias	Molecular function	Intracellular localization
GFP-CsnA interacting proteins	**Primary metabolism and development**			
	AN7895/ Q5AUY5	*cipB*	Zinc-binding alcohol dehydrogenase[1]	cytoplasm[1M]
	Secondary metabolism			
	AN7902/ Q5AUX8	*dbaH*[4]	FAD-binding monooxygenase, member of the *dba* gene cluster[2]	plasma membrane[1M]
GFP-CsnD interacting proteins	**Primary metabolism and development**			
	AN0271/ Q5BGQ9	DUT1	Putative dUTP pyrophosphatase with a predicted role in pyrimidine metabolism[2]	cytoplasm[2], nucleus[2]
	AN4888/ P87208	*pdcA*	Pyruvate decarboxylase[2]	cytoplasm[1M]
	AN0687/ G5EAU1	*spdA*	Spermine or spermidine synthase with a predicted role in arginine metabolism[2]	cytoplasm[2], nucleus[2], secreted[1M2]
	AN5975/ Q5B0F5	*mpdA*	Mannitol-1-phosphate 5-dehydrogenase[12]	cytoplasm[1M], secreted[1M]
	AN3748/ C8V7A0	HIS1	Putative ATP phosphoribosyl transferase, ortholog catalyzes the first histidine biosynthesis step[2]	cytoplasm[1A]
	AN4793/ Q5B3T7	HOM2	Putative aspartate semialdehyde dehydrogenase with predicted role in glycine, serine, threonine metabolism[2]	cytoplasm[2], nucleus[2], plasma membrane[2]
	AN1007/ P22944	*niiA*[4]	Nitrite reductase[2]	ND
	AN2436/ Q5BAJ4	*aclB*	ATP citrate synthase[12]	cytoplasm[1M]
	AN5626/ P16928	*facA/ acuA/ acsA*	Acetyl-coenzyme A synthetase[12]	cytoplasm[2], nucleus[2], secreted[1M2]
	AN1263/ Q5BDW7	*mecD*	Adenosylhomocysteinase with a predicted role in methionine metabolism[2]	cytoplasm[1M]
	AN5907/ Q5B0M3	*rpiB*	Putative ribose-5-phosphate isomerase[123]	ND
	AN9094/ G5EAX7	*ungA*	UDP-N-acetylglucosamine pyrophosphorylase with a predicted role in chitin biosynthesis[2]	ND
	AN7657/ Q5AVM3	*gelA*	1,3-beta-transglycosidase[23]	cell wall[1M], plasma membrane[1A2]
	AN4443/ C8V8J7	*metH*	Methionine synthase with a predicted role in methionine metabolism[2]	cytoplasm[2], plasma membrane[2], secreted[1M]

	AN4501/ Q5B4M9	*artA* or rad24 or BMH2	14-3-3 protein, role in hyphal morphogenesis, induced by carbon starvation, autophagy[2]	cytoplasm[22], nucleus[22] secreted[1M]
GFP-CsnD interacting proteins	**Secondary metabolism**			
	AN7914/ Q5AUW6	*orsE*[4]	Alcohol dehydrogenase, F9775/orsellinic acid secondary metabolite gene cluster member[2]	cytoplasm[1M]
	Transcription and transcriptional regulation			
	AN1782/ Q5BCE8	hst2 or HST1	Putative sirtuin 2-type histone deacetylase domain containing protein[1]	nucleus[1]
	AN9080/ C8VH67	HMF1	Putative L-PSP endoribonuclease and p14.5[2] family protein predicted to be active on ssmRNA[1], heat shock inducible[2]	cytoplasm[1M], mitochondria[1M], nucleus[4]
	Protein biosynthesis and folding			
	AN4015/ Q5B615	HYP2/ eIF5A	Putative eukaryotic translation initiation factor 5A[12]	cytoplasm[2], nuclear periphery[2]
	AN4038/ Q5B5Z2	FUN12/ eIF5B	Putative eukaryotic translation initiation factor 5B[12]	mitochondria[1A]
	AN8605/ Q5ASX5	*cyp1*[2]	Peptidyl-prolyl cis-trans isomerase with a predicted role in protein folding, cyclophilin[2]	cytoplasm[1M], secreted[1M]
	Ubiquitin-proteasome pathway			
	AN2917/ Q5B963	RPT1	Putative ATPase of the base particle of the 19S regulatory particle of the 26S proteasome[2], AAA domain-containing protein[1] subunit 1	cytoplasm[1A]
	AN4236/ Q5B5E4	RPT5	Putative ATPase of the 19S regulatory particle of the 26S proteasome[2], AAA domain-containing protein[1] subunit 5	cytoplasm[1A], nucleus[1A]
	AN5784/ Q5B0Z6	pam1 or PRE7	Putative 20S proteasome core component of the 26S proteasome, beta 6 subunit[1]	cytoplasm[1M], nucleus[1A]
	AN8054/ C8V668	PRE6	Putative 20S proteasome core component of the 26S proteasome, alpha 4 subunit[12]	cytoplasm[1M],mitochondria[1A] nuclear periphery[1A], nucleus[1M]
	Stress response			
	AN10223/ C8VNU1; AN3973/ Q5B657	tpx1 or PRX1	Putative peroxiredoxin[2]	cytoplasm[1M], mitochondria[1M]
	Protein of unknown function			
	AN5141/ Q5B2T9	ND	Uncharacterized disordered protein with coiled coil domains[1]	ND
	AN2208/ Q5BB72	ND	Putative NAD binding Rossmann fold containing galactose 1-dehydrogenase[2]	ND

Table S6. Interaction partners of GFP-CsnA and GFP-CsnF in the Δ*csnD*Δ*csnE* strain.
Source of information: [1]UniProt, where [A]Automatic annotation and [M]Manual annotation, [2]AspGD, [3]FungiDB, [4]PubMed. ND: no data, ER: endoplasmic reticulum, Acc.no.: Accession number. The gene names of the orthologs are written in color, where blue: *Saccharomyces cerevisiae,* green: *Schizosaccharomyces pombe.* Protein of unknown function: neither data, nor characterized ortholog was found up to date. Updated: 2021.05.10.

	Acc.no./ UniProt ID	Gene name/ alias	Molecular function	Intracellular localization
GFP-CsnA interacting proteins	**Primary metabolism and development**			
	AN10709/ C8VFD3	*gfaA* or GFA1	Putative glutamine-fructose-6-phosphate transaminase[2]	ND
	AN7895/ Q5AUY5	*cipB*	Zinc-binding alcohol dehydrogenase[1]	cytoplasm[1M]
	Intracellular transport			
	AN1379/ G5EAY9	*sonA*[4]	Nuclear pore complex protein[2], WD repeats region domain-containing protein[1]	cytoplasm[1A], nuclear pore[1M]
	AN4317/ Q5B563	SEC13	Putative nuclear pore complex protein[12], subunit of the COPII vesicle coat required for ER-to-Golgi transport[2]	nucleus[1M], ER[1M]
	Protein biosynthesis and folding			
	AN4218/ C8V4B4	tef101 or TEF1	Putative translational elongation factor 1-alpha[1]	cytoplasm[2], vacuole membrane[2], mitochondria[2]
	Ubiquitin-proteasome pathway			
	AN1700/ Q5BCN0	RPN2	Putative subunit of the base particle of the 19S regulatory particle of the 26S proteasome[2]	nucleus[1M2]
	Stress response			
	AN0241/ Q9HEY7	*sodA*[4]	Cu/Zn-superoxide dismutase	cytoplasm[1AM]
GFP-CsnF interacting proteins	**Primary metabolism and development**			
	AN8866/ C8V9B1	SER3	Putative phosphoglycerate dehydrogenase[12]	cytoplasm[1M]
	AN2526/ Q5BAA4	ILV5	Putative ketol-acid reductoisomerase with a predicted role in Coenzyme A and pantothenate biosynthesis or amino acid metabolism[2]	mitochondria[1A]
	AN10492/ G5EAZ2	*thiA*	Thiamine thiazole synthase[1]	cytoplasm[1M],nucleus[1M]
	AN7893/ C8V4J1	isp7	Fe(II) 2-oxoglutarate-dependent dioxygenase domain-containing protein[12]	cytoplasm[2], nucleus[2]
	AN0565/ O93937	*pyrABCN*[4]	Multifunctional carbamoyl-phosphate synthase and aspartate carbamoyltransferase, role in pyrimidine biosynthesis[2]	cytoplasm[1M]
	AN6048/ Q5B082	AAT2/ ASP5	Aspartate transaminase[1]	cytoplasm[1]
	AN1222/ Q5BE08	SAM1/SAM2	S-adenosylmethionine synthase[1]	cytoplasm[1]
	AN4159/ Q96V52	*glnA*	Glutamine synthetase[13]	cytoplasm[1]
	AN2150 /Q5BBD0	prs1	Proline tRNA ligase[13]	cytoplasm[1]

GFP-CsnF interacting proteins	**Intracellular transport**			
	AN6542/ P20359	*actA*	Gamma-actin[12]	cytoplasm/cytoskeleton[1M]
	AN6257/ Q5AZM3	SEC31	SEC31 ortholog COPII coatomer protein[1] subunit of the COPII vesicle coat required for ER-to-Golgi transport	ER[1]
	AN8268/ Q5ATW2	BRE5	Ubiquitin protease cofactor; coregulates transport between the ER and Golgi, deubiquitinating COPII and COPI vesicle coat constituents[3]	cytoplasm[1]
	Protein biosynthesis and folding			
	AN1162/ Q5BE68	tef5 or EFB1	Putative eukaryotic translation elongation factor 1 subunit Eef1-beta[12]	cytoplasm[1A]
	AN1851/ Q5BC79	CCT8	Putative chaperonin-containing T-complex 1 subunit theta, predicted role in unfolded protein binding[2]	cytoplasm[1A]
	AN2068/ Q5BBL2	vgl1 or SCP160	Putative RNA binding effector protein[1]	cytoplasm[1M],nucleus[12M], ER[2]
	AN1282/ Q5BDU8	SGT2	Putative co-chaperone, glutamine-rich protein[1]	cytoplasm[1M], ER[1M2] nucleus[3]
	AN1904/ C8VKS4	CCT5	Putative chaperonin-containing T-complex 1 subunit epsilon[1] predicted role in unfolded protein binding[2]	cytoplasm[1A]
	AN10474/ C8V6D1	ARC1	Putative methionyl-and glutamyl-tRNA synthetase cofactor[1], has domain(s) with predicted tRNA binding activity[2]	cytoplasm[1M]
	Ubiquitin-proteasome pathway			
	AN2917/ Q5B963	RPT1	Putative ATPase of the base particle of the 19S regulatory particle of the 26S proteasome[2], AAA domain-containing protein subunit 1[1]	cytoplasm[1A]
	AN4492/ C8V8E2	RPN11	Putative Rpn11 isopeptidase subunit of the lid particle of the 19S regulatory particle of the 26S proteasome[12]	cytoplasm[2], nucleus[2], mitochondria[2]

Table S7. Interaction partners of GFP-CsnA and GFP-CsnD in the Δ*csnF*Δ*csnE* strain.
Source of information: [1]UniProt, where [A]Automatic annotation and [M]Manual annotation, [2]AspGD, [3]FungiDB, [4]PubMed. ND: no data, Acc.no.: Accession number. The gene names of the orthologs are written in color, where blue: *Saccharomyces cerevisiae,* green: *Schizosaccharomyces pombe*, purple: *Aspergillus niger*. Protein of unknown function: neither data, nor characterized ortholog was found up to date. Updated: 2021.05.10.

	Acc.no./ UniProt ID	Gene name/ alias	Molecular function	Intracellular localization
GFP-CsnA interacting proteins	**Primary metabolism and development**			
	AN7895/ Q5AUY5	*cipB*	Zinc-binding alcohol dehydrogenase[1]	cytoplasm[1M]
	AN2526/ Q5BAA4	ILV5	Putative ketol-acid reductoisomerase with a predicted role in coenzyme A and pantothenate biosynthesis or amino acid metabolism[2]	mitochondria[1A]

	AN10709/ C8VFD3	*gfaA* or GFA1	Putative glutamine-fructose-6-phosphate transaminase[2]	ND
	Secondary metabolism			
	AN7902/ Q5AUX8	*dbaH*[4]	FAD-binding monooxygenase, member of the *dba* gene cluster[2]	plasma membrane[1M]
	Intracellular transport			
	AN3026/ C8VIU7	*copA*[4]	Alpha-COP coatomer-related protein involved in the establishment and maintenance of polarized growth[2]	cytoplasm[1A], Golgi apparatus[1]
	Protein of unknown function			
	AN7710/ Q5AVH0	ND	Putative HAD-superfamily hydrolase[1]	ND
GFP-CsnD interacting proteins	**Primary metabolism and development**			
	AN5975/ Q5B0F5	*mpdA*	Mannitol-1-phosphate 5-dehydrogenase[12]	cytoplasm[1M], secreted[1M]
	AN5907/ Q5B0M3	*rpiB*	Putative ribose-5-phosphate isomerase[123]	ND
	Intracellular transport			
	AN4463/ Q5B4R7	CHC1	Putative clathrin heavy chain, intracellular transport[12]	cytoplasm[1A]/cytoskeleton[1], Golgi apparatus[1A]
	AN4997/ Q5B383	spo20 or SEC14	Putative phosphatidylinositol/ phosphatidylcholine transporter[123]	cytoplasm[2],nucleus[1A2], Golgi apparatus[2]
	AN0347/ C8VTZ0	*rabE*/ *srgE*	GTPase with a predicted role in intra-Golgi transport[123]	cytoplasm[2], Golgi apparatus[1M]
	Transcription and transcriptional regulation			
	AN1782/ Q5BCE8	hst2 or HST1	Putative sirtuin 2-type histone deacetylase domain containing protein[1]	nucleus[1]
	Ubiquitin-proteasome pathway			
	AN4872/ G5EB17	*ubi1*[2]	Putative fusion of N-terminal ubiquitin and C-terminal extension protein of the small ribosomal subunit[1]	cytoplasm[1M], nucleus[1M], ribosome[1A]
	AN4236/ Q5B5E4	RPT5	Putative ATPase of the base particle of the 19S regulatory particle of the 26S proteasome[2], AAA domain-containing protein[1] subunit 5	cytoplasm[1A], nucleus[1A]

Table S8. Interaction partners of GFP-CsnA and GFP-CsnD in the Δ*csnG*Δ*csnE* strain.
Source of information: [1]UniProt, where [A]Automatic annotation and [M]Manual annotation, [2]AspGD, [3]FungiDB, [4]PubMed. ND: no data, ER: endoplasmic reticulum, Acc.no.: Accession number. The gene names of the orthologs are written in color, where blue: *Saccharomyces cerevisiae,* green: *Schizosaccharomyces pombe*, purple: *Aspergillus niger*. Protein of unknown function: neither data, nor characterized ortholog was found up to date. Updated: 2021.05.10.

	Acc. no./ UniProt ID	Gene name/ alias	Molecular function	Intracellular localization
	Primary metabolism and development			
	AN10709/ C8VFD3	*gfaA* or GFA1	Putative glutamine-fructose-6-phosphate transaminase[2]	ND
	AN9403/ C8VRK6	*pdhC*	Pyruvate dehydrogenase[12]	mitochondria[1M]

	AN7895/ Q5AUY5	*cipB*	Zinc-binding alcohol dehydrogenase[1]	cytoplasm[1M]
	Transcription and transcriptional regulation			
GFP-CsnA interacting proteins	AN0327/ Q5BGK3	RVB2	Putative 3'-5' DNA helicase[12]	nucleus[1M]
	Ubiquitin-proteasome pathway			
	AN4492/ C8V8E2	RPN11	Putative Rpn11 isopeptidase subunit of the lid particle of the 19S regulatory particle of the 26S proteasome[12]	cytoplasm[2], nucleus[2], mitochondria[2]
	AN1922/ Q5BC08	*rpnG* or RPN7	Putative Rpn7 subunit of the lid particle of the 19S regulatory particle of the 26S proteasome[12]	nucleus[1A]
	AN2904/ C8VJ79	RPT3	Putative ATPase of the base particle of the 19S regulatory particle of the 26S proteasome[2], AAA domain-containing protein[123] subunit 3	cytoplasm[1M], nucleus[1A] nuclear periphery[2]
GFP-CsnD interacting proteins	**Primary metabolism and development**			
	AN5907/ Q5B0M3	*rpiB*	Putative ribose-5-phosphate isomerase[123]	ND
	AN7657/ Q5AVM3	*gelA*	1,3-beta-transglycosidase[23]	cell wall[1M], plasma membrane[1A2]
	AN0565/ O93937	*pyrABCN*[4]	Multifunctional carbamoyl-phosphate synthase and aspartate carbamoyltransferase, role in pyrimidine biosynthesis[2]	cytoplasm[1M]
	AN5975/ Q5B0F5	*mpdA*	Mannitol-1-phosphate 5-dehydrogenase[12]	cytoplasm[1M], secreted[1M]
	AN1007/ P22944	*niiA*[4]	Nitrite reductase[2]	ND
	AN5626/ P16928	*facA/ acuA/ acsA*	Acetyl-coenzyme A synthetase[12]	cytoplasm[2], nucleus[2], secreted[1M2]
	AN4793/ Q5B3T7	HOM2	Putative aspartate semialdehyde dehydrogenase with a predicted role in glycine, serine, and threonine metabolism[2]	cytoplasm[2], nucleus[2], plasma membrane[2]
	AN7893/ C8V4J1	isp7	Fe(II) 2-oxoglutarate-dependent dioxygenase domain-containing protein[12]	cytoplasm[2], nucleus[2]
	Intracellular transport			
	AN0347/ C8VTZ0	*rabE/ srgE*	GTPase with a predicted role in intra-Golgi transport[123]	cytoplasm[2], Golgi apparatus[1M]
	AN11139= AN12237 /C8VLV0	*abpA*[4]	Actin binding protein[2]	cytoplasm/cytoskeleton[2]
	Transcription and transcriptional regulation			
	AN6505/ C8V0I4	*rcoA*[4]	WD40 repeat protein, required for sexual development and for sterigmatocystin production[2]	nucleus[2]
	Protein biosynthesis and folding			
	AN2068/ Q5BBL2	vgl1 or SCP160	Putative RNA binding effector protein[1]	cytoplasm[1M], nucleus[1M2], ER[2]
	AN4218/ C8V4B4	tef101 or TEF1	Putative translational elongation factor 1-alpha[1]	cytoplasm[2], vacuole membrane[2], mitochondria[2]
	AN1282/ Q5BDU8	SGT2	Putative co-chaperone, glutamine-rich protein[1]	cytoplasm[1M], ER[1M2] nucleus[3]

	AN3134/ Q5B8J6	cct3	Putative chaperonin-containing T-complex 1 subunit gamma[1,2] predicted role in unfolded protein binding[2]	cytoplasm[1A]
GFP-CsnD interacting proteins	AN2918/ C8VJ63	CCT4	Putative chaperonin-containing T-complex 1 subunit delta[1] predicted role in unfolded protein binding[2]	cytoplasm[1AM2]
	AN5713/ Q5B167	CCT7	Putative chaperonin-containing T-complex 1 subunit eta, predicted role in unfolded protein binding[2]	cytoplasm[1A]
	AN1851/ Q5BC79	CCT8	Putative chaperonin-containing T-complex 1 subunit theta, predicted role in unfolded protein binding[2]	cytoplasm[1A]
	Ubiquitin-proteasome pathway			
	AN2917/ Q5B963	RPT1	Putative ATPase of the base particle of the 19S regulatory particle of the 26S proteasome[2], AAA domain-containing protein[1] subunit 1	cytoplasm[1A]
	AN2213/ Q5BB67	RPT2	Putative ATPase of the base particle of the 19S regulatory particle of the 26S proteasome[2], AAA domain-containing protein[1] subunit 2	cytoplasm[1A]
	AN4236/ Q5B5E4	RPT5	Putative ATPase of the base particle of the 19S regulatory particle of the 26S proteasome[2], AAA domain-containing protein[1] subunit 5	cytoplasm[1A], nucleus[1A]
	AN8054/ C8V668	PRE6	Putative 20S proteasome core component of the 26S proteasome, beta 4 subunit[12]	cytoplasm[1M],mitochondria[1A],nuclear periphery[1A], nucleus[1M]
	AN5784/ Q5B0Z6	pam1 or PRE7	Putative 20S proteasome core component of the 26S proteasome, beta 6 subunit[1]	cytoplasm[1M], nucleus[1A]
	AN2304/ C8VN52	RAD23	Putative ubiquitin binding domain containing protein with predicted role in UV excision repair[12]	cytoplasm[1A], nucleus[1A]
	Protein of unknown function			
	AN2208/ Q5BB72	ND	Putative NAD binding Rossmann fold containing galactose 1-dehydrogenase[2]	ND

Table S9. Interaction partners of GFP-CsnA and GFP-CsnD in the Δ*csnH*Δ*csnE* strain.
Source of information: [1]UniProt, where [A]Automatic annotation and [M]Manual annotation, [2]AspGD, [3]FungiDB, [4]PubMed. ND: no data, ER: endoplasmic reticulum, Acc.no.: Accession number The gene names of the orthologs are written in color, where blue: *Saccharomyces cerevisiae,* green: *Schizosaccharomyces pombe.* Protein of unknown function: neither data, nor characterized ortholog was found up to date. Updated: 2021.05.10.

	Acc. no./ UniProt ID	Gene name/ alias	Molecular function	Intracellular localization
	Primary metabolism and development			
	AN0443/ C8VT88	BDH1	Putative zinc containing alcohol dehydrogenase[123]	cytoplasm[2]
	AN1523/ C8VMQ7; AN10626 C8V7Z2	ATP-1	Putative proton-transporting ATP synthase subunit alpha catalytic core F(1)[1]	plasma membrane[1M2]

GFP-CsnA interacting proteins	AN2526/ Q5BAA4	ILV5	Putative ketol-acid reductoisomerase, predicted role in coenzyme A and pantothenate biosynthesis or amino acid metabolism[2]	mitochondria[1A]
	AN6246/ P38091	*cycA*[4]	Cytochrome C[123]	mitochondrial intermembrane space[1M]
	AN7000/ C8VC98	LSC2	Putative succinate-CoA ligase (ADP-forming) with a predicted role in the TCA cycle[123]	mitochondria[1AM2]
	AN7657/ Q5AVM3	*gelA*	1,3-beta-transglycosidase[23]	cell wall[1M], plasma membrane[1A2]
	AN7895/ Q5AUY5	*cipB*	Zinc-binding alcohol dehydrogenase[1]	cytoplasm[1M]
	Secondary metabolism			
	AN7914/ Q5AUW6	*orsE*[4]	Alcohol dehydrogenase, F9775/orsellinic acid secondary metabolite gene cluster member[2]	cytoplasm[1M]
	AN7902/ Q5AUX8	*dbaH*[4]	FAD-binding monooxygenase, member of the *dba* gene cluster[2]	plasma membrane[1M]
	Intracellular transport			
	AN4317/ Q5B563	SEC13	Putative nuclear pore complex protein[12], subunit of the COPII vesicle coat required for ER-to-Golgi transport[2]	nucleus[1M], ER[1M]
	Protein biosynthesis and folding			
	AN5662/ Q5B1B8	THS1	Threonyl-tRNA synthetase[1]	cytoplasm[1A2]
	AN6010/ Q5B0C0	*sgdE*	Heat shock protein 70[123]	cytoplasm[1M], mitochondria[1AM]
	AN1282/ Q5BDU8	SGT2	Putative co-chaperone, glutamine-rich protein[1]	cytoplasm[1M], ER[1M2] nucleus[3]
	AN0381/ Q5BGE9	CCT2	Putative chaperonin-containing T-complex 1 subunit beta[1] predicted role in unfolded protein binding[23]	cytoplasm[1A], nucleus[3]
	Ubiquitin-proteasome pathway			
	AN4869/ C8V9V1	SCL1	Putative 20S proteasome core component of the 26S proteasome[23], alpha 1 subunit[12]	cytoplasm[1A], nucleus[1A]
	AN8054/ C8V668	PRE6	Putative 20S proteasome core component of the 26S proteasome, beta 4 subunit[12]	cytoplasm[1M],mitochondria[1A] nuclear periphery[1A], nucleus[1M]
	Protein of unknown function			
	AN7710/ Q5AVH0	ND	Putative HAD-superfamily hydrolase[1]	ND
GFP-CsnD interacting proteins	**Primary metabolism and development**			
	AN5626/ P16928	*facA/ acuA/ acsA*	Acetyl-coenzyme A synthetase[12]	cytoplasm[2], nucleus[2], secreted[1M2]
	AN5975/ Q5B0F5	*mpdA*	Mannitol-1-phosphate 5-dehydrogenase[12]	cytoplasm[1M], secreted[1M]
	Intracellular transport			
	AN0347/ C8VTZ0	*rabE/ srgE*	GTPase with predicted role in intra-Golgi transport[123]	cytoplasm[2], Golgi apparatus[1M]
	AN6542/ P20359	*actA*	Gamma-actin[12]	cytoplasm/ cytoskeleton[1M]
	AN4463/ Q5B4R7	CHC1	Putative clathrin heavy chain, intracellular transport[12]	cytoplasm[1A]/ cytoskeleton[1],Golgi apparatus[1A]

GFP-CsnD interacting proteins	Transcription and transcriptional regulation			
	AN1782/ Q5BCE8	hst2 or HST1	Putative sirtuin 2-type histone deacetylase domain containing protein[1]	nucleus[1]
	Protein biosynthesis and folding			
	AN4218/ C8V4B4	tef101 or TEF1	Putative translational elongation factor 1-alpha[1]	cytoplasm[2], vacuole membrane[2], mitochondria[2]
	AN1851/ Q5BC79	CCT8	Putative chaperonin-containing T-complex 1 subunit theta, predicted role in unfolded protein binding[2]	cytoplasm[1A]
	AN10719/ C8VFC9	LSM6	Putative RNA binding protein with a role in RNA splicing[1]	nucleolus[12M]
	Ubiquitin-proteasome pathway			
	AN1167/ Q5BE63	RPN13	Putative subunit of the 19S regulatory base particle of the 26S proteasome[21]	cytoplasm[1A2],nucleus[1A2]
	AN1757/ Q5BCH3	*ssfA*[4]	20S proteasome core component of the 26S proteasome, alpha 3 subunit[123]	cytoplasm[1A], nucleus[1A]
	AN2917/ Q5B963	RPT1	Putative ATPase of the 19S regulatory base particle of the 26S proteasome[2], AAA domain-containing protein[1] subunit 1	cytoplasm[1A]
	AN4236/ Q5B5E4	RPT5	Putative ATPase of the 19S regulatory base particle of the 26S proteasome[2], AAA domain-containing protein[1] subunit 5	cytoplasm[1A], nucleus[1A]
	Protein of unknown function			
	AN5141/ Q5B2T9	ND	Uncharacterized disordered protein with coiled coil domains[1]	ND

Table S10. Interaction partners of GFP-CsnA, GFP-CsnB, GFP-CsnD and GFP-CsnF in wild type background.
Source of information: [1]UniProt, where [A]Automatic annotation and [M]Manual annotation, [2]AspGD, [3]FungiDB, [4]PubMed. ND: no data, ER: endoplasmic reticulum, Acc.no.: Accession number. The gene names of the orthologs are written in color, where blue: *Saccharomyces cerevisiae,* green: *Schizosaccharomyces pombe.* Protein of unknown function: neither data, nor characterized ortholog was found up to date. Updated: 2021.05.10.

	Acc.no./ UniProt ID	**Gene name/ alias**	**Molecular function**	**Intracellular localization**
GFP-CsnA interacting proteins	**Primary metabolism and development**			
	AN1049/ G5EAZ2	*thiA*	Thiamine thiazole synthase[1]	cytoplasm[1M],nucleus[1M]
	Ubiquitin-proteasome pathway			
	AN1491/ Q5BD89	*csnA*	Subunit 1 of the COP9 signalosome[12]	cytoplasm[1M],nucleus[1M]
	AN4783/ Q5B3U7	*csnB*	Subunit 2 of the COP9 signalosome[12]	cytoplasm[1M],nucleus[1M]
	AN5798/ Q5B0Y2	*csnC*	Subunit 3 of the COP9 signalosome[12]	cytoplasm[1M],nucleus[1M]
	AN1539/ Q9C467	*csnD*	Subunit 4 of the COP9 signalosome[12]	cytoplasm[1M],nucleus[1M]
	AN2129/ Q5BBF1	*rri1*/ *csnE*	Subunit 5 of the COP9 signalosome[12]	cytoplasm[1M],nucleus[1M]
	AN2233/ Q5BB47	*csnF*	Subunit 6 of the COP9 signalosome[12]	cytoplasm[1M],nucleus[1M]

	AN3623/ Q00648	*acoB*/ *csnG*	Subunit 7 of the COP9 signalosome[12]	cytoplasm[1M],nucleus[1M]
	AN1020/ P0C624	*csnH*	Subunit 8 of the COP9 signalosome[12]	cytoplasm[1M],nucleus[1M]
	Stress response			
	AN9339/ P78619	*catB*	Catalase B[12]	cytoplasm[1M]
	Protein of unknown function			
	AN8072/ Q5AUF8	ND	Uncharacterized disordered protein[1]	cytoplasm[1]
GFP-CsnB interacting proteins	**Primary metabolism and development**			
	AN10709/ C8VFD3	*gfaA* or GFA1	Putative glutamine-fructose-6-phosphate transaminase[2]	ND
	Ubiquitin-proteasome pathway			
	AN1491/ Q5BD89	*csnA*	Subunit 1 of the COP9 signalosome[12]	cytoplasm[1M],nucleus[1M]
	AN4783/ Q5B3U7	*csnB*	Subunit 2 of the COP9 signalosome[12]	cytoplasm[1M],nucleus[1M]
	AN5798/ Q5B0Y2	*csnC*	Subunit 3 of the COP9 signalosome[12]	cytoplasm[1M],nucleus[1M]
	AN1539/ Q9C467	*csnD*	Subunit 4 of the COP9 signalosome[12]	cytoplasm[1M],nucleus[1M]
	AN2129/ Q5BBF1	*rri1*/ *csnE*	Subunit 5 of the COP9 signalosome[12]	cytoplasm[1M],nucleus[1M]
	AN2233/ Q5BB47	*csnF*	Subunit 6 of the COP9 signalosome[12]	cytoplasm[1M],nucleus[1M]
	AN3623/ Q00648	*acoB*/ *csnG*	Subunit 7 of the COP9 signalosome[12]	cytoplasm[1M],nucleus[1M]
	AN10208 /P0C624	*csnH*	Subunit 8 of the COP9 signalosome[12]	cytoplasm[1M],nucleus[1M]
	Stress response			
	AN9339/ P78619	*catB*	Catalase B[12]	cytoplasm[1M]
GFP-CsnD interacting proteins	**Primary metabolism and development**			
	AN7895/ Q5AUY5	*cipB*	Zinc-binding alcohol dehydrogenase[1]	cytoplasm[1M]
	AN10492 /G5EAZ2	*thiA*	Thiamine thiazole synthase[1]	cytoplasm[1M],nucleus[1M]
	Secondary metabolism			
	AN7902/ Q5AUX8	*dbaH*[4]	FAD-binding monooxygenase, member of the *dba* gene cluster[2]	plasma membrane[1M]
	Ubiquitin-proteasome pathway			
	AN1491/ Q5BD89	*csnA*	Subunit 1 of the COP9 signalosome[12]	cytoplasm[1M],nucleus[1M]
	AN4783/ Q5B3U7	*csnB*	Subunit 2 of the COP9 signalosome[12]	cytoplasm[1M],nucleus[1M]
	AN5798/ Q5B0Y2	*csnC*	Subunit 3 of the COP9 signalosome[12]	cytoplasm[1M],nucleus[1M]
	AN1539/ Q9C467	*csnD*	Subunit 4 of the COP9 signalosome[12]	cytoplasm[1M],nucleus[1M]
	AN2129/ Q5BBF1	*csnE*	Subunit 5 of the COP9 signalosome[12]	cytoplasm[1M],nucleus[1M]
	AN2233/ Q5BB47	*csnF*	Subunit 6 of the COP9 signalosome[12]	cytoplasm[1M],nucleus[1M]
	AN3623/ Q00648	*csnG*	Subunit 7 of the COP9 signalosome[12]	cytoplasm[1M],nucleus[1M]

	AN1020/ P0C624	*csnH*	Subunit 8 of the COP9 signalosome[12]	cytoplasm[1M],nucleus[1M]
	AN5872/ Q5B0Q8	PUP2	Putative alpha 5 subunit of the 20S proteasome[2]	cytoplasm[1A],nucleus[1A]
	Stress response			
	AN9339/ P78619	*catB*	Catalase B[12]	cytoplasm[1M]
	Protein of unknown function			
	AN7710/ Q5AVH0	ND	Putative HAD-superfamily hydrolase[1]	ND
GFP-CsnF interacting proteins	**Primary metabolism and development**			
	AN7895/ Q5AUY5	*cipB*	Zinc-binding alcohol dehydrogenase[1]	cytoplasm[1M]
	Ubiquitin-proteasome pathway			
	AN1491/ Q5BD89	*csnA*	Subunit 1 of the COP9 signalosome[12]	cytoplasm[1M],nucleus[1M]
	AN4783/ Q5B3U7	*csnB*	Subunit 2 of the COP9 signalosome[12]	cytoplasm[1M],nucleus[1M]
	AN5798/ Q5B0Y2	*csnC*	Subunit 3 of the COP9 signalosome[12]	cytoplasm[1M],nucleus[1M]
	AN1539/ Q9C467	*csnD*	Subunit 4 of the COP9 signalosome[12]	cytoplasm[1M],nucleus[1M]
	AN2129/ Q5BBF1	*csnE*	Subunit 5 of the COP9 signalosome[12]	cytoplasm[1M],nucleus[1M]
	AN2233/ Q5BB47	*csnF*	Subunit 6 of the COP9 signalosome[12]	cytoplasm[1M],nucleus[1M]
	AN3623/ Q00648	*csnG*	Subunit 7 of the COP9 signalosome[12]	cytoplasm[1M],nucleus[1M]
	AN1020/ P0C624	*csnH*	Subunit 8 of the COP9 signalosome[12]	cytoplasm[1M],nucleus[1M]
	AN5784/ Q5B0Z6	pam1 or PRE7	Putative 20S proteasome core component of the 26S proteasome, beta 6 subunit[1]	cytoplasm[1M],nucleus[1A]
	AN5121/ C8VEY3	RPN8	Putative Rpn8 subunit of the 19S regulatory lid particle of the 26S proteasome[2]	cytoplasm[2]
	AN1167/ Q5BE63	RPN13	Putative subunit of the 19S regulatory base particle of the 26S proteasome[21]	cytoplasm[1A2],nucleus[1A2]
	AN3019/ C8VIV4	RPN12	Putative subunit of the 19S regulatory lid particle of the 26S proteasome[21]	nucleus[1]
	Stress response			
	AN9339/ P78619	*catB*	Catalase B[12]	cytoplasm[1M]

Table S11. Southern hybridization strategy for verifying the genotype of *Aspergillus nidulans* strains constructed in this work.

The table summarizes the created fungal strains with regard to the parental strains and the DNA fragment used for transformation. In addition, the applied restriction enzymes and genetic probes are listed, which were used in the Southern hybridization experiments. Glossary: +m: the fungal strain contains the recyclable marker cassette, *: The ectopic integration of the plasmid was checked by confocal microscopy of the resulting fungal strains carrying the pME3173 plasmid and producing RFP-Histone 2A, **: Due to insufficient fragment size differences between wild type (WT) and mutant strain in Southern blotting after marker excision, the genotype was additionally verified by sequencing of the PCR fragment of the genomic region of interest.

Fungal strain		**Southern hybridization**	
Name	**Description**	**(fragment sizes are given in base pairs)**	
AnFB35	Δ*csnE,gfp:csnD* +m	see AnFB37	
AnFB37	Δ*csnE,gfp:csnD*	5´pME4702, *Eco*RI *gfp:csnD*: 2644 WT: 1888	3´pME4702,*Kpn*I *gfp:csnD*: 3960 WT: 2988
AnFB36	Δ*csnE,gfp:csnF* +m	see AnFB38	
AnFB38	Δ*csnE,gfp:csnF*	5´pME5437,*Kpn*I *gfp:csnF*: 2901 WT: 2144	3´pME5437,*Hind*III *gfp:csnF*: 4289 WT: 3322
AnFB39	Δ*csnA*Δ*csnE,gfp:csnD* +m	see AnFB46	
AnFB46	Δ*csnA*Δ*csnE,gfp:csnD*	5´pME5430,*Psi*I Δ*csnA*: 5004 WT: 6557	3´pME5430,*Kpn*I Δ*csnA*: 3961 WT: 4263
AnFB40	Δ*csnB*Δ*csnE,gfp:csnD* +m	see AnFB47	
AnFB47	Δ*csnB*Δ*csnE,gfp:csnD*	5´pME5431,*BamH*I Δ*csnB*: 3716 WT: 5296	3´pME5431,*Pvu*II Δ*csnB*: 2669 WT: 4249
AnFB41	Δ*csnC*Δ*csnE,gfp:csnD* +m	see AnFB48	
AnFB48	Δ*csnC*Δ*csnE,gfp:csnD*	5´pME5432,*Pst*I Δ*csnC*: 3984 WT: 5600	3pME5432,*Hind*III Δ*csnC*: 2610 WT: 4226
AnFB42	Δ*csnD*Δ*csnE,gfp:csnF* +m	see AnFB49	
AnFB49	Δ*csnD*Δ*csnE,gfp:csnF*	5´pME5433,*Sac*I Δ*csnD*: 4711 WT: 5835	3´pME5433,*Eco*RV Δ*csnD*: 3383 bp WT: 4507 bp
AnFB43	Δ*csnF*Δ*csnE,gfp:csnD* +m	see AnFB50	
AnFB50	Δ*csnF*Δ*csnE,gfp:csnD*	5´pME5434,*Pst*I Δ*csnF*: 3356 WT: 4516	3´pME5434,*Hind*III Δ*csnF*: 2126 WT: 3322
AnFB44	Δ*csnG*Δ*csnE,gfp:csnD* +m	see AnFB51	
AnFB51	Δ*csnG*Δ*csnE,gfp:csnD*	5´pME5435,*Blp*I Δ*csnG*: 2477 WT: 2028	3´pME5435,*BamH*I Δ*csnG*: 4336 WT: 5217
AnFB45	Δ*csnH*Δ*csnE,gfp:csnD* +m	see AnFB52	
AnFB52	Δ*csnH*Δ*csnE,gfp:csnD*	5´pME5436, *Eco*RV Δ*csnH*: 4475 WT: 5128	3´pME5436,*Eco*NI Δ*csnH*: 2172 WT: 2825
AnFB53	WT,*gfp:csnF* +m	see AnFB54	
AnFB54	WT,*gfp:csnF*	5´pME5437,*Pst*I *gfp:csnF*: 5483 WT: 4516	3´pME5437,*Hind*III *gfp:csnF*: 4289 WT: 3322
AnFB57	Δ*csnA* +m	see AnFB109	
AnFB58	Δ*csnB* +m	see AnFB105	
AnFB59	Δ*csnC* +m	see AnFB110	
AnFB60	Δ*csnD* +m	see AnFB106	
AnFB61	Δ*csnF* +m	see AnFB101	
AnFB62	Δ*csnG* +m	see AnFB111	

AnFB63	Δ*csnH* +m	see AnFB107	
AnFB64	Δ*csnA*Δ*csnE* +m	see AnFB71	
AnFB65	Δ*csnB*Δ*csnE* +m	see AnFB72	
AnFB66	Δ*csnC*Δ*csnE* +m	see AnFB73	
AnFB67	Δ*csnD*Δ*csnE* +m	see AnFB74	
AnFB68	Δ*csnF*Δ*csnE* +m	see AnFB75	
AnFB69	Δ*csnG*Δ*csnE* +m	see AnFB76	
AnFB70	Δ*csnH*Δ*csnE* +m	see AnFB77	
AnFB71	Δ*csnA*Δ*csnE*	5´pME5430,*Psi*I Δ*csnA:* 5004 WT:6557	3´pME5430,*Kpn*I Δ*csnA:* 4263 WT:3961
AnFB72	Δ*csnB*Δ*csnE*	5´pME5431,*BamH*I Δ*csnB:* 3716 WT: 5296	3´pME5431,*Pvu*II Δ*csnB:* 2669 WT: 4249
AnFB73	Δ*csnC*Δ*csnE*	5´pME5432,*Pst*I Δ*csnC:* 3984 WT: 5600	3´pME5432,*Hind*III Δ*csnC:* 2610 WT: 4226
AnFB74	Δ*csnD*Δ*csnE*	5´pME5433,*Sac*I Δ*csnD:* 4711; WT: 5835	
AnFB75	Δ*csnF*Δ*csnE*	5´pME5434,*Pst*I Δ*csnF:* 3356 WT: 4516	3´pME5434,*Hind*III Δ*csnF:* 2162 WT: 3322
AnFB76	Δ*csnG*Δ*csnE*	5´pME5435,*Blp*I Δ*csnG:* 2477 WT: 2028	3´pME5435,*BamH*I Δ*csnG:* 4336 WT: 5217
AnFB77	Δ*csnH*Δ*csnE*	5´pME5436,*EcoR*V Δ*csnH:* 4475; WT: 5128	
AnFB78	Δ*csnA*Δ*csnE,gfp:csnB* +m	see AnFB87	
AnFB79	Δ*csnB*Δ*csnE,gfp:csnA* +m	see AnFB88	
AnFB80	Δ*csnC*Δ*csnE,gfp:csnA* +m	see AnFB89	
AnFB81	Δ*csnD*Δ*csnE,gfp:csnA* +m	see AnFB90	
AnFB82	Δ*csnF*Δ*csnE,gfp:csnA* +m	see AnFB91	
AnFB83	Δ*csnG*Δ*csnE,gfp:csnA* +m	see AnFB92	
AnFB84	Δ*csnH*Δ*csnE,gfp:csnA* +m	see AnFB93	
AnFB85	Δ*csnE,gfp:csnA* +m	see AnFB94	
AnFB86	WT,*gfp:csnA* +m	see AnFB95	
AnFB87	Δ*csnA*Δ*csnE,gfp:csnB*	5´pME5441,*BamH*I *gfp:csnB:* 6173; WT: 5296	
AnFB88	Δ*csnB*Δ*csnE,gfp:csnA*	5´pME5439,*Sac*I *gfp:csnA:* 4380; WT: 3624	
AnFB89	Δ*csnC*Δ*csnE,gfp:csnA*	5´pME5439,*Sac*I *gfp:csnA:*4380; WT: 3624	
AnFB90	Δ*csnD*Δ*csnE,gfp:csnA*	5´pME5439,*Sac*I *gfp:csnA:*4380; WT: 3624	
AnFB91	Δ*csnF*Δ*csnE,gfp:csnA*	5´pME5439,*Sac*I *gfp:csnA:*4380; WT: 3624	
AnFB92	Δ*csnG*Δ*csnE,gfp:csnA*	5´pME5439,*Sac*I *gfp:csnA:*4380; WT: 3624	
AnFB93	Δ*csnH*Δ*csnE,gfp:csnA*	5´pME5439,*Sac*I *gfp:csnA:*4380; WT: 3624	
AnFB94	Δ*csnE,gfp:csnA*	5´pME5439,*Sac*I *gfp:csnA:*4380; WT: 3624	
AnFB95	WT,*gfp:csnA*	5´pME5439,*Sac*I	

		*gfp:csnA:*4380; WT: 3624	
AnFB96	Δ*csnE,gfp:csnB* +m	see AnFB98	
AnFB97	WT,*gfp:csnB* +m	see AnFB99	
AnFB98	Δ*csnE,gfp:csnB*	3´pME5441,*Xho*I *gfp:csnB*: 6586; WT: 5709	
AnFB99	WT,*gfp:csnB*	5´pME5441,*BamH*I *gfp:csnB*: 6173; WT: 5296	
AnFB101	Δ*csnF*	5´pME5434,*Pst*I Δ*csnF*: 3355; WT: 4516	
AnFB105	Δ*csnB*	5´pME5431,*Bam*HI Δ*csnB*: 3716; WT: 5296	
AnFB106	Δ*csnD*	3´pME5433,*Eco*RV Δ*csnD*: 3383; WT: 4507	
AnFB107	Δ*csnH*	5´pME5436,*EcoR*V Δ*csnH*: 4475 WT: 5128	3´pME5436,*Xag*I Δ*csnH*: 2172 WT: 2825
AnFB109	Δ*csnA*	5´pME5439,*Sac*I Δ*csnA:* 3636 WT: 3624	3´pME5439,*Kpn*I Δ*csnA*: 4263 WT: 3961
AnFB110	Δ*csnC*	5´pME5432,*Pst*I Δ*csnC*: 3984 WT: 5600	3´pME5432,*Hind*III Δ*csnC*: 2610 WT: 4226
AnFB111	Δ*csnG*	5´pME5435,*Blp*I Δ*csnG*: 2477 WT: 2028	3´pME5435,*BamH*I Δ*csnG*: 4336 WT: 5217
AnFB115*	Δ*csnA*Δ*csnE,gfp:csnB, mrfp::h2a*	-	
AnFB117*	WT,*gfp:csnA,mrfp::h2a*	-	
AnFB120*	WT,*gfp:csnD,mrfp::h2a*	-	
AnFB136*	Δ*csnB*Δ*csnE,gfp:csnD, mrfp::h2a*	-	
AnFB137*	Δ*csnB*Δ*csnE,gfp:csnA, mrfp::h2a*	-	
AnFB138*	WT, *mrfp::h2a*	-	
AnFB139	Δ*csnB::gfp:csnB* +m	3´pME5441,*Hind*III *gfp:csnB*: 8963; WT: 3322	
AnFB140	Δ*csnB::gfp:csnB*	3´pME5441,*Hind*III *gfp:csnB*: 4087; WT: 3322	
AnFB141	WT,*gfp:csnE* +m	see AnFB142	
AnFB142	WT,*gfp:csnE*	5´pME5446,*Bgl*II *gfp:csnE*:3599 WT:2729	3´pME5446,*Eco*RV *gfp:csnE*:6724 WT:5854
AnFB143	Δ*csnE::gfp:csnE* +m	5´pME5446,*Pvu*II *gfp:csnE*: 6780; WT: 6024	
AnFB144	Δ*csnE::gfp:csnE*	5´pME5446,*Bgl*II *gfp:csnE*:3599 WT:2729	3´pME5446,*Eco*RV *gfp:csnE*:6724 WT:5854
AnFB145	Δ*csnB,gfp:csnE* +m	5´pME5446,*Pvu*II *gfp:csnE*: 6780; WT: 6024	
AnFB146	Δ*csnB,gfp:csnE*	5´pME5446,*Bgl*II *gfp:csnE*:3599 WT:2729	3´pME5446,*Eco*RV *gfp:csnE*:6724 WT:5854
AnFB156	Δ*csnA::gfp:csnA* +m	see AnFB157	
AnFB157	Δ*csnA::gfp:csnA*	5´pME5439,*Sac*I *gfp:csnA:*4384 WT:3624	3´pME5439,*KpnI* *gfp:csnA:*4076 WT:3961
AnFB158	Δ*csnF::gfp:csnF* +m	see AnFB159	

AnFB159	Δ*csnF::gfp:csnF*	5´pME5437,*Pst*I *gfp:csnF:* 5483; WT: 4516	
AnFB160	Δ*csnD::gfp:csnD* +m	see AnFB161	
AnFB161	Δ*csnD::gfp:csnD*	3´pME4702,*Kpn*I *gfp:csnD:* 3960; WT: 2988	
AnFB162	Δ*csnB::gfp:csnB*$^{\Delta NLS2}$ +m	5´pME5444,*BamH*I *gfp:csnB*$^{\Delta NLS2}$: 7759; WT: 5296	
AnFB163	Δ*csnB::gfp:csnB*$^{\Delta NLS2}$	5´pME5444,*BamH*I *gfp:csnB*$^{\Delta NLS2}$: 6133; WT: 5296	
AnFB164**	Δ*csnB::gfp:csnB*$^{\Delta NLS1}$ +m	5´pME5444,*BamH*I *gfp:csnB*$^{\Delta NLS1}$: 7710; WT: 5296	
AnFB165**	Δ*csnB::gfp:csnB*$^{\Delta NLS1}$	5´pME5444,*BamH*I *gfp:csnB*$^{\Delta NLS1}$: 6054; WT: 5296	
AnFB166**	Δ*csnB::gfp:csnB**^{NLS2} +m	see AnFB167	
AnFB167**	Δ*csnB::gfp:csnB**^{NLS2}	5´pME5444,*BamH*I *gfp:csnB**^{NLS2}: 6154; WT: 5296	
AnFB168**	Δ*csnB::gfp:csnB**^{NLS1} +m	see AnFB169	
AnFB169**	Δ*csnB::gfp:csnB**^{NLS1}	5´pME5444,*BamH*I *gfp:csnB**^{NLS1}: 6154; WT: 5296	
AnFB182	Δ*csnH::csnH* +m	3´pME5436,*Xag*I Δ*csnH::csnH:* 5303; WT: 2825	
AnFB183	Δ*csnH::csnH*	see AnFB182	
AnFB184	Δ*csnG::csnG* +m	see AnFB185	
AnFB185	Δ*csnG::csnG*	5´pME5435,*Blp*I Δ*csnG::csnG:* 2028 WT: 2028	3´pME5435,*BamH*I Δ*csnG::csnG:* 5217 WT: 5217

7 List of abbreviations

Abbreviation	Meaning
α	alpha
aa	amino acid
AAA domain	ATPases associated with diverse cellular activities
Acc. No.	accession number
ADP	adenosine diphosphate
amp.	ampicillin
APS	ammonium persulphate
ATP	adenosine triphosphate
ATPase	adenosine triphosphatase
b	bottom
β	beta
bp	base pair
biol.	biological replicate
µ	micro
Δ	delta
%	percent
°C	Celsius
CCT	chaperonin containing tailless complex polypeptide 1
CID	collision-induced dissociation
COPI and II	coat protein complex I and II
COP9	constitutive photomorphogenesis 9
CSN	COP9 signalosome complex
CRL	cullin-RING ubiquitin E3 ligase
DAPI	4′,6-diamidino-2-phenylindole
DIC	differential interference contrast
DNA	deoxyribonucleic acid
DMSO	dimethyl sulfoxide
e1/e2/e3	elution fraction 1/ elution fraction 2/ elution fraction 3
EDTA	ethylenediamine tetraacetic acid
FAD	flavin adenine dinucleotide
FDR	false discovery rate
L	linker
LB	lysogeny broth
LC	loading control
LC-MS/MS	liquid chromatography mass spectrometry-mass spectrometry
LFQ	label-free quantification
GFP	green fluorescent protein
GTP	Guanosine-5'-triphosphate
GTPase	Guanosine-5'-triphosphatase
MS/MS count	number of the LC-MS/MS counts
n	number of replicates
NAD	nicotinamide adenine dinucleotide
NADH	1,4-dihydronicotinamide adenine dinucleotide
ND	no data
n.s.	not significant
PP	precision protease
PMSF	phenylmethylsulfonyl-fluoride
PCR	polymerase chain reaction
pre-CSN	pre-assembled COP9 signalosome complex
rel.	relative
RFP	red fluorescent protein
RNA	ribonucleic acid
RNaseA	ribonuclease A
SCF CRL	Skp1/A-Cul1/A-F-box cullin-RING E3 ligase
SDS	sodium dodecyl sulphate
SEM	standard error of the mean

TAP	tandem affinity purification
t	top
TCA cycle	tricarboxylic acid cycle
tech.	technical replicate
TEMED	tetramethylethylenediamine
TRiC	tailless complex polypeptide 1 ring complex
U.p.	uncharacterized protein
UP	unique peptide
UPP	ubiquitin-proteasome pathway
UV	ultraviolet
v/v %	volume per volume percent
w/v %	weight per volume percent
X/G	xylose-glucose

8 List of figures

9 List of tables

10 References

Ambroggio XI, Rees DC & Deshaies RJ (2003) JAMM: A metalloprotease-like zinc site in the proteasome and signalosome. *PLoS Biol* 2: e2

Amit M, Weisberg SJ, Nadler-Holly M, McCormack EA, Feldmesser E, Kaganovich D, Willison KR & Horovitz A (2010) Equivalent mutations in the eight subunits of the chaperonin CCT produce dramatically different cellular and gene expression phenotypes. *J Mol Biol* 401: 532–543

Amm I, Sommer T & Wolf DH (2014) Protein quality control and elimination of protein waste: The role of the ubiquitin–proteasome system. *Biochim Biophys Acta - Mol Cell Res* 1843: 182–196

Anfinsen CB (1973) Principles that govern the folding of protein chains. *Science (80-)* 181: 223–230

Araujo-Bazán L, Peñalva MA & Espeso EA (2008) Preferential localization of the endocytic internalization machinery to hyphal tips underlies polarization of the actin cytoskeleton in *Aspergillus nidulans*. *Mol Microbiol* 67: 891–905

Asimaki E, Petriukov K, Renz C, Meister C & Ulrich HD (2021) Fast friends – Ubiquitin-like modifiers as engineered fusion partners. *Semin Cell Dev Biol* in press

Axelrod DE, Gealt M & Pastushok M (1973) Gene control of developmental competence in *Aspergillus nidulans*. *Dev Biol* 34: 9–15

Baek K, Scott DC & Schulman BA (2021) NEDD8 and ubiquitin ligation by cullin-RING E3 ligases. *Curr Opin Struct Biol* 67: 101–109

Bai M, Zhao X, Sahara K, Ohte Y, Hirano Y, Kaneko T, Yashiroda H & Murata S (2019) In-depth analysis of the lid subunits assembly mechanism in mammals. *Biomolecules* 9: 213

Bailly AP, Perrin A, Serrano-Macia M, Maghames C, Leidecker O, Trauchessec H, Martinez-Chantar ML, Gartner A & Xirodimas DP (2019) The balance between mono- and NEDD8-chains controlled by NEDP1 upon DNA damage is a regulatory module of the HSP70 ATPase activity. *Cell Rep* 29: 212-224.e8

Barth E, Hübler R, Baniahmad A & Marz M (2016) The evolution of COP9 signalosome in unicellular and multicellular organisms. *Genome Biol Evol* 8: 1279–1289

Basenko E, Pulman J, Shanmugasundram A, Harb O, Crouch K, Starns D, Warrenfeltz S, Aurrecoechea C, Stoeckert C, Kissinger J, *et al* (2018) FungiDB: An integrated bioinformatic resource for fungi and oomycetes. *J Fungi* 4: 39

Bateman A, Martin MJ, Orchard S, Magrane M, Agivetova R, Ahmad S, Alpi E, Bowler-Barnett EH, Britto R, Bursteinas B, *et al* (2021) UniProt: The universal protein knowledgebase in 2021. *Nucleic Acids Res* 49: D480–D489

Bayram Ö & Braus GH (2012) Coordination of secondary metabolism and development in fungi: the velvet family of regulatory proteins. *FEMS Microbiol Rev* 36: 1–24

Bayram Ö, Krappmann S, Ni M, Bok JW, Helmstaedt K, Valerius O, Braus-Stromeyer S, Kwon N-J, Keller NP, Yu J-H, *et al* (2008) VelB/VeA/LaeA complex coordinates light signal with fungal development and secondary metabolism. *Science (80-)* 320

Bayram Ö, Sarikaya-Bayram Ö, Ahmed YL, Maruyama J-I, Valerius O, Rizzoli SO, Ficner R, Irniger S & Braus GH (2012) The *Aspergillus nidulans* MAPK module AnSte11-Ste50-Ste7-Fus3 controls development and secondary metabolism. *PLoS Genet* 8: e1002816

Bech-Otschir D, Kraft R, Huang X, Henklein P, Kapelari B, Pollmann C & Dubiel W (2001) COP9 signalosome-specific phosphorylation targets p53 to degradation by the ubiquitin system. *EMBO J* 20:

1630–1639

Beckmann EA, Köhler AM, Meister C, Christmann M, Draht OW, Rakebrandt N, Valerius O & Braus GH (2015) Integration of the catalytic subunit activates deneddylase activity in vivo as final step in fungal COP9 signalosome assembly. *Mol Microbiol* 97: 110–124

Bertani G (1951) Studies on lysogenesis. I. The mode of phage liberation by lysogenic *Escherichia coli*. *J Bacteriol* 62: 293–300

Bhat KP & Greer SF (2011) Proteolytic and non-proteolytic roles of ubiquitin and the ubiquitin proteasome system in transcriptional regulation. *Biochim Biophys Acta - Gene Regul Mech* 1809: 150–155

Brachmann CB, Sherman JM, Devine SE, Cameron EE, Pillus L & Boeke JD (1995) The SIR2 gene family, conserved from bacteria to humans, functions in silencing, cell cycle progression, and chromosome stability. *Genes Dev* 9: 2888–2902

Braus GH, Irniger S & Bayram Ö (2010) Fungal development and the COP9 signalosome. *Curr Opin Microbiol* 13: 672–676

Breakspear A, Langford KJ, Momany M & Assinder SJ (2007) CopA:GFP localizes to putative Golgi equivalents in *Aspergillus nidulans*. *FEMS Microbiol Lett* 277: 90–97

Busch S & Braus GH (2007) How to build a fungal fruit body: from uniform cells to specialized tissue. *Mol Microbiol* 64: 873–876

Busch S, Eckert SE, Krappmann S & Braus GH (2003) The COP9 signalosome is an essential regulator of development in the filamentous fungus *Aspergillus nidulans*. *Mol Microbiol* 49: 717–730

Busch S, Schwier EU, Nahlik K, Bayram O, Helmstaedt K, Draht OW, Krappmann S, Valerius O, Lipscomb WN & Braus GH (2007) An eight-subunit COP9 signalosome with an intact JAMM motif is required for fungal fruit body formation. *Proc Natl Acad Sci U S A* 104: 8089–94

Caplan AJ, Cyr DM & Douglas MG (1992) YDJ1p facilitates polypeptide translocation across different intracellular membranes by a conserved mechanism. *Cell* 71: 1143–1155

Caplan AJ & Douglas MG (1991) Characterization of YDJ1: a yeast homologue of the bacterial dnaJ protein. *J Cell Biol* 114: 609–621

Cappadocia L & Lima CD (2018) Ubiquitin-like protein conjugation: structures, chemistry, and mechanism. *Chem Rev* 118: 889–918

Cerqueira GC, Arnaud MB, Inglis DO, Skrzypek MS, Binkley G, Simison M, Miyasato SR, Binkley J, Orvis J, Shah P, *et al* (2014) The Aspergillus Genome Database: Multispecies curation and incorporation of RNA-Seq data to improve structural gene annotations. *Nucleic Acids Res* 42 doi:10.1093/nar/gkt1029

Chamovitz DA (2009) Revisiting the COP9 signalosome as a transcriptional regulator. *EMBO Rep* 10: 352–358

Chamovitz DA, Wei N, Osterlund MT, von Arnim AG, Staub JM, Matsui M & Deng X-W (1996) The COP9 complex, a novel multisubunit nuclear regulator involved in light control of a plant developmental switch. *Cell* 86: 115–121

Cherry JM, Hong EL, Amundsen C, Balakrishnan R, Binkley G, Chan ET, Christie KR, Costanzo MC, Dwight SS, Engel SR, *et al* (2012) Saccharomyces Genome Database: The genomics resource of budding yeast. *Nucleic Acids Res* 40: 700–705

Christmann M, Schmaler T, Gordon C, Huang X, Bayram Ö, Schinke J, Stumpf S, Dubiel W & Braus GH (2013) Control of multicellular development by the physically interacting deneddylases DEN1/DenA

and COP9 signalosome. *PLoS Genet* 9: e1003275

Ciechanover A (2005) Proteolysis: from the lysosome to ubiquitin and the proteasome. *Nat Rev Mol Cell Biol* 6: 79–87

Ciechanover A & Schwartz AL (1998) The ubiquitin-proteasome pathway: The complexity and myriad functions of proteins death. *Proc Natl Acad Sci* 95: 2727–2730

CJ. Mousley, K. Tyeryar, KE. Ile GS & RL. Brost, C. Boone, X. Guan, MR. Wenk VB (2008) Trans-Golgi network and endosome dynamics connect ceramide homeostasis with regulation of the unfolded protein response and TOR signaling in yeast. *Mol Biol Cell* 19: 4785– 4803

Clutterbuck AJ (1990) The genetics of conidiophore pigmentation in *Aspergillus nidulans*. *J Gen Microbiol* 136: 1731–1738

Coleman KE, Békés M, Chapman JR, Crist SB, Jones MJ, Ueberheide BM & Huang TT (2017) SENP8 limits aberrant neddylation of NEDD8 pathway components to promote cullin-RING ubiquitin ligase function. *Elife* 6

Conlan RS, Gounalaki N, Hatzis P & Tzamarias D (1999) The Tup1-Cyc8 protein complex can shift from a transcriptional co-repressor to a transcriptional co-activator. *J Biol Chem* 274: 205–210

Conway P, Tyka MD, DiMaio F, Konerding DE & Baker D (2014) Relaxation of backbone bond geometry improves protein energy landscape modeling. *Protein Sci* 23: 47–55

La Cour T, Kiemer L, Mølgaard A, Gupta R, Skriver K & Brunak S (2004) Analysis and prediction of leucine-rich nuclear export signals. *Protein Eng Des Sel* 17: 527–536

Cox J & Mann M (2008) MaxQuant enables high peptide identification rates, individualized p.p.b.-range mass accuracies and proteome-wide protein quantification. *Nat Biotechnol* 26: 1367–1372

Dambacher CM, Worden EJ, Herzik MA, Martin A & Lander GC (2016) Atomic structure of the 26S proteasome lid reveals the mechanism of deubiquitinase inhibition. *Elife* 5

Davie JK, Edmondson DG, Coco CB & Dent SYR (2003) Tup1-Ssn6 interacts with multiple class I histone deacetylases in vivo. *J Biol Chem* 278: 50158–50162

Davie JK, Trumbly RJ & Dent SYR (2002) Histone-dependent association of Tup1-Ssn6 with repressed genes in vivo. *Mol Cell Biol* 22: 693–703

DeMartino GN & Gillette TG (2007) Proteasomes: machines for all reasons. *Cell* 129: 659–662

Derbyshire MK, Weinstock KG & Strathern JN (1996) HST1, a new member of the SIR2 family of genes. *Yeast* 12: 631–640

Deshaies RJ & Joazeiro CAP (2009) RING Domain E3 Ubiquitin Ligases. *Annu Rev Biochem* 78: 399–434

Deshaies RJ, Koch BD, Werner-Washburne M, Craig EA & Schekman R (1988) A subfamily of stress proteins facilitates translocation of secretory and mitochondrial precursor polypeptides. *Nature* 332: 800–805

Dohmann EMN, Levesque MP, De Veylder L, Reichardt I, Jurgens G, Schmid M & Schwechheimer C (2008) The *Arabidopsis* COP9 signalosome is essential for G2 phase progression and genomic stability. *Development* 135: 2013–2022

Dopie J, Skarp KP, Rajakylä EK, Tanhuanpää K & Vartiainen MK (2012) Active maintenance of nuclear actin by importin 9 supports transcription. *Proc Natl Acad Sci U S A* 109

Dressel U, Thormeyer D, Altincicek B, Paululat A, Eggert M, Schneider S, Tenbaum SP, Renkawitz R

& Baniahmad A (1999) Alien, a highly conserved protein with characteristics of a corepressor for members of the nuclear hormone receptor superfamily. *Mol Cell Biol* 19: 3383–3394

Drocourt D, Calmels T, Reynes J-P, Baron M & Tiraby G (1990) Cassettes of the *Streptoalloteichus hindustanus ble* gene for transformation of lower and higher eukaryotes to phleomycin resistance. *Nucleic Acids Res* 18: 4009–4009

Dubiel D, Rockel B, Naumann M & Dubiel W (2015) Diversity of COP9 signalosome structures and functional consequences. *FEBS Lett* 589: 2507–2513

Dubiel W, Chaithongyot S, Dubiel D & Naumann M (2020) The COP9 signalosome: a multi-DUB complex. *Biomolecules* 10: 1082

Duda DM, Borg LA, Scott DC, Hunt HW, Hammel M & Schulman BA (2008) Structural insights into NEDD8 activation of cullin-RING ligases: conformational control of conjugation. *Cell* 134: 995–1006

Duden R (2003) ER-to-Golgi transport: COP I and COP II function (Review). *Mol Membr Biol* 20: 197–207

Duden R, Hosobuchi M, Hamamoto S, Winey M, Byers B & Schekman R (1994) Yeast beta- and beta'-coat proteins (COP). Two coatomer subunits essential for endoplasmic reticulum-to-Golgi protein traffic. *J Biol Chem* 269: 24486–24495

Echalier A, Pan Y, Birol M, Tavernier N, Pintard L, Hoh F, Ebel C, Galophe N, Claret FX & Dumas C (2013) Insights into the regulation of the human COP9 signalosome catalytic subunit, CSN5/Jab1. *Proc Natl Acad Sci* 110: 1273–1278

Eckey M, Hong W, Papaioannou M & Baniahmad A (2007) The nucleosome assembly activity of NAP1 is enhanced by Alien. *Mol Cell Biol* 27: 3557–3568

Ellis RJ (1991) Molecular Chaperones. *Annu Rev Biochem* 60: 321–347

Ellisdon AM & Stewart M (2012) Structural biology of the PCI-protein fold. *Bioarchitecture* 2: 118–123

Elsasser S, Chandler-Militello D, Müller B, Hanna J & Finley D (2004) Rad23 and Rpn10 serve as alternative ubiquitin receptors for the proteasome. *J Biol Chem* 279: 26817–26822

Enchev RI, Schreiber A, Beuron F & Morris EP (2010) Structural Insights into the COP9 Signalosome and Its Common Architecture with the 26S Proteasome Lid and eIF3. *Structure* 18: 518–527

Enchev RI, Schulman BA & Peter M (2015) Protein neddylation: beyond cullin–RING ligases. *Nat Publ Gr* 16

Enninga J, Levay A & Fontoura BMA (2003) Sec13 shuttles between the nucleus and the cytoplasm and stably interacts with Nup96 at the nuclear pore complex. *Mol Cell Biol* 23: 7271–7284

Estrin E, Lopez-Blanco JR, Chacón P & Martin A (2013) Formation of an Intricate Helical Bundle Dictates the Assembly of the 26S Proteasome Lid. *Structure* 21: 1624–1635

Fang L, Kaake RM, Patel VR, Yang Y, Baldi P & Huang L (2012) Mapping the protein interaction network of the human COP9 signalosome complex using a label-free QTAX strategy. *Mol Cell Proteomics* 11: 138–147

Fernandez-Capetillo O, Lee A, Nussenzweig M & Nussenzweig A (2004) H2AX: the histone guardian of the genome. *DNA Repair (Amst)* 3: 959–967

Fidel S, Doonan JH & Morris NR (1988) *Aspergillus nidulans* contains a single actin gene which has unique intron locations and encodes a γ-actin. *Gene* 70: 283–293

Freilich S, Oron E, Kapp Y, Nevo-Caspi Y, Orgad S, Segal D & Chamovitz DA (1999) The COP9

signalosome is essential for development of *Drosophila melanogaster*. *Curr Biol* 9: 1187-S4

French ME, Koehler CF & Hunter T (2021) Emerging functions of branched ubiquitin chains. *Cell Discov* 7: 6

Fukunaga K, Kudo T, Toh-e A, Tanaka K & Saeki Y (2010) Dissection of the assembly pathway of the proteasome lid in *Saccharomyces cerevisiae*. *Biochem Biophys Res Commun* 396: 1048–1053

Fuzesi-Levi MG, Ben-Nissan G, Bianchi E, Zhou H, Deery MJ, Lilley KS, Levin Y & Sharon M (2014) Dynamic regulation of the COP9 signalosome in response to DNA damage. *Mol Cell Biol* 34: 1066–1076

Füzesi-Levi MG, Fainer I, Ivanov Enchev R, Ben-Nissan G, Levin Y, Kupervaser M, Friedlander G, Salame TM, Nevo R, Peter M, *et al* (2020) CSNAP, the smallest CSN subunit, modulates proteostasis through cullin-RING ubiquitin ligases. *Cell Death Differ* 27: 984–998

Gabler F, Nam S, Till S, Mirdita M, Steinegger M, Söding J, Lupas AN & Alva V (2020) Protein sequence analysis using the MPI bioinformatics toolkit. *Curr Protoc Bioinforma* 72: 1–30

García I, Mathieu M, Nikolaev I, Felenbok B & Scazzocchio C (2008) Roles of the *Aspergillus nidulans* homologues of Tup1 and Ssn6 in chromatin structure and cell viability. *FEMS Microbiol Lett* 289: 146–154

Gasteiger E, Gattiker A, Hoogland C, Ivanyi I, Appel RD & Bairoch A (2003) ExPASy: The proteomics server for in-depth protein knowledge and analysis. *Nucleic Acids Res* 31: 3784–3788

Gasteiger E, Hoogland C, Gattiker A, Duvaud S, Wilkins MR, Appel RD & Bairoch A (2005) Protein identification and analysis tools on the ExPASy server. In *The Proteomics Protocols Handbook* pp 571–607.

des Georges A, Dhote V, Kuhn L, Hellen CUT, Pestova T V., Frank J & Hashem Y (2015) Structure of mammalian eIF3 in the context of the 43S preinitiation complex. *Nature* 525: 491–495

Gerke J, Bayram Ö, Feussner K, Landesfeind M, Shelest E, Feussner I & Braus GH (2012) Breaking the silence: protein stabilization uncovers silenced biosynthetic gene clusters in the fungus *Aspergillus nidulans*. *Appl Environ Microbiol* 78: 8234–8244

Gerke J, Frauendorf H, Schneider D, Wintergoller M, Hofmeister T, Poehlein A, Zebec Z, Takano E, Scrutton NS & Braus GH (2020) Production of the fragrance geraniol in peroxisomes of a product-tolerant baker's yeast. *Front Bioeng Biotechnol* 8

Gerke J, Köhler AM, Wennrich J-P, Große V, Shao L, Heinrich AK, Bode HB, Chen W, Surup F & Braus GH (2021) Biosynthesis of antibacterial iron-chelating tropolones in *Aspergillus nidulans* as response to glycopeptide-producing *Streptomycetes*. *Front Fungal Biol* in press

Gillette TG, Gonzalez F, Delahodde A, Johnston SA & Kodadek T (2004) Physical and functional association of RNA polymerase II and the proteasome. *Proc Natl Acad Sci U S A* 101: 5904–5909

Giurgiu M, Reinhard J, Brauner B, Dunger-Kaltenbach I, Fobo G, Frishman G, Montrone C & Ruepp A (2019) CORUM: the comprehensive resource of mammalian protein complexes—2019. *Nucleic Acids Res* 47: D559–D563

Glickman MH, Rubin DM, Coux O, Wefes I, Pfeifer G, Cjeka Z, Baumeister W, Fried VA & Finley D (1998) A subcomplex of the proteasome regulatory particle required for ubiquitin-conjugate degradation and related to the COP9-signalosome and eIF3. *Cell* 94: 615–623

Gonzalez F, Delahodde A, Kodadek T & Johnston SA (2002) Recruitment of a 19 S proteasome subcomplex to an activated promoter. *Science (80-)* 296: 548–550

Greene ER, Goodall EA, de la Peña AH, Matyskiela ME, Lander GC & Martin A (2019) Specific lid-base

contacts in the 26s proteasome control the conformational switching required for substrate degradation. *Elife* 8: 1–27

Groisman R, Polanowska J, Kuraoka I, Sawada J, Saijo M, Drapkin R, Kisselev AF, Tanaka K & Nakatani Y (2003) The ubiquitin ligase activity in the DDB2 and CSA complexes is differentially regulated by the COP9 signalosome in response to DNA damage. *Cell* 113: 357–367

Gusmaroli G, Figueroa P, Serino G & Deng XW (2007) Role of the MPN subunits in COP9 signalosome assembly and activity, and their regulatory interaction with *Arabidopsis* cullin3-based E3 ligases. *Plant Cell Online* 19: 564–581

Gutierrez C, Chemmama IE, Mao H, Yu C, Echeverria I, Block SA, Rychnovsky SD, Zheng N, Sali A & Huang L (2020) Structural dynamics of the human COP9 signalosome revealed by cross-linking mass spectrometry and integrative modeling. *Proc Natl Acad Sci U S A* 117: 4088–4098

Han K-H, Han K-Y, Yu J-H, Chae K-S, Jahng K-Y & Han D-M (2001) The *nsdD* gene encodes a putative GATA-type transcription factor necessary for sexual development of *Aspergillus nidulans*. *Mol Microbiol* 41: 299–309

Harshuk-Shabso D, Castel N, Israeli R, Harari S & Pick E (2021) *Saccharomyces cerevisiae* as a toolkit for COP9 signalosome research. *Biomolecules* 11: 497

Hartmann T, Dümig M, Jaber BM, Szewczyk E, Olbermann P, Morschhäuser J & Krappmann S (2010) Validation of a self-excising marker in the human pathogen *Aspergillus fumigatus* by employing the βrec/six site-specific recombination system. *Appl Environ Microbiol* 76: 6313–17

Heck JW, Cheung SK & Hampton RY (2010) Cytoplasmic protein quality control degradation mediated by parallel actions of the E3 ubiquitin ligases Ubr1 and San1. *Proc Natl Acad Sci* 107: 1106–1111

Helmstaedt K, Laubinger K, Voßkuhl K, Hoppert M, Valerius O, Seiler S & Braus GH (2008) The nuclear migration protein NUDF /LIS1 forms a complex with NUDC and BNFA at spindle pole bodies. *Eukaryot Cell* 7: 1041–1052

Hernández-González M, Bravo-Plaza I, de los Ríos V, Pinar M, Pantazopoulou A & Peñalva MA (2019) COPI localizes to the early Golgi in *Aspergillus nidulans*. *Fungal Genet Biol* 123: 78–86

Hetfeld BKJ, Helfrich A, Kapelari B, Scheel H, Hofmann K, Guterman A, Glickman M, Schade R, Kloetzel P-M & Dubiel W (2005) The zinc finger of the CSN-associated deubiquitinating enzyme USP15 is essential to rescue the E3 ligase Rbx1. *Curr Biol* 15: 1217–1221

Hicks J, Lockington RA, Strauss J, Dieringer D, Kubicek CP, Kelly J & Keller N (2001) RcoA has pleiotropic effects on *Aspergillus nidulans* cellular development. *Mol Microbiol* 39: 1482–1493

Hinnebusch AG (2006) eIF3: a versatile scaffold for translation initiation complexes. *Trends Biochem Sci* 31: 553–562

Hong X, Xu L-G, Li X, Zhai Z & Shu H-B (2001) CSN3 interacts with IKKγ and inhibits TNF- but not IL-1-induced NF-κB activation. *FEBS Lett* 499: 133–136

Horianopoulos LC & Kronstad JW (2021) Chaperone networks in fungal pathogens of humans. *J Fungi* 7: 1–16

Howard B & Raistrick H (1955) Studies in the biochemistry of micro-organisms. *Biochem J* 59: 475–84

Huang X, Hetfeld BKJ, Seifert U, Kähne T, Kloetzel P-M, Naumann M, Bech-Otschir D & Dubiel W (2005) Consequences of COP9 signalosome and 26S proteasome interaction. *FEBS J* 272: 3909–3917

Inoue H, Nojima H & Okayama H (1990) High efficiency transformation of *Escherichia coli* with plasmids. *Gene* 96: 23–28

Isono E, Saito N, Kamata N, Saeki Y & Toh-e A (2005) Functional analysis of Rpn6p, a lid component of the 26 S proteasome, using temperature-sensitive *rpn6* mutants of the yeast *Saccharomyces cerevisiae*. *J Biol Chem* 280: 6537–6547

Jackson RJ, Hellen CUT & Pestova T V. (2010) The mechanism of eukaryotic translation initiation and principles of its regulation. *Nat Rev Mol Cell Biol* 11: 113–127

Jackson SP & Durocher D (2013) Regulation of DNA damage responses by ubiquitin and SUMO. *Mol Cell* 49: 795–807

Jayaraj GG, Hipp MS & Hartl FU (2020) Functional modules of the proteostasis network. *Cold Spring Harb Perspect Biol* 12: a033951

Jöhnk B, Bayram Ö, Abelmann A, Heinekamp T, Mattern DJ, Brakhage AA, Jacobsen ID, Valerius O & Braus GH (2016) SCF ubiquitin ligase F-box protein Fbx15 controls nuclear co-repressor localization, stress response and virulence of the human pathogen *Aspergillus fumigatus*. *PLOS Pathog* 12: e1005899

Kamitani T, Kito K, Fukuda-Kamitani T & Yeh ETH (2001) Targeting of NEDD8 and its conjugates for proteasomal degradation by NUB1. *J Biol Chem* 276: 46655–46660

Kang D, Wang X, Cao K, Sun C, Deng X-W & Wei N (2000) A gain-of-function phenotype conferred by over-expression of functional subunits of the COP9 signalosome in *Arabidopsis*. *Plant J* 23: 597–608

Kapelari B, Bech-Otschir D, Hegerl R, Schade R, Dumdey R & Dubiel W (2000) Electron microscopy and subunit-subunit interaction studies reveal a first architecture of COP9 signalosome. *J Mol Biol* 300: 1169–1178

Kato N, Brooks W & Calvo AM (2003) The expression of sterigmatocystin and penicillin genes in *Aspergillus nidulans* is controlled by *veA*, a gene required for sexual development. *Eukaryot Cell* 2: 1178–1186

Kloc M, Chanana P, Vaughn N, Uosef A, Kubiak JZ & Ghobrial RM (2021) New insights into cellular functions of nuclear actin. *Biology (Basel)* 10: 304

Köhler A, Meister C & Braus G (2016) *In vitro* deneddylation assay. *Bio-Protocol* 6

Köhler AM (2018) Specific ubiquitin-dependent protein degradation requires a trimeric CandA complex in *Aspergillus nidulans*. *D-NbInfo*

Köhler AM, Harting R, Langeneckert AE, Valerius O, Gerke J, Meister C, Strohdiek A & Braus GH (2019) Integration of fungus-specific CandA-C1 into a trimeric CandA complex allowed splitting of the gene for the conserved receptor exchange factor of cullinA E3 ubiquitin ligases in *Aspergilli*. *MBio* 10

Kolog Gulko M, Heinrich G, Gross C, Popova B, Valerius O, Neumann P, Ficner R & Braus GH (2018) Sem1 links proteasome stability and specificity to multicellular development. *PLOS Genet* 14: e1007141

Kosugi S, Hasebe M, Matsumura N, Takashima H, Miyamoto-Sato E, Tomita M & Yanagawa H (2009) Six classes of nuclear localization signals specific to different binding grooves of importinα. *J Biol Chem* 284: 478–485

Kotiguda GG, Weinberg D, Dessau M, Salvi C, Serino G, Chamovitz DA & Hirsch JA (2012) The organization of a CSN5-containing subcomplex of the COP9 signalosome. *J Biol Chem* 287: 42031–42041

Kragelund BB, Schenstrøm SM, Rebula CA, Panse VG & Hartmann-Petersen R (2016) DSS1/Sem1, a Multifunctional and Intrinsically Disordered Protein. *Trends Biochem Sci* 41: 446–459

Kranz A, Kinner A & Kölling R (2001) A family of small coiled-coil–forming proteins functioning at the late endosome in yeast. *Mol Biol Cell* 12: 711–723

Krappmann S, Jung N, Medic B, Busch S, Prade RA & Braus GH (2006) The *Aspergillus nidulans* F-box protein GrrA links SCF activity to meiosis. *Mol Microbiol* 61: 76–88

Krissinel E & Henrick K (2007) Inference of macromolecular assemblies from crystalline state. *J Mol Biol* 372: 774–797

Kück U & Hoff B (2006) Application of the nourseothricin acetyltransferase gene *(nat1)* as dominant marker for the transformation of filamentous fungi. *Fungal Genet Rep* 53: 9–11

Kunjappu MJ & Hochstrasser M (2014) Assembly of the 20S proteasome. *Biochim Biophys Acta - Mol Cell Res* 1843: 2–12

Kurz T, Özlü N, Rudolf F, O'Rourke SM, Luke B, Hofmann K, Hyman AA, Bowerman B & Peter M (2005) The conserved protein DCN-1/Dcn1p is required for cullin neddylation in *C. elegans* and *S. cerevisiae*. *Nature* 435: 1257–1261

Kwok SF, Staub JM & Deng X-W (1999) Characterization of two subunits of *Arabidopsis* 19S proteasome regulatory complex and its possible interaction with the COP9 complex. *J Mol Biol* 285: 85–95

Lander GC, Estrin E, Matyskiela ME, Bashore C, Nogales E & Martin A (2012) Complete subunit architecture of the proteasome regulatory particle. *Nature* 482: 186–191

Lasker K, Forster F, Bohn S, Walzthoeni T, Villa E, Unverdorben P, Beck F, Aebersold R, Sali A & Baumeister W (2012) Molecular architecture of the 26S proteasome holocomplex determined by an integrative approach. *Proc Natl Acad Sci* 109: 1380–1387

Lederkremer GZ, Cheng Y, Petre BM, Vogan E, Springer S, Schekman R, Walz T & Kirchhausen T (2001) Structure of the Sec23p/24p and Sec13p/31p complexes of COPII. *Proc Natl Acad Sci* 98: 10704–10709

Lee BN & Adams TH (1994) The *Aspergillus nidulans fluG* gene is required for production of an extracellular developmental signal and is related to prokaryotic glutamine synthetase I. *Genes Dev* 8: 641–651

Lee DH, Sherman MY & Goldberg AL (1996) Involvement of the molecular chaperone Ydj1 in the ubiquitin-dependent degradation of short-lived and abnormal proteins in *Saccharomyces cerevisiae*. *Mol Cell Biol* 16: 4773–4781

Lee M-H, Zhao R, Phan L & Yeung S-CJ (2011a) Roles of COP9 signalosome in cancer. *Cell Cycle* 10: 3057–3066

Lee M-K, Kwon N-J, Choi JM, Lee I-S, Jung S & Yu J-H (2014) NsdD is a key repressor of asexual development in *Aspergillus nidulans*. *Genetics* 197: 159–173

Lee MJ, Lee B-H, Hanna J, King RW & Finley D (2011b) Trimming of ubiquitin chains by proteasome-associated deubiquitinating enzymes. *Mol Cell Proteomics* 10: R110.003871

Lee WC, Xue ZX & Mélèse T (1991) The NSR1 gene encodes a protein that specifically binds nuclear localization sequences and has two RNA recognition motifs. *J Cell Biol* 113: 1–12

Li L (2003) The COP9 signalosome: an alternative lid for the 26S proteasome? *Trends Cell Biol* 13: 507–509

Lier S & Paululat A (2002) The proteasome regulatory particle subunit Rpn6 is required for Drosophila development and interacts physically with signalosome subunit Alien/CSN2. *Gene* 298: 109–119

Lima JF, Malavazi I, von Zeska Kress Fagundes MR, Savoldi M, Goldman MHS, Schwier E, Braus GH & Goldman GH (2005) The *csnD/csnE* signalosome genes are involved in the *Aspergillus nidulans* DNA

damage response. *Genetics* 171: 1003–1015

Lingaraju GM, Bunker RD, Cavadini S, Hess D, Hassiepen U, Renatus M, Fischer ES & Thomä NH (2014) Crystal structure of the human COP9 signalosome. *Nature* 512: 161–165

Liou S-T, Cheng M-Y & Wang C (2007) SGT2 and MDY2 interact with molecular chaperone YDJ1 in *Saccharomyces cerevisiae*. *Cell Stress Chaperones* 12: 59

Liu C, Guo L-Q, Menon S, Jin D, Pick E, Wang X, Deng XW & Wei N (2013) COP9 signalosome subunit Csn8 is involved in maintaining proper duration of the G1 phase. *J Biol Chem* 288: 20443–20452

Liu L, Sasse C, Dirnberger B, Valerius O, Fekete-Szücs E, Harting R, Nordzieke DE, Pöggeler S, Karlovsky P, Gerke J, *et al* (2021) Hülle-cell-mediated protection of fungal reproductive and overwintering structures against fungivorous animals. *Biochem Chem Biol Ecol*: 6

Livneh I, Cohen-Kaplan V, Cohen-Rosenzweig C, Avni N & Ciechanover A (2016) The life cycle of the 26S proteasome: From birth, through regulation and function, and onto its death. *Cell Res* 26: 869–885

Lobato-Gil S, Heidelberger JB, Maghames C, Bailly A, Brunello L, Rodriguez MS, Beli P & Xirodimas DP (2021) Proteome-wide identification of NEDD8 modification sites reveals distinct proteomes for canonical and atypical NEDDylation. *Cell Rep* 34: 108635

Lock A, Rutherford K, Harris MA, Hayles J, Oliver SG, Bähler J & Wood V (2019) PomBase 2018: user-driven reimplementation of the fission yeast database provides rapid and intuitive access to diverse, interconnected information. *Nucleic Acids Res* 47: D821–D827

Lodish H, Berk A, Kaiser CA, Kaiser C, Krieger M, Scott MP, Bretscher A, Ploegh H & Matsudaira P (2008) Molecular Cell Biology 4th ed. W. H. Freeman

Lykke-Andersen K, Schaefer L, Menon S, Deng X-W, Miller JB & Wei N (2003) Disruption of the COP9 signalosome Csn2 subunit in mice causes deficient cell proliferation, accumulation of p53 and cyclin E, and early embryonic death. *Mol Cell Biol* 23: 6790–6797

M.B. Wierman and J.S. Smith (2014) Yeast sirtuins and the regulation of aging. *FEMS Yeast Res* 14: 73–88

Ma W & Goldberg J (2013) Rules for the recognition of dilysine retrieval motifs by coatomer. *EMBO J* 32: 926–937

Madeira F, Park YM, Lee J, Buso N, Gur T, Madhusoodanan N, Basutkar P, Tivey ARN, Potter SC, Finn RD, *et al* (2019) The EMBL-EBI search and sequence analysis tools APIs in 2019. *Nucleic Acids Res* 47: W636–W641

Mandal AK, Nillegoda NB, Chen JA & Caplan AJ (2008) Ydj1 protects nascent protein kinases from degradation and controls the rate of their maturation. *Mol Cell Biol* 28: 4434–4444

Mani A & Gelmann EP (2005) The ubiquitin-proteasome pathway and its role in cancer. *J Clin Oncol* 23: 4776–4789

Mao Y-Q & Houry WA (2017) The role of pontin and reptin in cellular physiology and cancer etiology. *Front Mol Biosci* 4

Mao Y (2021) Structure, dynamics and function of the 26S proteasome. In *Subcellular Biochemistry* pp 1–151. Springer International Publishing

Markina-Iñarrairaegui A, Etxebeste O, Herrero-García E, Araújo-Bazán L, Fernández-Martínez J, Flores JA, Osmani SA & Espeso EA (2011) Nuclear transporters in a multinucleated organism: functional and localization analyses in *Aspergillus nidulans*. *Mol Biol Cell* 22: 3874–3886

Marsh JA, Hernández H, Hall Z, Ahnert SE, Perica T, Robinson C V. & Teichmann SA (2013) Protein

complexes are under evolutionary selection to assemble via ordered pathways. *Cell* 153: 461–470

Matalon O, Horovitz A & Levy ED (2014) Different subunits belonging to the same protein complex often exhibit discordant expression levels and evolutionary properties. *Curr Opin Struct Biol* 26: 113–120 doi:10.1016/j.sbi.2014.06.001

Maytal-Kivity V, Reis N, Hofmann K & Glickman MH (2002) MPN+, a putative catalytic motif fo und in a subset of MPN domain proteins from eukaryotes and prokar yotes, is critical for Rpn11 function. *Biomedcentral Biochem* 3: 1–12

Mazur P, Nakanishi K, El-Zayat AAE & Champe SP (1991) Structure and synthesis of sporogenic psi factors from *Aspergillus nidulans*. *J Chem Soc Chem Commun*: 1486

McCann T & Tansey W (2014) Functions of the proteasome on chromatin. *Biomolecules* 4: 1026–1044

McCord R, Pierce M, Xie J, Wonkatal S, Mickel C & Vershon AK (2003) Rfm1, a novel tethering factor required to recruit the Hst1 histone deacetylase for repression of middle sporulation genes. *Mol Cell Biol* 23: 2009–2016

McMahon HT & Mills IG (2004) COP and clathrin-coated vesicle budding: different pathways, common approaches. *Curr Opin Cell Biol* 16: 379–391

Meister C (2018) Interplay of the COP9 signalosome deneddylase and the UspA deubiquitinase to coordinate fungal development and secondary metabolism. *D-NbInfo*

Meister C, Kolog Gulko M, Köhler AM & Braus GH (2016) The devil is in the details: comparison between COP9 signalosome (CSN) and the LID of the 26S proteasome. *Curr Genet* 62: 129–136 doi:10.1007/s00294-015-0525-7

Meister C, Thieme KG, Thieme S, Köhler AM, Schmitt K, Valerius O & Braus GH (2019) COP9 signalosome interaction with UspA/Usp15 deubiquitinase controls Vea-mediated fungal multicellular development. *Biomolecules* 9: 238

Mergner J & Schwechheimer C (2014) The NEDD8 modification pathway in plants. *Front Plant Sci* 5: 1–15

Metzger MB, Hristova VA & Weissman AM (2012) HECT and RING finger families of E3 ubiquitin ligases at a glance. *J Cell Sci* 125: 531–537

Mosadeghi R, Reichermeier KM, Winkler M, Schreiber A, Reitsma JM, Zhang Y, Stengel F, Cao J, Kim M, Sweredoski MJ, *et al* (2016) Structural and kinetic analysis of the COP9-Signalosome activation and the cullin-RING ubiquitin ligase deneddylation cycle. *Elife* 5: 1–25

Mundt KE, Liu C & Carr AM (2002) Deletion mutants in COP9/signalosome subunits in fission yeast *Schizosaccharomyces pombe* display distinct phenotypes. *Mol Biol Cell* 13: 493–502

Mundt KE, Porte J, Murray JM, Brikos C, Christensen PU, Caspari T, Hagan IM, Millar JBA, Simanis V, Hofmann K, *et al* (1999) The COP9 signalosome complex is conserved in fission yeast and has a role in S phase. *Curr Biol* 9: 1427–1433

Murphy R, Watkins JL & Wente SR (1996) GLE2, a Saccharomyces cerevisiae homologue of the Schizosaccharomyces pombe export factor RAE1, is required for nuclear pore complex structure and function. *Mol Biol Cell* 7: 1921–1937

Musti AM, Treier M & Bohmann D (1997) Reduced ubiquitin-dependent degradation of c-Jun after phosphorylation by MAP Kinases. *Science (80-)* 275: 400–402

Nahlik K, Dumkow M, Bayram Ö, Helmstaedt K, Busch S, Valerius O, Gerke J, Hoppert M, Schwier E, Opitz L, *et al* (2010) The COP9 signalosome mediates transcriptional and metabolic response to hormones, oxidative stress protection and cell wall rearrangement during fungal development. *Mol*

Microbiol 78: 964–979

Neutzner M & Neutzner A (2012) Enzymes of ubiquitination and deubiquitination. *Essays Biochem* 52: 37–50

Nguyen Ba AN, Pogoutse A, Provart N & Moses AM (2009) NLStradamus: A simple Hidden Markov Model for nuclear localization signal prediction. *BMC Bioinformatics* 10: 1–11

Niepel M, Molloy KR, Williams R, Farr JC, Meinema AC, Vecchietti N, Cristea IM, Chait BT, Rout MP & Strambio-De-Castillia C (2013) The nuclear basket proteins Mlp1p and Mlp2p are part of a dynamic interactome including Esc1p and the proteasome. *Mol Biol Cell* 24: 3920–3938

Noventa-Jordão MA, Do Nascimento AM, Goldman MHS, Terenzi HF & Goldman GH (2000) Molecular characterization of ubiquitin genes from *Aspergillus nidulans*: mRNA expression on different stress and growth conditions. *Biochim Biophys Acta - Gene Struct Expr* 1490: 237–244

Oh E, Akopian D & Rape M (2018) Principles of ubiquitin-dependent signaling. *Annu Rev Cell Dev Biol* 34: 137–162

Oron E, Tuller T, Li L, Rozovsky N, Yekutieli D, Rencus-Lazar S, Segal D, Chor B, Edgar BA & Chamovitz DA (2007) Genomic analysis of COP9 signalosome function in *Drosophila melanogaster* reveals a role in temporal regulation of gene expression. *Mol Syst Biol* 3: 108

Osherov N & May G (2000) Conidial Germination in *Aspergillus nidulans* Requires RAS Signaling and Protein Synthesis. *Genetics* 155: 647–656

Osmani AH, Davies J, Liu H-L, Nileand A & Osmani SA (2007) Systematic deletion and mitotic localization of the nuclear pore complex proteins of *Aspergillus nidulans*. *Mol Biol Cell* 17: 4946–4961

Pantazopoulou A (2016) The Golgi apparatus: insights from filamentous fungi. *Mycologia* 108: 603–622

Park H-S, Lee M-K, Han K-H, Kim M-J & Yu J-H (2019) Developmental decisions in *Aspergillus nidulans*. In *Biology of the Fungal Cell* pp 63–80. Cham: Springer International Publishing

Park H-S, Ni M, Jeong KC, Kim YH & Yu J-H (2012) The role, interaction and regulation of the velvet regulator VelB in *Aspergillus nidulans*. *PLoS One* 7: e45935

Pathare GR, Nagy I, Bohn S, Unverdorben P, Hubert A, Korner R, Nickell S, Lasker K, Sali A, Tamura T, *et al* (2012) The proteasomal subunit Rpn6 is a molecular clamp holding the core and regulatory subcomplexes together. *Proc Natl Acad Sci* 109: 149–154

Pathare GR, Nagy I, Sledz P, Anderson DJ, Zhou H-J, Pardon E, Steyaert J, Forster F, Bracher A & Baumeister W (2014) Crystal structure of the proteasomal deubiquitylation module Rpn8-Rpn11. *Proc Natl Acad Sci* 111: 2984–2989

Payne GS & Schekman R (1985) A test of clathrin function in protein secretion and cell growth. *Science (80-)* 230: 1009–1014

Peng Z, Shen Y, Feng S, Wang X, Chitteti BN, Vierstra RD & Deng XW (2003) Evidence for a physical association of the COP9 signalosome, the proteasome, and specific SCF E3 ligases *in vivo*. *Curr Biol* 13: R504–R505

Peth A, Berndt C, Henke W & Dubiel W (2007a) Downregulation of COP9 signalosome subunits differentially affects the CSN complex and target protein stability. *BMC Biochem* 8: 27

Peth A, Boettcher JP & Dubiel W (2007b) Ubiquitin-dependent proteolysis of the microtubule End-Binding Protein 1, EB1, is controlled by the COP9 signalosome: possible consequences for microtubule filament stability. *J Mol Biol* 368: 550–563

Pick E & Bramasole L (2014) Moonlighting and pleiotropy within two regulators of the degradation

machinery: the proteasome lid and the CSN. *Biochem Soc Trans* 42: 1786–1791

Pick E, Golan A, Zimbler JZ, Guo L, Sharaby Y, Tsuge T, Hofmann K & Wei N (2012) The minimal deneddylase core of the COP9 signalosome excludes the Csn6 MPN-domain. *PLoS One* 7: 1–10

Pick E, Hofmann K & Glickman MH (2009) PCI complexes: Beyond the proteasome, CSN, and eIF3 troika. *Mol Cell* 35: 260–264

Pierce NW, Lee JE, Liu X, Sweredoski MJ, Graham RLJ, Larimore EA, Rome M, Zheng N, Clurman BE, Hess S, *et al* (2013) Cand1 promotes assembly of new SCF complexes through dynamic exchange of F-box proteins. *Cell* 153: 206–215

Pijnappel WWMP, Schaft D, Roguev A, Shevchenko A, Tekotte H, Wilm M, Rigaut G, Séraphin B, Aasland R & Stewart AF (2001) The *S. cerevisiae* SET3 complex includes two histone deacetylases, Hos2 and Hst1, and is a meiotic-specific repressor of the sporulation gene program. *Genes Dev* 15: 2991–3004

Pinar M, Arst HN, Pantazopoulou A, Tagua VG, de los Ríos V, Rodríguez-Salarichs J, Díaz JF & Peñalva MA (2015) TRAPPII regulates exocytic Golgi exit by mediating nucleotide exchange on the Ypt31 ortholog RabE RAB11. *Proc Natl Acad Sci* 112: 4346–4351

Pinar M & Peñalva MA (2017) *Aspergillus nidulans* BapH is a RAB11 effector that connects membranes in the Spitzenkörper with basal autophagy. *Mol Microbiol* 106: 452–468

Pöggeler S, Nowrousian M & Kück U (2006) Growth, Differentiation and Sexuality Kües U & Fischer R (eds) Berlin/Heidelberg: Springer-Verlag

Pöggeler S, Nowrousian M, Teichert I, Beier A & Kück U (2018) Fruiting-body development in *Ascomycetes*. In *Physiology and Genetics* pp 1–56. Cham: Springer International Publishing

Pontecorvo G, Roper JA, Chemmons LM, Macdonald KD & Bufton AWJ (1953) The genetics of *Aspergillus nidulans*. *Adv Genet* 5: 141–238

Punt PJ & van den Hondel CAMJJ (1992) Transformation of filamentous fungi based on hygromycin b and phleomycin resistance markers. In *Methods Enzymol.* pp 447–457.

Purschwitz J, Müller S & Fischer R (2009) Mapping the interaction sites of *Aspergillus nidulans* phytochrome FphA with the global regulator VeA and the White Collar protein LreB. *Mol Genet Genomics* 281: 35–42

Rao-Naik C, DelaCruz W, Laplaza JM, Tan S, Callis J & Fisher AJ (1998) The Rub family of ubiquitin-like proteins. *J Biol Chem* 273: 34976–34982

Rappsilber J, Mann M & Ishihama Y (2007) Protocol for micro-purification, enrichment, pre-fractionation and storage of peptides for proteomics using StageTips. *Nat Protoc* 2: 1896–1906

Richardson KS & Zundel W (2005) The emerging role of the COP9 signalosome in cancer. 3: 645–653

Rodríguez-Urra AB, Jiménez C, Nieto MI, Rodríguez J, Hayashi H & Ugalde U (2012) Signaling the induction of sporulation involves the Interaction of two secondary metabolites in *Aspergillus nidulans*. *ACS Chem Biol* 7: 599–606

Rozen S, Füzesi-Levi MG, Ben-Nissan G, Mizrachi L, Gabashvili A, Levin Y, Ben-Dor S, Eisenstein M & Sharon M (2015) CSNAP Is a Stoichiometric Subunit of the COP9 Signalosome. *Cell Rep* 13: 585–598

Russo VEA, Cove DJ, Edgar LG, Jaenisch R & Salamini F (1999) Development Russo VEA Cove DJ Edgar LG Jaenisch R & Salamini F (eds) Berlin, Heidelberg: Springer Berlin Heidelberg

Salama NR, Chuang JS & Schekman RW (1997) Sec31 encodes an essential component of the COPII

coat required for transport vesicle budding from the endoplasmic reticulum. *Mol Biol Cell* 8: 205–217

Sanchez JF, Chiang YM, Szewczyk E, Davidson AD, Ahuja M, Elizabeth Oakley C, Woo Bok J, Keller N, Oakley BR & Wang CCC (2010) Molecular genetic analysis of the orsellinic acid/F9775 gene cluster of *Aspergillus nidulans*. *Mol Biosyst* 6: 587–593

Santamaría PG, Finley D, Ballesta JPG & Remacha M (2003) Rpn6p, a proteasome subunit from *Saccharomyces cerevisiae*, is essential for the assembly and activity of the 26 S proteasome. *J Biol Chem* 278: 6687–6695

Sarikaya-Bayram Ö, Bayram Ö, Valerius O, Park HS, Irniger S, Gerke J, Ni M, Han K-H, Yu J-H & Braus GH (2010) LaeA control of velvet family regulatory proteins for light-dependent development and fungal cell-type specificity. *PLoS Genet* 6: e1001226

Sarikaya-Bayram Ö, Palmer JM, Keller N, Braus GH & Bayram Ö (2015) One Juliet and four Romeos: VeA and its methyltransferases. *Front Microbiol* 6: 1–7

Scheel H & Hofmann K (2005) Prediction of a common structural scaffold for proteasome lid, COP9-signalosome and eIF3 complexes. *BMC Bioinformatics* 6: 1–10

Schinke J, Kolog Gulko M, Christmann M, Valerius O, Stumpf SK, Stirz M & Braus GH (2016) The DenA/DEN1 interacting phosphatase DipA controls septa positioning and phosphorylation-dependent stability of cytoplasmatic DenA/DEN1 during fungal development. *PLoS Genet* 12

Schmidt S (1997) Sce3, a suppressor of the Schizosaccharomyces pombe septation mutant cdc11, encodes a putative RNA-binding protein. *Nucleic Acids Res* 25: 3433–3439

Schwechheimer C (2004) The COP9 signalosome (CSN): an evolutionary conserved proteolysis regulator in eukaryotic development. *Biochim Biophys Acta - Mol Cell Res* 1695: 45–54

Schwechheimer C & Isono E (2010) The COP9 signalosome and its role in plant development. *Eur J Cell Biol* 89: 157–162

Seeger M, Kraft R, Ferrell K, Bech-Otschir D, Dumdey R, Schade R, Gordon C, Naumann M & Dubiel W (1998) A novel protein complex involved in signal transduction possessing similarities to 26S proteasome subunits. *FASEB J* 12: 469–478

Sen N, Gui B & Kumar R (2014) Physiological functions of MTA family of proteins. *Cancer Metastasis Rev* 33: 869–877

Sha Z, Brill LM, Cabrera R, Kleifeld O, Scheliga JS, Glickman H, Chang EC & Wolf DA (2010) The eIF3 interactome reveals the translasome, a supercomplex linking protein synthesis and degradation machineries. *Mol Cell* 36: 141–152

Shaikhqasem A, Schmitt K, Valerius O & Ficner R (2021) Crystal structure of human CRM1, covalently modified by 2-mercaptoethanol on Cys528, in complex with RanGTP. *Acta Crystallogr Sect F Struct Biol Commun* 77: 70–78

Sharon M, Mao H, Boeri Erba E, Stephens E, Zheng N & Robinson C V (2009) Symmetrical modularity of the COP9 signalosome complex suggests its multifunctionality. *Structure* 17: 31–40

Sharon M, Taverner T, Ambroggio XI, Deshaies RJ & Robinson C V (2006) Structural Organization of the 19S Proteasome Lid: Insights from MS of Intact Complexes. *PLoS Biol* 4: e267

Shmueli MD, Sheban D, Eisenberg-Lerner A & Merbl Y (2021) Histone degradation by the proteasome regulates chromatin and cellular plasticity. *FEBS J*: febs.15903

Shortt J & Johnstone RW (2012) Oncogenes in cell survival and cell death. *Cold Spring Harb Perspect Biol* 4: a009829–a009829

Silvera D, Formenti SC & Schneider RJ (2010) Translational control in cancer. *Nat Rev Cancer* 10: 254–266

Singer R, Atar S, Atias O, Oron E, Segal D, Hirsch JA, Tuller T, Orian A & Chamovitz DA (2014) *Drosophila* COP9 signalosome subunit 7 interacts with multiple genomic loci to regulate development. *Nucleic Acids Res* 42: 9761–9770

Smith RL & Johnson AD (2000) Turning genes off by Ssn6–Tup1: a conserved system of transcriptional repression in eukaryotes. *Trends Biochem Sci* 25: 325–330

Snyder NA & Silva GM (2021) Deubiquitinating enzymes (DUBs): Regulation, homeostasis, and oxidative stress response. *J Biol Chem* 297: 101077

Song Y, DiMaio F, Wang RY-R, Kim D, Miles C, Brunette T, Thompson J & Baker D (2013) High resolution comparative modeling with RosettaCM. *Structure* 21: 1735–42

Southern EM (1975) Detection of specific sequences among DNA fragments separated by gel electrophoresis. *J Mol Biol* 98: 503–517

Souza CP De, Hashmi SB, Nayak T, Berl Oakley A & Osmani SA (2009) Mlp1 acts as a mitotic scaffold to spatially regulate spindle assembly checkpoint proteins in Aspergillus nidulans. *Mol Biol Cell* 20: 2146 –2159

Strambio-de-Castillia C, Blobel G & Rout MP (1999) Proteins connecting the nuclear pore complex with the nuclear interior. *J Cell Biol* 144: 839–855

Stratmann JW & Gusmaroli G (2012) Many jobs for one good cop - The COP9 signalosome guards development and defense. *Plant Sci* 185–186: 50–64

Sun C, Todorovic A, Querol-Audi J, Bai Y, Villa N, Snyder M, Ashchyan J, Lewis CS, Hartland A, Gradia S, *et al* (2011) Functional reconstitution of human eukaryotic translation initiation factor 3 (eIF3). *Proc Natl Acad Sci* 108: 20473–20478

Sun CW, Griffen S & Callis J (1997) A model for the evolution of polyubiquitin genes from the study of *Arabidopsis thaliana* ecotypes. *Plant Mol Biol* 34: 745–758

Sun L, Johnston SA & Kodadek T (2002) Physical association of the APIS complex and general transcription factors. *Biochem Biophys Res Commun* 296: 991–999

Swatek KN & Komander D (2016) Ubiquitin modifications. *Cell Res* 26: 399–422

Thieme KG (2017) The zinc cluster transcription factor ZtfA is an activator of asexual development and secondary metabolism and regulates the oxidative stress response in the filamentous fungus *Aspergillus nidulans*. *D-NbInfo*

Tiana M, Acosta-Iborra B, Puente-Santamaría L, Hernansanz-Agustin P, Worsley-Hunt R, Masson N, García-Rio F, Mole D, Ratcliffe P, Wasserman WW, *et al* (2018) The SIN3A histone deacetylase complex is required for a complete transcriptional response to hypoxia. *Nucleic Acids Res* 46: 120–133

Todd RB, Hynes MJ & Andrianopoulos A (2006) The *Aspergillus nidulans rcoA* gene is required for *veA*-dependent sexual development. *Genetics* 174: 1685–1688

Tomko RJ, Funakoshi M, Schneider K, Wang J & Hochstrasser M (2010) Heterohexameric ring arrangement of the eukaryotic proteasomal ATPases: Implications for proteasome structure and assembly. *Mol Cell* 38: 393–403

Tomoda K, Kubota Y, Arata Y, Mori S, Maeda M, Tanaka T, Yoshida M, Yoneda-Kato N & Kato J (2002) The cytoplasmic shuttling and subsequent degradation of p27Kip1 mediated by Jab1/CSN5 and the COP9 signalosome complex. *J Biol Chem* 277: 2302–2310

Torreira E, Jha S, López-blanco JR, Arias-palomo E, Cañas C, Ayora S, Dutta A, Llorca O, Nacional C, Cnb DB, *et al* (2009) Architecture of the pontin/reptin complex, essential in the assembly of several macromolecular complexes. *Structure* 16: 1511–1520

Trinci APJ & Morris NR (1979) Morphology and growth of a temperature-sensitive mutant of *Aspergillus nidulans* which forms aseptate mycelia at non-permissive temperatures. *J Gen Microbiol* 114: 53–59

Troppens DM, Köhler AM, Schlüter R, Hoppert M, Gerke J & Braus GH (2020) Hülle cells of *Aspergillus nidulans* with nuclear storage and developmental backup functions are reminiscent of multipotent stem cells. *MBio* 11

Tsuge T, Matsui M & Wei N (2001) The subunit 1 of the COP9 signalosome suppresses gene expression through its N-terminal domain and incorporates into the complex through the PCI domain. *J Mol Biol* 305: 1–9

Tyanova S, Temu T, Sinitcyn P, Carlson A, Hein MY, Geiger T, Mann M & Cox J (2016) The Perseus computational platform for comprehensive analysis of (prote)omics data. *Nat Methods* 13: 731–740

Uhle S, Medalia O, Waldron R, Dumdey R, Henklein P, Bech-Otschir D, Huang X, Berse M, Sperling J, Schade R, *et al* (2003) Protein kinase CK2 and protein kinase D are associated with the COP9 signalosome. *EMBO J* 22: 1302–1312

Vallim MA, Miller KY & Miller BL (2000) *Aspergillus* SteA (Sterile12-like) is a homeodomain-C2/H2-Zn+2 finger transcription factor required for sexual reproduction. *Mol Microbiol* 36: 290–301

Vijay-Kumar S, Bugg CE & Cook W (1992) Structure of porin refined at 1.8 Å resolution. *J Mol Biol* 227: 493–509

Wada H, Kito K, Caskey LS, Yeh ETH & Kamitani T (1998) Cleavage of the C-terminus of NEDD8 by UCH-L3. *Biochem Biophys Res Commun* 251: 688–692

Wang F, Brown EC, Mak G, Zhuang J & Denic V (2010) A chaperone cascade sorts proteins for posttranslational membrane insertion into the endoplasmic reticulum. *Mol Cell* 40: 159–171

Wang L, Zheng J-N & Pei D-S (2016) The emerging roles of Jab1/CSN5 in cancer. *Med Oncol* 33: 90

Wang X, Li W, Piqueras R, Cao K, Deng XW & Wei N (2009) Regulation of COP1 nuclear localization by the COP9 signalosome via direct interaction with CSN1. *Plant J* 58: 655–667

Watson AD, Edmondson DG, Bone JR, Mukai Y, Yu Y, Du W, Stillman DJ & Roth SY (2000) Ssn6–Tup1 interacts with class I histone deacetylases required for repression. *Genes Dev* 14: 2737–2744

Wei N, Chamovitz DA & Deng X-W (1994) *Arabidopsis* COP9 is a component of a novel signaling complex mediating light control of development. *Cell* 78: 117–124

Wei N & Deng XW (1992) COP9: a new genetic locus involved in light-regulated development and gene expression in *Arabidopsis*. *Plant Cell* 4: 1507–1518

Wei N & Deng XW (2003) The COP9 signalosome. *Annu Rev Cell Dev Biol* 19: 261–286

Wei N, Serino G & Deng XW (2008) The COP9 signalosome: more than a protease. *Trends Biochem Sci* 33: 592–600 doi:10.1016/j.tibs.2008.09.004

Wei N, Tsuge T, Serino G, Dohmae N, Takio K, Matsui M & Deng X-W (1998) The COP9 complex is conserved between plants and mammals and is related to the 26S proteasome regulatory complex. *Curr Biol* 8: 919–924

Wessel D & Flügge UI (1984) A method for the quantitative recovery of protein in dilute solution in the presence of detergents and lipids. *Anal Biochem* 138: 141–143

Whitby FG, Xia G, Pickart CM & Hill CP (1998) Crystal structure of the human ubiquitin-like protein NEDD8 and interactions with ubiquitin pathway enzymes. *J Biol Chem* 273: 34983–34991

Whittaker SL, Lunness P, Milward KJ, Doonan JH & Assinder SJ (1999) sodVIC is an α-COP-related gene which is essential for establishing and maintaining polarized growth in *Aspergillus nidulans*. *Fungal Genet Biol* 26: 236–252

Worden EJ, Padovani C & Martin A (2014) Structure of the Rpn11–Rpn8 dimer reveals mechanisms of substrate deubiquitination during proteasomal degradation. *Nat Struct Mol Biol* 21: 220–227

Yan J, Walz K, Nakamura H, Carattini-Rivera S, Zhao Q, Vogel H, Wei N, Justice MJ, Bradley A & Lupski JR (2003) COP9 signalosome subunit 3 is essential for maintenance of cell proliferation in the mouse embryonic epiblast. *Mol Cell Biol* 23: 6798–6808

Yao T & Cohen RE (2002) A cryptic protease couples deubiquitination and degradation by the proteasome. *Nature* 419: 403–407

Yébenes H, Mesa P, Muñoz IG, Montoya G & Valpuesta JM (2011) Chaperonins: two rings for folding. *Trends Biochem Sci* 36: 424–432

Yu J-H (2010) Regulation of development in *Aspergillus nidulans* and *Aspergillus fumigatus*. *Mycobiology* 38: 229

Yu JH (2006) Heterotrimeric G protein signaling and RGSs in *Aspergillus nidulans*. *J Microbiol* 44: 145–154

Yu Z, Armant O & Fischer R (2016) Fungi use the SakA (HogA) pathway for phytochrome-dependent light signalling. *Nat Microbiol* 1: 16019

Yu Z, Kleifeld O, Lande-Atir A, Bsoul M, Kleiman M, Krutauz D, Book A, Vierstra RD, Hofmann K, Reis N, *et al* (2011) Dual function of Rpn5 in two PCI complexes, the 26S proteasome and COP9 signalosome. *Mol Biol Cell* 22: 911–920

Zaman Z, Ansari AZ, Koh SS, Young R & Ptashne M (2001) Interaction of a transcriptional repressor with the RNA polymerase II holoenzyme plays a crucial role in repression. *Proc Natl Acad Sci* 98: 2550–2554

Zang Y, Jin M, Wang H, Cui Z, Kong L, Liu C & Cong Y (2016) Staggered ATP binding mechanism of eukaryotic chaperonin TRiC (CCT) revealed through high-resolution cryo-EM. *Nat Struct Mol Biol* 23: 1083–1091

von Zeska Kress MR, Harting R, Bayram Ö, Christmann M, Irmer H, Valerius O, Schinke J, Goldman GH & Braus GH (2012) The COP9 signalosome counteracts the accumulation of cullin SCF ubiquitin E3 RING ligases during fungal development. *Mol Microbiol* 83: 1162–1177

Zheng N, Schulman BA, Song L, Miller JJ, Jeffrey PD, Wang P, Chu C, Koepp DM, Elledge SJ, Pagano M, *et al* (2002) Structure of the Cul1–Rbx1–Skp1–F box-Skp2 SCF ubiquitin ligase complex. *Nature* 416: 703–709

Zhou C, Wee S, Rhee E, Naumann M, Dubiel W & Wolf DA (2003) Fission yeast COP9/signalosome suppresses cullin activity through recruitment of the deubiquitylating enzyme Ubp12p. *Mol Cell* 11: 927–938

Zingales V, Fernández-Franzón M & Ruiz M-J (2020) Sterigmatocystin: Occurrence, toxicity and molecular mechanisms of action – A review. *Food Chem Toxicol* 146: 111802

Acknowledgements

My gratitude goes to every person, who chaperoned me and my work during the last years and brought me forward in any ways. Working in the incomparable motivating and friendly atmosphere of AG Braus was a great experience, which helped me grow professionally and as a person.

I am truly grateful to Gerhard Braus for all the support I got during my work. This provided me with an inspiring atmosphere to work carefree, so I could go after my curiosity. I would like to extend my gratitude to Kai Heimel for all his valuable advices during our meetings and for encouraging me during the recent years. I would like to thank Ralf Ficner for his helpful comments and advices regarding my work as well as for allowing me to cooperate with members of the AG Ficner (Department for Molecular Structural Biology, GZMB, Göttingen). I thank the Stefanie Pöggeler, Michael Hoppert and Marcel Wiermer for being members of the examination board.

The enrollment in the Göttingen Graduate Center for Neurosciences, Biophysics, and Molecular Biosciences (GGNB) Microbiology and Biochemistry program allowed me to participate in exciting courses and to get to know fellow students. I enjoyed the workshops organized by the Georg-August University School of Science (GAUSS) Career Service. I thank the GGNB Office coordinators for the administrative help. This work was supported by the Deutsche Forschungsgemeinschaft (DFG) Sonderforschungsbereich (SFB) 860 and this gave me opportunity to meet and collaborate with researchers from other work groups.

I would like to express my gratefulness to Oliver Valerius and Kerstin Schmitt; not just for all the LCMS-MS measurements and proofreading of my thesis, but for the valuable suggestions and discussions, which contributed to this dissertation.

Members of the AG Ficner also always had an open ear to my questions. My gratitude goes to Piotr Neumann and Achim Dickmanns for protein structure predictions, brainstorming regarding work and life, which were always spent in a very friendly atmosphere.

Being a member of the lab 1.134 was a great experience and I am very lucky to have such wonderful colleagues. I am truly grateful to Anna Maria Köhler and Cindy Meister, not just for introducing me the COP9 signalosome and proofreading of my thesis, but also for supporting me during my work in so many ways. Understanding and tolerance gained a new meaning for me since I know them. I thank them for being on my side and I am proud to call them my friend! I thank Gaby Heinrich for her help in the lab and the motherly care for my professional as well as for my private life. I would like to express my thankfulness to Helena Stupperich. Her conscientious work during her master thesis and after that, together with her comments on the thesis, contributed to this work. Deep thank goes also to Anja Strohdiek for all the support, for always having an open ear for my concerns and the cheerful time we spent during the last years. I would like to thank the students, who participated in my work as my bachelor or internship students.

I would like to extend my gratefulness to Rebekka Harting to whom I could always turn with my questions. I thank for her advices during my work and for the comments on my thesis. I would like to thank Jessica Starke for proofreading my thesis. I very much appreciate the help and motivation I got from Jessica Starke and Miriam Leonard! It meant a lot for me. I thank Annalena Höfer for the helpful discussions about mass spectrometry and for the nice chats in the department. I thank Blagovesta Popova for the cheerful conversations and for encouraging me whenever I needed it. I thank Anja Abelmann for the fun in- and outside of the lab. Many thanks to Christoph Sasse for introducing me in the group of AG Braus and to

our former `lunch group´ members, Jennifer Gerke, Joshua Schinke and Bastian Jöhnk. I thank Jennifer Gerke also for providing plasmids. I thank Karl Thieme for providing primers and for the good times we had in the lab. I thank Anna Pinter (born Knapp) for being an honest friend, for all the cheerful moments we had the last years and for the whole Pinter family for being wonderful host during my Black Forest visits! I owe deep thank to Maire Holz for cheering for me and providing me with delicious deserts, which I needed especially in the last phase of my doctoral studies. I also would like to thank Heidi Northemann, Andrea Wäge, Maria Meyer and Nicole Scheiter for facilitating my daily life in the department as well as for the delightful conversations in- and outside of the department. I am thankful to the members of the `Werkstatt´, whose experience and helped me inside and out of the department.

My Hungarian heartland is supporting me form 1000 km distance. I would not be writing these lines and my life would be poorer without it. The high school years, which I will never forget, imprinted in me, thanks to all my wonderful former classmates! I express my gratitude to my friends Boglárka Torma, Szabina Papp, Anita Pokoraczki, Krisztián Bene and Zsófia Zsíros. We stay together since more than two decades, forming each other and sharing experiences of growing up. I admire their trust, warmth and courage; these pushed me to be bolder and for that I am forever grateful! I appreciate the helpful comments Krisztián Bene made on my thesis. I feel also very lucky to make wonderful friends at the University of Debrecen. My deepest thank to Nóra Hegedüs, Tímea Cihat and Szilvia Szaniszló for their loyal friendship, understanding, encouragement and for being on my side for all these years and for long before! They showed me the bright side of life, what helped me through difficult times. I am grateful to Melinda Szilágyi-Bónizs for introducing me the microbiology lab practice as my first supervisor and for being a friend, in spite of, and ever since. I always could and can count on Viktória Tóth, to whom I am very thankful to for being a great and honest friend!

André’s endless patience and love supported me during the recent years. I thank for this and for being my wonderful partner for life!

I have a lot to thank to my late grandparents, who were probably unaware of how much guidance they gave for my life. I am forever grateful for my parents, who always trusted and beyond their strength supported my decisions. I owe my gratitude to my sisters for their love and faith in me. I dedicate this work for my nephews and nieces Zalán, Zétény, Zoé, Zara Milla, István and Zorka for the endless joy it gives me watching them grow up. I hope I can live up to their trust. (Örökké hálás vagyok a szüleimnek, akik erejükön felül támogattak és mindig bíztak a döntéseimben. Köszönöm a testvéreimnek a szeretetüket és a belém vetett hitüket. Az unokaöccseimnek és az unokahugaimnak Zalánnak, Zéténynek, Zoénak, Zara Millának, Istvánnak és Zorkának ajánlom ezt az írást azért a végtelen örömért, amit az nyújt, hogy láthatom őket felnőni. Remélem, hogy megérdemlem a bizalmukat.)